MOLECULAR CLONING AND CHARACTERIZATION OF NOVEL GENES HEPN1, HEPACAM AND HEPT3 THAT ARE ALTERED IN HUMAN HEPATOCELLULAR CARCINOMA

ANGELA MOH MEI CHUNG

NATIONAL UNIVERSITY OF SINGAPORE

2006

MOLECULAR CLONING AND CHARACTERIZATION OF NOVEL GENES HEPN1, HEPACAM AND HEPT3 THAT ARE ALTERED IN HUMAN HEPATOCELLULAR CARCINOMA

ANGELA MOH MEI CHUNG

(B.Sc. (Hons.), University College London)

A THESIS SUBMITTED

FOR THE DEGREE OF DOCTOR OF PHILOSOPHY

DEPARTMENT OF PHYSIOLOGY

NATIONAL UNIVERSITY OF SINGAPORE

2006

ACKNOWLEDGEMENTS

I am eternally grateful to my supervisor Dr Shali Shen and sincerely appreciate her invaluable guidance and mentorship. Her seriousness at work, critical thinking at analyzing results, incredible ability at applying knowledge to practice, and emphasis on having right attitude towards research, have enormously helped improve many areas of my research. Her unfailing patience, encouragement and support, especially during difficult times, have been a great source of strength for me to come thus far.

My warmest thanks go to my colleague Lee Lay Hoon. It had been great working with you. Your generous help, understanding and unswerving support are deeply appreciated. I also owe my sincere thanks to my ex-colleague Zhang Chunli for her unwavering friendship, encouragement and her help in raising the antibody. A big thank you to the 'little kids' in the laboratory, Zhang Ting and Tian Qifeng, for keeping the atmosphere light and my spirits high during work. All the refreshing recreational activities outside the laboratory have truly added excitement to the exhausting daily routine.

I would like to take this opportunity to acknowledge all staff members and their respective laboratories in the Department of Physiology for generously sharing their research materials and equipment. I am particularly grateful to Assoc Prof Hooi Shing Chuan, the Head of Department of Physiology, for his energetic leadership and moral support, as well as, for facilitating the pleasant work environment and providing excellent research facilities. I also greatly appreciate Khaw Aik Kia's assistance in using computer software. My very special thanks go to all the administrative staff, especially Ms Asha Das for her help whenever and wherever needed.

My deepest gratitude and thanks are due to my parents for their never-ending love and wholehearted support. Thank you Mum for believing in me and encouraging me to finish my studies that you least understand. Sorry for having kept you waiting for many late nights just to prepare dinner for me. I am also indebted to my close friends Wenjiao, Cindy, Pauline and Jann for their continuous encouragement and for bringing joy into my life.

LIST OF PUBLICATIONS

Publications in International Peer-reviewed (NUS Tier I) Journals

Moh, M. C., Zhang, C., Luo, C., Lee, L. H., and Shen, S. (2005) Structural and functional analyses of a novel ig-like cell adhesion molecule, hepaCAM, in the human breast carcinoma MCF7 cells. *J. Biol. Chem.* **280**, 27366-27374

Moh, M. C., Lee, L. H., and Shen, S. (2005) Cloning and characterization of hepaCAM, a novel Ig-like cell adhesion molecule suppressed in human hepatocellular carcinoma. *J. Hepatol.* **42**, 833-841

Moh, M. C., Lee, L. H., Yang, X., and Shen, S. (2003) HEPN1, a novel gene that is frequently down-regulated in hepatocellular carcinoma, suppresses cell growth and induces apoptosis in HepG2 cells. *J. Hepatol.* **39**, 580-586

Oral presentations at International Scientific Conferences

Moh, M. C., Lee L. H., and Shen, S. hepaCAM, a novel immunoglobulin-like cell adhesion molecule, is associated with the actin cytoskeleton and the lipid rafts and is involved in cell-matrix interaction. ASBMB Annual Meeting and Centennial Celebration. April 1-5, 2006. San Francisco, CA, USA. (ASBMB, American Society for Biochemistry and Molecular Biology)

Moh, M. C., Lee, L. H., and Shen, S. Structural and functional analyses of a novel immunoglobulin-like cell adhesion molecule hepaCAM that is suppressed in a variety of human cancers. 18th Asia Pacific Cancer Conference. September 7-9, 2005. Seoul, South Korea.

Moh, M. C., Lee, L. H., and Shen, S. Identification and characterization of a putative noncoding RNA gene in human hepatocellular carcinoma. 5th Human Genetics Organization (HUGO) Pacific Meeting & 6th Asia-Pacific Conference on Human Genetics. November 17-20, 2004. Biopolis/ Singapore.

Poster presentations at International Scientific Conferences

Moh, M. C., Lee, L. H., Zhang, C., and Shen, S. Identification and characterization of CAMSIT as a novel immunoglobulin-like cell adhesion molecule that exhibits growth inhibitory effect on human cancer cells. 95th Annual Meeting of the American Association for Cancer Research. March 27-31, 2004. Orlando, Florida, USA.

Moh, M. C., and Shen, S. A novel intronless putative tumor suppressor gene, hepn1, frequently inactivated in hepatocellular carcinoma and multiple tumor types. 93rd Annual Meeting of the American Association for Cancer Research. April 6-10, 2002. San Francisco, CA, USA.

International Awards

Moh, M. C. 18th Asia Pacific Cancer Conference Travel Award. September 7-9, 2005. Seoul, South Korea.

Moh, M. C. 5th Human Genetics Organization (HUGO) Pacific Meeting & 6th Asia-Pacific Conference on Human Genetics Fellowship Award. November 17-20, 2004. Biopolis/ Singapore.

TABLE OF CONTENTS

SUMMARY

The liver executes a myriad of endocrine and exocrine functions vital for the normal functioning of many organs and systems of the body. Cancer of the liver arises when there is a loss of equilibrium between the positive and negative regulators of cell growth, differentiation and cellular adhesion. The major form of primary liver cancer in human is hepatocellular carcinoma (HCC). HCC is one of the most common malignancies worldwide, especially in Asia and sub-Saharan Africa. Despite a few advances made in the diagnosis and treatment of HCC, the overall prognosis of HCC remains extremely poor. Hopefully, understanding the yet unclear molecular pathogenesis of HCC will provide a rational basis for the development of new diagnostic and prognostic interventions as well as identifying novel targets for a more effective management of HCC.

Using the technique of suppression subtractive hybridization, 45 novel genes differentially expressed in HCC were identified. Among these genes, a transcript, designated as *HEPN1*, was found to be frequently lost while the other, *HEPT3*, was frequently elevated in HCC patients. Intriguingly, the identification of *HEPN1* led to the isolation of another novel gene, *hepaCAM*, which contained the full-length cDNA of *HEPN1* on its antisense strand in the 3'-untranslated region. The aim of this study was to clone the full-length cDNAs of *HEPN1*, *hepaCAM* and *HEPT3*, as well as to investigate their expression and biological functions in HCC and other malignant cells. The data pertaining to these three novel genes, with particularly interesting findings and emphasis on *hepaCAM*, are presented in the thesis.

Gene *HEPN1* was downregulated in 22/23 of HCC samples and 4/4 of HCC cell lines, and completely lost in 10/12 of human cancer cell lines derived from different tumor types. Sequence analyses revealed that *HEPN1* was an intronless gene mapped to human chromosome 11q24.2. The gene encoded a putative 10-kDa peptide of 88 amino acids that had no homology to known proteins. The peptide was predominantly localized in the cytoplasm of mammalian cells. Re-expression of HEPN1 in HCC cell line HepG2 inhibited cell growth and induced apoptosis. The data suggest that silencing of *HEPN1* may be associated with carcinogenesis of hepatocytes.

Gene *hepaCAM* was expressed in a wide variety of normal human tissues, but frequently suppressed in HCC and diverse tumors. The gene was mapped to human chromosome 11q24.2 and contained 7 exons. The gene product of 416 amino acids displayed the typical structure of immunoglobulin (Ig)-like cell adhesion molecules, including an extracellular domain comprising a signal peptide and two Ig-like loops, a transmembrane segment, and a cytoplasmic tail. Biochemical analyses demonstrated that hepaCAM was glycosylated and phosphorylated, and formed *cis*-homodimers on cell surface. The subcellular localization of hepaCAM appeared cell density-dependent; in well spread cells, hepaCAM was distributed to cell protrusions, whereas in confluent cells, hepaCAM was predominantly accumulated at the sites of cell-cell contact on the plasma membrane. In polarized cells, hepaCAM was recruited to the basolateral membrane, and, lacking physical interaction, colocalized with E-cadherin at the lateral membrane. Furthermore, deletion mutagenesis of hepaCAM revealed that the extracellular/transmembrane domains of hepaCAM were essential for its dimerization and localization on plasma membrane. Exogenous expression of hepaCAM inhibited colony formation, arrested cell proliferation, and activated the

tumor suppressor p53, suggesting a role of hepaCAM as a negative regulator of cell growth. Furthermore, cell adhesion and motility assays demonstrated that hepaCAM increased cell spreading on matrices fibronectin and matrigel, delayed cell detachment, and enhanced cell migration. Deletion of the cytoplasmic domain significantly reduced cell-matrix adhesion and abolished wound healing, indicating that hepaCAM modulates cell-matrix interaction and cell migration essentially through its cytoplasmic domain.

Cell adhesion and migration signaling require the coordinated interaction amongst transmembrane proteins, actin cytoskeleton and membrane lipids. Detergent solubility assay showed that hepaCAM was partially insoluble in Triton X-100, suggesting a possible interaction between hepaCAM and the actin cytoskeleton and/or lipid rafts. Extensive deletion mutagenesis of hepaCAM revealed that while the cytoplasmic domain, specifically residues located within 319-416, conferred the detergent-resistant nature of the molecule, the extracellular Ig domains regulated the insolubility. Colocalization studies showed that hepaCAM colocalized with cytoskeletal filamentous actin (F-actin). Depolymerization of F-actin altered the solubility and disrupted the subcellular distribution of hepaCAM. When the cytoplasmic domain of hepaCAM was cloned and transfected into cells, the protein was no longer localized on the plasma membrane, and its solubility could not be affected by F-actin depolymerization, suggesting that recruitment of the cytoplasmic domain to the plasma membrane is necessary for its interaction with F-actin. In addition, sucrose density gradients demonstrated that hepaCAM, preferentially its dimeric form, partitioned into the lipid rafts. Dispersion of cholesterol in the lipid rafts affected the buoyancy of hepaCAM. Furthermore, hepaCAM colocalized with the lipid raft

markers caveolin-1 and fyn. These results indicate that hepaCAM interacts with the actin cytoskeleton and resides in the lipid rafts, implicating an involvement of the glycoprotein in cell signaling.

Gene *HEPT3* was transcriptionally upregulated in 20/23 of HCC patients and 5/5 of HCC cell lines. *HEPT3* was an intronless gene mapped to human chromosome 6q13-14. The gene transcript lacked extensive open reading frame and contained an Alu sequence near the 5' terminus, indicating that *HEPT3* encoded a noncoding RNA. Antisense studies showed that, when endogenous *HEPT3* expression level was reduced, colony formation and cell growth of HCC cell line C3A were significantly inhibited. The data suggest that the *HEPT3* may function through its noncoding RNA and its overexpression may play a role in hepatocarcinogenesis.

In conclusion, the data generated to date have demonstrated the importance of *HEPN1*, *hepaCAM*, and *HEPT3* in cell signaling and growth regulation, as well as their possible involvement in carcinogenesis. The frequent alterations of their expression in HCC and other malignancies suggest that these novel genes may emerge as biomarkers/targets for diagnosis/management of human cancer. However, further studies are to be carried out to elucidate the molecular mechanisms of tumor suppression by *HEPN1* and *hepaCAM*, and tumor promotion by *HEPT3*.

LIST OF TABLES

LIST OF FIGURES

ABBREVIATIONS

5-FU	5-fluorouracil
AFP	alpha-fetoprotein
ANOVA	analysis of variance
APAF	apoptosis protease-activating factor
APC	adenomatous polyposis coli
APS	ammonium persulfate
AS	antisense
ATM	ataxia telangiectasia mutated
ATP	adenosine triphosphate
ATR	ATM and Rad3-related
BCLC	barcelona clinic liver cancer staging
bFGF	basic fibroblast growth factor
bp	base pair
BRCC	breast cancer cell
BS3	bis(sulfosuccinimidyl) suberate
BSA	bovine serum albumin
CAM	cell adhesion molecule
CAR	coxsackie virus and adenovirus receptor
CD2AP	CD2-interacting adapter
CDK	cyclin-dependent kinase
cDNA	complementary DNA
CEACAM	carcinoembryonic antigen cell adhesion molecule
CIP	calf intestinal alkaline phosphatase

CLIP	cancer of the liver italian program
CT	computed tomography
DAPI	4',6-Diamidino-2-phenylindole
DEPC	diethylpyrocarbonate
DIG	digoxigenin
DMEM	Dulbecco's modified Eagle's medium
DMSO	dimethyl sulfoxide
DNA	deoxyribonucleic acid
DNase	deoxyribonuclease
dNTP	deoxynucleotide triphosphate
DRM	detergent-resistant membrane
DTSSP	3, 3'-Dithiobis (sulphosuccinimidyl propionate)
DTT	dithiothreitol
ECM	extracellular matrix
EDTA	ethylenediaminetetraacetic acid
ELISA	enzyme-linked immunosorbent assay
EP-CAM	epithelial cell adhesion molecule
ER	endoplasmic reticulum
ERK	extracellular signal-regulated kinase
ESAM	endothelial cell-selective adhesion molecule
EST	expressed sequence tag
F-ACTIN	filamentous actin
FAK	focal adhesion kinase
FBS	fetal bovine serum
FITC	fluorescein isothiocyanate

FNIII	fibronectin type III
Fz	frizzled
G-ACTIN	globular actin
GAP	GTPase-activating protein
GAPDH	glyceraldehyde 3-phosphate dehydrogenase
GDP	guanidine diphosphate
GEF	guanine nucleotide exchange factor
GFP	green fluorescent protein
GPI	glycosylphosphatidylinositol
GSK	glycogen synthase kinase
GTP	guanidine triphosphate
HBSS	Hanks' balanced salt solution
HBV	hepatitis B virus
HBX	hepatitis B virus X protein
HCC	hepatocellular carcinoma
HCV	hepatitis C virus
HDV	hepatitis D virus
ICAM	intercellular adhesion molecule
IGF-II	insulin-like growth factor 2
Ig	immunoglobulin
IgSF	immunoglobulin superfamily
IPTG	isopropyl-beta-D-thiogalactopyranoside
JAM	junctional adhesion molecule
JAK	janus kinase
JIS	japan integrated staging

kb	kilobase
kDa	kilodalton
KI	potassium iodide
LB	Luria-Bertani
LEF	lymphoid enhancing factor
LOH	loss of heterozygosity
LRP	low-density lipoprotein receptor related protein
MAGUK	membrane-associated guanylate kinase
MAPK	mitogen-activated protein kinase
MCD	methyl-β-cyclodextrin
MDCK	Madin-Darby canine kidney
MEM	minimum essential medium
MHC	major histocompatibility complex
MHz	megahertz
min	minute(s)
mJ	millijoules
MOPS	3-[N-morpholino] propanesulfonic acid
MORF4	mortality factor 4
MRI	magnetic resonance imaging
mRNA	messenger RNA
MTT	3-(4,5-dimethylthiazol-2-yl)-2,5-diphenyltetrazolium bromide
MW	molecular weight
NCAM	neural-cell adhesion molecule
NCBI	National Center for Biotechnology Information
ncRNA	noncoding RNA

NFκB	nuclear factor kappa B
n-OG	*N*-octyl-β-D-glucopyranoside
OD	optical density
OPCML	opioid-binding protein/cell adhesion molecule-like
ORF	open reading frame
P	probability
PAK	p21-associated kinase
PCR	polymerase chain reaction
PECAM	platelet-endothelial-cell adhesion molecule
PEI	percutaneous ethanol injection
pI	isoelectric point
PI3K	phosphoinositide 3-kinase
PIP	phosphatidylinositol phosphate
PIPES	piperazine-*N*,*N*'-bis(2-hydroxypropanesulfonic acid)
PKB	protein kinase B
PNGase F	peptide *N*-glycosidase F
PS	phosphatidylserine
PTP	protein tyrosine phosphatase
PTTG	pituitary tumor transforming gene
PVDF	polyvinylidene difluoride
RACE	rapid amplification of cDNA ends
Rb	retinoblastoma
RFA	radiofrequency ablation
RHAMM	receptor for hyaluronate mediated motility
RIPA	radioimmunoprecipitation assay

ROCK	rho-associated kinase
RNA	ribonucleic acid
RNase	ribonuclease
rpm	revolutions per minute
RPMI-1640	Roswell Park Memorial Institute-1640
RPTP	receptor protein tyrosine phosphatase
RT-PCR	reverse transcriptase-polymerase chain reaction
SDS	sodium deodecyl sulphate
SDS-PAGE	SDS-polyacrylamide gel electrophoresis
sec	seconds
SH3	src homology 3
SINE	short interspersed repetitive sequence
SSC	standard sodium citrate
SSH	suppression subtractive hybridization
STAT	signal transducer and activator of transcription
TACE	trans-arterial chemoembolization
TAE	tris-acetate EDTA
TBS	tris-buffered saline
TBS-T	TBS-Tween-20
TCA	tricholoracetic acid
TCF	T-cell factor
TGF	transforming growth factor
Tm	melting temperature
TNF	tumor necrosis factor
TNM	tumor node metastasis

TRITC	tetramethylrhodamine isothiocyanate
TSLC	tumor suppressor in lung cancer
TUSC	tumor suppressor candidate
UTR	untranslated region
UV	ultraviolet
VCAM	vascular-cell adhesion molecule
VSV	vesicular stomatitis virus
WASP	Wiskott-Aldrich Syndrome protein
X-GAL	5-bromo-4-chloro-3-indolyl-β-D-galactoside
XIST	X (inactive)-specific transcript
ZO	zonula occludens

CHAPTER 1 INTRODUCTION

1.1 Liver – The metabolic centre

The liver is the largest internal organ in the human body and it executes a myriad of endocrine and exocrine functions essential for the normal functioning of many organs and systems of the body. It is involved in the regulation, synthesis, storage, and secretion of many important proteins and nutrients; as well as the purification, transformation, and removal of toxic or unwanted substances. Broadly, these functions can be classified into the following three overlapping categories.

1.1.1 Regulation, synthesis, and secretion

1.1.1.1 Glucose

The liver plays a major role in maintaining the homeostasis of blood glucose, either by storing glucose in the form of glycogen or releasing glucose when needed, in response to the pancreatic hormones insulin and glucagon.

1.1.1.2 Proteins

The liver produces and secretes the majority of blood proteins such as albumin. It also produces most of the proteins required for blood clotting including the prothrombin group of clotting factors. Furthermore, it is the centre for synthesis of lipoproteins, ceruloplasmin, transferrin and glycoproteins.

1.1.1.3 Lipids

The liver is involved in fat metabolism. It converts excess carbohydrates and proteins into fatty acids and triglycerides, which are then exported and stored in the adipose

tissues. Additionally, it manufactures cholesterol from acetate. Cholesterol is a type of lipid present on cell membranes that helps maintain the physical integrity of cells. It is packaged after synthesis and is then distributed to the body to be used or excreted into bile for removal from the body. The liver also synthesizes lipoproteins, which are made up of cholesterol, triglycerides, phospholipids and proteins. Lipoproteins circulate in the blood and transport cholesterol and fatty acids between the liver and body tissues.

1.1.1.4 Bile

The liver produces bile which contains cholesterol, phospholipids, bilirubin and bile salts. Bile is secreted into bile canaliculus that joins the bile duct. The bile duct then transports the bile to the gallbladder where it is drained into the small intestine to digest and absorb dietary fats. Bile also facilitates the absorption of substances such as vitamins A, D, E and K.

1.1.2 Storage

The liver stores important substances such as glycogen, fat-soluble vitamins (vitamins A, D, E and K), folate, vitamin B_{12}, and minerals such as copper and iron.

1.1.3 Purification, transformation, and clearance

The liver eliminates harmful substances from the blood to maintain homeostasis and protect the body against ingested toxins. It is capable of metabolizing or modifying toxins into less harmful compounds. These toxic substances include poisons, ammonia and bilirubin. In addition, the liver metabolizes most hormones and drugs to either a more or a less active product.

1.2 Liver organogenesis

In vertebrate models, the development of liver can be conceptualized in a series of stages that require intimate cooperation between cell adhesion and signaling events (Zaret, 2002; Gumbiner, 1996). Figure 1-1 depicts the sequence of events. During gastrulation, the endoderm forms a monolayer-thick sheet that covers the mesoderm and ectoderm of the embryo, which will eventually develop into liver, pancreas, lung, thyroid, and epithelial cells of the gastrointestinal system (Wells and Melton, 1999). Subsequent morphogenetic movements result in the patterning of the endoderm into broad domains along the anterior-posterior axis. The anterior endoderm then gains competence to generate the foregut. A combination of external positive inductive signals from the cardiogenic mesoderm and suppressive signals from the trunk mesoderm specifies a mass of cells in the ventral foregut endoderm to develop into a liver (Fukuda-Taira, 1981; Gualdi *et al*., 1996; Le Douarin, 1975). The hepatic endoderm epithelium thickens, proliferates, and migrates into the surrounding septum transversum mesenchyme to form the liver bud. Sustained epithelial/mesenchymal interactions promote cell propagation and morphogenesis as the embryonic liver matures. Remodelling of extracellular matrix (ECM) and formation of cell-cell and cell-ECM contacts accompany this event. The undifferentiated cells in the liver bud, known as hepatoblasts, are bi-potential, and have the ability to differentiate into either hepatocytes or biliary epithelial cells. The hepatocytes become polarized with three distinct membrane domains: sinusoidal (basal), lateral, and canalicular (apical). The basal membrane faces the sinusoids that contain blood. The lateral surface is associated with the adjacent hepatocyte. The apical domain lines the bile canaliculi that connect to bile ducts. Primitive endothelial cells residing near the hepatoblasts also play a crucial role in stimulating the early outgrowth of hepatoblasts as well as in

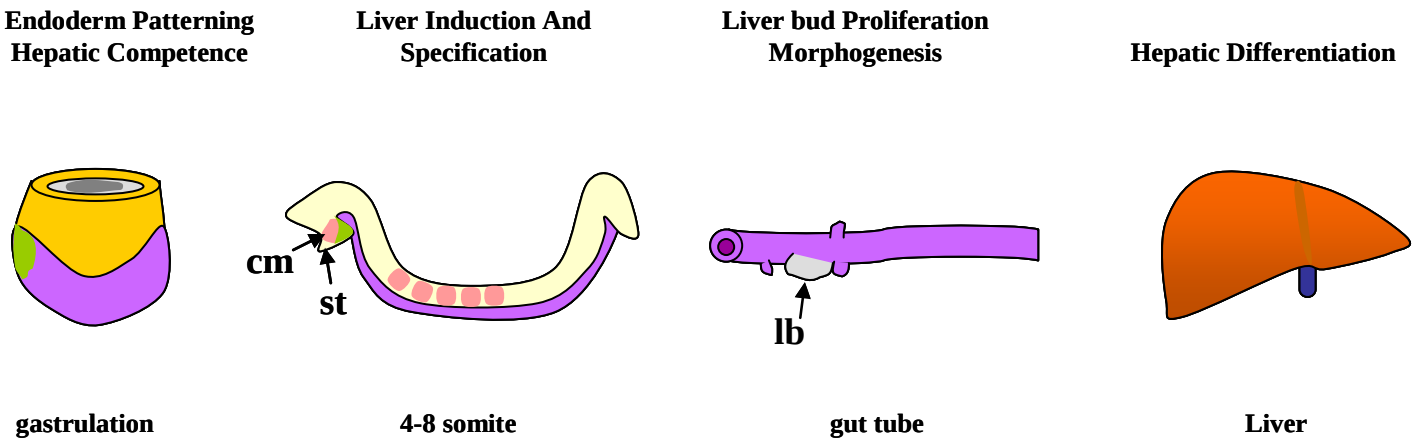

FIGURE 1-1 Organogenesis of liver. The liver development in mouse at four developmental stages; gastrula (far left), 4-8 somite stage, isolated gut tubes at liver bud , and adult liver (far right). During gastrulation, the endoderm (yellow) is specified and patterned so that the anterior endoderm (pink) acquires the competence to form foregut lineages. Between 4-8 somite stages, a subset of the ventral foregut endoderm (arrows) is induced by the adjacent cardiogenic mesoderm (cm) to adopt a hepatic fate. The hepatic epithelium then invades the septum transversum mesenchyme (st) and proliferates to form the liver bud (lb), which eventually differentiates and forms the mature liver. Anterior is to the left.

contributing to the development of blood vessels in which hematopoietic cells later invade.

1.3 Liver architecture

1.3.1 The liver is composed of acinar units

The liver is arranged into lobules that can be described as a collection of acini which are the basic subunits of liver structure. Each liver acinus is a small three-dimensional mass of hepatocytes supplied by the terminal branches of the portal vein and hepatic artery, and drained by the terminal branches of the hepatic vein (Figure 1-2). It can be divided into 3 zones that are anatomically related to the liver's blood supply and drainage. The blood enters zone one first, and then passes through the second and third zones before leaving the liver. The hepatocytes at zone 1 closest to the portal areas receive the most oxygen and nutrients as well as a high concentration of enzymes important for oxidative energy metabolism, amino acid metabolism, ureagenesis, gluconeogenesis, cholesterol synthesis, and bile formation. The hepatocytes in zone 3 closest to the central veins receive the least oxygen and nutrients and are predominantly involved in glycogen synthesis, glycolysis, liponeogenesis, ketogenesis, xenobiotic metabolism, and glutamine formation. Therefore, the hepatocytes in zone 3 are more specialized in the detoxification processes and the biotransformation of drugs. Zone 2 is the intermediate area of hepatocytes between zones 1 and 3 (Gumucio, 1983).

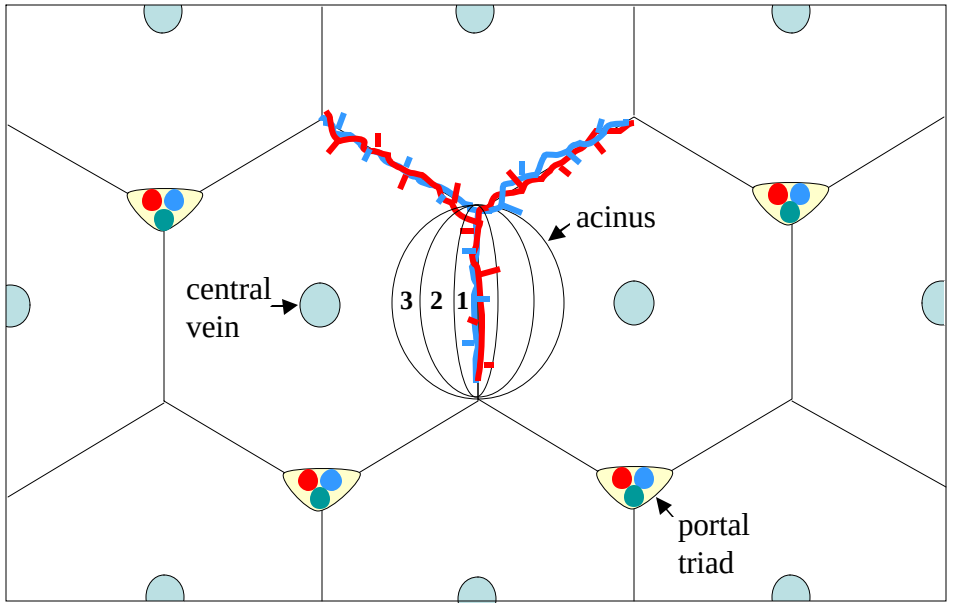

FIGURE 1-2 The acinus is divided into zones that correspond to distance from the arterial blood supply. Hepatocytes closest to the arterioles (zone 1) are the best oxygenated, while those farthest from the arterioles (zone 3) have the least supply of oxygen.

1.3.2 The liver has a unique dual blood supply, but a single venous drainage system

The liver receives a dual blood supply. The hepatic portal vein contributes about 70-80% of the liver's blood supply while the hepatic artery provides the remaining 20-30%. The hepatic artery supplies the liver with blood from the heart that is rich in oxygen and the portal vein carries nutrient-rich blood from the gastrointestinal tract. Blood from both the portal vein and the hepatic artery branch eventually converge together as they enter the sinusoids in the liver. The sinusoids flow into the central veins, coalesce into hepatic vein, and subsequently leave the liver to join the inferior vena cava.

1.3.3 Major cell types in liver

The liver cells are made up of parenchymal and non-parenchymal cells. As shown in Table 1-1, hepatocytes are the main parenchymal cells which constitute 80% of all liver cells, while the non-parenchymal cells consisting of sinusoidal endothelial cells, stellate cells, kupffer cells, pit cells, and biliary cells constitute the remaining 20-25%.

TABLE 1-1 Cell types in liver (modified from http://hupo.org/files/hlpp/HLPP_Summary_030930.pdf)

	Parenchyma	**Non-Parenchyma**
Cell type	Hepatocytes	Endothelial, Ito, Kupffer, Pit, Biliary
% Liver Cells	80%	20-25% **Fraction of Non-parenchymal cells** Endothelial: 70% Ito: 10% Kupffer: 20% Pit: 1% Biliary: 10%

1.3.3.1 Parenchymal cells

1.3.3.1.1 Hepatocytes

Hepatocytes are the functional units of the liver and they perform the majority of liver functions. The prominent intracellular golgi system and rough endoplasmic reticulum in hepatocytes enable the cells to synthesize and secrete large amounts of proteins into the blood. These cells are also involved in protein storage; transformation of carbohydrates; synthesis of cholesterol, bile salts and phospholipids; as well as detoxification, modification, and excretion of exogenous and endogenous substances. The hepatocytes also form and secrete bile.

Hepatocytes are arranged in one-cell thick hepatic plates that anastomose with one another (Figure 1-3). The cells are polygonal in shape and separate the tiny canalicular lumen containing bile from the sinusoid containing blood. The basal domains of the hepatocytes are in contact with ECM components in the space of Disse which separates the hepatocytes from the cells of the hepatic sinusoids.

1.3.3.2 Non-parenchymal cells

1.3.3.2.1 Sinusoidal endothelial cells

The sinusoidal endothelial cells form a fenestrated monolayer that separates hepatocytes from the passing blood (Figure 1-3). They serve as sieve-like plates that permit ready exchange of plasma solutes between the blood and hepatocytes. Unique from other endothelial cells, the sinusoidal endothelial cells lack basement membranes and their structures are supported by the reticular fibers in the space of Disse.

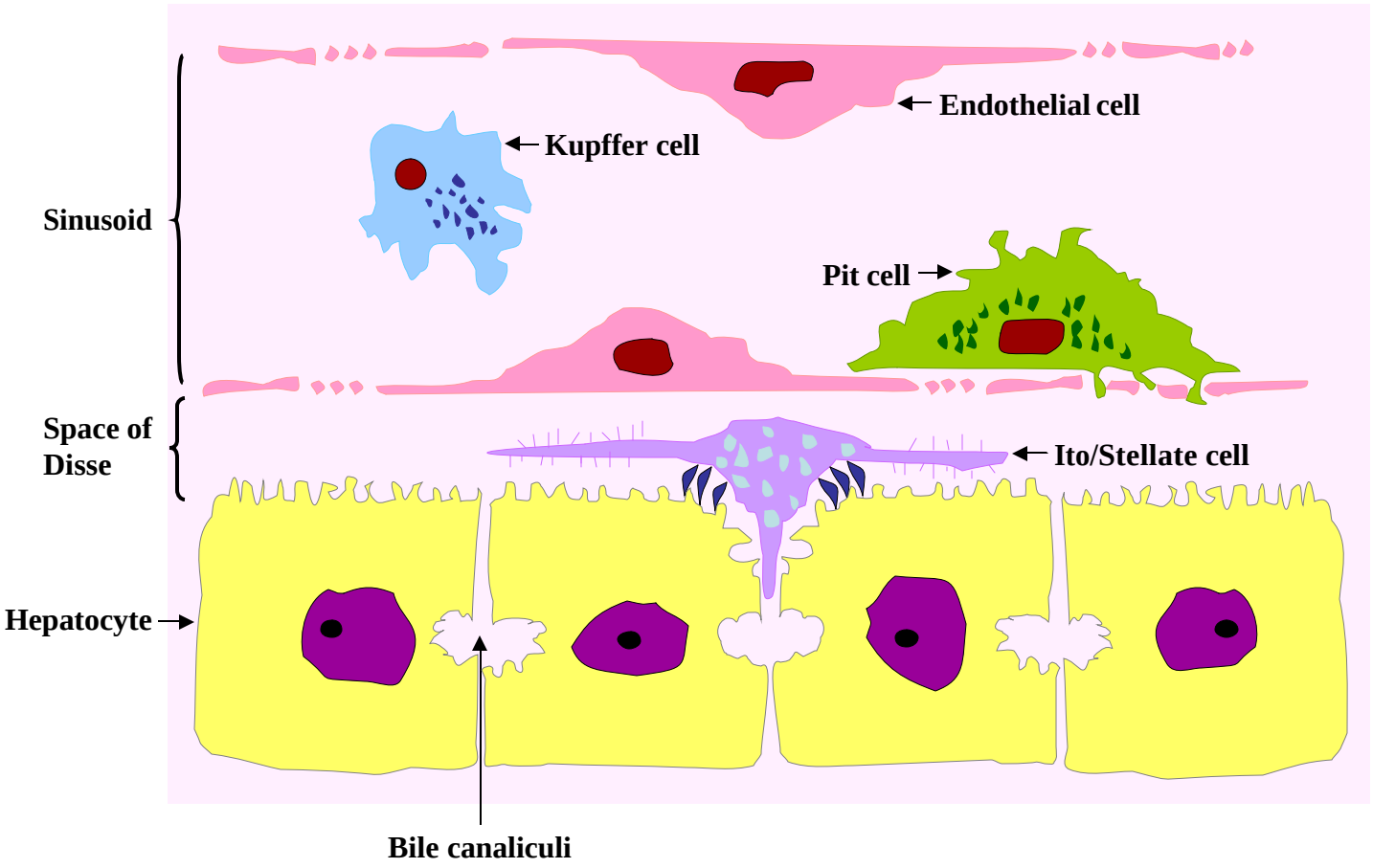

FIGURE 1-3 Diagrammatic representation of the liver cell plate.

1.3.3.2.2 Kupffer cells

Kupffer cells are associated with the endothelial cells within the lumen of the sinusoids (Figure 1-3) and function as resident macrophages that phagocytize particulates and unwanted materials (e.g. bacteria, virus particles, fibrin-fibrinogen complexes, damaged erythrocytes, and immune complexes) from the circulation. In addition, they modulate the immune response through the release of mediators and cytotoxic agents.

1.3.3.2.3 Ito/Stellate cells

Ito/Stellate cells are fat-storing cells found between the sinusoidal endothelial cells and hepatocytes in the perisinusoidal space of Disse (Figure 1-3; Wake, 1980). They are involved in vitamin A metabolism and are responsible for the storage of 80-90% of the vitamin A in the liver in the form of lipid droplets (Hendriks *et al*., 1985). In addition, these cells are the main source of ECM macromolecules such as collagen and ECM-degrading enzymes (Arthur, 2000). Furthermore, they are involved in releasing an array of proinflammatory cytokines and recruiting leukocytes. Therefore, upon liver damage, the ito cells may contribute to host defense, inflammation, and ultimately to fibrogenesis and the development of liver cirrhosis (Weiler-Normann and Rehermann, 2004).

1.3.3.2.4 Pit cells

Pit cells are large, mobile, granular lymphocytes that are found in the sinusoids and often adhere to the endothelial cells (Figure 1-3). Pseudopodia of pit cells can penetrate the pores of the endothelial cells to enter the space of Disse. They function as natural killer cells (Luo *et al*., 2000).

1.3.4 Extracellular space

The extracellular space is made up of perisinusoidal space of Disse, hepatic sinusoids, bile canaliculi and ECM (Stamatoglou and Hughes, 1994).

1.3.4.1 Space of Disse

The perisinusoidal space of Disse is located in between the sinusoidal domain of hepatocyte plasma membrane and the endothelial cells that form the walls of the hepatic sinusoids (Figure 1-3). This location where substances released from sinusoidal blood and hepatocytes mix is filled with microvilli of the hepatocytes. These microvilli will absorb nutrients, oxygen, and toxins from the blood as well as release their endocrine secretory products e.g. albumin and prothrombin to the blood via this perisinusoidal space. The space of Disse also functions as the liver's lymphatic capillary. Lymph flows through the space of Disse to collect in small lymphatic capillaries in the portal spaces.

1.3.4.2 Hepatic sinusoids

Hepatic sinusoids carry the blood flow from the portal vein and the hepatic artery. The four major sinusoidal cells are endothelial cells, kupffer cells, ito cells and pit cells (Figure 1-3; Wisse *et al*., 1996). Sinusoids lack basement membrane and are composed of a discontinuous layer of fenestrated endothelial cells. The pores can undergo dynamic changes in size to permit most solutes, except for large complexes, to gain access to the intervening space of Disse. Blood from the hepatic sinusoids enters the central vein before draining into the hepatic vein.

1.3.4.3 Biliary canaliculi

The bile canaliculi are formed by the invaginations between the adjacent plasma membranes of two hepatocytes (Figure 1-3). Bile secreted by the hepatocytes accumulates in canaliculi, drains via collecting ducts to small liver ducts, and finally to the hepatic duct that joins the cystic duct from the gallbladder to form the common bile duct.

1.3.4.4 Extracellular matrix

The ECM components occupy the space of Disse and are composed of type IV collagen, laminin, fibronectin and heparan sulfate proteoglycans (Hughes and Stamatoglou, 1987).

1.4 Liver and immunity

The liver plays a vital role in fighting infections. Functionally, the liver is involved in the uptake, metabolism, detoxification, and storage of a plethora of macromolecules. Therefore, it is constantly exposed to pathogens and foreign antigens. To protect against infectious pathogens, the liver must be able to induce immune responses against these harmful substances while maintain tolerance against food antigens. A large population of resident and migratory cells that patrol the liver including kupffer cells, pit cells, dendritic cells, and lymphocytes carry out these immunological functions. Lymphocytes, for example, in the presence of the appropriate migratory signals, have the capacity to bind to adhesion molecules expressed on the endothelial cells and migrate across the endothelial cells to the tissue where they follow a chemotactic gradient towards the site of inflammation (Weiler-Normann and Rehermann, 2004; Lalor and Adams, 2002).

1.5 Liver regeneration

The liver possesses the extraordinary ability to heal after severe liver injury or resection. This process involves controlled hyperplasia (cell division). In a normal healthy adult liver, the vast majority of hepatocytes are in a state of growth arrest at the G0 phase of the cell cycle, during which cells do not proliferate. It has been shown that partial hepatectomy stimulates ~95% of quiescent hepatocytes within the acinar architecture of the intact liver to rapidly re-enter the cell cycle. Liver regeneration is regulated by endogenous growth factors and cytokines such as tumor necrosis factor-alpha (TNF-α), interleukin-6, and hepatocyte growth factor. These growth factors and cytokines activate signaling cascades and thus induce the hepatocytes to undergo several cycles of proliferation and to migrate in order to restore the lost parenchymal liver mass and functional capacity. Restorative growth ceases when the organ reaches the appropriate size (Michalopoulos and DeFrances, 1997; Fausto *et al*., 1995).

In severe or chronic liver injury caused by hepatitis viral infections or alcohol when hepatocytes undergo recurring necrosis, subsequent chronic inflammation, regeneration and liver matrix remodeling will result in a fibrotic liver that may eventually progress to cirrhosis. The increased turnover rate of hepatocytes is likely to promote genetic alterations, and through clonal expansion of cells with a proliferation advantage over normal cells, hepatocellular carcinoma may finally develop (Thomas, 2005).

1.6 Hepatocellular carcinoma

Hepatocellular carcinoma (HCC) is the most common form of primary liver cancer in adults. It arises from hepatocytes, the major cell type in liver. HCC accounts for 80-90% of primary liver cancers and is one of the most frequent malignancies worldwide. The major risk factors for the development of HCC have been identified and characterized. Despite few advances in the treatment of HCC, the overall prognosis remains poor. The pitfalls in the conventional diagnosis, staging, and treatment of HCC urged scientists to unravel the yet unclear mechanism of HCC pathogenesis in the hope of developing new effective interventions to improve the management of HCC.

1.6.1 Global epidemiology of HCC

Hepatocellular carcinoma is one of the most frequent malignancies in the world, and its incidence varies greatly with geographic location, ethnic background and gender. In year 2000, an estimated 564,000 new cases of HCC and almost as many deaths were recorded (Ferlay *et al*., 2001; Parkin *et al*., 2001). As shown in Table 1-2, the geographic areas with a very high incidence (>20 cases/100,000 inhabitants) of HCC include Asia and sub-Saharan Africa. Southern Europe, Argentina and Switzerland are at intermediate risk (5-10 cases/100,000). Geographic areas of lowest incidence (<5 cases/100,000) include Western Europe and the United States (Thomas, 2005). In most parts of the world, the incidence of HCC is escalating. The incidence of HCC in the United States increased from 1.4/100,000 per year from 1976-1980 to 2.4/100,000 per year from 1991-1995 (El-Serag and Mason, 1999). Similar increases have also been registered in Japan and Western Europe (Thomas, 2005; Taylor-Robinson *et al*.,

TABLE 1-2 Epidemiology of HCC (Thomas, 2005)

Region	Incidence in Males (occurrences/100,000 population)	Incidence in Females (occurrences/100,000 population)	Major Risk Factors
Asia, Sub-Saharan Africa	30-120	9-30	HBV, aflatoxin
Japan	10-30	3-9	HCV
Southern Europe, Argentina, Switzerland	5-10	2-5	HCV
Western Europe	< 5	< 3	HCV
United States	< 5	< 3	HCV, alcohol

1997; Deuffic *et al*., 1998). In all regions studied, men are at greater risk of developing liver cancer than women. The average sex ratio for age-adjusted incidence rates (men/women) for year 2000 is 2.72 (Bosch and Ribes, 2002).

The incidence of HCC also varies with ethnic groups and regions of origin of patients who have migrated. For example, in the United States during 1988-1992, lower rates are found in the non-Hispanic white population, when compared to American Indians, Blacks and Hispanics. The highest incidence rates for North Americans have been observed among immigrants from high-risk countries, especially Chinese, Filipinos, Japanese and Koreans, although their United States-born descendents showed lower incidence rates (Bosch and Ribes, 2002). In addition, a local study showed that HCC is the third most frequent cancer among Singapore males, with more than 1,500 cases diagnosed between 1998 and 2002. HCC is more common in men than women, with a sex ratio of 3.4:1. The Chinese has the highest rates of HCC compared to Malays and Indians (Seow *et al*., 2004).

The majority of HCC patients do not survive for more than a year. The five-year relative survival rate in Europe (1985-1989) and North America (1983-1988) was 5% and 6%, respectively. There are no differences in the survival rates of male and female HCC patients. In Europe, the relative survival rate is higher in young patients (<45 years of age), which is attributed to curative treatment such as liver transplantation. In developing countries, however, HCC is inevitably fatal.

1.6.2 Risk factors of HCC

The etiological factors responsible for development of HCC are now well recognized. The geographical variability in HCC incidence rates strongly suggests differences in exposure to the risk factors. The major viral and environmental agents linked to HCC consisting of chronic infections with hepatits B virus and hepatitis C virus, and aflatoxin B1 exposure account for about 80% of HCC (Bosch *et al*., 1999). Furthermore, synergistic interplays between HBV and aflatoxin B1 (Kew, 2003), and between HCV and alcohol (Regev and Jeffers, 1999) have been documented to amplify the risk of HCC development. However, it is still debated whether various chemical agents are responsible for the recently observed increase in HCC incidences.

1.6.2.1 Hepatitis B virus infection

Hepatitis B virus (HBV) infection is the major cause of HCC in developing countries like China and Africa. Chronic HBV infection causes liver cirrhosis, and in most patients with HBV-associated HCC, the tumor occurs in the setting of cirrhosis. Therefore, with increasing duration or severity of chronic HBV infection, the chance of infected hepatocytes undergoing malignant transformation becomes progressively higher.

It has been implicated that the oncogenic mechanism of HBV is attributed to the integration of HBV DNA into the host cell genome (Shafritz *et al*., 1981), leading to undesired activation of multiple cellular genes as well as chromosomal instability. Specifically, integration of the hepatitis B virus X protein (HBX), a known causative agent in the formation of HCC, has been shown to stimulate cytoplasmic signal transduction pathways, including NFκB (Su and Schneider, 1996), PI3K/Akt (Shih *et*

al., 2000), AP-1 (Benn *et al*., 1996), Ras/Raf/MAPK (Benn and Schneider, 1994), JAK/STAT (Lee and Yun, 1998) and Wnt (Cha *et al*., 2004), thus promoting cell survival and initiating HCC development.

Indirectly, persistent HBV infection provokes an immune response and chronic inflammation with continuous regeneration and fibrosis that may eventually lead to cirrhosis. It is known that HBV-infected liver cells can be killed by cytotoxic T cells or injured by the cytokines from other specific cells. To retain adequate liver function, the liver cells must regenerate to replace the loss. These two events of immune-mediated injuries and reactive hyperplasia of the infected liver cells roll into a vicious cycle, and inevitably increase the risk of mutations which can be passed on to the daughter cells during proliferation (Thomas, 2005).

In addition, synergistic interactions between HBV and other factors such as aflatoxin B1 exposure, hepatitis D virus (HDV), HCV, and alcohol have been found to promote HCC development (Yeh *et al*., 1989; Sheen *et al*., 1994; Okuda and Ohnishi, 1994).

1.6.2.2 Hepatitis C virus infection

Hepatitis C virus (HCV) infection is also associated with the development of HCC, particularly in developed countries e.g. Japan and United States, and it contributes to the increasing rise in HCC incidence in these countries (Kiyosawa and Tanaka, 2002; Hassan *et al*., 2002). HCV is a plus-strand RNA virus that is not reverse transcribed into cDNA, and therefore is not integrated into the host genome. The mechanism in which HCV causes HCC is still obscure. Persistent infection with HCV will result in inflammation, cellular injury, regeneration, and cirrhosis, signifying an indirect role of

HCV in the pathogenesis of HCC. However, it is possible for an individual who has HCV but no cirrhosis to develop HCC. Growing evidence show that the core protein of HCV is capable of modulating cell proliferation by impeding apoptosis through interacting with Bax (Chung *et al*., 2003), interfering the normal function of tumor suppressors p53 and $p21^{waf1/cip1}$ (Ray *et al*., 1997; Kao *et al*., 2004; Oka *et al*., 2003), or upregulating cell growth-related genes, particularly Wnt-1 (Fukutomi *et al*., 2005). An observation that 15% of alcoholics with cirrhosis were infected with low level of HCV implicates that alcoholics may have increased exposure and acquisition of persistent HCV infection for unknown reasons (von Weizsacker *et al*., 1995).

1.6.2.3 Aflatoxin B1

Aflatoxin B1 has long been linked to the development of HCC because areas with a large dietary consumption of this toxin coincide with areas with a high incidence of HCC. Aflatoxin B1 is a toxic product of a mold called *Aspergillus flavus*, which is found in food that has been stored in a hot and humid environment. In most countries of sub-Saharan Africa, and some parts of China and Southeast Asia, food including peanuts, rice, soybeans, corn, and wheat is often highly contaminated with aflatoxin B1. Experimental studies have shown clearly that aflatoxin B1 is capable of causing HCC (Busby and Wogan, 1984). It is a very potent mutagen that is metabolized by the liver into the exo-8,9-epoxide intermediate. This epoxide binds selectively to guanine in DNA to form the N7 guanine adduct (Groopman *et al*., 1985), inducing a specific genetic change that is associated with development of HCC. The frequent base change is a specific G to T mutation at the third position of codon 249 of the tumor suppressor gene p53 (Lasky and Magder, 1997). In addition, the synergistic effect of

coexposures to aflatoxin B1 and HBV infection has been documented to increase the risk of HCC by 3-fold (Sun *et al*., 1999).

1.6.2.4 Alcohol

Chronic alcohol abuse is well known to cause liver injury and development of cirrhosis. Furthermore, the risk of developing cirrhosis among individuals who drink heavily is significantly increased by the coexistence of chronic HBV (Ohnishi *et al*., 1982) or HCV (Regev and Jeffers, 1999) infection. Alcohol has not been experimentally proven to initiate liver carcinogenesis. Rather, it has been proposed that alcohol may cause chronic liver damage and cirrhosis which may eventually lead to HCC formation.

1.6.2.5 Oral contraceptives

Studies have revealed that sex steroids (either estrogen or testosterone) may be associated with the development of liver adenomas (Dourakis and Tolis, 1998). These are benign liver tumors that occasionally developed into HCC in women who are long-term users of oral contraceptives. In countries like Europe and the United States, where oral contraceptives are widely used and HBV infection is rare, many cases of HCC developing in women appear to correlate with the long term use of oral contraceptives (Deugnier and Turlin, 1997).

1.6.2.6 Hemochromatosis

HCC will develop in up to 30% of patients with hereditary hemochromatosis (Powell *et al*., 1980). Hereditary hemochromatosis is a disorder characterized by the progressive accumulation of iron in the body. Patients at the greatest risk are those

who develop cirrhosis with their hemochromatosis. Once cirrhosis is established, effective removal of excess iron will not decrease the risk of developing HCC.

1.6.2.7 Cirrhosis

Individuals with liver cirrhosis are prone to developing HCC. Approximately 70-90% of HCC develop on a background of cirrhosis (Okuda *et al*., 1982). In addition to the conditions described above (HBV, HCV, alcohol, and hemochromatosis), alpha 1 anti-trypsin deficiency, a hereditary condition that can cause emphysema and cirrhosis, may also result in HCC development (Eriksson *et al*., 1986). Liver cancer is also strongly associated with hereditary tyrosinemia, a childhood biochemical abnormality that leads to early cirrhosis (Dehner *et al*., 1989).

1.6.3 Diagnosis of HCC

HCC is generally asymptomatic and is often advanced at the time of diagnosis when no curative therapy can be offered. Early diagnosis of small asymptomatic HCC, especially in high-risk patients, may prolong the survival of patients. Several diagnostic tools have been routinely employed for early detection of HCC.

1.6.3.1 Blood tests

Blood tests may be used to assess liver function. The most commonly used biochemical blood test is alpha-fetoprotein (AFP), a protein normally produced by immature liver cells in the fetus. At birth, infants have relatively high levels of AFP, which declines to normal adult levels by one year old. In addition, pregnant women carrying babies with neural tube defects may have high levels of AFP. Serum AFP levels are elevated in majority of primary liver cancer patients. AFP greater than

500 ng/ml is very indicative of HCC, and this level rapidly normalizes after HCC resection. The AFP test, however, cannot be used solely to confirm a diagnosis of liver cancer, because chronic hepatitis or cirrhosis can also produce high AFP levels.

1.6.3.2 Imaging studies

Imaging is used regularly to detect HCC in high-risk patients together with serum AFP assay, as well as to provide information relating to the location of the tumor, size of the tumor, the number of tumors, and whether the tumor has involved major blood vessels locally or spread outside of the liver. Ultrasound allows screening of the entire liver in a noninvasive manner and successfully visualizes HCC nodules as small as 0.5 cm in diameter. Computed tomography (CT) scan is useful in the diagnosis of HCC in patients when ultrasound is unsuccessful because of intervening bones, air in the intestine or lung, dense post-operative scar tissue, or presence of fatty tissue. It can detect HCC, differentiate various focal lesions of the liver, evaluate the location and extension of these lesions, and determine the size of tumors post-treatment. Magnetic resonance imaging (MRI) can provide very high-resolution, multiplanar images of the body. MRI is very useful for the differential diagnosis of hepatic masses and is slightly more sensitive than CT in detecting smaller tumors. Imaging studies, however, cannot tell the difference between a hepatoma and other abnormal nodules in the liver. A sample of liver tissue for biopsy is needed to make the definitive diagnosis of primary liver cancer. CT or ultrasound can be used to guide the doctor in selecting the best location for obtaining the biopsy sample.

1.6.3.3 Liver biopsy

Liver biopsy is considered to provide the definite diagnosis of liver cancer. This technique can target tumors as small as 0.5 cm in diameter. A sample of the liver or tissue fluid is removed with a fine needle, which is directed through the skin of the abdomen into the liver under ultrasound or CT guidance; and the biopsy is examined under a microscope for cancer cells. One drawback is that post biopsy bleeding can be fatal in cirrhotic patients with low platelet count, prolonged clotting time, and enlarged blood vessels that are under high pressure (portal hypertension).

1.6.4 Staging of HCC

Clinical staging of HCC provides guides to the prediction of prognosis and directs the appropriate therapeutic interventions. It is also an essential research tool that enables comparison between groups in clinical trials and between different studies. The ideal staging system should incorporate parameters related to: (a) the stage, aggressiveness, and growth rate of the tumor; (b) the general health of the patient; (c) the liver function of the patient; and (d) the specific therapeutic intervention. Staging systems that omit some factors or use only one factor will have a poor survival predictive power. Several staging systems have been proposed. However, there is no worldwide consensus on which is the most accurate.

The most commonly used classifications for HCC are the Child-Pugh score (Pugh *et al*., 1973), Okuda classification (Okuda *et al*., 1985), and the tumor node metastasis (TNM) classification (UICC, 1997). However, each has its own limitations for classifying patients. The Child-Pugh score is used for identification of HCC candidates for therapy. However, it only includes the functional capacity of the liver

without considering tumor-related parameters including tumor size, number, location, vascular invasion and metastasis. Conversely, the tumor node metastasis (TNM) classification uses tumor-related parameters without addressing the functional capacity of the liver. TNM classification is widely used in HCC candidates for treatment by hepatic resection or transplantation. The Okuda classification provides a tool for the combined assessment of both tumor characteristics and liver function factors including ascites, serum albumin and serum total bilirubin. Nevertheless, it lacks a means of assessing important tumor factors, such as whether the tumor is unifocal, multifocal or diffuse; or whether there is vascular invasion; all of which have important prognostic significance.

New staging paradigms have recently been proposed. The Barcelona clinic liver cancer (BCLC) staging classification was developed to address the weakness of the TNM and Okuda staging systems (Llovet *et al*., 1999). It considers tumor stage, liver functional status, physical status, and cancer-related symptoms; divides patients into early, intermediate, advanced, and end-stage categories (Sala *et al*., 2005); and links the prognostic prediction to a treatment algorithm. The Cancer of the Liver Italian Program (CLIP) score combines the Child-Pugh classification with tumor size, portal vein invasion, and AFP; and predicts patient survival more precisely than the Okuda staging system. However, it failed to identify patients at early stages of disease and is only applicable to patients with advanced tumors (Colombo and Sangiovanni, 2004). The Japan Integrated Staging (JIS) score includes TNM stage and Child-Pugh grade. BCLC scoring system has been demonstrated to provide a better prediction of prognosis in patients with disease diagnosed at early stage (Grieco *et al*., 2005); and

JIS was shown to perform better than the CLIP scoring system in selecting the best prognostic patient group (Kudo *et al*., 2003).

1.6.5 Treatment of HCC

HCC is extremely difficult to manage. Early-stage HCC is typically clinically silent, and HCC is often advanced at the time of diagnosis. Without treatment, HCC is relentlessly progressive, with a 5-year survival rate of less than 5% (Clark *et al*., 2005). The current management of HCC is confusing due to the lack of consensus guidelines for treatment as well as the lack of well-designed, randomized clinical trials comparing various treatment modalities. The treatment options are dictated by the stage of HCC, patient's clinical state, and hepatic function. Surgical interventions including tumor resection and liver transplantation offer the best curative treatment. Surgery is limited to patients whose tumors are less than 5 cm and confined to the liver, with no invasion of the blood vessels, cirrhosis, jaundice, or ascites. Therefore, only a few patients are eligible for surgery. All the other therapies to treat unresectable HCC are palliative and are with limitations. A downstaging of unresectable HCC can be achieved by trans-arterial chemoembolization (TACE) or percutaneous ablation using ethanol injection, cryosurgery and radiofrequency. Percutaneous treatments provide good results but are unable to achieve response rates and outcomes comparable to those of surgical treatments. Small solitary tumors of less than 2 cm can be completely ablated using the percutaneous approach. However, when tumor size exceeds 3 cm and/or the number of nodules is greater than 3, the success rate of treatment is significantly decreased. In patients with well-preserved liver function and large/multifocal asymptomatic tumors without vascular invasion, the sole option that has been demonstrated to provide treatment efficacy with modest

improvement in survival is chemoembolization. There is no proven chemotherapy regimen for HCC. Systemic administration of chemotherapeutic agents such as 5-fluorouracil (5-FU), doxorubicin and cisplatin has resulted in unsatisfactory clinical effects (Clark *et al*., 2005; Blum, 2005; Carr, 2004; Beaugrand *et al*., 2005; Llovet, 2005). Long-term survival of patients is uncommon because of the frequent recurrence after tumor resection, metastasis, or the development of new primary tumors. Overall, despite advances made in the diagnosis and management of HCC, the prognosis of HCC remains poor, especially in patients with unfavorable tumor characteristics. Therefore, elucidation of the genetic and molecular pathogenesis of HCC may provide new insights that will lead to the development of innovative strategies to manage HCC.

1.6.5.1 Liver resection

The goal of liver resection is to completely remove the tumor and the appropriate surrounding liver tissue. This option is limited to patients with one or two small (3 cm or less) tumors and excellent liver function without cirrhosis. Hence, very few patients with HCC are suitable to undergo liver resection. When a portion of a normal liver is removed, the remaining liver can regenerate to the original size within one to two weeks.

The greatest concern about resection is that the patient may develop liver failure after operation. Liver failure can occur if the remaining portion of the liver is inadequate to provide the necessary support for life. Even in carefully selected patients, about 10% of them are expected to die shortly post-surgery, usually as a result of liver failure. For patients whose tumors are successfully resected, the five-year survival is about 30

to 40% (Cha *et al*., 2003). However, the probability of recurrence of HCC elsewhere in the liver of these patients is high.

1.6.5.2 Liver transplantation

Liver transplantation is the best option for patients with tumors that are less than 5 cm in size and with signs of liver failure. Patients with small tumors less than 3 cm and no involvement of blood vessels have a less than 15% risk of recurrent HCC after transplant (Befeler and Di Bisceglie, 2002). Conversely, patients with tumors greater than 5 cm or with involvement of blood vessels have a very high risk of recurrence.

Biopsy or aspiration of HCC should be avoided in patients considering liver transplantation to prevent seeding cancer cells from the tumor by the needle into the liver along the needle track. Patients who have undergone liver transplantation must consume powerful anti-rejection medications to prevent the patient's immune system from rejecting the new liver. However, the suppressed immune system may allow new foci of cancer to develop.

1.6.5.3 Percutaneous ethanol injection

Ethanol treatment of HCC involves injecting pure ethanol percutaneously into the tumor using a very thin needle with the help of ultrasound or CT visual guidance. Alcohol induces tumor destruction by dehydrating the cytoplasm of tumor cells, leading to the denaturation of cellular protein structures and eventually necrosis. It may take up to several sessions of injections to completely destroy the tumor.

Percutaneous ethanol injection (PEI) therapy is only suitable for patients with fewer than three tumors, each less than 3-4 cm in size or with small single lesions less than 5 cm. In addition, patients with HCC undergoing alcohol injection should have no signs of chronic liver failure, such as ascites or jaundice.

The most common side effect of PEI therapy is leakage of alcohol onto the surface of the liver and into the abdominal cavity, causing pain and fever. It is important that the blood vessels and/or bile ducts that are adjacent to a tumor are clearly identified to protect them from accidental injection or injury during the procedure.

1.6.5.4 Cryosurgery

Cryosurgery is performed percutaneously laparoscopically, or more frequently, during an open surgey. The procedure involves freezing the tumor to stop its growth. Cryoprobes are placed directly into the liver and supercooled liquid nitrogen/argon gas circulates through the probes to freeze the tumor and a half inch margin of normal liver, resulting in cellular crystallization, cell shrinkage and membrane damage. Thawing leads to further damage as the area becomes hypotonic and smaller crystals re-crystallize to larger ones. Usually, two freeze-thaw cycles are carried out in each area because it has been shown to produce a better destruction of cancer cells than a single cycle. The tumor is not removed and the destroyed cancer cells are left in the body. Cryosurgery may have fewer side effects than other types of treatments, and is less expensive and requires shorter recovery time.

1.6.5.5 Radiofrequency ablation

Radiofrequency ablation (RFA) is a thermal technique that can be performed percutaneously laparoscopically or during an open surgery. An electrode is placed in the tumor and radio waves in the frequency range of 200 to 1200 MHz cause cells to oscillate. The heat generated ranging from 80°C to 110°C causes necrosis of tumor cells. The ideal size of an HCC tumor for RFA is less than 3 cm. Tumors that are larger may require more than one session. It is relatively safe and can be performed minimally invasively.

1.6.5.6 Trans-arterial chemoembolization

Liver tumors receive its blood supply exclusively from the hepatic artery unlike normal liver parenchyma that is supplied by both portal vein and hepatic artery. A downstaging of unresectable HCC can be achieved by trans-arterial chemoembolization (TACE). In this technique, small branches of the tumor hepatic artery are directly infused with chemotherapeutic agents before occlusion (embolization) with various types of materials, such as gelatin sponge or small metal coils. The tumor is thus exposed to high concentrations of anticancer agents which are confined locally since they are not carried away by the bloodstream. Furthermore, the technique deprives the tumor of blood supply, leading to tissue ischemic and eventually necrosis.

1.6.5.7 Chemotherapy

Chemotherapy of HCC is administered either intra-arterially or systemically. The most commonly used chemotherapeutic agents for HCC are doxorubicin, 5-FU, mitoxantrone, mitomycin C and cisplatin. These drugs are relatively toxic and no

established chemotherapeutic regimens have produced a responsive effect against HCC. The failure of treatment could be caused by suboptimal dosages of anticancer drugs, tumor heterogeneity, or overexpression of the multidrug resistance gene (Lai *et al*., 1990; Dexter and Leith, 1986; Huang *et al*., 1992).

1.7 Role of cell adhesion in liver

Cell adhesion in the liver plays a key role in liver organogenesis, immunity, regeneration, and HCC development. Cell adhesion is mediated by a large and complex number of cell adhesion molecules (CAMs) expressed on the cell surface that interact with one another in a spatially and temporally regulated manner. Intracellularly, the cytosolic domains of the CAMs associate with cytoplasmic plaque or peripheral membrane proteins. The cytoplasmic plaque proteins function as a bridge that links the adhesion systems to the cytoskeleton. Therefore, apart from linking cells to each other or to components of the ECM, an exciting concept that has emerged from recent cell biological research is that CAMs function also as receptors critical in modulating signal transduction (Gumbiner, 1996). Such interactions are vital for the regulation of a wide variety of cellular processes such as cell morphology, cell adhesion and cell motility; and are regulated by signaling complexes formed by the assembly of transmembrane and cytosolic proteins and membrane lipids (Engqvist-Goldstein and Drubin, 2003; Sechi and Wehland, 2000; Fais and Malorni, 2003).

1.7.1 Classification of cell adhesion molecules

Cell adhesion molecules are responsible for adhesion of cells to neighbouring cells or to the ECM components in the extracellular environment. According to their

structural and functional features, these transmembrane receptors can be generally classified into six families: the immunoglobulin superfamily, integrins, cadherins, selectins, hyaluronate receptors, and receptor protein tyrosine phosphatases.

1.7.1.1 Immunoglobulin superfamily

Immunoglobulin superfamily (IgSF) is one of the largest protein families in vertebrates and is widely expressed in a variety of cell types, including neurons, leukocytes, epithelial and endothelial cells. The IgSF CAMs are calcium-independent transmembrane glycoproteins that function by both homophilic and heterophilic interactions. The heterogeneous expression pattern of these CAMs implicates their involvement in diverse biological processes including immune responses, morphogenesis, brain development, tissue sorting, and development of the vascular network.

A typical IgSF CAM comprises of an extracellular domain which contains several Ig-like intrachain disulfide-bonded loops with conserved cysteine residues, a transmembrane domain, and a cytoplasmic domain. In addition, the ectodomain of these CAMs may possess several fibronectin type III (FNIII) repeats. Members of the IgSF include intercellular adhesion molecule (ICAM), vascular-cell adhesion molecule (VCAM), platelet-endothelial-cell adhesion molecule (PECAM), and neural-cell adhesion molecule (NCAM). Typically, they are capable of binding to other members of the Ig superfamily or to integrins.

1.7.1.2 Integrins

Integrins are cell-surface receptors important for a variety of cellular functions such as growth, development, immune response, and wound repair. They constitute non-covalently bound heterodimer composed of an α and a β subunit. To date, there are at least 22 integrin heterodimers composed of different combinations of the 17 α subunits and 8 β subunits. However, not every α and β combination exist. Although both subunits contribute to adhesion, the binding specificity of integrins primarily depends on the extracellular portion of the α-subunit. The β1 and β3 subfamilies predominantly mediate cell-matrix interactions, while members of the β2 classes are cell-cell adhesion molecules. Integrins are capable of mediating cell-ECM and cell-cell interactions (Hynes, 1987). They can bind to a variety of ECM proteins including fibronectin, fibrinogen, laminin, collagen, vitronectin and von Willenbrand factor (Haas and Plow, 1994). They can also associate with adhesion molecules like E-cadherin (Cepek *et al*., 1994) and those belonging to the IgSF such as ICAM and VCAM.

Integrins are constitutively expressed, but require activation in order to bind their ligand to mediate cell-cell or cell-ECM adhesion. Moreover, integrins play a critical role in signal transduction, exhibiting both "inside-out" and "outside-in" signaling properties. An example of "inside-out" signaling occurs when a cell stimulus, for example, triggering of the TCR/CD3 complex on an immune cell, stimulates the integrin receptor, leading to its activation via binding to its ligand. "Inside-out" signaling may also downregulate integrin activation. "Outside-in" signaling occurs after the integrin receptor binds its ligand and a signal is transmitted from the integrin receptor into the cell. Among the signaling molecules involved in integrin-mediated

cell survival is focal adhesion kinase (FAK), which is activated following integrin ligation (Nojima *et al*., 1995). It activates downstream survival pathways, such as PI3K, Akt and MAPK/ERK. The affinity of integrins for their ligands is not very strong. Therefore, to form effective cell-cell or cell-ECM contacts in response to specific stimuli, integrins that are usually diffusely distributed over the cell surface cluster at focal contacts (Jockusch *et al*., 1995). Their combined affinities create a region with sufficient adhesive capacity to adhere to the ECM. This allows cells to bind to a large number of matrix molecules simultaneously while still maintaining their ability to explore their environment. Integrins are capable of binding divalent cations such as calcium, magnesium and manganese. Magnesium and manganese alone are capable of activating integrins.

1.7.1.3 Cadherins

Cadherins are transmembrane glycoproteins that function as regulators of a wide variety of processes such as cell adhesion, cell sorting, cell survival, morphogenesis, formation of intercellular junctions, maintenance of tissue integrity, and tumorigenesis. They have been divided into several families, including type I (classical) and type II cadherins which are linked to the actin cytoskeleton; protocadherins which are expressed primarily in the central nervous system; and desmosomal cadherins (desmocollins and desmogleins) which are attached to intermediate filaments (Buxton *et al*., 1993).

Classical cadherins include E-, N-, and VE-cadherins. They were named after the tissues in which they were first identified (epithelial, neural, and vascular endothelial cells, respectively; Wheelock and Johnson, 2003; Pece and Gutkind; 2000). They are

single-pass transmembrane proteins that mediate Ca^{2+}-dependent homophilic cell-cell adhesion. Interestingly, there is evidence suggesting a heterophilic interaction between E-cadherin and $\alpha_E\beta_7$ integrin on the surface of lymphocytes (Cepek *et al*., 1994). Structurally, cadherins consist of five tandem repeated extracellular domains that are important for promoting cell-cell adhesion, a membrane-spanning segment, and a cytoplasmic region which links to the cytoskeleton via adaptor proteins like catenins and plakoglobin. These adhesion molecules depend on calcium for their adhesive function and prevention of protease digestion (Grunwald *et al*., 1981; Hyafil *et al*., 1981; Takeichi, 1977, 1988; Yoshida and Takeichi, 1982). In addition, they have been implicated to participate in transducing extracellular signals to the cytoplasm of cells (Juliano, 2002).

1.7.1.4 Selectins

Selectins are important for leukocyte recruitment. They are expressed on the surface of leukocytes, endothelial cells and platelets; and are responsible for mediating transient attachment and rolling of leukocytes along the activated vascular endothelium before development of tight adhesion and subsequent extravasation of leukocytes at sites of vascular injury and inflammation. The selectins have characteristic extracellular regions composed of an amino-terminal calcium-dependent lectin domain that binds a carbohydrate ligand, an epidermal growth factor-like domain, and two to nine short consensus repeat units similiar to domains found in complement binding proteins. There are three major groups of selectins: the L-selectins, which are homing receptors for specific adhesion of lymphocytes to endothelial cells of peripheral lymph nodes; the E-selectins, which are important mediators of inflammatory reactions and are upregulated within hours after

stimulation by inflammatory mediators; and P-selectins, which are expressed in endothelial cells and contained in storage granules of platelets whereby they are released during clotting and at times of platelet activation. P-selectins also mediate adhesion between leukocytes and platelets (Tedder *et al*., 1995; Freemont and Hoyland, 1996).

1.7.1.5 Hyaluronate receptors

Hyaluronan (also called hyaluronic acid or hyaluronate) is a naturally occurring member of the glycosaminoglycan family and is a linear polysaccharide composed of alternating glucuronic acid and *N*-acetylglucosamine $[\beta1,4\text{-GlcUA-}\beta1,3\text{-GlcNAc-}]_n$. Hyaluronan is an important structural element localized in ECM, at cell surface, and inside cells. It is ubiquitously distributed in the tissues of vertebrates, but is particularly abundant in extracellular matrices surrounding proliferating and migrating cells (Toole, 2002). Cells can bind to hyaluronan through cell surface hyaluronate receptor proteins such as CD44 and receptor for hyaluronate mediated motility (RHAMM; Peach *et al*., 1993; Yang *et al*., 1993), thereby modulating important biological processes including angiogenesis (Savani *et al*., 2001), proliferation (Mast *et al*., 1993; Wiig *et al*., 1996), cell motility (Chen *et al*., 1989), wound healing (Nishida *et al*., 1991), and cell adhesion (Klein *et al*., 1996).

1.7.1.6 Receptor protein tyrosine phosphatases

Receptor protein tyrosine phosphatases (RPTPs) form a subfamily of the classical protein tyrosine phosphatases (PTPs) and are involved in intracellular signaling and regulation of cell-cell adhesion (Tonks, 1993; Beckman and Bork, 1993). While the intracellular domains of other cell adhesion molecules need another molecule to link

to enzymes within the cytoplasm to influence intracellular events, the RPTPs have catalytic active cytosolic tyrosine phosphatase domains that have the potential to modulate intracellular signaling events directly (Freemont, 1998). Their extracellular domains are highly variable but many contain motifs of cell adhesion molecules that may function as ligand binding domains. Some RPTPs such as PTP-μ have CAM-like extracellular segments that mediate homophilic cell-cell interaction and associate with cadherins *in vivo* (Brady-Kalnay *et al*., 1998). On the other hand, PTP-α localizes to focal adhesions (Lammers *et al*., 2000). Cells overexpressing PTP-α show increased cell-substratum association (Harder *et al*., 1998), while cells deficient of PTP-α exhibit defective spreading on fibronectin (Su *et al*., 1999).

1.7.2 Types of cell adhesions

Cell adhesion mediated by cell-cell and cell-matrix interactions is necessary for tissue organization and integrity. Specialized cell-cell and cell-matrix junctions exist with their particular constellation of multiprotein complexes that connect the cytoskeleton to the plasma membrane to form stable adhesive contacts between cells and their extracellular environment.

1.7.2.1 Cell-cell adhesions

Cells are linked to one another via four distinct junctional complexes – gap junctions, adherens junctions, desmosomes, and tight junctions. Both tight junctions and adherens junctions are linked to the actin cytoskeleton while desmosomes are linked to intermediate filaments.

1.7.2.1.1 Gap junctions

Gap junctions form cylindrical hydrophilic channels that serve as direct connections between adjacent cells, allowing passive diffusion of the ions and small molecules in aqueous intercellular channels (connexons) between the cytoplasm of the neighbouring cells (Kumar and Gilula, 1996). Most cells in normal tissues including epithelial cells, endothelial cells, and the cells of cardiac and smooth muscle communicate via these junctions. Each gap junction is composed of an assembly of 6 transmembrane proteins called connexins.

1.7.2.1.2 Adherens junctions

Adherens junctions, also known as zonula adherens, are made up of calcium-dependent homophilic interactions between the extracellular domains of cadherins of adjoining cells and are critical for the establishment and maintenance of epithelial layers. Actin filaments are associated with the intracellular domains of cadherins via catenins located at the undercoat of the adherens junctions (Geiger and Ginsberg, 1991). E-cadherin, for example, is capable of binding to β-catenin or to γ-catenin (plakoglobin), which in turn, forms the linkage to α-catenin that connects to the actin cytoskeleton (Yamada and Geiger, 1997).

1.7.2.1.3 Desmosomes

Desmosomes are specialized form of adherens junctions that connect intermediate filaments such as cytokeratins along the lateral membrane of adjacent epithelial cells (Schwarz *et al*., 1990). Desmosomal structures consist of members of the cadherin superfamily known as desmogleins and desmocollins; and they are linked to the

intermediate filament network by several cytoplasmic plaque proteins including the desmoplakins and plakoglobin (Garrod, 1993; Gumbiner, 1996).

1.7.2.1.4 Tight junctions

Tight junctions are the most apical intercellular junctions that create physiological semi-permeable barriers between epithelial or endothelial cells. They maintain distinct tissue compartments and prevent protein and lipid diffusion between the apical and basolateral plasma membrane domains (Tsukita *et al*., 1999). The proteins involved in the formation of tight junctions include integral membrane proteins such as occludin, claudin and junctional adhesion molecule (JAM); and peripheral membrane proteins such as membrane-associated guanylate kinase (MAGUK) homologue proteins including ZO-1, -2, -3, cingulin, symplekin, 19B1 and AF-6 (Furuse *et al*., 1993, 1998; Martin-Padura *et al*., 1998; Stevenson *et al*., 1986; Jesaitis and Goodenough, 1994; Haskins *et al*., 1998; Citi *et al*., 1988). The cytoplasmic domains of claudin and occludin interact with F-actin-binding scaffold molecules, ZO-1, -2, and -3 (Furuse *et al*., 1994; Jesaitis and Goodenough, 1994; Fanning *et al*., 1998; Itoh *et al*., 1999; Haskins *et al*., 1998); and JAM interacts with ZO-1 (Martin-Padura *et al*., 1998; Bazzoni *et al*., 2000; Ebnet *et al*., 2000).

1.7.2.2 Cell-matrix adhesions

Cell-matrix adhesion occurs at specialized zones on the cell surface, where activated or clustered adhesion molecules bind to their respective ECM ligands and link intracellularly to the cytoskeleton. The importance of such adhesion is underscored by the existence of many genetic and autoimmune diseases caused by the perturbations of ECM structure or adhesion of cells to the ECM (Gumbiner, 1996). Cell-matrix

adhesion junctions can be classified into focal adhesions, hemidesmosomes, and dystroglycan complex.

1.7.2.2.1 Focal adhesions

Focal adhesions are the structural connections between the ECM and the actin cytoskeleton. At these sites, integrins make linkage with the actin cytoskeleton via vinculin, talin, α-actinin, paxillin, FAK, and Src family tyrosine kinases to control the assembly of focal adhesion (Beckerle *et al*., 1987; Jaken *et al*., 1989; Burridge and Chrzanowska-Wodnicka, 1996; Kaplan *et al*., 1994; Zamir and Geiger, 2001).

1.7.2.2.2 Hemidesmosomes

Hemidesmosomes are multimeric protein complexes that attach epithelial cells to their underlying matrix and serve as cell surface anchorage sites for the keratin intermediate filaments. They are morphologically similar to desmosomes and are localized to the basal surface of some epithelial cell types (Garrod, 1993). Keratin bundles associate to the hemidesmosome plaques via protein complexes consisting of α6β4 integrin and BP180 that act as transmembrane proteins, and BP230 and plectin that act as cytoplasmic plaque proteins (Green and Jones, 1996).

1.7.2.2.3 Dystroglycan complex

Dystroglycan is the transmembrane adhesive receptor that links the ECM protein laminin to the actin cytoskeleton via its cytoplasmic plaque protein dystrophin. Duchenne muscular dystrophy is caused by a mutation in the dystrophin gene (Campbell, 1995).

1.7.3 Cell migration

Cell-matrix adhesion is a key aspect of cell migration. Cell migration is a highly integrated multistep process that choreographs a wide variety of biological phenomena. Cell movement is important for morphogenesis throughout embryogenesis. Migration remains prominent during adulthood, in normal physiology involving tissue repair, regeneration and immune surveillance, as well as in pathology involving angiogenesis, tumor invasion and metastasis (Ridley *et al*., 2003).

1.7.3.1 The migration cycle

In general, cell migration can be conceptualized as a cyclic process of attachment and detachment of cell across the substratum (Lauffenburger and Horwitz, 1996). In response to migratory stimulus, the cell becomes polarized by intracellular actin cytoskeleton polymerization, coordinately elongates its protrusions in the direction of migration, and forms new adhesions at the leading edge. These protrusions can be either lamellipodia or filopodia (Welch and Mullins, 2002). Both lamellipodia and filopodia are stabilized by adhering to the ECM or adjacent cells via transmembrane adhesion receptors, which are linked intracellularly to the actin cytoskeleton, either directly or indirectly via cytoplasmic adaptors. Such adhesions serve as traction sites for migration as the cell moves forward over them; and disassembly of these adhesive contacts and cytoskeletal-dependent retraction at the tailing edge then lead to the detachment of cell at its rear end (Webb *et al*., 2002; Ridley *et al*., 2003).

1.7.3.2 Organization of actin cytoskeleton during cell motility

The actin cytoskeleton is a highly dynamic filamentous network composed of crosslinked polymers of actin filaments and a myriad of associated proteins. It

undergoes extensive remodeling in motile cells fundamental for the regulation of cell adhesion, cell spreading and motility (Mitchison and Cramer, 1996). The ability of a eukaryotic cell to move is largely driven by the assembly of actin filaments from the actin monomers near the plasma membrane and by the myosin motors that contract the filaments. Cellular actin exists in two forms: as monomeric globular actin (G-actin) and as filamentous actin (F-actin). In the physiological ATP-magnesium ion-rich cell medium, ATP-G-actin and F-actin are maintained in a dynamic steady state. In response to actin polymerization, the flux of ATP-G-actin binding onto the barbed, fast growing ends of the filaments at the leading edge is balanced by the dissociation flux of hydrolyzed actin subunits from the pointed (slower growing) ends of the filaments at the rear. This cycle is continuous and is known as treadmilling. F-actin is generally organized into filopodia — finger-like protrusions that contain a backbone of actin filaments organized into long parallel bundles in the direction of the protrusion; lamellipodia — branching "dendritic" network of actin filaments that dominates the leading edges of motile cells; and stress fibers — bundles of actin filaments that traverse the cell and are linked to the ECM through focal adhesions.

1.7.3.3 Roles of Rho GTPases in migration

Precise actin cytoskeleton remodeling entails tight spatial and temporal regulation of actin filament assembly and organization. The activity of the actin cytoskeleton is regulated by proteins of the Rho family GTPases, of which Rho, Rac, and Cdc42 are best characterized. Cdc42 activation maintains cell polarity and induces filopodium extension (Kozma *et al*., 1995; Nobes and Hall, 1995). Activation of Rac results in the formation of lamellipodia and membrane ruffles (Ridley *et al*., 1992). Rho activation stimulates the formation of integrin-containing focal adhesions and assembly of

actomyosin bundles into stress fibres (Ridley and Hall, 1992). Stimulation of Cdc42 and Rac suppresses Rho activity. Most Rho GTPases alternate between an active GTP-bound form and inactive GDP-bound form. Their activity is regulated by guanine nucleotide exchange factors (GEFs), which promote the exchange of GDP for GTP, and GTPase-activating proteins (GAPs) that promote GTP hydrolysis. In their active GTP-bound conformation, these central regulatory proteins act on the membrane and recruit a hierarchical cascade of effector proteins, mainly either kinases such as p21-associated kinase (PAK), Rho-associated kinase (ROCK), phosphatidylinositol phosphate (PIP) 5-kinase, or scaffolding proteins such as Wiskott-Aldrich Syndrome protein (WASP), IRSp53 and mDIA. These effector proteins then trigger actin-based cell motility via activating diverse signaling pathways that promote nucleating, capping, severing, or crosslinking of actin filaments (Ahmadian *et al*., 2002; Hall, 1994; Lauffenburger and Horwitz, 1996).

1.7.3.4 Receptor-mediated adhesion during migration

For migration to occur, a protrusion must form and be stabilized by adhering to the environment. Many different adhesion receptors have been reported to participate in migration, and integrins are the established class of migration-promoting receptors. Integrins are capable of mediating adhesion of cells to ECM proteins. Activated integrins cluster in the membrane to form organized adhesive contacts called focal adhesions. Focal adhesions recruit scaffolding and signaling components to link the ECM proteins to the actin cytoskeleton as well as to transduce signals important for cell movement (Lauffenburger and Horwitz, 1996; Klemke *et al*., 1997; Liu *et al*., 2000; Sastry and Burridge, 2000). These adhesions are stationary at the leading edge and serve as traction sites for the migrating cell. On the other hand, they are actively

retracting at the rear of the cell (Ballestrem *et al*., 2001). Recently, it has also become apparent that integrin-mediated adhesion to the ECM regulates the activity of the Rho family of small GTP-binding proteins (GTPases; Barry *et al*., 1997; Clark *et al*., 1998; Price *et al*., 1998).

Apart from integrins, members of the IgSF have also been documented to regulate migration. For example, studies have shown that nectins are capable of binding to afadin, an F-actin binding protein, through their cytoplasmic domains (Takahashi *et al*., 1999). These Ig-like adhesion molecules can induce the activation of Cdc42 and Rac protein (Kawakatsu *et al*., 2002) and associate with Par-3, a cell polarity protein (Takekuni *et al*., 2003). Through these activities, nectins modulate a range of cellular functions consisting of cell adhesion, migration and polarization. It is also known that another Ig-like adhesion molecule, L1, stimulates neuronal cell migration (Lindner *et al*., 1983), and neurite fasciculation and outgrowth (Lagenaur and Lemmon, 1987). Furthermore, Ll has been found to be a heterophilic ligand for members of the integrin family (Felding-Habermann *et al*., 1997).

1.7.3.5 Lipid rafts

For more than 30 years, the Singer-Nicolson fluid mosaic concept has provided the foundation of the structure of cell membrane. This model proposes that both lipids and membrane proteins are free to diffuse in the membrane bilayer, implying a random organization of proteins in lipid (Singer and Nicolson, 1972). More recently, however, it has been recognized that the biological membranes exhibit a much more complex structure. Within the disordered fluid membrane bilayer, cellular lipids can segregate into ordered lipid microdomains enriched with sphingolipids and

cholesterol. These microdomains have the ability to recruit and spatially organize signaling molecules as well as regulate actin dynamics and recruit cytoskeletal associated proteins important for many signaling processes. They are most abundant on the plasma membrane, but can also be found in intracellular membranes such as the endocytotic pathway or the Golgi apparatus (Gkantiragas *et al*., 2001).

The unique lipid composition of these sphingolipid-cholesterol microdomains makes them resistant to solubilization by cold non-ionic detergents such as Triton X-100. In addition, because of their high lipid content, these detergent-resistant membrane (DRM) complexes float to low density in sucrose gradients and are rich in raft-associated proteins and lipids. Therefore, sucrose density gradient ultracentrifugation provides a simple means for isolating and identifying raft components (Brown and Rose, 1992; Brown and London, 1998).

DRMs can be subdivided into lipid rafts and its derivative, caveolae. Lipid rafts are presumed to be too small and transient to be directly identified in cells, while caveolae are microscopically identifiable flask-shaped invaginations of the plasma membrane. Caveolae are distinguished from lipid rafts by the presence of cholesterol-binding caveolin-1 that stabilizes the invaginated structure of caveolae. Both lipid rafts and caveolae are enriched with proteins such as glycosylphosphatidylinositol (GPI)-anchored proteins; doubly acylated proteins including tyrosine kinases of the Src family; and transmembrane receptors and adhesion molecules. Because these microdomains can move laterally and cluster into larger patches, they have been implicated to function as platforms for the attachment and trafficking of proteins in biosynthetic and endocytic pathways, as well as in the assembly of signaling

complexes to facilitate signal transduction (Niethammer *et al*., 2002; Roepstorff *et al*., 2002; Quest *et al*., 2004; Simons and Toomre, 2000; Simons and Ikonen, 1997).

1.8 Molecular pathogenesis of HCC

The development of HCC, or hepatocarcinogenesis, is a multifactorial and multistage process. It represents a sequential process that drives hepatocytes to develop a malignant phenotype. In the background of chronic hepatitis infection and/or cirrhosis, the inflamed liver displays accelerated proliferation of hepatocytes, resulting in the development of a more aberrant monoclonal population of hepatocytes in focal lesions, and subsequently giving rise to hyperplastic hepatocyte nodules which escalate to dysplastic nodules that evolve into HCC (Thorgeirsson and Grisham, 2002).

Distortion of normal tissue morphology is one of the early events observed in the development of HCC and other malignant tumors. Since cell adhesion molecules play a crucial role in the formation and maintenance of normal tissue architecture as well as regulation of cellular interactions, it is extremely relevant for these molecules to contribute to cancer development. There are accumulating evidence suggesting that perturbations of cell adhesion molecules accompany tumor progression, invasion, and subsequent metastatic dissemination of tumor cells (Stamatoglou and Hughes, 1994).

Although the major risk factors of HCC are now well recognized, knowledge on the molecular interactions implicated in HCC development is still fragmentary. Genomic alterations, regarded as the hallmark of cancers, are commonly identified during the course of HCC development (Coleman, 2003). Genetic (including chromosomal

deletions, rearrangements, aneuploidy, gene amplifications, and mutations) and epigenetic aberrations (including DNA hypermethylation) combine to inactivate tumor suppressor genes and activate proto-oncogenes, resulting in cells with autonomous growth potential. The extensive genetic heterogeneity of HCC suggests that multiple and different regulatory pathways may participate in the genesis of subsets of hepatocellular neoplasms. Therefore, functional characterization of both known and unknown genes altered in HCC is essential to refine our understanding on the molecular pathogenesis of this malignancy.

1.8.1 Tumor suppressor genes

Tumor suppressor genes usually encode proteins that regulate cell division, DNA repair, apoptosis and cell adhesion; and they function in important cellular processes involved in growth, development, and cell signaling pathways. Loss of function of these genes results in uncontrolled cell growth. Knudson's two-hit paradigm of tumor suppressor genes (Knudson *et al*., 1975) stipulates that mutation of both alleles of a tumor suppressor gene is required to initiate tumorigenesis. Because tumor suppressor genes are recessive, inheritance of an inactivated allele (the first hit) of a suppressor gene from a parent increases the risk of cancer development. It is only after the successive loss of the second allele (the second hit) that then triggers deregulated proliferation. However, this concept is now being challenged by increasing evidences showing that disruption of a single allele of a tumor suppressor gene may be sufficient to exert a cellular phenotype, and, as a consequence, lead to tumor formation without having to inactivate the second allele. This conjecture is supported by haploinsufficient genes that require the inactivation of only one allele (Largaespada, 2001), and genes inactivated by epigenetic hypermethylation (Issa *et al*., 1994).

1.8.1.1 Rb

Expression of tumor suppressor genes involved in cell cycle progression is important for effective inhibition of cell division. The Rb gene encodes a cell cycle regulator protein critical for the regulation of G1-S phase transition of the cell cycle. Hypophosphorylated Rb can form complexes with and repress transcriptional activation of E2F transcription factors, blocking cell cycle progression during G1 phase. In response to mitogenic signaling, cyclin-dependent kinase (Cdk) 4/6 complexes with cyclin D and phosphorylates Rb. This inactivated form of Rb then dissociates from E2F, allowing E2F to promote transcription of major S phase genes such as cyclin E, driving cell cycle progression. The cyclin D-Cdk4/6 complexes are, in turn, antagonized by Cdk inhibitors e.g. $p16^{INK4A}$ and $p15^{INK4B}$.

Aberrant expression of Rb is a common and significant event in human hepatocarcinogenesis. The Rb gene can be inactivated by different modes, including loss of heterozygosity (LOH; Walker *et al*., 1991; Murakami *et al*., 1991), mutations, loss of TGF-β responsiveness, and alterations of Rb regulatory proteins such as $p16^{INK4A}$, $p15^{INK4B}$, cyclin D, or Cdk4/6 (Hanahan and Weinberg, 2000; Levy *et al*., 2002). In HCC, mutations of Rb are observed in about 15% of the cases (Kekule *et al*., 1993). LOH at chromosome 13q14 where Rb is located is frequently observed in HCC, with a prevalence of 30% (Kekule *et al*., 1993). In addition, it has been shown that Rb expression is significantly decreased in 30-50% of tumors (Hsia *et al*., 1994). Silencing of p16 by promoter methylation is a major mode of inhibiting Rb (Levy *et al*., 2002). The discovery of a new oncogene, termed gankyrin, defines a novel pathway leading to Rb inactivation. Gankyrin is a six ankyrin-repeat protein homologous to the p28 subunit of the 26S proteosome. It is overexpressed in all HCC.

It is capable of binding to Rb and promoting degradation by the ubiquitin-proteosome pathway (Higashitsuji *et al*., 2000). An amplification of cyclins has been observed in about 10-13% of HCC cases (Zhang *et al*., 1993). Cyclin D is a known oncogene and a key regulator of cell cycle progression. The upregulated expression of the cyclin D gene has been associated with aggressive forms of human HCC (Nishida *et al*., 1994). It has recently been shown in a transgenic mouse model that overexpression of cyclin D is sufficient to initiate hepatocarcinogenesis (Deane *et al*., 2001). The transduction of antisense cyclin D arrests tumor growth in a xenograft hepatoma model (Ivorra *et al*., 2003).

1.8.1.2 p53

The p53 tumor suppressor gene is known as the guardian of the genome and is responsible for regulating cell cycle checkpoints and apoptosis (Levine, 1997). In response to DNA damage induced by chemicals, irradiation or other causes, wildtype p53 is activated. p53 induces cell cycle arrest by activating $p21^{waf1/cip1}$ protein which suppresses Cdk2, thereby arresting transition from G1 phase to S phase to permit DNA repair. DNA repair is carried out by a DNA mismatch repair gene, predominantly hMLH1 and hMLH2. In HCC, both hMLH1 and hMLH2 are rarely altered or mutated, implying that defective DNA mismatch repair does not play a significant role in HCC development (Macdonald *et al*., 1998; Salvucci *et al*., 1999). In the event when the damaged DNA is beyond repair, a normal cell undergoes self-destruction through apoptosis. p53 is capable of inducing the transcription of several key players of apoptosis, including apoptosis protease-activating factor-1 (Apaf-1; Moroni *et al*., 2001) and Bax protein (Miyashita and Reed, 1995). Bax protein translocates to the mitochondria where it triggers cytochrome C release. The caspase

cascade is then activated and apoptosis takes place. Normally, MDM2 binds to p53 preventing its expression and promoting p53 ubiquitination for proteasomal degradation. MDM2, however, can be sequestered by $p14^{ARF}$, leading to the stabilization of p53 and promotion of cell growth arrest or apoptosis (Weber *et al*., 2002).

p53 is commonly mutated or inactivated in human cancers through LOH and missense mutations. These mutations occur mainly at the DNA binding domain of p53 (Pavletich *et al*., 1993) that is critical for correct folding of the protein (Balagurumoorthy *et al*., 1995). Mutations of p53 are also associated with a prolonged half-life of the protein, which accumulates in the cell nuclei, suggesting that it has acquired an oncogenic gain of function.

In HCC, mutations of p53 are common. LOH at chromosome 17p13 has been observed in 25-60% of tumors, and p53 mutations were found in about 28% of HCC worldwide (Levy *et al*., 2002). The frequency and type of mutations differ depending on geographic location and cause of the tumor. There is a strong correlation between p53 mutations, large tumor size, and poor differentiation state. HBV infection or the presence of HBV DNA in the tumor has been associated with the functional inactivation of p53. It has been shown that HBX can bind to p53 and block p53-mediated transcriptional transactivation *in vivo* (Truant *et al*., 1995). Furthermore, HBX interferes with *in vitro* associations of p53 with transcription factors involved in nucleotide excision repair such as XPB (ERCC3) or XPD (Wang *et al*., 1994). These observations suggest that HBX is capable of disrupting the normal cellular surveillance mechanisms of p53, leading to genetic instability that is characteristic of

HCC. It is now clear that the unique "hot spot" 249 missense mutation of p53 is the hallmark of dietary exposure to aflatoxin B1. In regions where aflatoxin exposure is rare, p53 mutations remain prevalent but occur at sites other than codon 249 (Murakami *et al*., 1991; Nishida *et al*., 1993; Sheu *et al*., 1992).

1.8.1.3 E-cadherin

Several proteins involved in cell adhesion inhibit tumor dispersion, prevent loss of contact inhibition, and inhibit metastasis. E-cadherin is an adhesion molecule that functions as a potent tumor suppressor of epithelial tumor cell invasion and metastasis (Birchmeier and Behrens, 1994; Takeichi, 1993). The cytoplasmic domain of E-cadherin interacts with α- and β-catenin molecules that establish an intracellular linkage with the actin cytoskeleton. This E-cadherin-catenin complex plays a crucial role in epithelial cell-cell adhesion for the maintenance of tissue architecture, migration and signal transduction. Consequently, perturbation in the expression or function of this complex disrupts the mediated intercellular adhesion and signaling, leading to tumor progression and metastasis.

E-cadherin is commonly downregulated in poorly differentiated HCC (Endo *et al*., 2000). While somatic mutations of E-cadherin have been described in poorly differentiated breast (Berx *et al*., 1995) and gastric cancers (Becker *et al*., 1994), E-cadherin is rarely mutated in HCC. However, alterations of E-cadherin caused by LOH or hypermethylation are evident in HCC (Matsumura *et al*., 2001; Kanai *et al*., 1997). Loss of E-cadherin activity has been associated with enhanced cell invasiveness and metastasis of several human tumors; and E-cadherin gene knockouts

in mice result in lethality at a very early stage (Laure *et al*., 1994). Aberrant expression of β-catenin also contributes to the inhibition of E-cadherin.

1.8.1.4 Transforming growth factor-β

Transforming growth factor (TGF)-β is a multifunctional cytokine that functions as a potent growth inhibitor involved in cell proliferation (Wollenberg *et al*., 1987), cellular differentiation (Nagy *et al*., 1989), fibrogenesis (Gressner *et al*., 2002), and apoptosis in the liver (Gressner *et al*., 1997). TGF-β signaling pathway constitutes TGF-β Type I and Type II receptors which are serine-threonine kinases that signal through the Smad family of proteins. Binding of TGF-β to its cell surface receptor Type II leads to the phosphorylation of the Type I receptor. Activated TGF-β Type I receptor then activates cytoplasmic Smad2 and Smad3 by phosphorylation, allowing them to form a heteromeric complex with Smad4. This Smad complex can induce TGF-β responsive gene transcription after it is translocated to nucleus and bound to the specific target nuclear matrix site. Genetic alterations of the TGF-β pathway are mediated by mutations of the Smad2 and Smad4 genes, which occur in about 10% of HCC cases. Mutations of the TGF-β receptor II gene have been detected in patients with HCC and may also abrogate TGF-β signaling.

1.8.2 Oncogenes

Oncogenes are mutated forms of proto-oncogenes, which are the genes involved in promoting the differentiation and proliferation of normal cells. When a proto-oncogene mutates into an oncogene, it becomes permanently "turned on" and results in the malignant transformation of normal cells into cancerous tumor cells. A number

of oncogenes encode oncoproteins that function as signal transducers, apoptosis regulators, transcription factors, growth factors or their receptors.

1.8.2.1 Ras

The Ras family consists of 3 highly conserved genes, H-Ras, K-Ras and N-Ras. Localized in the inner plasma membrane, Ras proteins relay mitogenic and growth signals from growth factor receptors via multiple downstream effector pathways and thereby regulate important cellular processes such as differentiation, proliferation and apoptosis. They function as G-regulatory proteins, which act as molecular switches that alternate between inactive GDP-bound and active GTP-bound states. Upon ligand-stimulated activation of growth factor receptors, Ras becomes activated by exchanging GDP for GTP. In its GTP-bound state, the wildtype Ras stimulates its effector pathways such as the Raf/MAPK and PI3K/PKB pathways (Rebollo and Martínez-A, 1999). Elevated expression of Ras induced by hypomethylation (Shen *et al*., 1998) or point mutations (Pascale *et al*., 1993) has been implicated in HCC. The constitutively active GTP-bound Ras promotes hepatocarcinogenesis by incessantly triggering downstream effector pathways in the absence of extracellular stimuli. These signaling pathways, in turn, induce cell growth as well as cooperate with other oncogenes, such as c-myc, in oncogenesis (Born *et al*., 1994; Feitelson, 2005).

1.8.2.2 c-myc

c-myc encodes a transcription factor and has been implicated to regulate cell proliferation, differentiation, immortalization, transformation, angiogenesis and apoptosis (Amati *et al*., 1998; Oster *et al*., 2002). It induces G1-S progression through activation of the cyclin E-Cdk2 complex as well as inhibits Cdk inhibitors such as

$p21^{waf1/cip1}$ and $p27^{Kip1}$ from binding to cyclin E-Cdk2. In addition, c-myc induces synthesis of cyclin D (Perez-Roger *et al*., 1999; Bouchard *et al*., 1999).

In HCC, upregulation of c-myc and its gene product occurs by hypomethylation (Shen *et al*., 1998), point mutation (Pascale *et al*., 1993), or gene amplification (Abou-Elella *et al*., 1996). Transgenic animal models have shown that elevation of myc can induce HCC formation (Sandgren *et al*., 1989; Murakami *et al*., 1993; Wu *et al*., 2002). Conversely, inhibition of myc results in a loss of the carcinoma's neoplastic properties (Simile *et al*., 2003). Furthermore, Shachaf *et al*. demonstrated that myc stimulates the malignant expansion of immature liver cells with stem cell features. Upon inactivation of myc, the tumors begin to differentiate into normal cellular lineages and tissue structures of liver, while retaining their latent potential to become cancerous again upon reactivation of myc (Shachaf *et al*., 2004).

1.8.2.3 Transforming growth factor-α

Transforming growth factor (TGF)-α is a potent mitogen for hepatocyte growth. It was found to be present at elevated levels in human HCC (Harada *et al*., 1999; Kira *et al*., 1997; Heinze *et al*., 1999), often in association with HBV infection (Jakubczak *et al*., 1997). Specifically, TGF-α is detected more frequently in patients whose adjacent non-tumorous livers have detectable HBV surface antigen and/or HBV core antigen than in those whose livers lack these viral proteins. It is still unclear if increased expression of this growth factor is mechanistically related to hepatocarcinogenesis or if it results from liver regeneration in response to chronic HBV infection since elevated TGF-α expression is typically observed in the livers of patients with chronic

hepatitis and without HCC. TGF-α may promote tumor angiogenesis by upregulating vascular endothelial growth factor.

1.8.2.4 β-catenin

Apart from linking E-cadherin transmembrane receptors to the actin cytoskeleton (Aberle *et al*., 1996), β-catenin also plays an important role in the Wingless/Wnt signal transduction pathway during embryonic development. In the absence of Wnt signaling, β-catenin is localized at the plasma membrane in complex with E-cadherin and α-catenin at the sites of adherens junctions. Excess β-catenin is normally bound to axin and the adenomatous polyposis coli (APC) protein, phosphorylated at the N-terminal serine/threonine residues by glycogen synthase kinase 3β (GSK3β), and subsequently targeted for ubiquitination and degradation in the 26S proteasome, thus reducing the level of cytosolic β-catenin (Rubinfeld *et al*., 1996; Kishida *et al*., 1998). The Wnt signal is stimulated when the Wnt ligand binds a frizzled (Fz)/low-density lipoprotein receptor related protein (LRP) complex and activates the cytoplasmic protein dishevelled (Dsh in Drosophila and Dvl in vertebrates). Dsh/Dvl stabilizes the cytosolic β-catenin by preventing GSK3β from phosphorylating β-catenin. The stabilized β-catenin will then translocate into the nucleus and binds members of the T-cell factor (TCF)/Lymphoid enhancing factor (LEF) family of transcription factors (Behrens *et al*., 1996), leading to the transcriptional activation of Wnt-responsive genes.

Mutations of the β-catenin gene, particularly at exon 3 which encodes serine/threonine phosphorylation residues for GSK3β, confer resistance to phosphorylation and ubiquitination, resulting in the accumulation of cytoplasmic and

nuclear β-catenin (Miyoshi *et al*., 1998; Orford *et al*., 1997; Rubinfeld *et al*., 1996). It was reported that the nuclear accumulation of β-catenin mutants in HCC promotes tumor cell growth (Van Nhieu *et al*., 1999). Conversely, in non-tumorous livers, dysplastic lesions and cirrhotic nodules, β-catenin immunostaining is restricted to the plasma membrane. Furthermore, it was shown that cyclin D, which facilitates the inactivation of tumor suppressor Rb, is one of the target genes of the β-catenin/TCF complex (Shtutman *et al*., 1999) A significant correlation between β-catenin and cyclin D was detected in breast (Lin *et al*., 2000) and colon cancers (Tetsu and McCormick; 1999), and more recently, in HCC (Ueta *et al*., 2002). Somatic mutations of APC are rare in HCC, but biallelic inactivation of APC gene may contribute to the development of HCC in patients with familial adenomatous (Su *et al*., 2001). Axin is mutated in about 10% of HCC cases (Satoh *et al*., 2000), leading to an activation of the Wnt pathway. Loss of function of axin induces β-catenin accumulation in the nucleus. Tyrosine phosphorylation of β-catenin in v-Src- (Behrens *et al*., 1993) or Ras- (Kinch *et al*., 1995) transformed cells or in cells stimulated with epidermal growth factor (Hoschuetzky *et al*., 1994) induces disassembly of the E-cadherin-catenin complex from the cytoskeleton and abolishes cell adhesion.

CHAPTER 2 OBJECTIVES

Hepatocellular carcinoma (HCC) is one of the most common malignancies worldwide, and its incidence is escalating. Extensive epidemiologic studies have identified multiple risk factors of HCC, including hepatitis viral infections, liver cirrhosis, and environmental carcinogens like aflatoxin B1. Differences in exposure to these risk factors contribute to the wide geographical variation in incidence, with the highest frequencies observed in the sub-Saharan Africa and Asia. HCC is generally asymptomatic and is often at the advanced stage when diagnosed. No curative therapy can be offered to these patients who are often presented with large and/or multi-focal HCC. Despite progresses made in the treatment of HCC, surgery remains as the most effective therapeutic modality. However, long-term survival is uncommon because of the propensity of HCC recurrence after surgery. Moreover, current methodologies for staging of HCC are still evolving and none is widely accepted. The limitations present in each staging system impede the selection of an optimal treatment strategy for the individual HCC patient. Furthermore, the lack of effective palliation to prolong the survival of patients contributes to the pitfalls of HCC management. All these difficulties in treating HCC resulted in the overall poor prognosis of the disease. Hence, there is an urgent need of developing accurate measures to determine the degree of the malignancy as well as to design new interventions for a more efficacious management of HCC.

Identification of key molecular targets and pathways involved in the onset and progression of HCC may provide a rational basis for the development of new diagnostic and prognostic tools as well as novel targets for therapy. Although, the

genetic mechanism leading to HCC has not yet been fully elucidated, it is well established that HCC arises because of a loss of equilibrium between the positive and negative regulators of cell growth, differentiation and cellular adhesion. Therefore, the long-term goal of this research is to unravel the genetic changes that contribute to HCC of different etiologies, and to understand the correlation between these changes and tumor progression.

The groundwork was initiated by examining the differences in gene expression between a pair of HCC tumor and its surrounding non-tumorous liver tissues using the technique of suppression subtractive hybridization. With this approach, a total of 272 differentially expressed transcripts of both known and unknown genes were identified. Among these genes, 142 genes (18 novel genes) were upregulated while 130 genes (27 novel genes) were downregulated in the tumor. Subsequently, using RT-PCR to screen the expressions of all the novel genes against a panel of liver specimens, it was found that one transcript, designated as *HEPN1*, was frequently lost while the other, *HEPT3*, was frequently elevated in HCC patients. Intriguingly, the identification of *HEPN1* led to the isolation of an uncharacterized gene, *hepaCAM*, containing the full-length cDNA of *HEPN1* on its antisense strand in the 3'-noncoding region. Therefore, this study aimed to clone the full-length cDNAs of these three novel genes and to characterize them by investigating their expressions and functions in HCC and in other malignancies.

The principal objectives of this study include:

1. Examination of *HEPN1*, *hepaCAM* and *HEPT3* expression levels in HCC patients and human HCC cell lines, and in tissues and cell lines derived from different human tumor types;
2. Isolation and cloning of the full-length cDNA sequences of *HEPN1*, *hepaCAM* and *HEPT3*;
3. Sequence and structural analyses of *HEPN1*, *hepaCAM* and *HEPT3*;
4. Biochemical analyses of hepaCAM protein;
5. Functional explorations of *HEPN1*, *hepaCAM* and *HEPT3*.

CHAPTER 3 MATERIALS AND METHODS

3.1 Cell cultures

3.1.1 Cell lines and culture conditions

Twenty human cancer cell lines including Huh7 (HCC), C3A (HCC), HepG2 (HCC), Hep3B (HCC), SK-HEP1 (HCC), HT29 (colorectal cancer), Colo205 (colorectal cancer), HCT116 (colorectal cancer), Jurkat (leukaemia), HL60 (leukaemia), K562 (leukaemia), NCI-H82 (lung cancer), NCI-H23 (lung cancer), NCI-H69 (lung cancer), NCI-H2066 (lung cancer), MCF7 (breast cancer), Hs683 (glioblastoma), SK-N-SH (neuroblastoma), HeLa (cervical cancer) and M14 (melanoma); a HeLa-contaminated immortalized non-tumor liver cell line Chang liver; and a mouse fibroblast cell line NIH3T3 were purchased from the American Type Culture Collection (Manassas, VA) and used in the study. All cells were maintained in an incubator at 37°C with 5% CO_2 humidified atmosphere in different culture media.

Chang liver, C3A, HepG2, Hep3B, MCF7, Hs683, HeLa, M14, NCI-H2066 and NIH3T3 cells were cultured in Dulbecco's modified Eagle's medium (DMEM; Sigma, St. Louis, MO) supplemented with 10% fetal bovine serum (FBS; Gibco BRL, Life Technologies, Gaithersburg, MD).

HCT116 and HT29 cells were cultured in McCoy's medium containing 10% FBS.

SK-N-SH and SK-HEP1 cells were cultured in minimum essential medium (MEM; Sigma) containing 10% FBS.

Huh7, Colo205, NCI-H82, NCI-H69, NCI-H23, Jurkat, K562 and HL60 cells were maintained in Roswell Park Memorial Institute (RPMI)-1640 medium (Sigma) supplemented with 10% FBS.

3.1.2 Passaging cells

Cells were subcultured when they reached 80-100% confluence. The culture medium was removed and the cells were washed once with 1X PBS. To cells in T75 flasks, 2 ml of 1X Trypsin/EDTA (Gibco BRL) was added and incubated at 37°C for 2-5 min or until the cells were detached. Approximately 5 ml of culture medium was added to the flask and the cells in clumps were dispersed by repeated pipetting. Five milliliters of cells were removed and fresh medium was added to the remaining cells in the flask to a final volume of 10 ml. If cells were to be counted, 50 µl of the cell suspension was mixed with 50 µl of 0.8 mM trypan blue in PBS on a piece of parafilm. The mixture was then applied to a haemocytometer and at least 100 cells were counted. The number of cells/ml was calculated using the following formula:

Number of cells/ml = the average count per square of haemocytometer X the dilution factor X 10^4

3.1.3 Storing cells

Trypsinized cells were pelleted at 1,000 rpm for 5 min. The supernatant was discarded and the cells were resuspended in fresh freezing medium made up of 8% DMSO in culture medium containing 10% FBS. The concentration of cells should be about 2 X 10^6 cells/ml of freezing medium. One milliliter-aliquot of the suspension was

dispensed into each cryotube and stored at -80°C for overnight before transferring to liquid nitrogen for long-term storage.

3.2 Liver tissue specimens

Paired liver specimens from 23 patients (HCC together with its adjacent non-tumorous liver tissue) and normal liver tissues were collected from the No. 3 Hospital of Chongqing in China. Each sample was snap-frozen and stored in liquid nitrogen before experiment. The final diagnosis of HCC was confirmed and classified by histological examination.

3.3 Determination of nucleic acid concentration

The concentration and purity of DNA and RNA were determined by measuring their optical density (OD) at 260 and 280 nm. The concentration of DNA or RNA in a diluted solution was calculated using the molar extinction coefficient (OD_{260} = 1 = 50 µg/µl for DNA or OD_{260} = 1 = 40 µg/µl for RNA) as given below.

OD_{260} X dilution factor X 50 µg/µl = Concentration of DNA µg/µl

OD_{260} X dilution factor X 40 µg/µl = Concentration of RNA µg/µl

The ratio OD_{260}/OD_{280} was determined to estimate the purity of nucleic acids. Pure DNA or RNA has a ratio of 1.8-2.0. A ratio less than 1.8 indicates that there may be proteins and/or other UV (ultraviolet) absorbers in the sample. A ratio higher than 2.0 indicates that the samples may be contaminated with chloroform or phenol.

3.4 Isolation of total RNA from cells or tissues

Total RNA was prepared from either liver tissues or cultured cells using the RNeasy Kit (Qiagen, Hilden, Germany), and when necessary, contaminating DNA was digested on-column using the RNase-Free DNase Set (Qiagen). Tissues or cells were resuspended in 600 µl of β-mercaptoethanol-containing RLT buffer and homogenized by repeated pipetting or by passing through a 20-guage needle fitted to syringe. One volume of 70% ethanol was then added to the lysate and mixed. The mixture was applied to an RNeasy spin column with a 2-ml collection tube and centrifuged. The flow-through was discarded and 350 µl of buffer RW1 was pipetted into the spin column. After centrifugation, the spin column was transferred to a new 2-ml collection tube and washed twice with 500 µl of buffer RPE. The RNA was then eluted into a fresh collection tube from the spin column by adding 30 µl of RNase free water and centrifuging at 10,000 rpm for 1 min. Unless otherwise stated, all centrifugations were carried out at 10,000 rpm for 15 sec.

Digestion of DNA could be carried out during RNA extraction. After immobilization of RNA on the spin column and washing with buffer RW1, DNase I mix containing 10 µl (30 units) of DNase I stock solution and 70 µl of buffer RDD was added directly onto the spin column membrane and incubated at room temperature for 20 min. The reaction was terminated by the addition of 350 µl of buffer RW1 for 5 min. After centrifugation, the column was washed with buffer RPE as described above.

To ensure the integrity of RNA, samples of the purified RNA were separated by gel electrophoresis using standard 1% agarose gels containing ethidium bromide as described in Section 3.13. The 28S and 18S ribosomal RNAs should appear as distinct

bands on the stained gel. In addition, the intensity of the 28S ribosomal RNA band should be approximately twice the amounts of the 18S RNA.

3.5 Northern blot analysis

Northern blot analysis is a standard method for detection and quantitation of mRNA levels; and is the preferred method for determining transcript size and for detecting alternatively spliced transcripts. Northern analysis was carried out with the DIG high prime DNA labeling and detection starter kit I (Roche, Basel, Switzerland). Solutions and gel apparatus were treated with 0.1% DEPC accordingly.

3.5.1 Random primed labeling of probe

The probe used in Northern analysis was non-isotopically labeled. An 893 bp *HEPT3* cDNA was synthesized by PCR using T3seq-f1 (5'ctactcgggaggctgaggcag3') and T3seq-r1 (5'gtaacatctcctaggtaacag3'), electrophoresed, and purified from agarose gel. Five hundred nanograms of the cDNA template in a final volume of 16 µl was boiled for 10 min and rapidly chilled on ice. Four microliters of digoxigenin-11-dUTP (DIG)-high primer was then added to the denatured sample and incubated overnight at 37°C. The reaction was terminated by adding 2 µl of 0.2 M EDTA pH 8.0 and heating the sample to 65°C for 10 min. The yield of the labeled probe was quantitated by spotting various dilutions of the probe on a positively charged nylon membrane (Hybond-XL; Amersham Pharmacia, Germany) and detecting DIG in the spots with chemiluminescence according to the manufacturer's instructions.

3.5.2 Electrophoresis of RNA on denaturing formaldehyde/MOPS gel

Forty micrograms of total RNA mixed with 2 volumes of freshly made loading buffer was denatured at 65°C for 10 min and chilled on ice until use. The sample was electrophoresed on a 1% formaldehyde/MOPS gel in 1X MOPS buffer at 40 V for 2-3 hours or until the RNA was well-separated. The quality of the RNA after electrophoresis was assessed under UV light.

3.5.3 Transferring RNA to nylon membrane

The gel was soaked twice for 15 min in 20X SSC to remove formaldehyde. The RNA was transferred overnight from the gel to the nylon membrane using the transfer set-up as shown in Figure 3-1. On the following day, the RNA was immobilized onto the membrane by UV crosslinking using a UV Stratalinker at 120 mJ.

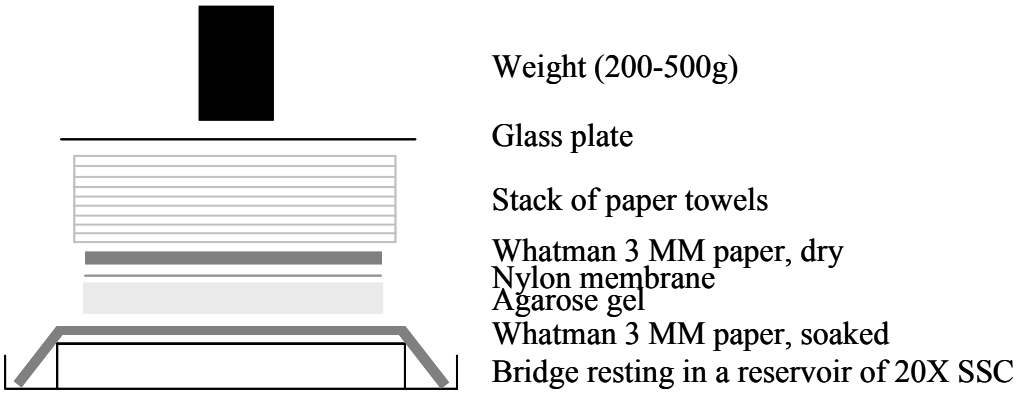

FIGURE 3-1 Northern blot transfer by capillary action.

3.5.4 Pre-hybridization, hybridization with probe and washing of blot

The blot was placed in a roller bottle and blocked with 8 ml of DIG Easy Hyb buffer for 1 hour at 50°C. Towards the end of pre-hybridization, 50 ng of labeled probe was added to 50 µl of H_2O and denatured by boiling for 5 min. The probe was

immediately cooled on ice prior to mixing with 8 ml of fresh prewarmed DIG Easy Hyb buffer. The pre-hybridization buffer was discarded and replaced with the probe-containing DIG Easy Hyb buffer. After overnight incubation at 50°C, the blot was washed twice for 5 min in Low Stringency buffer at room temperature to remove the hybridization solution and unhybridized probe, followed by two 15-min washes with preheated High Stringency buffer at 60°C to remove partially hybridized molecules.

3.5.5 Detection

Detection was performed at room temperature. The membrane was incubated in Washing buffer followed by Blocking solution for 2 min and 30 min, respectively. Antibody solution was added to the membrane for 30 min and the membrane was washed twice for 15 min in Washing buffer. The membrane was then equilibrated for 3 min in Detection buffer. Subsequently, CSPD was applied over the surface of the blot and incubated for 5 min prior to autoradiography.

3.6 Dot blotting of Matched Tumor/Normal Expression Array

The Matched Tumor/Normal Expression Array (Clontech, Palo Alto, CA, USA) is a nylon membrane dotted and immobilized with full-length cDNAs synthesized from human tumors and the corresponding normal tissues. Dot blotting was carried out according to the manufacturer's instructions with modifications. A 550 bp probe of *hepaCAM* cDNA was generated by PCR using primers hCAM-F2 (5'cgagatctccatcaccgacgacacc3') and hCAM-R (5'cttccgttcctgctcaccacttcga3') and then labeled with DIG (Roche) as described in Section 3.5.1. The probe was denatured with 150 µg of sheared salmon testis DNA (Sigma) and 50 µl of 20X SSC in a total volume of 200 µl before application. Following pre-hybridization in a

solution of ExpressHyb and heat-denatured sheared salmon testis DNA for 1 hour, the denatured probe mixed in fresh pre-hybridization solution was allowed to hybridize onto the array for overnight at 65°C. The array was washed at 65°C in prewarmed Wash solution 1 and then Wash solution 2 for 30 min each. A final 5-min wash in 2X SSC was performed before detection using the DIG detection system (Roche) as described in Section 3.5.5. The probe was stripped by boiling the membrane in 0.5% SDS solution for 10 min. A second hybridization with the provided human ubiquitin control cDNA probe was performed to normalize the relative gene expression.

3.7 Semi-quantitative RT-PCR

RT-PCR was performed to screen the mRNA expression of the gene of interest in HCC patients and in cell lines derived from various tumor types. RT-PCR reactions were prepared using the OneStep RT-PCR kit (Qiagen).

TABLE 3-1 Primers for RT-PCR

Primer name	Sequence
***HEPN1*:**	
N1-F	5'atccaagtcctgctgcctctt3'
N1-R	5'ctcctaaactccagctctgat3'
***hepaCAM*:**	
hCAM-F	5'cagcctgcctgtcaagatcaccgta3'
hCAM-R	5'cttccgttcctgctcaccacttcga3'
***HEPT3*:**	
T3-F	5'cagtgagagtaggcttgttttac3'
T3-R	5'ggcctcaagacaacataagatag3'
T3frag-f	5'ggtatacatgtgtctctgta3'
T3frag-r	5'ggtatacatgtgtctctgta3'
Housekeeping genes:	
***β-actin*:**	
β-actin-f	5'ctcttccagccttccttcct3'
β-actin-r	5'tgtggacttgggagaggact3'
***GAPDH*:**	
GAPDH-f	5'cggatttggtcgtattgggc3'
GAPDH-r	5'ggcagagatgatgacccttttg3'

TABLE 3-2 Semi-quantitative RT-PCR components

Component	Volume (µl)
H_2O	11
5X 1-step RT-PCR buffer	5
dNTP Mix (10 mM)	1
Primer 1 (10 µM)	1.5
Primer 2 (10 µM)	1.5
DNase-treated RNA (50 ng/µl)	4
1-step RT-PCR Enzyme Mix	1
Final volume	25

Q solution was added into the reaction for amplifying template with high GC content.

TABLE 3-3 Semi-quantitative RT-PCR conditions

Reaction	Temperature	Time	Cycles
RT	50 or 55°C (55°C for GC-rich template)	30 min	1
Inactivation of RT	95°C	15 min	1
Denaturation	95°C	30 sec	
Annealing	50-60°C	30 sec	35
Extension	72°C	1 min	
Final Extension	72°C	10 min	1

3.8 Real-time RT-PCR

The expression level of gene transcript was quantitated by real-time RT-PCR using the LightCycler (Roche). Reactions were prepared in 20-µl volumes using the LightCycler RNA Amplification Kit SYBR Green I (Roche) in thin-walled glass capillaries. PCR primer pairs used for quantitative RT-PCR were those used in semi-quantitative RT-PCR. The results were normalized and presented as percentage against the expression level of the internal control GAPDH.

TABLE 3-4 Real-time RT-PCR components

Component	Volume (µl)
H_2O	6.2
SYBR Green I	4
$MgCl_2$ solution	2.4
Primer 1 (10 µM)	1
Primer 2 (10 µM)	1
DNase-treated RNA (50 ng/µl)	5
RT-PCR Enzyme Mix	0.4
Final volume	20

TABLE 3-5 Real-time RT-PCR conditions

Reaction	Temperature	Time	Cycles
RT	55°C	10 min	1
Inactivation of RT	95°C	30 sec	1
Denaturation	95°C	5 sec	
Annealing	50-60°C	10 sec	45
Extension	72°C	15 sec	
Final Extension	72°C	7 min	1

3.9 Rapid amplification of cDNA ends

The Normal Human Liver Marathon-Ready cDNA used in rapid amplification of cDNA ends (RACE) was purchased from Clontech.

3.9.1 5' RACE

5' RACE was performed on the Human Liver Marathon-Ready cDNA using the gene-specific primers listed in Table 3-6 in combination with the provided adapter primer AP1 or nested adapter primer AP2 to amplify the 5' portion of the *HEPN1*, *hepaCAM* and *HEPT3* cDNAs. Advantage 2 PCR Enzyme System (Clontech) was used to set up the PCR reaction. Standard or touchdown PCR cycling parameters were used

depending on the Tm of the primers used. The amplified product was cloned in the pGEM-T vector (Promega, Madison, WI) and sequenced.

TABLE 3-6 Gene-specific primers for 5' RACE

Primer name	Sequence
***HEPN1*:**	
N1-RACE-R	5'cagggcacagaaaaaggcagactcc3'
N1-RACE-nR (nested primer)	5'cctagtctcctaaactccagctctg3'
***hepaCAM*:**	
hCAM-RACE-R	5'ttcatcaaaagtttattgagcatcc3'
***HEPT3*:**	
T3-RACE-R	5'gtccgacagaagcctctaccgagaacgt3'
T3-RACE-nR (nested primer)	5'cctcatagggagaaatcttgccaagggag3'

TABLE 3-7 5' RACE PCR components

Component	Volume (µl)
H_2O	36
10X cDNA PCR Reaction buffer	5
dNTP Mix (10 mM)	1
Gene-specific primer (10 µM)	1
AP1 or AP2 (10 µM)	1
Human Liver Marathon-Ready cDNA	5
Advantage 2 Polymerase Mix (50X)	1
Final volume	50

Q solution was added into the reaction for amplifying template with high GC content.

TABLE 3-8 Standard PCR conditions

Reaction	Temperature	Time	Cycles
Initial Denaturation	94°C	5 min	1
Denaturation	95°C	30 sec	
Annealing	60-65°C	30 sec	35
Extension	72°C	1-3 min	
Final Extension	72°C	10 min	1

TABLE 3-9 Touchdown PCR conditions (if gene-specific primer Tm >70°C)

Reaction	Temperature	Time	Cycles
Denaturation	94°C	5 sec	5
Annealing/Extension	72°C	4 min	
Denaturation	94°C	5 sec	5
Annealing/Extension	70°C	4 min	
Denaturation	94°C	5 sec	20-25
Annealing/Extension	68°C	4 min	

3.9.2 3' RACE

3' RACE was performed on the Human Liver Marathon-Ready cDNA using the gene-specific primers listed in Table 3-10 in combination with the provided adapter primer AP1 or nested adapter primer AP2 to amplify the 3' portion of the *HEPN1* and *HEPT3* cDNAs. The PCR reaction set-up and PCR conditions used were as described in Section 3.9.1. The amplified product was cloned in the pGEM-T vector and sequenced.

TABLE 3-10 Gene-specific primers for 3' RACE

Primer name	Sequence
***HEPN1*:**	
N1-RACE-F	5'tatccaagtcctgctgcctcttcca 3'
***HEPT3*:**	
T3-RACE-F	5'cagtgggagtaggcttgttttac3'
T3-RACE-nF (nested primer)	5'ctatttctagccagtgggttgtg3'

3.10 Plasmid constructs

The cDNA insert of a plasmid construct was generated by PCR using the respective pair of primers listed in Table 3-11. The PCR product was purified, digested with the appropriate restriction enzymes, and cloned in the desired vector or plasmid.

TABLE 3-11 Primers for generating cDNA insert

Construct name	Primer name	Primer sequence	Cloned into
		End-to-end PCR	
N1-pGEMT	N1ful-F N1ful-R	5'cactctgctggatgctagtaa3' 5'ccactttcccagaatccacag3'	pGEM-T vector
T3-pGEMT	T3ful-F T3ful-R	5'attaggaaacactagaatggaaagg3' 5'tccttatttcaacagtgttcttctc3'	pGEM-T vector
		***HEPN1* constructs**	
HEPN1-EGFP	N1-GFP-F N1-GFP-R	5'gtaagctttgtggaggtgatgggtaactg 3' 5' ccggatccacactaacatcaaaataaagag 3'	pEGFP-N2 vector
HEPN1-pcDNA	N1-GFP-F N1-pcDNA-R	5'gtaagctttgtggaggtgatgggtaactg 3' 5'ccggatcctcacactaacatcaaaataaag3'	pCDNA3.1 vector
HEPN1-V5	N1-GFP-F N1-V5-R	5'gtaagctttgtggaggtgatgggtaactg 3' 5'aaggatcccactaacatcaaaataaagag3'	pcDNA6B/V5-His vector
		***hepaCAM* constructs**	
hepaCAM-GFP	hCAM-GFP-F hCAM-GFP-R	5'caagcttcaaaatggagagagaaaaggggagc3' 5' aggatccaggcgctgatctccaccg3'	pEGFP-N2 vector
hCAM△320-GFP	hCAM-GFP-F hCAM320-GFP-R	5'caagcttcaaaatggagagagaaaaggggagc3' 5'aggatcctctccggggagtccttgt3'	pEGFP-N2 vector
hCAM△263-GFP	hCAM-GFP-F hCAM263-GFP-R	5'caagcttcaaaatggagagagaaaaggggagc3' 5'tggatccagcaggcacagactgtcacc3'	pEGFP-N2 vector
hepaCAM-V5	hCAM-V5-F hCAM-V5-R	5'taagcttgccaccatgaagagagaaaaggggag3' 5'aggatccggcccaggcgctgatctccacc3'	pcDNA6B/V5-His vector
hCAM△318-V5	hCAM-V5-F hCAM318-V5-R	5'taagcttgccaccatgaagagagaaaaggggag3' 5'ctggatccggagtccttgtccttcag3'	pcDNA6B/V5-His vector
hCAM△290-V5	hCAM-V5-F hCAM290-V5-R	5'taagcttgccaccatgaagagagaaaaggggag3' 5'gaggatcctttcaggcggtcatcattcc3'	pcDNA6B/V5-His vector
hCAM△263-V5	hCAM-V5-F hCAM263-V5-R	5'taagcttgccaccatgaagagagaaaaggggag3' 5'tggatccgcaggcacagactgtcacca3'	pcDNA6B/V5-His vector
hCAM△32-V5	hCAM-V5-F hCAM32-V5-R	5'taagcttgccaccatgaagagagaaaaggggag3' 5'aaggatccgatgttcacccccctccagg3'	pcDNA6B/V5-His vector
hCAMΔ1st Ig-V5	hCAM145-V5-F hCAM-V5-R	5'caggatccatttcgaggccacaggtg 3' 5'aggatccggcccaggcgctgatctccacc3'	hCAM△32-V5 plasmid
hCAM△154-V5	hCAM-V5-F hCAM154-V5-R	5'taagcttgccaccatgaagagagaaaaggggag3' 5'acggatcctgaagccaccaacacctgtg3'	pcDNA6B/V5-His vector

hCAMΔ2nd Ig-V5	hCAM228-V5-F hCAM-V5-R	5'acggatccagcctgcctgtcaagatcac3' 5'aggatccggcccaggcgctgatctccacc3'	hCAM△154-V5 plasmid
hCAMΔIgs-V5	hCAM228-V5-F hCAM-V5-R	5'acggatccagcctgcctgtcaagatcac3' 5'aggatccggcccaggcgctgatctccacc3'	hCAM△32-V5 plasmid
hCAM_tail-V5	Tail-V5-F hCAM-V5-R	5'ataagcttaaaatgggcatcttcctccttgtgacc3' 5'aggatccggcccaggcgctgatctccacc3'	pcDNA6B/V5-His vector
		***HEPT3* constructs**	
HEPT3 (AS)-pcDNA3.1	T3-AS-F T3-AS-R	5'gctcgagattaggaaacactagaatgg3' 5'cgaattctactcccagtgtaacataag3'	pcDNA3.1 vector

TABLE 3-12 PCR components for generating cDNA insert

Component	Volume (µl)
H_2O	36
10X cDNA PCR Reaction buffer	5
dNTP Mix (10 mM)	2
Primer 1 (10 µM)	2
Primer 2 (10 µM)	2
Template (1 ng/µl)	2
Advantage 2 Polymerase Mix (50X)	1
Final volume	50

Q solution was added into the reaction for amplifying template with high GC content.

TABLE 3-13 PCR conditions for generating cDNA insert

Reaction	Temperature	Time	Cycles
Initial Denaturation	95°C	3 min	1
Denaturation	94°C	15 sec	35
Annealing	55-60°C	15 sec	
Extension	72°C	1 min/kb	
Final Extension	72°C	7 min	1

3.11 Preparation of $CaCl_2$ competent *E. coli* cells

E. coli strain JM109 frozen stock was streaked onto an LB agar plate and incubated overnight at 37°C. Following the protocol obtained from the Current Protocols in Molecular Biology, a single bacterial colony was inoculated into 50 ml of LB medium

and cultured overnight at 37°C with shaking at 250 rpm. Two milliliters of bacterial culture was added into 200 ml of prewarmed LB medium and grown to an OD_{590} of 0.375. The bacteria were aliquoted into four 50-ml prechilled, sterile polypropylene tubes and incubated on ice for 10 min. The cells were harvested by centrifugation without brake at 3,000 rpm for 7 min at 4°C. Each pellet was gently resuspended on ice in 10 ml of ice-cold $CaCl_2$ solution followed by centrifugation at 2,500 rpm for 5 min at 4°C. A second resuspension in 10 ml of ice-cold $CaCl_2$ solution was carried out. The cells were incubated for 30 min on ice before centrifugation. Finally, each pellet was resuspended in 2 ml of ice-cold $CaCl_2$ solution and dispensed in 100 µl-aliquots into pre-chilled sterile 1.5-ml microcentrifuge tubes before storing at -80°C.

3.12 Restriction endonuclease digestion of DNA

Most restriction digestions were generally carried out in a final volume of 20 µl or 50 µl containing the DNA, restriction enzyme/s, bovine serum albumin (BSA) and applicable buffer as supplied by Promega. The reactions were incubated for a minimum of 1 hour at 37°C. Double digests were carried out simultaneously unless the buffer conditions were not suitable for both enzymes. In the latter cases, one digest was performed, purified with the QIAquick PCR Purification kit (Qiagen) as described in Section 3.14.2, and followed by the second enzyme digest.

3.13 Agarose gel electrophoresis

DNA or RNA was usually separated on a 1% agarose gel. To prepare a 1% SeaKem LE agarose (BioWhittaker, Walkersville, MD) gel, 0.5 g of agarose was added to 50 ml of 1X TAE buffer and microwaved until the agarose was completely dissolved. The agarose mixture was cooled under running tap water to about 45°C before adding

2.5 µl of 10 mg/ml ethidium bromide (Biorad, Richmond, CA). The mixture was then poured into a cast with a well comb and allowed to solidify. Once set, the comb was removed and the gel was submerged in 1X TAE buffer in the electrophoresis tank. Samples were mixed with gel loading buffer prior to application to the wells. The gel was then electrophoresed at 120 V for approximately 45 min. The nucleic acid was visualized under UV light.

3.14 Purification of DNA from agarose gel

The desired DNA fragment was quickly excised under UV light and the DNA was recovered by centrifuging the gel slice over siliconized glasswool in a 0.6-ml microcentrifuge tube placed in a 1.5-ml microcentrifuge tube. The DNA eluant was purified using either the phenol/chloroform method or the QIAquick PCR Purification kit (Qiagen).

3.14.1 Phenol/chloroform method

The DNA eluant was mixed with 1 volume of phenol (Invitrogen, Carlsbad, CA), vortexed, and centrifuged at 13,000 rpm for 5 min. The aqueous layer was transferred into a tube containing 1 volume of chloroform and mixed. After a 5-min centrifugation at 13,000 rpm, the aqueous layer was precipitated with 2.5 volumes of -20°C absolute ethanol and 1/10 volume of 3 M sodium acetate for 30 min at -80°C. The precipitated DNA was pelleted at 13,000 rpm for 15 min at 4°C and washed once with 70% ethanol. The pellet was air-dried and resuspended in the desired amount of H_2O.

3.14.2 QIAquick PCR Purification kit

Five volumes of buffer PB were added to 1 volume of the eluant. The mixture was transferred into a QIAquick spin column and centrifuged. The column was washed with 750 µl of buffer PE. Subsequently, DNA was eluted with 10-50 µl of H_2O. All centrifugation steps were carried out at 13,000 rpm for 1 min at room temperature.

3.15 DNA ligation

In a ligation reaction, T4 DNA ligase (Promega) covalently links the phosphodiester bonds between the insert DNA and the vector DNA to join the two fragments together. Ligation was performed in a total volume of 10 µl containing appropriate molar ratios of vector and insert DNA (usually 1:2), 1 µl T4 DNA ligase and 1X ligase buffer, and incubated either for 1-2 hours at room temperature or overnight at 4°C.

3.16 Transformation of *E. coli*

Transformation facilitates the uptake and expression of DNA by a living cell. Ten microliters of ligation mix was added to 100 µl of JM109 competent cells, mixed, and left on ice for 30 min. The cells were then heat-shocked at 42°C for 45 sec before rapidly returning the tube to ice for two min. After addition of 900 µl of LB medium, the bacteria were incubated with shaking at 150 rpm for 90 min at 37°C. The cells were then pelleted by centrifugation at 2,000 rpm for 3 min. Excess supernatant was discarded, leaving approximately 200 µl in the tube. The cells were then resuspended and plated onto LB agar plates containing the appropriate antibiotic. For blue/white selection, the LB agar plates were spread with 20 µl of X-Gal and 100 µl of IPTG prior to plating of bacteria. The plates were incubated for 18-24 hours at 37°C.

3.17 Screening of bacterial colony by PCR

Screening of bacteria colonies by PCR enables the identification of positive bacteria clones that contain the transformed plasmid. In this procedure, each bacterial colony was picked with a sterile pipette tip and transferred into a 1.5-ml microcentrifuge tube containing 50 µl of sterile H_2O. The tip was agitated in the H_2O to remove the colony from the tip. An aliquot of the bacteria was used as template in the PCR reaction. The presence of the insert was determined by using either two insert-specific primers or two vector-specific primers. If insert orientation needs to be determined, a vector-specific primer paired with an insert-specific primer was used. The PCR reaction was prepared in a final volume of 25 µl using Promega's *Taq* DNA polymerase. The resulting PCR products were checked on an agarose gel for the presence of the predicted band. Positive bacteria in H_2O were directly inoculated in LB medium containing the appropriate antibiotic and cultured overnight for plasmid miniprep.

TABLE 3-14 PCR components for screening of bacterial colony

Component	Volume (µl)
10X buffer	2.5
$MgCl_2$	2
dNTP Mix (10 mM)	1
Primer 1 (10 µM)	0.5
Primer 2 (10 µM)	0.5
Bacteria in H_2O	18.25
Taq DNA polymerase	0.25
Final volume	25

Q solution was added into the reaction for amplifying template with high GC content.

TABLE 3-15 PCR conditions for screening bacterial colony

Reaction	Temperature	Time	Cycles
Initial Denaturation	95°C	5 min	1
Denaturation	94°C	30 sec	
Annealing	50-60°C	30 sec	35
Extension	72°C	1 min/kb	
Final Extension	72°C	7 min	1

3.18 Plasmid miniprep

A bacterial colony or an aliquot of bacterial glycerol stock was inoculated into 3 ml of LB medium supplemented with the appropriate antibiotic. The inoculated bacteria were cultured at 37°C overnight with shaking at 250 rpm. Two milliliters of bacteria were pelleted by centrifugation at 13,000 rpm for 1 min. Plasmid extraction was carried out using the Wizard Mini-prep kit from Promega according to the manufacturer's instruction. The pellet was resuspended in 250 µl of Cell Resuspension solution before lysing in 250 µl of Cell Lysis solution. The mixture was gently inverted several times till a clear and viscous lysate was obtained. Ten microliters of Alkaline Protease were pipetted into the solution, mixed, and incubated for 5 min. Unwanted materials including bacterial cell wall fragments, proteins, and chromosomal DNA were precipitated by the addition of 350 µl of Neutralization solution and centrifugation at 13,000 rpm for 10 min. The clear supernatant containing plasmid DNA was transferred to a spin column and centrifuged at 13,000 rpm for 1 min. The column was washed with a 750 µl and a subsequent 250 µl of wash buffer. Plasmid DNA was then eluted with 50 µl of sterile H_2O and stored at -20°C.

3.19 Bacterial glycerol stock

Glycerol was diluted to 50% in H_2O and filter-sterilized. Three hundred and fifty microliters of bacterial culture was mixed with 150 μl of 50% glycerol and stored at -80°C.

3.20 Automated DNA sequencing

DNA Sequencing reactions were performed with the ABI PRISM Big Dye Reaction Terminator Cycle Sequencing Kit version 3.1 (Applied Biosystems, Foster City, CA) with slight modifications to the manufacturer's instruction.

TABLE 3-16 Primers for sequencing

Primer name	Sequence
pEGFP-N2 vector-specific:	
GFP-F	5'aaatgggcggtaggcgtg3'
GFP-R	5'cctcgcccttgctcac3'
pcDNA3.1 or pcDNA6B/V5-His vector-specific:	
T7 (forward primer)	5'aatacgactcactataggg3'
pcDNA3.1bgh-R	5'tagaaggcacagtcgagg3'
pGEM-T vector-specific:	
pGEM-F	5'tgtaaaacgacggccagt3'
pGEM-R	5'aagctatgcatccaacgc3'
***HEPN1*-specific:**	
N1-F	5'atccaagtcctgctgcctctt3'
N1-R	5'ctcctaaactccagctctgat3'
***hepaCAM*-specific:**	
hCAMint-F	5'caatgactcgagaatgctcctgtcc 3'
hCAM-R	5'cttccgttcctgctcaccacttcga3'
***HEPT3*-specific:**	
T3-RACE-R	5'gtccgacagaagcctctaccgagaacgt3'
T3-RACE-nR	5'cctcatagggagaaatcttgccaagggag3'
HepT3(ngsp-forward)	5'cctattacagagacacatgtatacc3'
T3seq-r1	5'gtaacatctcctaggtaacag3'
T2seq-f1	5'ctactcgggaggctgaggcag3'

TABLE 3-17 Sequencing components

Component	Volume (µl)
Double-stranded plasmid	300-500 ng
Big Dye terminator mix	4
5X Sequencing buffer	2
Primer (10 µM)	0.5
Final volume	Add H_2O to a final volume of 20 µl

TABLE 3-18 Sequencing conditions

Reaction	Temperature	Time	Cycles
Denaturation	96°C	10 sec	
Annealing	55°C	5 sec	25
Extension	60°C	4 min	

The sequencing product was precipitated with 2 µl of 125 mM EDTA, 2 µl of 3 M sodium acetate and 50 µl of absolute ethanol for 15 min at room temperature before centrifugation at 13,000 rpm for 15 min at 4°C. The pellet was washed in 250 µl of 70% ethanol and centrifuged at 13,000 rpm for 5 min at 4°C. The final pellet was air-dried before being reconstituted in sequencing loading buffer and analyzed on an ABI PRISM™ TM 337 automated sequencer (Applied Biosystems).

3.21 Transient and stable transfection

Cells used for transfection were seeded one day before transfection at a density such that they would be 40-70% confluent on the day of transfection. Transfections were carried out with the reagent of Lipofectamine Plus (Invitrogen) according to the manufacturer's instructions. Cells were transfected in serum-free DMEM with DNA precomplexed with PLUS and Lipofectamine reagents for 3-5 hours, after which, the medium containing the complexes was removed and replaced with DMEM medium supplemented with 10% FBS.

For stable transfections, cells transfected in 35-mm plates were reseeded into 100-mm plates or T75 flasks after 24 hours of transfection and selected under 800 μg/ml of G418 (Sigma) or 10 μg/ml of blasticidin (Invitrogen) for 2 weeks. Thereafter, the cells were trypsinized and each cell picked under microscope was transferred into a well of a 24-well plate containing parental cells at 20% confluence. Parental cells were added to stimulate the growth of the stable cell. The cells were then allowed to propagate in culture medium without antibiotics for two days before replacing with selection medium. The cells were kept in selection medium until all the parental cells were killed and the stable clone reached confluence. Alternatively, after trypsinizing the stable cells, the cells were seeded at very low density to allow it to grow into a small colony of about 40 cells. Under microscope, the colony was gently detached and aspirated using a pipette tip and transferred to a 24-well plate. The cells were maintained until confluent in selection medium. Once the cells were confluent, a fraction of them was used for Western blot analysis and immunocytochemistry to confirm the expression of the desired protein and cell homogeneity, respectively. The positive clones were subsequently expanded.

For transient transfections, the transfected cells were cultured without antibiotic selection for 24-48 hours before assaying.

For transient transfections with time-course, HepG2 cells were transfected with either HEPN1-EGFP or vector pEGFP-N2 and examined by fluorescence microscopy between 8 and 24 hours after transfection with 2-hour interval.

3.22 Immunocytochemistry

3.22.1 Visualization of V5-tagged protein expression

Cells grown on coverslips were washed twice with PBS and fixed with 3.7% paraformaldehyde for 15 min at 37°C. The subsequent steps were all carried out at room temperature. Following three 5-min washes with PBS, the cells were permeabilized with 0.2% Triton X-100 in PBS for 5 min. A second set of washing was carried out and the nonspecific sites on coverslips were blocked in 10% normal goat serum (Santa Cruz, Santa Cruz, CA) in PBS. The cells were then incubated for 1 hour with mouse anti-V5 antibody (Invitrogen; 1:200 dilution) diluted in 1.5% normal goat serum, washed, and exposed for 1 hour to biotin-conjugated goat anti-mouse IgG antibody (Santa Cruz; 1.5:100 dilution) diluted in 3% normal goat serum. After washing, avidin-fluorescein isothiocyanate (FITC; Santa Cruz; 2:100 dilution) in PBS was added to the cells and incubated for 15 min in the dark. Excess avidin-FITC was removed by washing in PBS. After a final rinse in H_2O, the coverslips were mounted onto the microscopic slides with FluorSave reagent (Calbiochem, La Jolla, CA), and analyzed by fluorescence microscopy (Carl Zeiss, Germany) or confocal microscopy (LSM 510; Carl Zeiss).

3.22.2 Disruption of cellular F-actin

Cellular F-actin was disrupted by cytochalasin B (Sigma). Stock solution of cytochalasin B was prepared in DMSO at a concentration of 10 mM. Cells were incubated with 10 μM of cytochalasin B in culture medium containing 10% FBS for 90 min at 37°C prior to immunocytochemistry.

3.22.3 Detection of mitochondria

Mitochondria were detected by treating cells with Mitotracker-orange (Molecular Probes, Inc., Eugene, OR). Stock solution of 1 mM was prepared in DMSO. To detect mitochondria, live cells were treated with 250 nM of Mitotracker-orange (Molecular Probes, Inc., Eugene, OR) diluted in culture medium containing 10% FBS for 25 min at 37°C. The cells were then rinsed with culture medium before fixing in paraformaldehyde.

3.22.4 Labeling of F-actin

F-actin may be efficiently labeled with fluorescent phalloidin conjugates. Phalloidin is a fungal toxin produced by the poisonous mushroom *Amanita phalloides* that acts by binding to and stabilizing F-actin. Stock solution of tetramethylrhodamine isothiocyanate (TRITC)-conjugated phalloidin (Sigma) was prepared in DMSO at 1 mg/ml. F-actin of fixed and permeabilized cells was labeled with 1 μg/ml of TRITC-conjugated phalloidin diluted in PBS for 1 hour at room temperature.

3.22.5 Nuclear staining

4',6-Diamidino-2-phenylindole (DAPI; Roche) stock was prepared as 1 mg/ml in DMSO. Fixed cell nuclei were stained with 1 μg/ml of DAPI in PBS for 15 min at 37°C.

3.22.6 Colocalization of hepaCAM-GFP and E-cadherin in polarized cells

MCF7 cells stably expressing hepaCAM-GFP were seeded at 10% confluence and allowed to grow to confluence on 0.4-μm Transwell filters (Costar, Cambridge, MA). The filters were fixed, permeabilized, and blocked as described in Section 3.22.1.

E-cadherin was detected by mouse anti-E-cadherin antibody (Zymed, San Francisco, CA; 1.2:100 dilution), biotin-conjugated goat anti-mouse IgG antibody, and subsequently avidin-TRITC conjugate (Sigma; 1:100 dilution). To mount the filter, the excised filter with the cells side up was placed onto a drop of mountant on a microscopic slide. Another drop of mountant was dropped onto the cell surface and a coverslip was gently placed over it. The cells were examined by confocal microscopy (LSM 510) with sectioning performed at 0.5 μm.

3.22.7 Localization of detergent-resistant hepaCAM-V5 proteins

MCF7 cells on coverslips were transiently transfected with hepaCAM-V5 for 48 hours before permeabilizing with ice-cold 1% Triton X-100 in PBS for 3 min. The cells were then fixed and blocked, and the detergent-insoluble hepaCAM-V5 was detected by mouse anti-V5 antibody as described in Section 3.22.1. The control cells were fixed prior to permeabilization with 1% Triton X-100.

3.22.8 Colocalization of hepaCAM-V5 with lipid raft proteins

NIH3T3 cells grown on coverslips were transiently transfected with hepaCAM-V5 for 48 hours. The cells were permeabilized with ice-cold 0.5% Triton X-100 in PBS for 3 min prior to fixing and blocking. Double-staining of hepaCAM and caveolin-1 or fyn was carried out with mouse anti-V5 antibody and rabbit anti-caveolin-1 (Santa Cruz; 1:100 dilution) or rabbit anti-fyn antibody (Santa Cruz; 1:100 dilution) diluted in 1.5% normal goat serum. The anti-V5 antibody was detected with FITC-conjugated goat anti-mouse IgG antibody (Santa Cruz; 1:50 dilution) while anti-caveolin-1 and anti-fyn antibodies were detected with biotin-conjugated goat anti-mouse IgG

antibody (1.5:200 dilution) and avidin-TRITC conjugate (Sigma; 1:100 dilution). The cells were analyzed by confocal microscopy.

3.23 MTT assay

3-(4,5-dimethylthiazol-2-yl)-2,5-diphenyltetrazolium bromide (MTT) assay measures cell viability. The assay is based on the reduction of the yellow MTT into purple formazan crystals catalyzed by enzymes produced only in metabolically active live cells.

To evaluate cell viability, a volume of 100 µl of MTT (Roche; 5 mg/ml in PBS) was added to cells transfected for 48 h in a 6-well culture plate. After 3 h of incubation at 37°C, cells were lysed and formazan crystals were dissolved in 1 ml of isopropanol with 0.4 N HCl. Wells containing all admixtures except cells were used as blanks. Optical density was read at 570 nm using an ELISA reader. Transfection efficiency, approximately 40% in this study, was detected by transfecting HepG2 cells with the pEGFP-N2 vector and calculated based on the number of flouorescent cells against the total number of cells in the test. Cell viability (CV) was computed by the following equation:

$$CV\,(\%) = \left(\, 1 - \frac{ODc - ODe}{TE \times ODc} \,\right) \times 100\%$$

where TE = transfection efficiency, i.e., 40% in this study; ODe = OD reading of experiment; ODc = OD reading of control. Cell viability of control was regarded as 100%.

To assess the rate of cell proliferation, 2 X 10^4 cells were seeded and cultured in six 6-well plates in triplicates. MTT assay was carried out once the cells had attached to establish the base line of cell growth. At every 24 hours of cell culture for 5 days, MTT assay was performed to evaluate the cell viability. The growth rate of each cell line was presented as fold of increase in cell viability against the respective base line obtained on the day of seeding cells.

3.24 Colony formation

This assay was performed to evaluate the effect of the gene of interest on cell growth in colony form. Transfected cells were cultured in selection medium containing 10 μg/ml of blasticidin or 800 μg/ml of G418 for 2 weeks without trypsinization while medium was refreshed every 2 days or 3-4 days, respectively. The cell colonies formed at the end of experiment were visible and the number of colonies was counted.

3.25 Detection of apoptosis by Annexin V

ApoAlert Annexin V (Clontech) was used to detect changes in the position of phosphatidylserine (PS) in the cell membrane characteristic of apoptosis. At 16 hours after transfection, cells grown on coverslips were rinsed with 1X binding buffer, incubated with 5 μl of Annexin V and 10 μl of propidium iodide for 10 minutes, and examined by fluorescence microscopy

3.26 Cell aggregation assay

In the cell aggregation study, cells were washed once with PBS and detached by incubation with 1 mM EDTA in PBS at 37°C for about 15 minutes. Culture medium was added to the cells and the cells were sedimented by centrifugation at 1,000 rpm

for 5 min. The cell pellet was washed once with Ca^{2+}-free Hanks' balanced salt solution (HBSS; JRH Biosciences, Lenexa, KS) and resuspended in Ca^{2+}-free HBSS. Single-cell suspensions were prepared by passing the cells through an 18-gauge needle for 20 passages. The cells were counted using the trypan blue method as described in Section 3.1.2. Single cells were seeded at a concentration of 4 X 10^5 cells/ml in a final volume of 3 ml into 60-mm petri-dishes precoated overnight at 4°C with 1% BSA. The cells were incubated for 1 hour at 37°C with gentle agitation at 100 rpm. The cell aggregates formed were observed under the inverted light microscope.

3.27 Cell spreading assay

Coverslips were coated with either matrigel (40 μg/ml; Clontech) or fibronectin (10 μg/ml; Santa Cruz) and allowed to polymerize for 1 hour at 37°C or at room temperature, respectively. Cells were seeded onto the coated coverslips and incubated under standard culture conditions. Cell morphology was observed by microscopy. Unspread cells were defined as round cells while spread cells were defined as cells with extended processes (Richardson *et al*., 1997). The percentage of cells demonstrating spread morphology was quantified in 10 randomly selected fields.

3.28 Cell detachment assay

A confluent monolayer of cells was detached in 1 mM EDTA in PBS at 37°C. Cell detachment was observed under the inverted microscope at 5 minutes and 15 minutes of incubation. Concurrently, the dissociated cells were harvested and counted in 10 randomly selected fields.

3.29 Boyden chamber assay

Cell migration was assessed using the transwell chambers with 8-μm pore size membrane (Costar) coated with 20 μg of matrigel in 24-well plate. The cells were starved overnight in serum-free DMEM medium containing 0.1% BSA prior to initiation of the assay. Fifty thousand cells resuspended in DMEM with 1% FBS were loaded into the upper transwell chamber and allowed to migrate through the membrane into the bottom chamber containing DMEM supplemented with 10% FBS which acted as a chemoattractant. Migrated cells were harvested 24 hours later by trypsinizing the lower surface of the membrane and collected into a new 24-well plate. The migration activity was quantified by blind counting of the migrated cells in 10 randomly selected microscopic fields.

3.30 Wound healing assay

Cell motility was also assessed by the wound healing experiment on monolayer cells. Cells were seeded in 35-mm culture plates at high density and allowed to form confluent monolayers overnight. Wounds were made by sterile plastic 200-μl micropipette tips and allowed to be healed in culture medium containing 10% FBS. Microscopic pictures representing the changes in diameter (*D*) of each wound were taken at 24 and 48 hours. By measuring the remaining gap space on the pictures, the percentage of wound closure was computed into ratio ($D_{24/48h}/D_{initial}$ X 100%).

3.31 *N*-linked glycosylation analysis

For inhibiting *N*-linked glycosylation, cells were cultured in tunicamycin (Sigma) after transient transfection at the indicated concentrations for 24 hours before lysis. For enzymatic digestion of *N*-linked oligosaccharides, cell lysate was treated with

peptide *N*-glycosidase F (PNGase F; NEB, Beverly, MA) according to the manufacturer's instructions. A 10-µl reaction containing 20 µg of cell lysate and 1X glycoprotein denaturing buffer was denatured at 100°C for 10 minutes, followed by 1 hour incubation at 37°C in 1X G7 buffer, 1% Nonidet P-40 and 1,000 units of PNGase F. A control without PNGase F was treated concurrently. These samples were then subjected to Western blot analysis.

3.32 Alkaline phosphatase treatment

Cell lysate was incubated in dephosphorylation buffer for 10 min at 30°C. Calf intestinal alkaline phosphatase (CIP; Roche) was added and incubated for a further 15-60 min prior to Western blot analysis.

3.33 Chemical crosslinking

A monolayer or a single suspension of cells was incubated in PBS containing 3 mM bis(sulfosuccinimidyl) suberate (BS3; Pierce, Rockford, IL) or 3,3'-Dithiobis (sulphosuccinimidyl propionate) (DTSSP; Pierce) at room temperature for 30 min. The reaction was quenched with the addition of 20 mM Tris-HCl pH 7.5 for 15 min. Single-cell suspension was assured by microscopic observation before and after chemical crosslinking reaction. DTSSP-crosslinked proteins were resuspended in Laemmli sample buffer without reducing agent 50 mM dithiothreitol (DTT) unless indicated. Cell lysate was prepared in radioimmunoprecipitation assay (RIPA) buffer containing 10 mM iodoacetamide to inhibit formation of nonspecific disulfide linkages (Masuda *et al*., 2002).

3.34 Preparation of whole cell extracts

Cells were scraped in RIPA buffer containing protease inhibitors followed by sonication or incubation on ice for 15 min. Tissues were homogenized in RIPA buffer using a Dounce homogenizer. The cell lysate was cleared by centrifugation at 13,000 rpm for 10 min at 4°C. Protein samples were mixed with an equal volume of 2X or ¼ volume of 5X Laemmli sample buffer and boiled for 5 min before Western blot analysis.

3.34.1 Subcellular fractionation

Cells grown on 100-mm plate or T75 flask were scraped using a rubber policeman in hypotonic buffer supplemented with protease inhibitors. The cell lysate was incubated on ice for 10 min prior to 20-40 strokes of Dounce homogenization at 4°C. The cell homogenate was centrifuged at 1,500 rpm for 10 min to remove nuclei, cell debris and unbroken cells. The supernatant (S1) was then centrifuged for 1 hour at 100,000 g in an SW55Ti rotor (Beckman, Columbia, Md) at 4°C, resulting in the supernatant (S100) and the pellet (P100). The S100 supernatant contained cytoplasmic components while the P100 pellet contained the cellular membrane and cytoskeletal components.

3.34.2 Detergent extraction

For detergent solubility assay, cells or P100 fractions were resuspended in 1 volume of ice-cold 1% Triton X-100 in PBS containing protease inhibitors and incubated on ice for 15 min. One molar of potassium iodide (KI; Sigma) was added into the 1% Triton X-100 buffer wherever indicated to depolymerize F-actin. The detergent-

insoluble material was pelleted at 13,000 rpm for 10 min at 4°C, and boiled in 1 volume of 2X Laemmli sample buffer for 10 min.

To investigate if hepaCAM might be associated with the detergent-resistant membrane (DRM), P100 pellet was resuspended in 1 volume of ice-cold 1% Triton X-100 in PBS and placed on ice for 15 min. The Triton X-100-resistant material was pelleted at 13,000 rpm for 10 min at 4°C. To solubilize some DRM, the Triton X-100-insoluble pellet was further resuspended in 1 volume of ice-cold 100 mM *N*-octyl-β-D-glucopyranoside (n-OG; Fluka Biochemika, Buchs, Switzerland) in PBS, placed on ice for 15 min, followed by another centrifugation at 13,000 rpm for 10 min at 4°C. The remaining pellet containing the detergent-insoluble DRM was resuspended in 1 volume of 2X Laemmli sample buffer and boiled for 10 min.

An equal volume of each fraction was resolved by SDS-PAGE and subjected to Western blot analysis.

3.35 Sucrose density gradient ultracentrifugation

Forty-eight hours post-transfection, transfected NIH3T3 cells in 100-mm plates were washed twice in PBS, lysed in 500 µl of ice-cold lysis buffer supplemented with protease inhibitors, incubated on ice for 20 min, and homogenized with a Dounce homogenizer. The lysates were adjusted to a final concentration of 40% sucrose by adding 500 µl of 80% sucrose in TNE buffer to the samples. Reverse layering of gradient was performed to minimize disturbance caused during layering. In an ultra-clear centrifuge tube (Beckman), using 21-guage needle fitted on 3-ml syringe, the gradient was created by first loading 1 ml of 10% sucrose, followed by the addition of

1.5 ml of 30% sucrose, and finally the samples to the bottom of the tubes. Samples were spun at 100,000 g for 24 h at 4°C in an SW55Ti rotor. After centrifugation, seven 0.5-ml fractions were collected starting from the bottom layer to the top. Proteins were precipitated by the tricholoracetic acid (TCA)/ethanol precipitation method. Five hundred microliters of 20% TCA in H_2O was added to each fraction, placed on ice for 20 min, and spun at 13,000 rpm for 15 min at 4°C. The pellet was washed with absolute ethanol, dried, resuspended in 40 µl of 2X Laemmli sample buffer, and boiled for 10 min. Twenty microliters of each fraction were electrophoresed by SDS-PAGE and analyzed by Western blotting.

3.36 Cholesterol depletion

For cholesterol depletion, cells were washed twice with PBS and then incubated with 10 mM methyl-β-cyclodextrin (MCD; Sigma) in DMEM at 37°C for 30 min prior to cell lysis.

3.37 Determination of protein concentration by the Bradford method

The Bradford assay is a dye-binding assay based on the differential color change of Coomassie blue G dye as it binds to protein. In this study, the concentrations of proteins were determined by Bradford assay (Biorad) at OD_{595}.

One part of the Dye Reagent Concentrate was diluted in 4 parts of H_2O to constitute the working solution. Twenty microliters of protein diluted in PBS was mixed with 1 ml of working dye solution and the absorbance measured. A standard curve was plotted by measuring the absorbance of BSA at concentrations ranging from 0-1

mg/ml (Figure 3-2). The concentrations of test proteins were then determined from this curve.

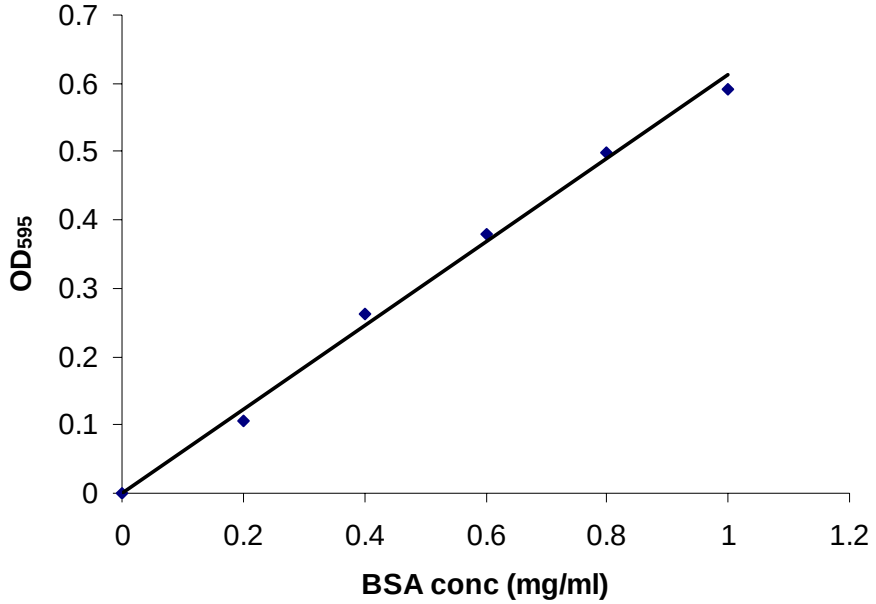

FIGURE 3-2 Protein standard curve.

3.38 Western blot analysis

3.38.1 Separation of proteins by polyacrylamide gel electrophoresis

Denatured protein samples were loaded usually onto 10% SDS-PAGE gel and resolved by running in 1X SDS-PAGE running buffer at 150 V for 70 min or until the desired distance was reached.

3.38.2 Protein transfer

After electrophoresis, proteins were transferred from the gel onto PVDF membrane (Biorad) using BioRad's Mini Trans-Blot Electrophoretic Transfer Cell. The gel, membrane, Whatman filter papers and fiber pads were equilibrated in Towbin buffer for 15 min before assembly as illustrated in Figure 3-3. The proteins were transferred

from the gel (negative electrode) to the membrane (positive electrode) at 100 V for 60 minutes in Towbin buffer containing 0.1% SDS.

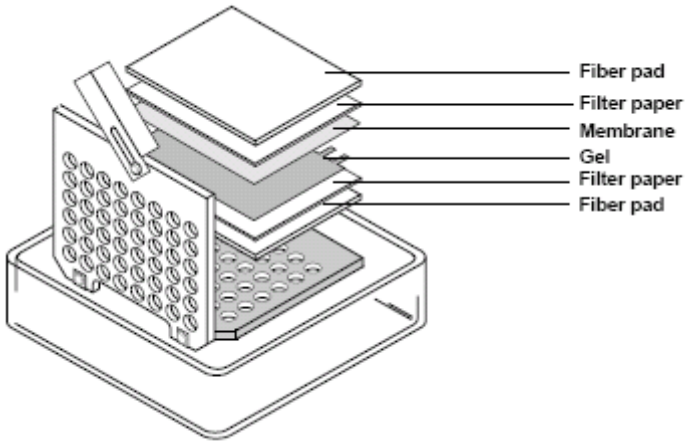

FIGURE 3-3 Assembly for protein transfer. (Source: instruction manual of Biorad's Mini Trans-Blot Electrophoretic Transfer Cell)

3.38.3 Western blotting

The membrane was rinsed with 1X TBS and blocked in blocking buffer for 1 hour. Incubation with primary antibodies diluted in blocking buffer was carried out either at room temperature for 1 hour or 4°C overnight. The primary antibodies used included rabbit anti-hepaCAM polyclonal antiserum (1:2,000 dilution; generated by Miss Zhang Chunli), mouse anti-V5 antibody (1:5,000 dilution), mouse anti-GFP antibody (Santa Cruz; 1:200 dilution), mouse anti-p53 (Santa Cruz; 1:5,000 dilution), mouse anti-E-cadherin (1:500 dilution), rabbit anti-caveolin-1 antibody (1:200 dilution), or goat anti-actin antibody (Santa Cruz; 1:100 dilution). Blots were then washed three times in TBS-T, 5 min each, and then incubated for 1 hour in the appropriate horseradish peroxidase-conjugated secondary antibody (Santa Cruz; 1:5,000 dilution). After four 5-min washes, the enzymatic activity was detected with chemiluminescence luminol reagent (Santa Cruz) and autoradiography.

3.38.4 Stripping of Western blot

The Western blot to be re-probed was stripped in two 15-min washes of Stripping buffer. The membrane was then rinsed with 1X TBS before re-blocking.

3.39 Immunoprecipitation

Immunoprecipitation was used to detect protein-protein interactions. Cell lysate prepared in RIPA buffer was precleared with Protein G-agarose beads (Santa Cruz) for 1 hour at 4°C with agitation. The supernatant was recovered by centrifugation at 2,500 rpm for 1 min. The precleared lysate was then mixed with protein G-agarose beads and specific antibody, and incubated overnight at 4°C before washing four times with RIPA buffer or PBS when a reduced stringency was desired. The beads were resuspended in 2X Laemmli sample buffer, boiled for 10 min and the eluted proteins were subjected to Western blot analysis.

3.40 Bioinformatics and statistical analysis

Database searches were carried out using National Center for Biotechnology Information (NCBI), Ensembl, ExPASy and Swiss-Prot; and motif searches were performed with programs like Scansite, PROSCAN, PROSITE, PSORT II, RepeatMasker, MatInspector, big-PI and NetPhos2.0. Mann-Whitney test was performed to compare two means of samples with small sample size (n = 6). Two-tailed Student's *t* test was used to assess data with sample size larger than 6. Nonparametric ANOVA was performed to compare the difference among more than two means. Fisher's exact test was used to assess the correlation between two parameters. Software InStat 3.0 (GraphPad) was employed and $P < 0.05$ was considered as significant.

CHAPTER 4 RESULTS

4.1 Gene *HEPN1*

4.1.1 Loss of *HEPN1* expression in human tumors

4.1.1.1 Suppression of *HEPN1* in HCC patients

Suppression subtractive hybridization (SSH) revealed that a novel gene, designated as *HEPN1*, was downregulated in HCC. Based on the partial *HEPN1* cDNA sequence information obtained from SSH, a pair of *HEPN1*-specific primers, N1-F and N1-R, was synthesized and used in semi-quantitative RT-PCR to analyze the frequency of *HEPN1* suppression in 23 HCC patients. The RT-PCR result (Figure 4-1) showed that *HEPN1* was ubiquitously expressed in 23 non-tumorous liver tissues, but either downregulated or lost in 22 HCC tissues (except for sample 16), demonstrating suppression of *HEPN1* in 95.7% of 23 HCC samples tested. Real-time RT-PCR was further performed on the same batch of liver specimens to quantitate the level of *HEPN1* expression (Figure 4-2). In addition to obtaining reproducible results pertaining to the frequency of *HEPN1* suppression in HCC by both experimental approaches, real-time RT-PCR detected a significant reduction of *HEPN1* expression in HCC. The average expression level in HCC (7.2±10.4) was 5.7-fold lower than that in non-tumorous liver tissues (40.8±10.0), $P < 0.0001$. No correlations between *HEPN1* and the clinicopathologic parameters could be detected. This could be due to the high rate of *HEPN1* suppression in the HCC samples examined (Table 4-1).

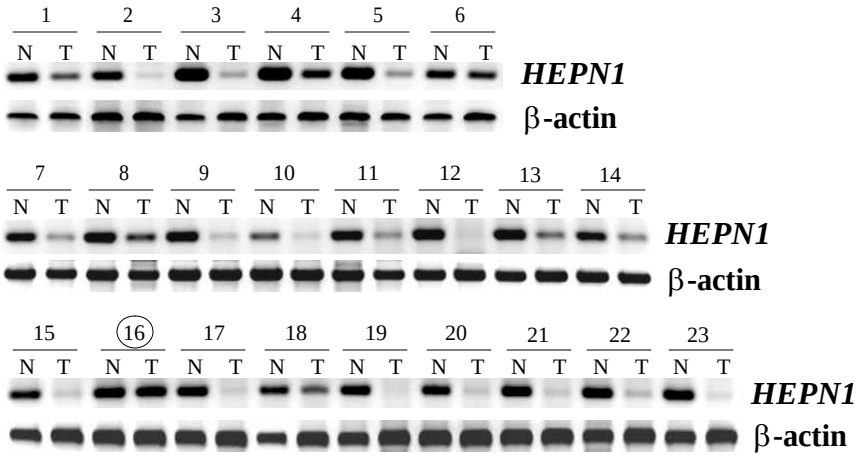

FIGURE 4-1 Expression of *HEPN1* transcript in 23 HCC patients by semi-quantitative RT-PCR. RT-PCR products of *HEPN1* generated by primers N1-F and N1-R were analyzed by gel electrophoresis. β-actin was included as internal control. ◯, sample that shows no clear difference in *HEPN1* expression; N, non-tumorous liver tissue; T, HCC liver tissue.

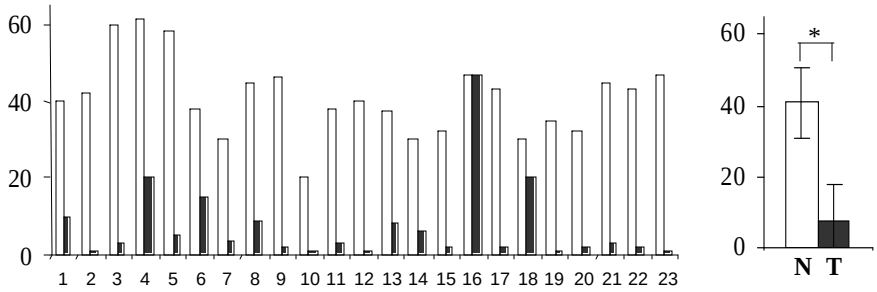

FIGURE 4-2 Expression of *HEPN1* transcript in 23 HCC patients by quantitative real-time RT-PCR. The expression level of *HEPN1* in each sample was determined by real-time RT-PCR. Results were normalized and converted into percentage against the expression level of GAPDH. The average level of expression (mean ± SD, n = 23) is represented on the right, * $P < 0.0001$. N, non-tumorous liver tissue; T, HCC liver tissue.

TABLE 4-1 Correlation between *HEPN1* suppression and the clinicopathologic parameters in 23 HCC patients

Parameters	*HEPN1* Suppression	Unchanged *HEPN1*	Suppression Rate (%)	*P*
Total number	22	1	95.7	
Sex				
Male	16	2	89	NS
Female	4	1	80	NS
Grade				
well	3	0	100	NS
moderate	12	2	86	NS
poor	5	1	83	NS
Cirrhosis	16	3	84	NS
Hepatitis virus				
HBV	18	2	90	NS
HCV	3	0	100	NS
HBV + HCV	2	0	100	NS

Grade, histological differentiation of HCC; NS, not significant; *P* was revealed by the Fisher's exact test.

4.1.1.2 Suppression of *HEPN1* in HCC cell lines

Furthermore, in 4 HCC cell lines tested, semi-quantitative RT-PCR showed that *HEPN1* was significantly suppressed in Hep3B, Huh7 and SK-Hep1, and completely silenced in HepG2 cells as compared to a non-tumorous liver specimen (Figure 4-3).

4.1.1.3 Suppression of *HEPN1* in cell lines derived from diverse cancers

HEPN1 mRNA expression was screened in a panel of human cancer cell lines consisting of Jurkat, HL60, K562, HT29, HCT116, Colo205, MCF7, SK-N-SH, NCI-H82, NCI-H23, NCI-H69, and NCI-H2066 derived from leukemia, colorectal cancer, breast cancer, neuroblastoma and lung cancer (Figure 4-4). Semi-quantitative RT-PCR showed that *HEPN1* was expressed in Jurkat and HCT116 cells, but markedly suppressed in HL60, K562, HT29 and Colo205 cells, and undetectable in MCF7, SK-N-SH, NCI-H82, NCI-H23, NCI-H69 and NCI-H2066 cells, representing a significant loss of *HEPN1* in 83.3% (10/12) of the cell lines.

4.1.2 Isolation of *HEPN1* full-length cDNA

The technique of RACE was used to extend the sequence knowledge of *HEPN1*. 5'- and 3' RACE were performed to isolate the respective 5' and 3' ends of *HEPN1* from human normal liver cDNA library. 5' RACE using gene-specific primer N1-RACE-R and adaptor primer AP1, followed by a nested 5' RACE using nested primers N1-RACE-nR and AP2 yielded a fragment of ~600 bp (Figure 4-5). A single round of 3'-RACE using primers N1-RACE-F and AP1 generated a 3' cDNA fragment of ~1.2 kb. The RACE fragments were cloned separately into the pGEM-T vector and sequenced. The overlapping sequences of the 5' and 3' RACE products were aligned together to obtain a 1448 bp full-length cDNA of *HEPN1* (Figure 4-6). The sequence

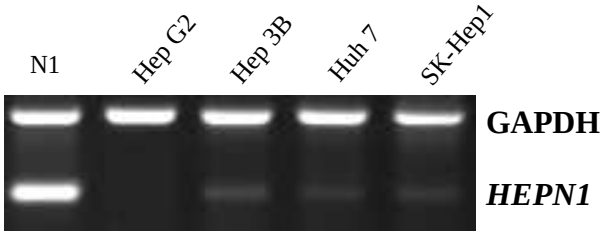

FIGURE 4-3 Expression of *HEPN1* transcript in 4 HCC cell lines. Semi-quantitative RT-PCR was used to amplify *HEPN1* mRNA and GAPDH (an internal control). RT-PCR products were analyzed by gel electrophoresis. The expression of *HEPN1* in four HCC cell lines, HepG2, Hep3B, Huh7 and SK-Hep1, was compared to that in the non-tumorous liver tissue from patient number one (N1).

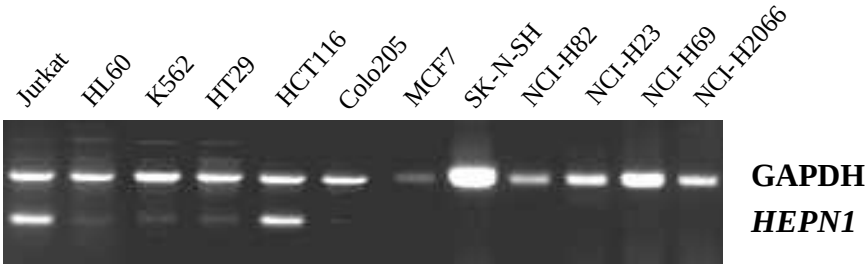

FIGURE 4-4 Expression of *HEPN1* transcript in cell lines derived from different tumor types. Semi-quantitative RT-PCR was performed to amplify *HEPN1* mRNA and GAPDH (an internal control). RT-PCR products were analyzed by gel electrophoresis.

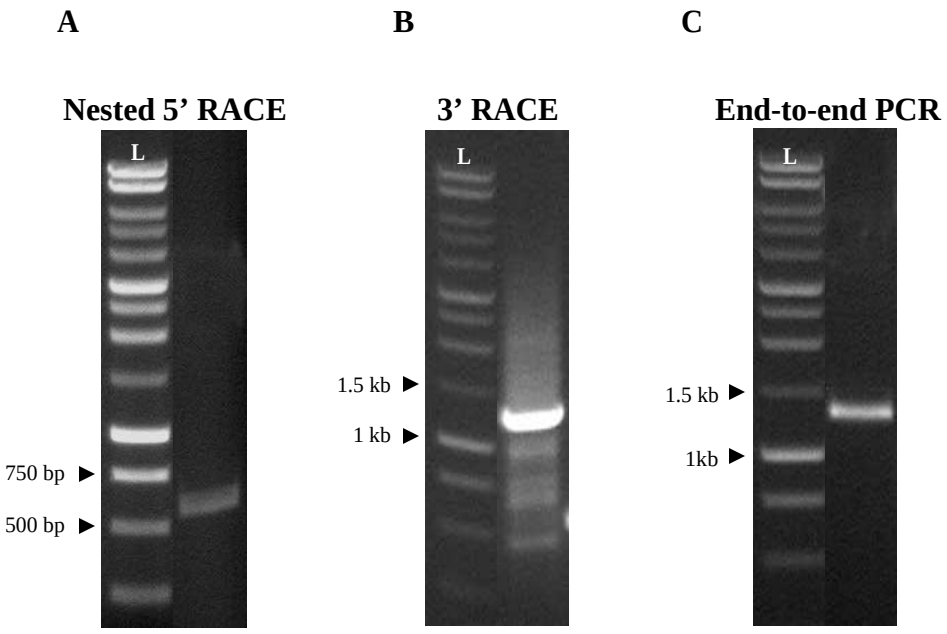

FIGURE 4-5 Isolation of *HEPN1* full-length cDNA by RACE. RACE-PCR products were analyzed by gel electrophoresis. A, Nested 5' RACE product was generated by primers N1-RACE-nR and AP2; B, 3' RACE product was generated by primers N1-RACE-F and AP1; C, Full-length *HEPN1* cDNA was amplified by end-to-end PCR using primers N1ful-F and N1ful-R. L, 1 kb DNA ladder.

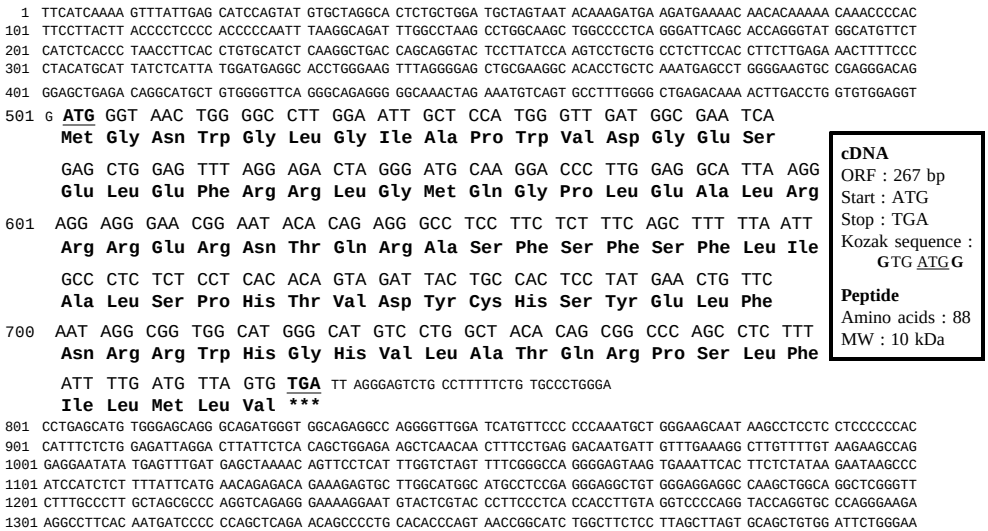

FIGURE 4-6 Sequences of *HEPN1* cDNA and the predicted amino acid. The full-length cDNA of *HEPN1* is approximately 1.4 kb long. The open reading frame (ORF), start codon (ATG), stop codon (TGA), and the Kozak sequence are highlighted. The sequence data for *HEPN1* is available in GenBank Accession no. AY275431.

was deposited into the GenBank (Accession no. AY275431). Based on this sequence, primers N1ful-F and N1ful-R corresponding to the 5' and 3' ends of *HEPN1* cDNA were synthesized and applied in end-to-end PCR to amplify the complete cDNA of *HEPN1*. The cDNA was then cloned into the pGEM-T vector and sequenced for verification.

4.1.3 Sequence characteristics of *HEPN1*

4.1.3.1 Sequence analysis of *HEPN1* cDNA

The full-length cDNA of *HEPN1* (Figure 4-6) contained an open reading frame (ORF) of 267 base pairs. The start codon ATG, the stop codon TGA, and the Kozak sequence (Kozak, 1990) surrounding the initiation codon were identified. However, no consensus polyadenylation signal was detected upstream of the poly-A tail. Searching *HEPN1* against human EST databases yielded a number of aligned fragments identified mainly in the brain.

4.1.3.2 Sequence analysis of HEPN1 protein

The putative HEPN1 peptide consisted of 88 amino acids (Figure 4-6) with a calculated molecular weight of ~10 kDa and a pI (isoelectric point) of 9.29. The gene product was predicted to be unstable with a half-life of ~30 hours in mammalian cells. The peptide had neither motifs nor significant structural or sequence homology in the available databases of proteins and peptides.

4.1.3.3 Sequence analysis of *HEPN1* genomic DNA

A BLAST search against the human genome database revealed that *HEPN1* was mapped to the sense strand of human chromosome 11 at q24.2 (Figure 4-7). Screening

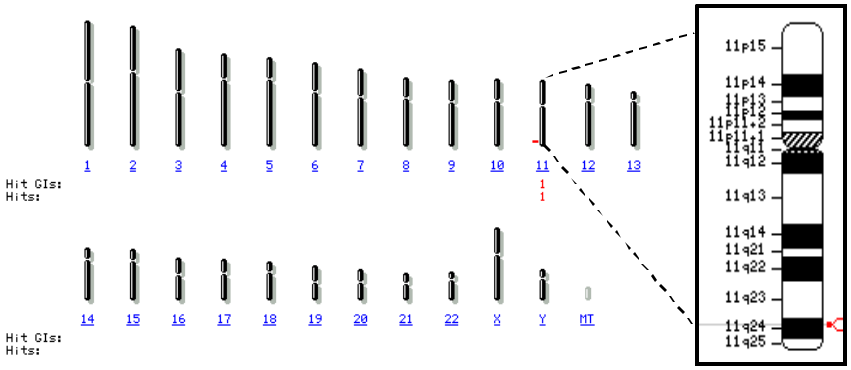

FIGURE 4-7 Chromosomal localization of *HEPN1* in human genome. *HEPN1* is mapped to chromosome 11q24.2.

the genomic sequence of *HEPN1* using the MatInspector program revealed a TATA box (TATTTAA) at position -57 upstream of the transcriptional start, indicative of a promoter. Comparative analysis revealed that *HEPN1* cDNA was collinear to the genomic sequence, suggesting that gene *HEPN1* is intronless.

4.1.4 Subcellular localization of HEPN1 in HepG2 cells

To localize *HEPN1* gene product in living cells, the construct expressing HEPN1-V5 fusion protein was transiently transfected into HEPN1-null HepG2 cells (Figure 4-3) for 48 hours and the distribution of the protein was detected by immunostaining with anti-V5 antibody. Cells transfected with pcDNA6B/V5-His vector served as control. Fluorescence microscopy showed that HEPN1 peptide was predominantly distributed in the cytoplasm (Figure 4-8).

4.1.5 Growth suppression in HepG2 cells by HEPN1

The biological role of HEPN1 was assessed in HepG2 cells. The construct HEPN1-pcDNA was transiently transfected into HepG2 cells. Cells transfected with pcDNA3.1 vector served as control. At 48 hours after transfection, the cells were subjected to light microscopy, MTT assay, and real-time RT-PCR analysis. Cell viability detected by MTT assay was computed into percentage against the control. As shown in Figure 4-9, re-expression of HEPN1 (real-time RT-PCR) decreased cell density, altered cell morphology (light microscopy), and reduced cell viability to 37.5±2.5% ($P = 0.001$).

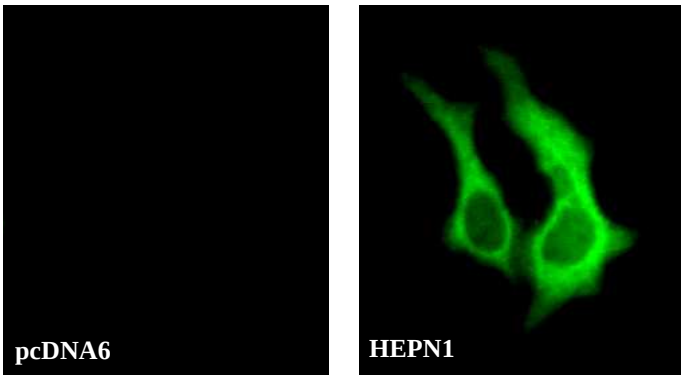

FIGURE 4-8 Subcellular localization of HEPN1 in HepG2 cells. HepG2 cells were transiently transfected with either pcDNA6B/V5-His vector (pcDNA6) or HEPN1-V5 construct (HEPN1) for 48 hours. Immunostaining with anti-V5 antibody visualized that HEPN1 was predominantly distributed in the cytoplasm.

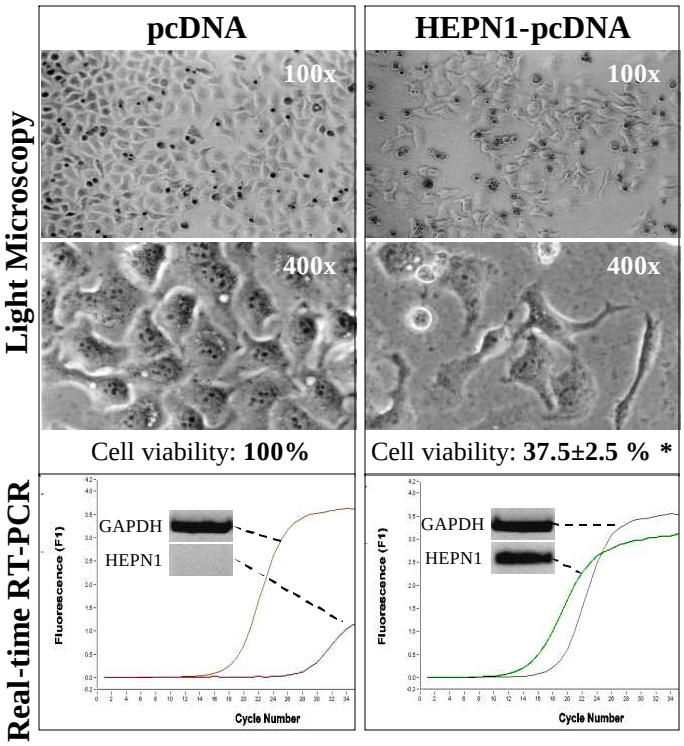

FIGURE 4-9 Growth inhibition of HepG2 cells by HEPN1. Transient transfection for 48 hours. Light microscopic photographs demonstrate the density (100x) and morphology (400x) of HepG2 cells transfected with HEPN1-pcDNA (right panel) in contrast to the control, cells transfected with pcDNA3.1 vector alone (left panel). Cell viability (mean ± SD, n = 12) was detected by MTT assay and computed into percentage against the control; * P = 0.001. Real-time RT-PCR results show the expression level of *HEPN1* in the transfected HepG2 cells. GAPDH was used as control. The RT-PCR products were analyzed by gel electrophoresis to verify the specificity.

Colony formation was performed to confirm the inhibitory effect of HEPN1 on cell growth. HepG2 cells transfected with HEPN1-EGFP and selected in 800 μg/ml of G418 antibiotic for 2 weeks were compared with those transfected with pEGFP-N2 vector. Green fluorescent protein facilitated the visualization of cells in each colony. The results (Figure 4-10) demonstrated that, in addition to the significant reduction of the number of colonies formed, the number of fluorescent cells in the cells transfected with HEPN1-EGFP was extremely low as compared to that in the cells transfected with pEGFP-N2 vector alone.

4.1.6 Apoptosis induction in HepG2 cells by HEPN1

To explore if HEPN1 could promote cell death, HepG2 cells were transfected with either HEPN1-EGFP construct or pEGFP-N2 vector. Between 8 and 24 hours post-transfection, cells were analyzed by fluorescence microscopy every 2 hourly. Figure 4-11 showed the cell behaviour of HepG2 cells transfected with *HEPN1* in contrast with the control cells. After transfection, 1) at hour 8, HEPN1 started being expressed predominantly in cytoplasm; 2) at hour 10, the expression level was increased and concentrated in granular structures; 3) at hour 12, HEPN1 was distributed more in the perinuclear region; 4) at hour 14, HEPN1 started translocating into cell nuclei; and from hour 16 onwards, typical apoptotic morphology including cytoplasm shrinking (16 h), cell blebbing (18 h), and nuclear fragmentation (20h and 22h) was observed. At hour 24, the number of cells transfected with HEPN1-EGFP was considerably reduced compared to that at hour 12 presented in the inset. The control cells transfected with pEGFP-N2 vector alone remained unchanged throughout.

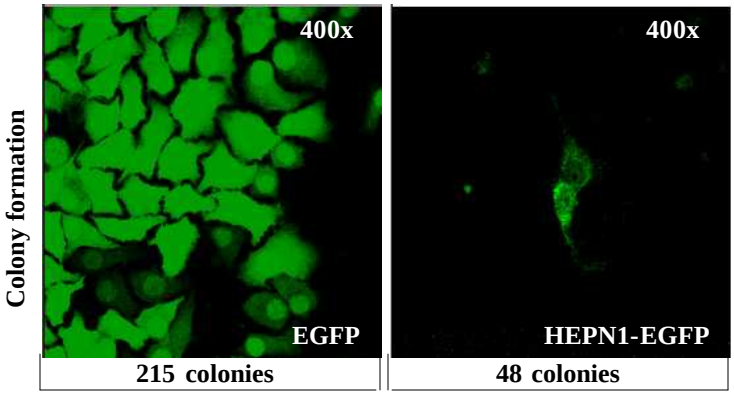

FIGURE 4-10 Inhibition of colony formation by HEPN1. HepG2 cells transfected with the plasmid HEPN1-EGFP (right panel) or pEGFP-N2 vector (left panel) were cultured in the presence of 800 μg/ml of G418 for 2 weeks before confocal microscopy. The density and morphology of cells in a colony were visualized by green fluorescence. The number of colonies presented at the bottom of each picture was counted manually.

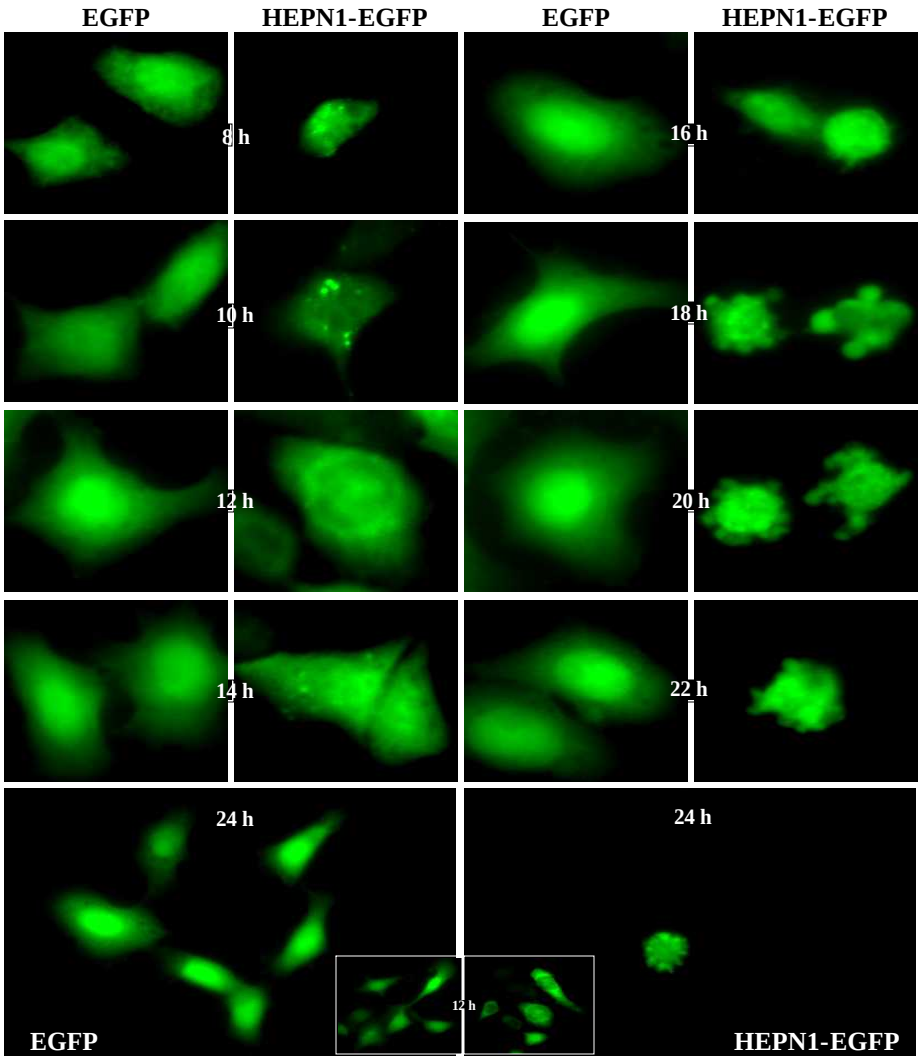

FIGURE 4-11 Induction of apoptosis in HepG2 cells by HEPN1. HepG2 cells were transfected with either pEGFP-N2 vector (EGFP) or HEPN1-EGFP construct. Between 8 and 24 hours after transfection, cells were analyzed by fluorescence microscopy every 2 hourly to visualize cell number, cell morphology and distribution of HEPN1. Microphotographs are presented at each time point and indicated as 8h, 10h, 12h, 14h, 16h, 18h, 20h, 22h, and 24h, respectively. An entire microscopic view at 24h is compared to that at 12h (inset), showing the reduction of cell number when HEPN1 was re-expressed.

In addition, Annexin V was used to determine if cells were indeed undergoing apoptosis. Since Annexin V detects changes in the position of PS in the cell membrane, one of the earliest changes of apoptotic cells, HepG2 cells were examined at 16 hours after transfection. As shown in Figure 4-12, positive Annexin V-PS binding on the cell membrane was observed in cells transfected with HEPN1-pcDNA but not in the cells transfected with pcDNA3.1 vector alone.

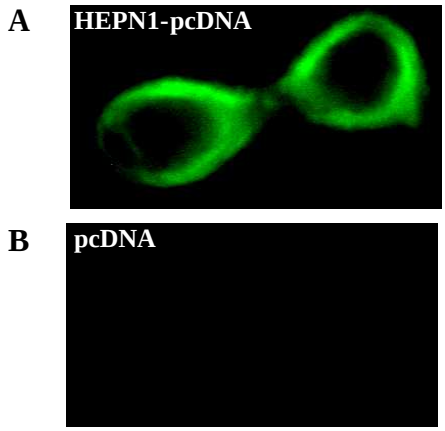

FIGURE 4-12 Detection of HEPN1-induced apoptosis by Annexin V assay. The fluorescent rings represent positive binding of Annexin V with PS in the cell membrane, an early indication of apoptosis. A, HepG2 cells transfected with HEPN1-pcDNA construct; B, HepG2 cells transfected with the empty vector pcDNA3.1 (pcDNA).

4.2 Gene *hepaCAM*

4.2.1 Identification of *hepaCAM*

As illustrated in Figure 4-13, an updated BLAST search with *HEPN1* revealed an uncharacterized mRNA sequence of 2465 bp in the database (GenBank Accession no. AL834419). AL834419 contained the entire antisense strand of *HEPN1* in its 3' UTR and encoded an incomplete hypothetical protein of 165 amino acids at the 5' terminus of the sequence. The lack of 5' UTR and putative start codon (ATG) on AL834419 implicated that the sequence was incomplete.

4.2.2 Isolation of *hepaCAM* full-length cDNA

The primer hCAM-RACE-R was designed at the 5'-end of *HEPN1* antisense strand. Used in combination with adaptor primer AP1 in 5' RACE (Figure 4-14), the complete cDNA of a novel gene, designated as *hepaCAM*, was isolated from human normal liver cDNA library. Q solution was added into the RACE-PCR reaction admixture as a PCR enhancer for amplifying the GC-rich template of *hepaCAM*. The cDNA was cloned into pGEM-T vector and sequenced. The full-length cDNA sequence of *hepaCAM* was submitted to the GenBank (Accession no. AY047587).

4.2.3 Sequence characteristics of *hepaCAM*

4.2.3.1 Sequence analysis of *hepaCAM* cDNA

The full-length cDNA of *hepaCAM* was 3244 bp long (Figure 4-15). It contained a 5' UTR of 44 bp, a deduced coding region of 1251 bp with ATG as start codon and TGA as stop codon, and a 3' UTR of 1949 bp. An in-frame termination codon TAG was present at 24 nucleotides upstream of the putative initiating methionine, indicating the completion of the ORF. A Kozak sequence (AAAATGA) surrounding the start codon

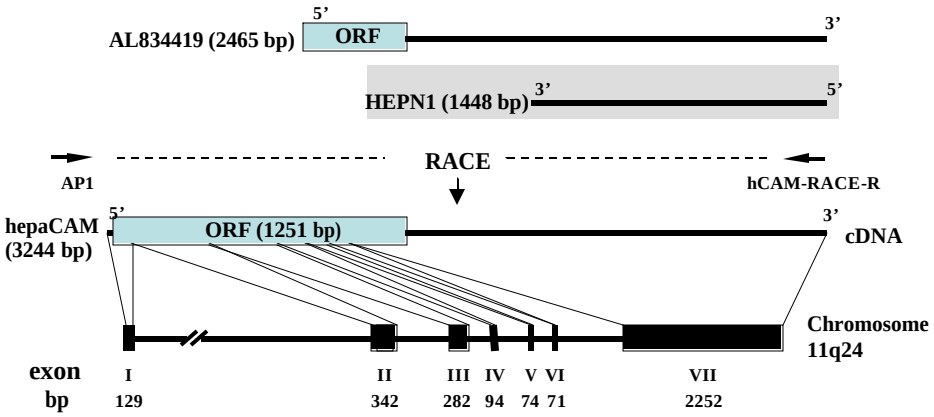

FIGURE 4-13 Molecular cloning of *hepaCAM*. The full-length cDNA of *hepaCAM* was isolated from normal human liver cDNA library by RACE. A forward primer on the adaptor (AP1) and a gene specific primer hCAM-RACE-R at the 5'-end of *HEPN1* antisense strand were used in the RACE reaction. The cDNA lengths of *hepaCAM*, *HEPN1* and sequence AL834419 are given in the brackets. The indications of 5' and 3' correspond to the orientations of the cDNAs. The genomic DNA of *hepaCAM* mapped to human chromosome 11q24 contains 7 exons indicated as I – VII and accompanied by their respective length in base pairs (bp).

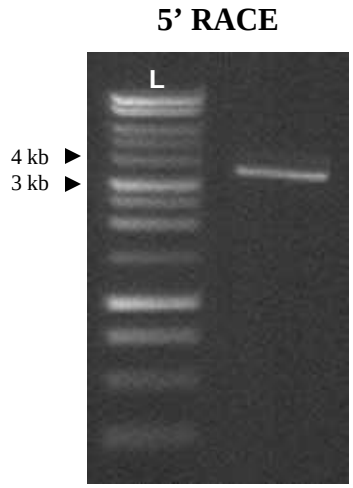

FIGURE 4-14 Isolation of *hepaCAM* full-length cDNA by 5’ RACE. 5’ RACE product was generated by primers hCAM-RACE-R and AP1. The RACE-PCR product was analyzed by gel electrophoresis. L, 1 kb DNA ladder.

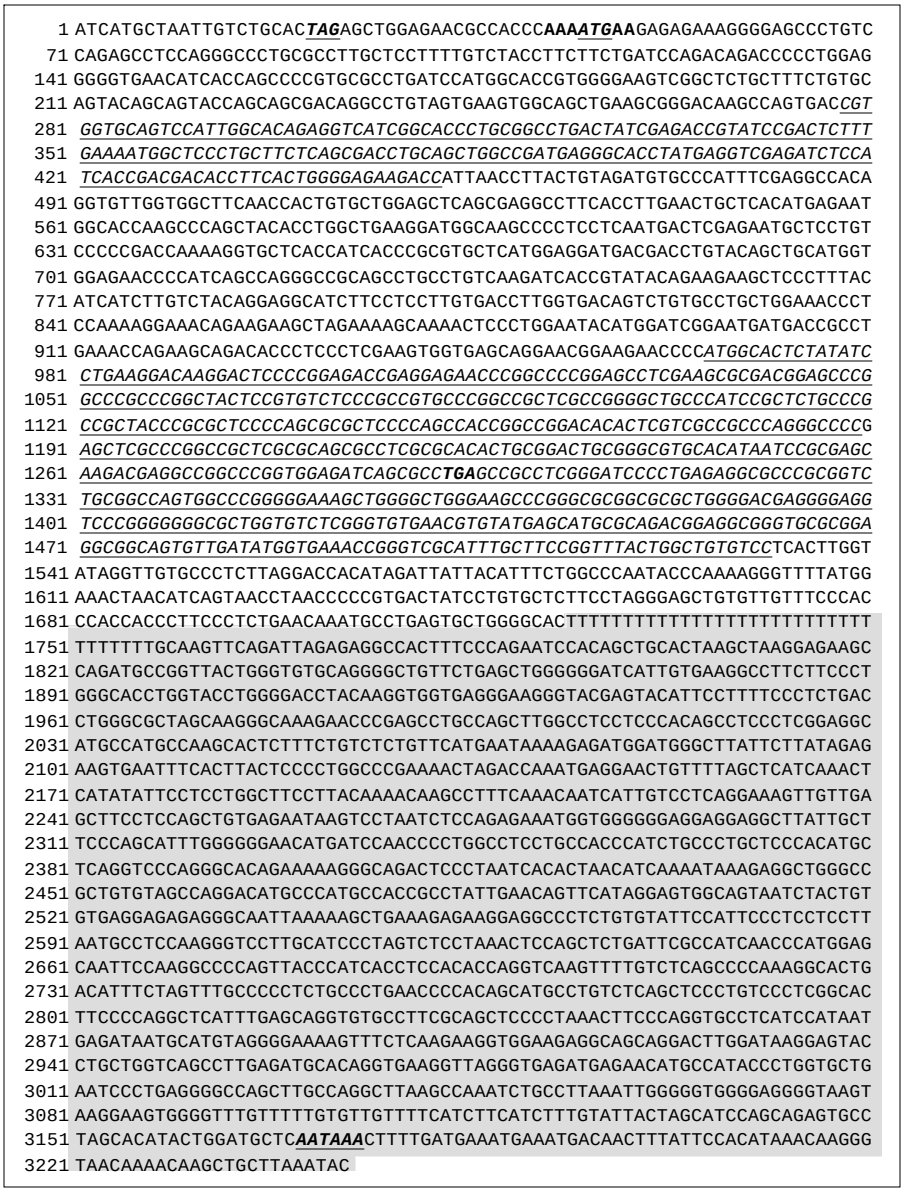

FIGURE 4-15 The full-length cDNA sequence of *hepaCAM*. The full-length cDNA contains an ORF that begins from the start codon (ATG) and ends at the stop codon (TGA). A 5'-untranslated region containing a termination signal (TAG) indicates the completion of the ORF. A consensus Kozak (AAAATGA; bold) sequence surrounds the start codon. The polyadenylation signal (AATAAA; bold italic) is identified near the 3'-terminus. The full-length sequence of *HEPN1* antisense strand (shaded) is localized within the 3'-untranslated region (1949 bp long). The GC-rich region is underlined and italicized. The sequence data for *hepaCAM* is available in GenBank Accession no. AY047587.

as well as a polyadenylation sequence (AATAAA), which signals for poly-A addition, was identified in the sequence. Interestingly, CpG plot analysis predicted a short GC-rich region of 176 bp (nucleotides 277-452) at the 5' ORF of *hepaCAM*; and a long GC-rich region of 566 bp (nucleotides 966-1531) that spanned the 3' ORF and 3' UTR of *hepaCAM* cDNA.

4.2.3.2 Protein sequence and structure of hepaCAM

Gene *hepaCAM* was predicted by the SMART algorithm and SignalP server to encode a novel type I integral transmembrane Ig-like cell adhesion molecule of 416 amino acids (Figure 4-16). The protein contained an extracellular domain comprising a signal peptide (residues 1-33) and two Ig-like loops (residues 40-142; 159-224), a transmembrane segment (residues 241-263), and a cytoplasmic tail (residues 264-416).

Motif searches by the PROSITE and PSORT II programs identified a leucine zipper (residues 181-202), a proline-rich region (residues 325-385) with 6 SH3-binding domains, a nuclear localization signal (residues 265-271), a cAMP- and cGMP-dependent protein kinase phosphorylation site (residues 237-240), a prokaryotic membrane lipoprotein lipid attachment site (residues 252-262), two tyrosine sulfation sites (residues 113-127; 274-288), two *N*-myristoylation sites (residues 33-38; 173-178), four casein kinase II phosphorylation sites (residues 60-63; 125-128; 156- 159; 331-334), six protein kinase C phosphorylation sites (residues 62-64; 90-92; 266-268; 357-359; 371-373; 394-396), and six *N*-glycosylation sites (residues 35-38; 104-107; 138-141; 167-170; 172-175; 189-192).

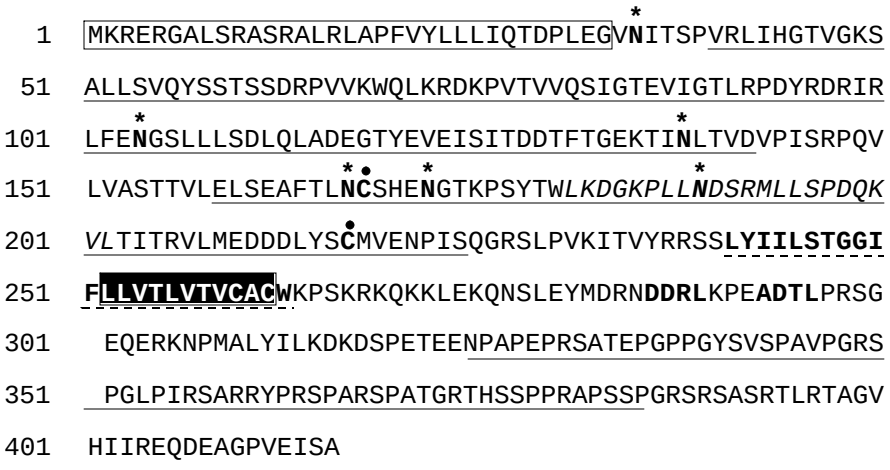

FIGURE 4-16 Predicted amino acid sequence of hepaCAM. Gene *hepaCAM* encodes a putative protein of 416 amino acids. The fragment highlighted in the box is the signal peptide (33 amino acids). The regions underlined with solid lines are the two immunoglobulin-like (Ig-like) domains (103 and 66 amino acids, respectively), while the one underlined with dashed line is the transmembrane domain (23 amino acids). Two cysteine residues (marked underneath the "•") are identified in the second Ig-like domain, which may be needed for the formation of the disulfide bond in the domain. Six asparagines (marked underneath the "*") are in the extracellular region, which represent the potential *N*-linked glycosylation sites. The leucine zipper is italicized. The prokaryotic membrane lipoprotein lipid attachment site (shaded) is located in the transmembrane domain; and a proline-rich region (dotted underline) is present in the cytoplasmic region.

Furthermore, scansite analysis of hepaCAM protein revealed binding sites for 14-3-3 (residues 333, 376, 390), ATM kinase (residue 127), ITK kinase (residue 242), p85 SH3 (residues 354; 365), Cbl-associated protein C-SH3 (residues 347; 385), Intersectin SH3 (residue 347), protein kinase C (residue 278), Akt kinase (residue 392), Clk2 kinase (residue 392), GSK3 kinase (residue 384), Cdk5 kinase (residues 377; 384), and Cdc2 kinase (residues 377; 384).

Other potential motifs included eight dileucine motifs (residues 22-23; 23-24; 57-57; 107-108; 108-109; 187-188; 194-195) distributed in the signal peptide, extracellular and transmembrane domains of hepaCAM. In addition, two potential palmitoylation sites were recognized in the transmembrane domain (Cys260; Cys262). The big-PI program predicted a potential C-terminal GPI-modification site at residue 399.

A database search on the deduced protein of *hepaCAM* revealed sequence homology, mainly at the extracellular domain, between hepaCAM and other Ig-like cell adhesion molecules (Figure 4-17) such as coxsackie virus and adenovirus receptor (CAR; GenBank Accession no: AAX41267) and CEACAM3 (GenBank Accession no: AAQ88451). Furthermore, hepaCAM displayed structural similarities to Ig-like cell adhesion molecules like JAM1, CAR and ESAM (Figure 4-18). Typically, they contained an extracellular domain with two Ig-like domains (V and C2 domains), a transmembrane segment, and a cytoplasmic tail. Two cysteine residues flanking the C2 Ig domain of hepaCAM contributed to the formation of intrachain disulfide-linked loop.

A

```
hepaCAM          1 MKRERGALSRASRALRLAPFVYLLLIQTDPLEGVNITSPVRLIHGTVGKS     50
                                || |  || ||    |      || |   |    |
CAR              1            malllc-fv-llcgvvdftrslsittpeemiekakget     36

hepaCAM         51 ALLSVQYSSTSSDR-PV-VKWQLKRDKPVTVVQSI----GTEVIGTLRPD     94
                   | |         |  |    |         | | |    |        ||
CAR             37 aylpckftlspedqgpldiewlispadnqkvdqviilysgdkiyddyypd     86

hepaCAM         95 YRDRIRLFEN------GSLLLSDLQLADEGTYEVEISITDDTFTGEKTIN    138
                      |     |       |     ||| | |||              | |
CAR             87 lkgrvhftsndlksgdasinvtnlqlsdigtyqckvkkapg--vankkih    134

hepaCAM        139 LTVDVPISRPQVLVASTTVLELSEAFTLNCSHENGTKP-SYTWLKDGKPL    187
                   | | |  |     |      |    |   |    |  |  | | |
CAR            135 lvvlvkpsgarcyvdgse--eigsdfkikcepkegslplqyewqk-----    177

hepaCAM        188 LNDSR-----MLLSPDQKVLTITRVLMEDDDLYSCMVENPISQGRSLPVK    232
                   | ||       |      |        |    ||| | |       |
CAR            178 lsdsqkmptswlaemtssvisvknasseysgtysctvrnrvgsdqcl-lr    226

hepaCAM        233 ITVYRRSS-----LYIILSTGGIFLLVTLVTVCACWKPSKRKQKKLEKQN    277
                     |   |         |  |     |  |   | | |  ||   | ||
CAR            227 lnvvppsnkagliagaiigtllalaligliifc-crk--krreekyeke-    272
```

B

```
hepaCAM          1        MKRE----RGALSRAS-RALRLAPFVYLLLIQTDPLEGVNITS     38
                            ||     | |  ||      ||    | |   | |
CEACAM3          1 mgppsacphrecipwqgllltaslltfwnapttawlfiasapfevae---     47

hepaCAM         39 PVRLIHGTVGKSALLSVQYSSTSSDRPVVKWQLKRDKPVTVVQSIGTEVI     88
                           |    ||| |                  | |   | |   ||
CEACAM3         48 ---------genvhlsvvylpen----lysygwykgktvepnqliaayvi     84

hepaCAM         89 GT-LR---PDYRDRIRLFENGSLLLSDLQLADEGTYEVEISITDDTFTGE    134
                    |  |   | |  |      | |      | | | |
CEACAM3         85 dthvrtpgpaysgretispsgdlhfqnvtledtgyynlqvtyrnsqie-q    133

hepaCAM        135 KTINLTVDVPISRPQVLVASTTVLELSEAFTLNCSHENGTKPSYTWLKDG    184
                       | |      |     |||| |      | | | | |  |  |
CEACAM3        134 ashhlrvyesvaqpsiqassttvte-kgsvvltc-htnntgtsfqwifnn    181

hepaCAM        185 KPLLNDSRMLLSPDQKVLTITRVLMEDDDLYSCMVENPISQGRSLPVKIT    234
                     |    || ||    ||||     ||   | | | || |  || | | |
CEACAM3        182 qrlqvtkrmklswfnhvltidpirqedageyqcevsnpvssnrsdplklt    231

hepaCAM        235 VYRRSSLYIILSTGGIFLLVTLVTVCACWKPSKRKQKKLEKQNSLEYMDR    284
                   |     | |     |      ||    |          |         |
CEACAM3        232 vkydntlgili---gvlvgsllvaalvcf---------lllrktgrasdq    269
```

FIGURE 4-17 Sequence comparison between hepaCAM protein and other immunoglobulin-like adhesion molecules. A, Sequence homology between hepaCAM and coxsackie virus and adenovirus receptor (CAR; GenBank Accession no: AAX41267). B, Sequence homology between hepaCAM and CEACAM3 (GenBank Accession no: AAQ88451). Bar represents identity.

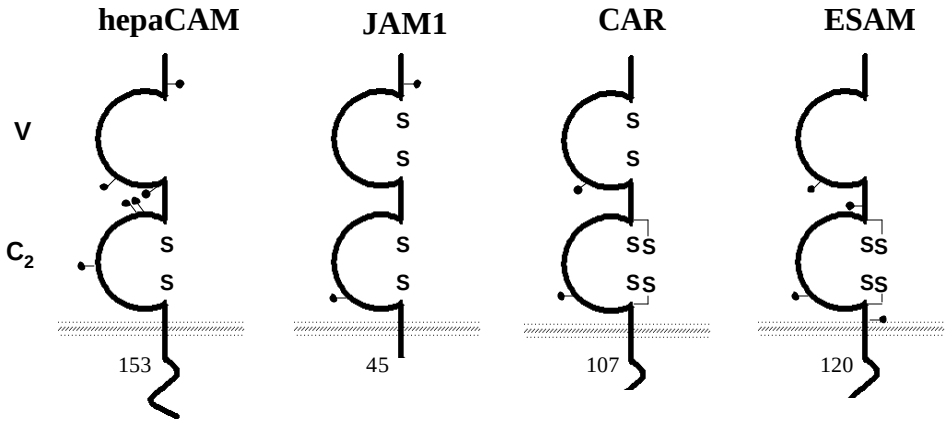

FIGURE 4-18 Structural comparison between hepaCAM protein and other immunoglobulin-like adhesion molecules. hepaCAM owns the typical structure of cell adhesion molecules belonging to the immunoglobulin superfamily. Like JAM1, CAR and ESAM, hepaCAM contains a V-type and a C2-type Ig-domain on its extracellular domain, a transmembrane segment, and a cytoplasmic tail. Putative *N*-linked glycosylation sites are marked by dots. Disulfide bridges and putative additional intramolecular disulfide bridges formed by cysteine residues in the C2-type Ig-domain are indicated. The lengths of the intracellular domains are indicated at the bottom of each molecule (Modified from Ebnet *et al*., 2004).

Alignment of the predicted amino acid sequence of human hepaCAM protein with those of chimpanzee (424 amino acids, GenBank Accession no. XP_522240), mouse (418 amino acids, GenBank Accession no. NP_780398), and dog (418 amino acids, GenBank Accession no. XP_852267) demonstrated an extremely conserved sequence with identities of 95%, 94% and 93%, respectively (Figure 4-19).

4.2.3.3 Sequence analysis of *hepaCAM* genomic DNA

A BLAST analysis was performed using the *hepaCAM* full-length cDNA sequence against the working draft sequences of the human genome in the NCBI database. Gene *hepaCAM* was mapped to the minus strand of the human chromosome 11q24.2 and contained 7 exons ranging in sizes from 71 to 2252 bp (Figure 4-13). The start codon was located in exon 1 and the stop codon was positioned in exon 7. Intron sizes varied greatly from the longest intron 1 (10,851 bp) to the shortest intron 5 (285 bp). As listed in Table 4-2, all the exon/intron boundaries conformed to the GT-AG splicing signal rules.

The MatInspector program predicted three binding sites for the tumor suppressor p53 in *hepaCAM* genomic DNA. Two of the binding sites were situated in intron 1 at nucleotides 256-276 (aaacatgtcagggaattcagg) and nucleotides 8294-8314 (caccatgcccggcctgtttct), while the other binding site was situated in intron 2 at nucleotides 11760-11780 (gttcatggcaaggcatttgga). No sequence pattern that resembled a promoter was detected in the genomic sequence of *hepaCAM* upstream of the transcriptional start.

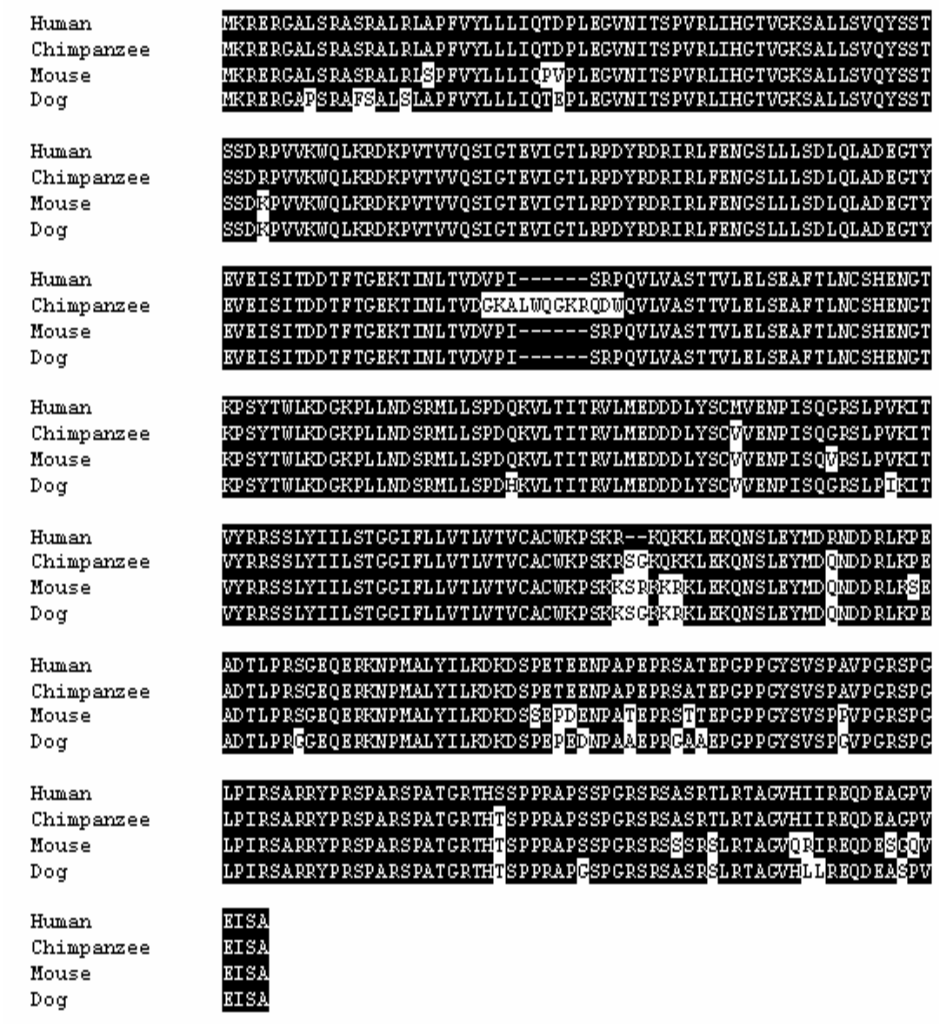

FIGURE 4-19 Comparison of hepaCAM orthologues. Inverted shade indicates identity. The sequence data for human, chimpanzee, mouse and dog are available in GenBank Accession nos. AY047587, XP_522240, NP_780398 and XP_852267, respectively.

TABLE 4-2 Intron/Exon boundaries of *hepaCAM*

Exon	Nucleotide position	3' Splice acceptor	Exon Size (bp)	5' Splice donor	Intron Size (bp)
1	1-129	ggag**aa**ATCATG	129	AGACAG**gt**agga	10,851
2	130-471	tcac**ag**ACCCCC	342	TAGATG**gt**aaag	716
3	472-753	gctc**ag**TGCCCA	282	TATACA**gt**gagt	294
4	754-847	ccct**ag**GAAGAA	94	CAAAAG**gt**ctgg	520
5	848-921	tcac**ag**GAAACA	74	CAGAAG**gt**gagc	285
6	922-992	gtgc**ag**CAGACA	71	GACAAG**gt**gagc	946
7	993-3244	ttgc**ag**GACTCC	2252		

Nucleotide sequences indicated at the intron (lowercase letters) and exon (uppercase letters) junctions. Exon and intron sizes are indicated in bp.

4.2.4 Expression of *hepaCAM* in human tissues and cell lines

4.2.4.1 Expression of *hepaCAM* in normal human tissues

hepaCAM mRNA and protein were found to be widely expressed in normal human tissues. A search of *hepaCAM* cDNA sequence against the human EST databases retrieved a number of fragments identified in normal tissues of the liver, brain, breast, muscle, lung, retina, uterus, and *etc*. In addition, according to the GeneNote database of human genes and their expression profiles in healthy tissues (http://genecards.weizmann.ac.il), *hepaCAM* was expressed in all 12 human tissues tested, with the highest expression in spinal cord (Figure 4-20). A pair of primers hCAM-F and hCAM-R that was specific for *hepaCAM* and not associated with the *HEPN1* sequence was used in semi-quantitative RT-PCR to detect the expression of *hepaCAM* in normal human liver tissues. The result showed that *hepaCAM* was ubiquitously expressed at a similar level in all the six normal liver tissues (Figure 4-21). Furthermore, Western blot analysis with anti-hepaCAM polyclonal antiserum confirmed the protein expression of hepaCAM in all the 6 normal liver tissues (Figure 4-22).

4.2.4.2 Suppression of *hepaCAM* in HCC tissues

Gene *HEPN1* was frequently downregulated in HCC. To evaluate if *hepaCAM* was also differentially expressed in HCC, the mRNA levels of *hepaCAM* were examined in 23 paired liver samples obtained from HCC patients using primers hCAM-F and hCAM-R. Semi-quantitative RT-PCR results showed that *hepaCAM* was downregulated in 87% (20/23) of HCC tissues when compared to their non-tumorous counterparts (Figure 4-23).

A

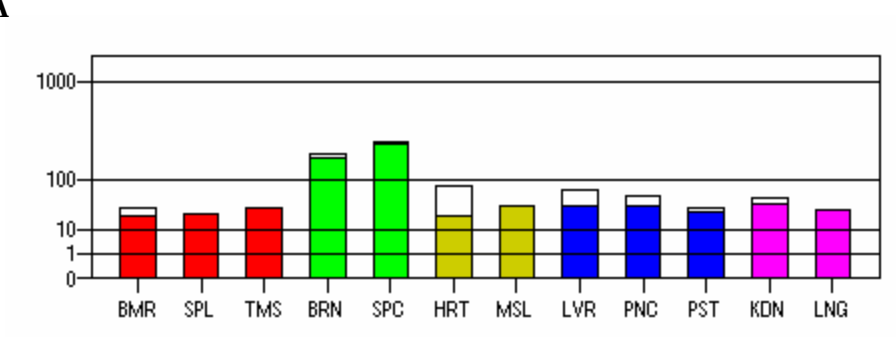

B

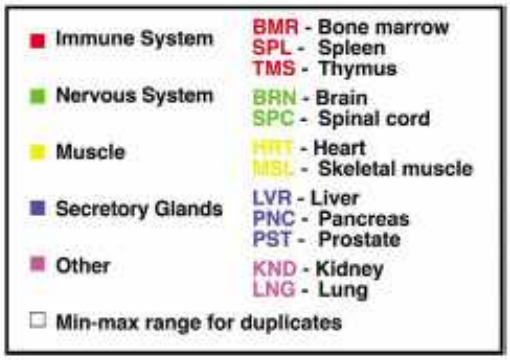

FIGURE 4-20 Expression of *hepaCAM* transcript in normal tissues (GeneNote expression array). A, The expression level of *hepaCAM* in normal human tissues was calculated from the normalized signals and is presented in a graphical way. Tissues were grouped according to their origin and the groups colored accordingly. The range between the lower and higher measurements was represented by a white box above the colored minimal measurement bar. The graph is presented on the *y*-axis with a special root scale $Y = X^{(1/B)}$ where $B = \log_2 10$ (Safran *et al.*, 2003). B, The tissue vector colored map.

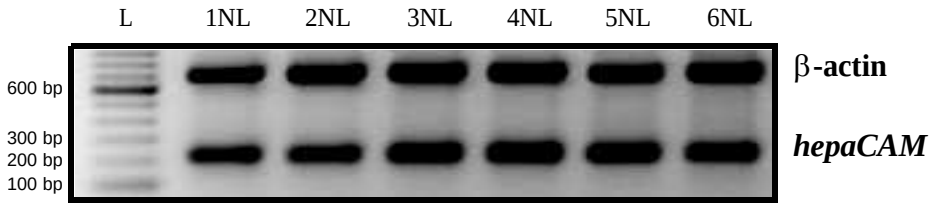

FIGURE 4-21 Expression of *hepaCAM* transcript in normal liver tissues. Semi-quantitative RT-PCR using *hepaCAM*-specific primers hCAM-F and hCAM-R was performed to determine the mRNA expression of hepaCAM in 6 normal liver tissues obtained from 6 individuals. RT-PCR products were analyzed by gel electrophoresis. β-actin were included in the RT-PCR reaction as internal control. The samples are labeled from 1 to 6; NL, normal liver. L, 100 bp DNA ladder.

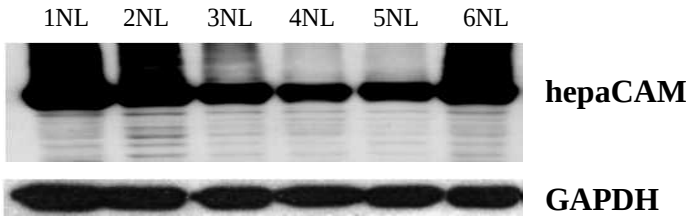

FIGURE 4-22 Expression of hepaCAM protein in normal liver tissues. Western blot analysis with rabbit anti-hepaCAM polyclonal antiserum revealed the endogenous hepaCAM protein levels in 6 normal liver tissues. GAPDH protein level indicates the loading quantity. The samples are labeled from 1 to 6; NL, normal liver.

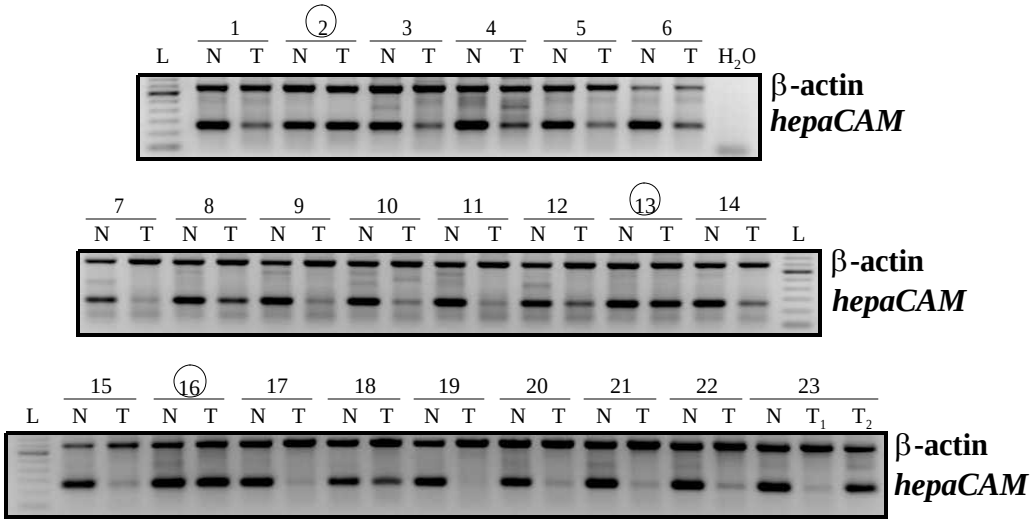

FIGURE 4-23 Expression of *hepaCAM* transcript in 23 HCC patients. Semi-quantitative RT-PCR products generated using *hepaCAM*-specific primers hCAM-F and hCAM-R were analyzed by gel electrophoresis. β-actin was included as internal control. ◯, sample that shows no clear difference in *hepaCAM* expression; L, 100 bp DNA ladder; N, non-tumorous liver tissue; T, HCC liver tissue; Patient 23 had two HCC nodules (T_1 and T_2) in the liver.

4.2.4.3 Suppression of *hepaCAM* in HCC cell lines

In addition, semi-quantitative RT-PCR using primers hCAM-F and hCAM-R was carried out to analyze the expression of *hepaCAM* in 5 human HCC cell lines HepG2, Hep3B, Huh7, SK-Hep1 and PLC-5 (Figure 4-24). While *hepaCAM* mRNA was detected in the normal liver tissue that was included as a positive control, the transcript was undetectable in all the five HCC cell lines.

4.2.4.4 Suppression of *hepaCAM* in cell lines derived from diverse tumors

Furthermore, the expression of *hepaCAM* transcript was screened in six human cancer cell lines M14, HL60, NCI-H23, MCF7, Hs683, and HCT116 derived from melanoma, leukemia, lung cancer, breast cancer, glioblastoma and colorectal cancer, respectively (Figure 4-24). Semi-quantitative RT-PCR showed that *hepaCAM* mRNA was undetectable in all these cell lines.

4.2.4.5 Suppression of *hepaCAM* in tissues derived from diverse tumors

The Matched Tumor/Normal Expression Array from Clontech was used to examine the expression profile of *hepaCAM* transcript in a panel of human tumors derived from kidney, breast, prostate, uterus, ovary, colon, lung, stomach and rectum (Figure 4-25). Dot blotting was performed on the membrane by using a DIG-labeled *hepaCAM* cDNA as a probe. Subsequently, the intensity of the dots obtained in the normal tissue as compared to its matched tumor was measured. Loading of the cDNAs was normalized for housekeeping gene ubiquitin to enable quantitative comparisons between gene expressions in different tissues. Downregulated expression of *hepaCAM* in tumor tissue as compared with the normal tissue was observed in 36.4% of the patients, while 44% showed no significant change in *hepaCAM* expression levels and

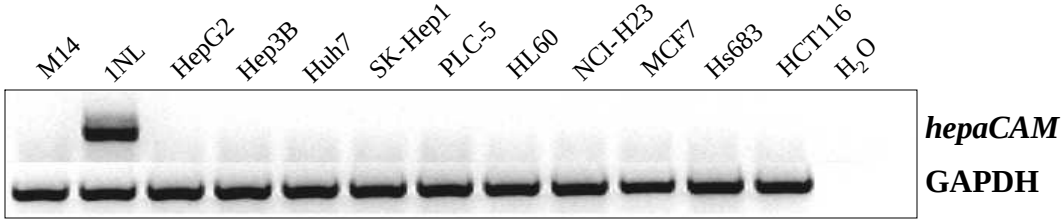

FIGURE 4-24 Expression of *hepaCAM* transcript in cancer cell lines. Semi-quantitative RT-PCR was used to amplify *hepaCAM* mRNA and GAPDH mRNA (internal control). RT-PCR products were analyzed by gel electrophoresis. The expression levels of *hepaCAM* in the cancer cell lines were compared to that in the normal liver tissue 1NL.

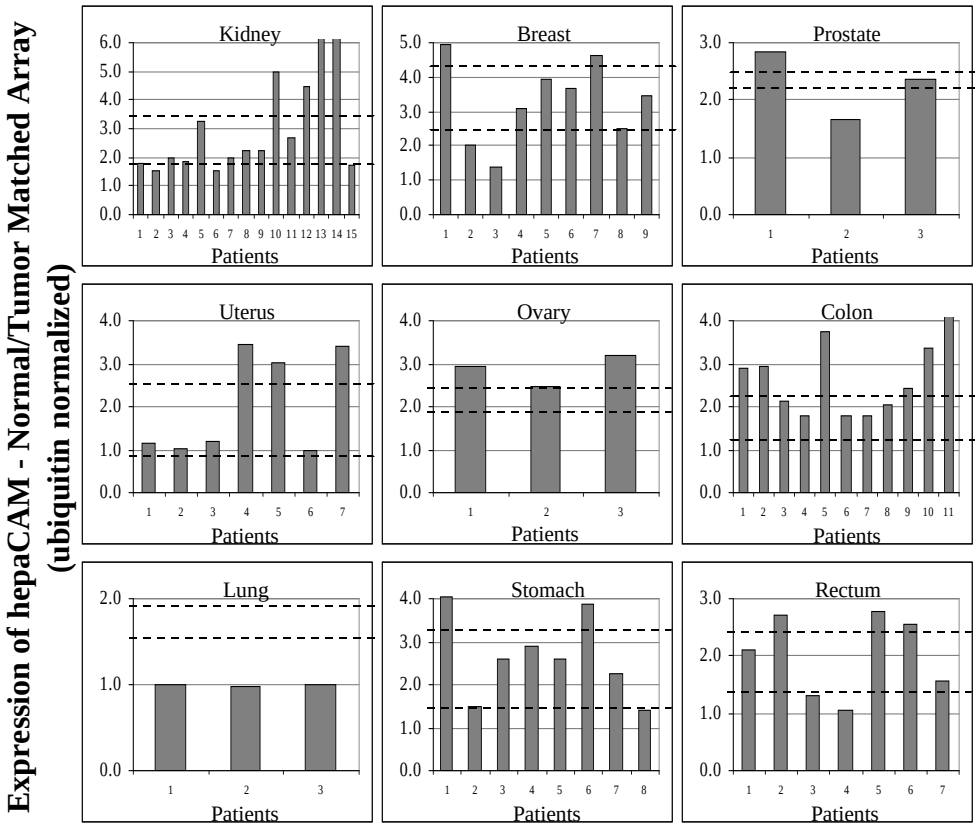

FIGURE 4-25 Expression of *hepaCAM* transcript in a panel of human tumors. *hepaCAM* mRNA expression was measured on the Matched Tumor/Normal Expression Array. Densitometric values were normalized to those for ubiquitin. The ratio obtained between normal and tumor tissue of each patient is shown. The broken line represents the standard deviation obtained from the hepaCAM/ubiquitin ratio derived from the normal tissues.

19.7% of tumors exhibited higher *hepaCAM* levels. The most striking examples were the ubiquitous decreased levels of *hepaCAM* mRNA in ovary tumor samples and the elevated levels of *hepaCAM* mRNA observed in all the lung tumor samples tested.

4.2.5 Plasmid constructs of wildtype and truncated mutants of *hepaCAM*

In order to investigate the function(s) and the structural significance of *hepaCAM*, a series of *hepaCAM* deletion mutants were constructed. Mutants with truncations at the cytoplasmic domain (Figure 4-26A) included hCAM△320 (deletion of residues 321-416); hCAM△318 (deletion of residues 319-416); hCAM△290 (deletion of residues 291-416); and hCAM△263 (deletion of the entire domain from residues 264-416); while those with truncations at the extracellular/transmembrane domains (Figure 4-26B) included hCAMΔ1st Ig (deletion of the 1st Ig domain at residues 33-145); hCAMΔ2nd Ig (deletion of the 2nd Ig domain at residues 155-227); hCAMΔIgs (deletion of the 1st and 2nd Ig domains at residues 33-227); and hCAM_tail (deletion of the signal peptide, extracellular and transmembrane domains).

Wildtype *hepaCAM*, hCAM△320, and hCAM△263 were fused in-frame at the N-terminal of the green fluorescent protein (GFP) gene of the expression vector pEGFP-N2. The resulting plasmids were named as hepaCAM-GFP, hCAM△320-GFP, and hCAM△263-GFP, respectively. In addition, wildtype *hepaCAM*, hCAM△318, hCAM△290, hCAM△263, hCAMΔ1st Ig, hCAMΔ2nd Ig, hCAMΔIgs, and hCAM_tail were inserted at the N-terminal of the V5 tag of the pcDNA6B/V5-His vector, and were designated as hepaCAM-V5, hCAM△318-V5, hCAM△290-V5, hCAM△263-V5, hCAMΔ1st Ig-V5, hCAMΔ2nd Ig-V5, hCAMΔIgs-V5, and

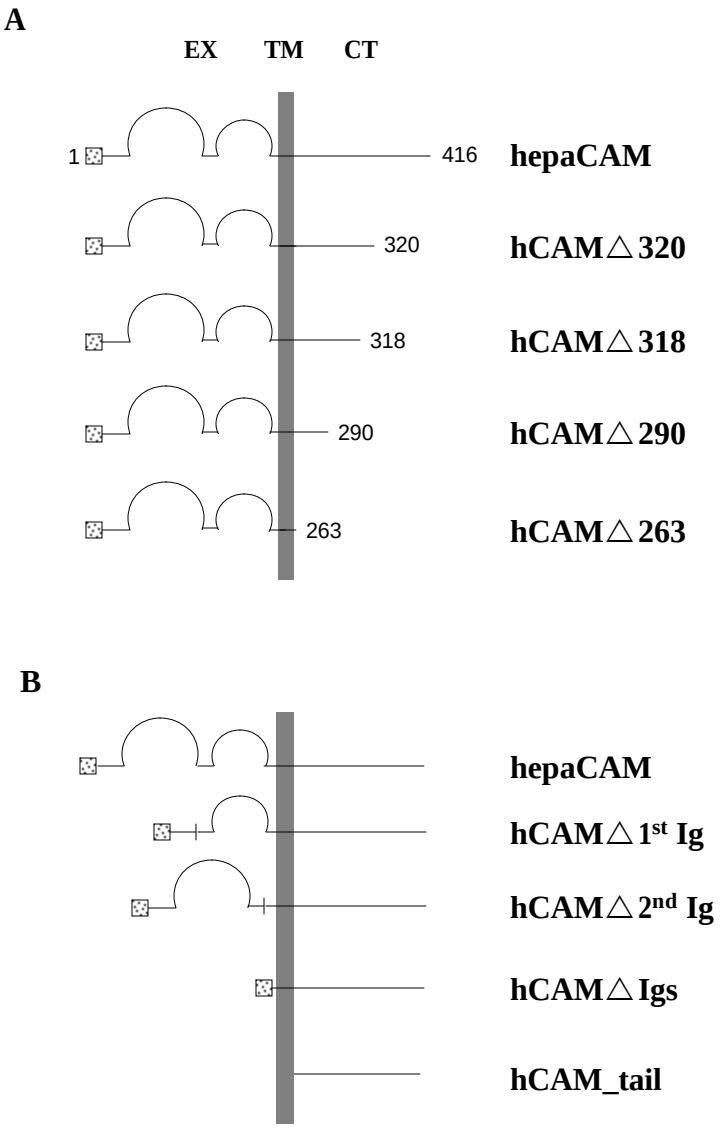

FIGURE 4-26 Schematic representation of wildtype hepaCAM and mutants. A, wildtype and cytoplasmic domain mutants of hepaCAM. B, wildtype and extracellular/transmembrane domain mutants of hepaCAM. EX, extracellular domain; TM, transmembrane domain (grey); CT, cytoplasmic domain; dotted box, signal peptide; loop, Ig domain; bar, sequence break.

hCAM_tail-V5, respectively.

4.2.6 Establishment of stable clones of HepG2 and MCF7 transfectants

4.2.6.1 HepG2 stable clones

HepG2 cells were stably transfected with pcDNA6B/V5-His vector and hepaCAM-V5. Two clones stably transfected with vector (V1 and V2) and 3 clones with hepaCAM-V5 (H1, H2 and H3) were screened. Cell lysates of these cells were subjected to Western blot analysis with anti-V5 antibody (Figure 4-27). The result showed that hepaCAM was absent in the vector clones V1 and V2, and expressed in 2 (among 3) hepaCAM clones H1 and H3. Real-time RT-PCR using *hepaCAM*-specific primers hCAM-F and hCAM-R showed that *hepaCAM* mRNA was expressed in clones H1 and H3 but not overexpressed when compared to the normal liver tissues, and was expectedly absent in clones V1, V2 and H2 (Figure 4-28). Immunostaining with anti-V5 antibody confirmed the establishment of homogenous cell clones (Figure 4-29). Clones V1, V2, H1, and H3 were therefore selected for the downstream functional exploration of *hepaCAM*.

4.2.6.2 MCF7 stable clones

MCF7 cells were stably transfected with pEGFP-N2 vector (MCF7/pEGFPN2), hepaCAM-GFP (MCF7/hepaCAM-GFP), hCAM△263-GFP (MCF7/hCAM△263-GFP), hCAM△320-GFP (MCF7/hCAM△320-GFP), pcDNA6B/V5-His vector (MCF7/pcDNA6), hepaCAM-V5 (MCF7/hepaCAM-V5) and hCAM△263-V5 (MCF7/hCAM△263-V5), and cloned. Samples of the cells were lysed and analyzed

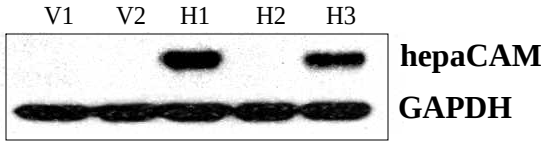

FIGURE 4-27 Protein expression of HepG2 stable clones transfected with pcDNA6B/V5-His vector or hepaCAM-V5. Anti-V5 antibody was used in the Western blot analysis to evaluate the protein levels of hepaCAM in 2 clones transfected with pcDNA6B/V5-His vector alone (V1 and V2) and 3 clones transfected with hepaCAM-V5 (H1, H2, and H3). The membrane was stripped and reprobed with anti-GAPDH antibody for loading control.

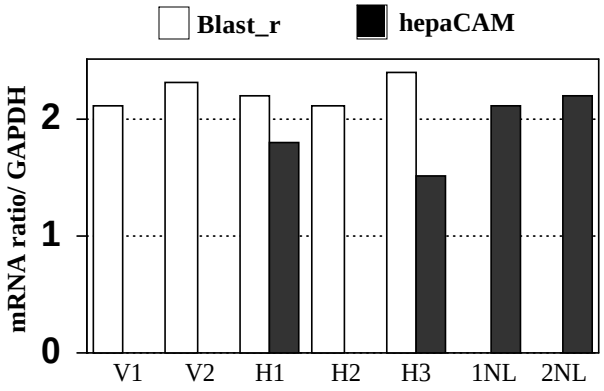

FIGURE 4-28 Real-time RT-PCR analysis of HepG2 stable transfectants. The mRNA levels of blasticidin resistant gene (Blast_r) and *hepaCAM* were determined in all the clones and 2 normal liver tissues (1NL and 2NL), and converted into ratio against GAPDH mRNA levels.

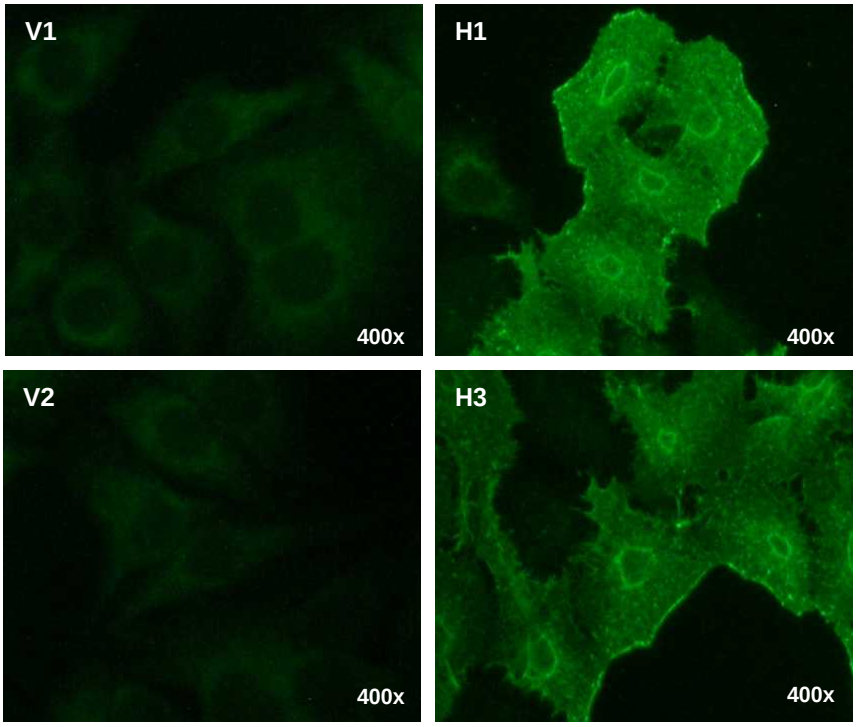

FIGURE 4-29 Confocal microscopy of HepG2 stable transfectants. Immunostaining with anti-V5 antibody was performed to visualize hepaCAM protein in both cells from the control clones V1 and V2 and cells from the clones expressing hepaCAM-V5 (H1 and H3). 400x, magnification.

by Western blotting using anti-GFP (Figure 4-30) or anti-V5 antibody (Figure 4-31) to confirm expression.

4.2.7 Subcellular localization of hepaCAM and mutants

4.2.7.1 hepaCAM is localized predominantly on plasma membrane

Two HCC cell lines Hep3B and HepG2 and a breast cancer cell line MCF7 (Figure 4-32) were transiently transfected with hepaCAM-V5. After 48 hours of transfection, the cells were immunostained with anti-V5 antibody and the mitochondria of MCF7 cells were labeled with Mitotracker-orange. Fluorescence microscopy showed that hepaCAM was scattered to punctuate structures in the cytoplasm, absent in the nucleus and predominantly localized on the plasma membranes of Hep3B, HepG2, and MCF7 cells. In addition, hepaCAM protein was not recruited to the mitochondria of MCF7 cells.

4.2.7.2 Subcellular localization of hepaCAM is cell density-dependent

The subcellular localization of hepaCAM appeared to be cell density-dependent (Figure 4-33). In well spread stable MCF7/hepaCAM-GFP cells, hepaCAM protein was localized to punctuate structures in the perinuclear membrane, cytoplasm, and at the tip of cell surface protrusions that were about to make contact with adjacent cell surfaces, forming zipper-like structures. Once cells became confluent, the protein was localized to a lesser extent in the perinuclear membrane and cytoplasm, and predominantly on the plasma membrane, particularly at the areas of cell-cell contact.

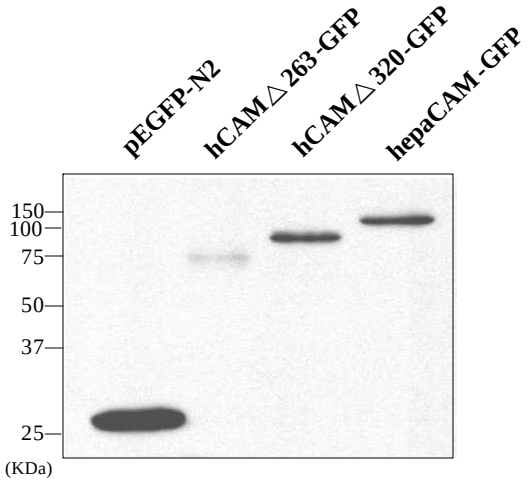

FIGURE 4-30 Protein expression of GFP-fused hepaCAM and cytoplasmic domain mutants in stable MCF7 cells. Proteins expressed by pEGFP-N2 vector as well as GFP-fused wildtype and cytoplasmic domain mutants of hepaCAM were detected by Western blot analysis with anti-GFP antibody. Positions of the molecular size markers are shown on the left panel.

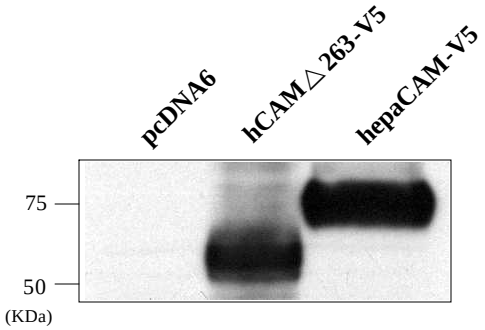

FIGURE 4-31 Protein expression of V5-fused hepaCAM and cytoplasmic domain mutant in stable MCF7 cells. Proteins expressed by pcDNA6B/V5-His vector (pcDNA6) as well as V5-fused wildtype hepaCAM and mutant hCAM△263 were detected by Western blot analysis with anti-V5 antibody. Positions of the molecular size markers are shown on the left panel.

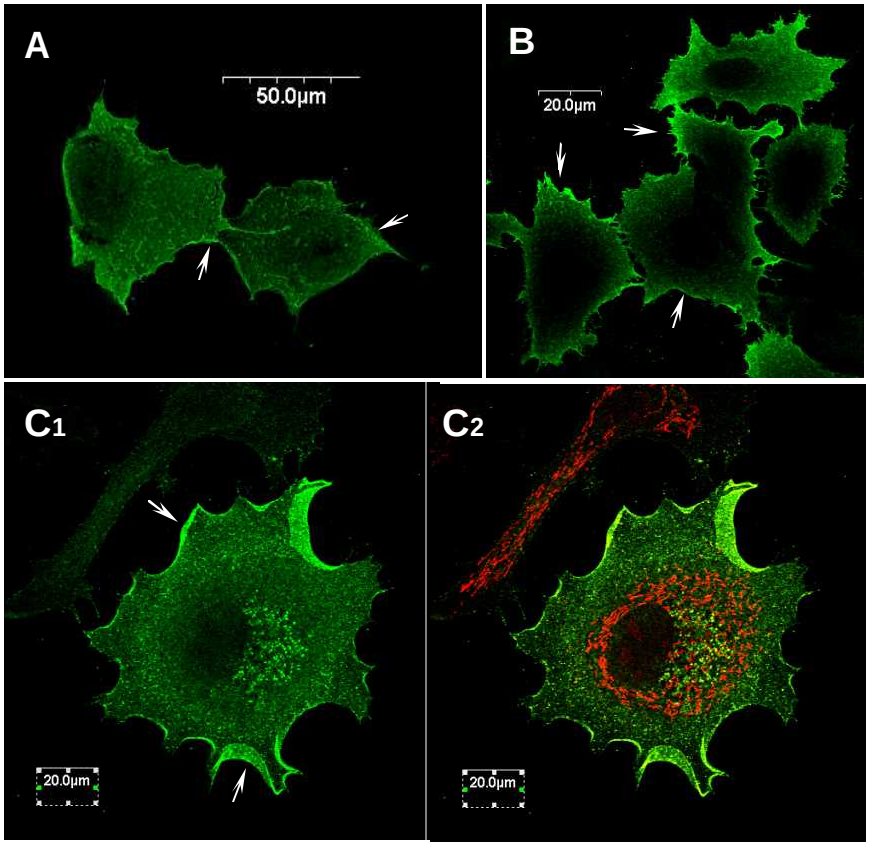

FIGURE 4-32 Subcellular localization of hepaCAM protein in cancer cell lines. Two HCC cell lines Hep3B (A) and HepG2 (B) cells and a breast cancer cell line MCF7 (C_1 and C_2) were transiently transfected with hepaCAM-V5 plasmid. Anti-V5 antibody was used for immunostaining to detect the expression and localization of hepaCAM. Confocal microscopy revealed that hepaCAM was scattered in the cytoplasm and predominantly localized on the plasma membrane (arrows). Mitochondria of MCF7 cell (C2) were stained with Mitotracker-orange.

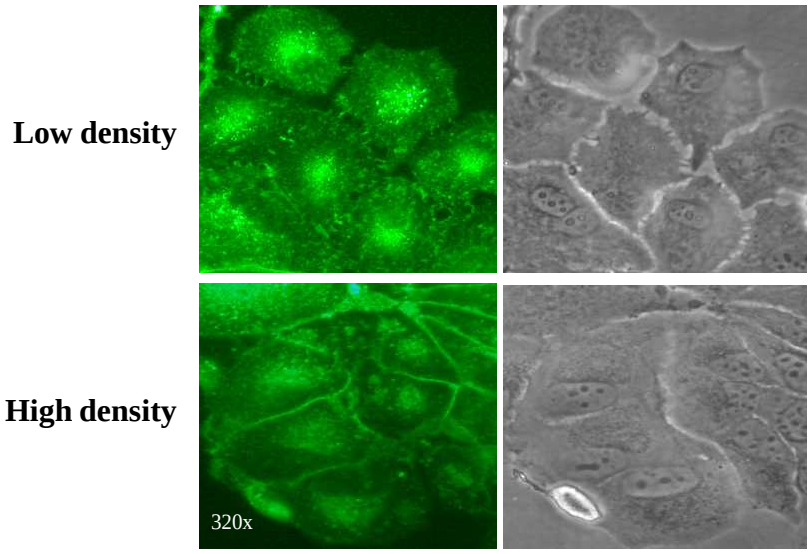

FIGURE 4-33 The localization of hepaCAM in MCF7/hepaCAM cells is cell density-dependent. MCF7/hepaCAM-GFP cells were seeded at low density and cultured for a few days. Upper panel, well-spread cells with surface protrusions; lower panel, confluent cells with clear cell-cell contacts. 320x, magnification.

4.2.7.3 Colocalization of hepaCAM with E-cadherin

The localizations of hepaCAM and E-cadherin were examined in confluent polarized MCF7/hepaCAM-GFP cells by confocal microscopy (Figure 4-34). The cells were seeded in low density and allowed to grow to confluence on 0.4-μm Transwell filters before immunostaining for E-cadherin, an adhesion molecule known to localize in the lateral cell surface. In the X-Y section, hepaCAM-GFP protein was distributed to honeycomb-like structures at cell-cell boundaries that significantly colocalized with E-cadherin. In the X-Z vertical cross-section, the distribution of E-cadherin along the entire lateral cell surface coincided with hepaCAM-GFP. Moreover, hepaCAM was also detected at the basal membrane in contact with the transwell membrane. Since hepaCAM and E-cadherin appeared to colocalize, coimmunoprecipitation was performed to investigate if there was any physical interaction between the two proteins (Figure 4-35). Cell lysate prepared from MCF7/hepaCAM-V5 cells was immunoprecipitated with anti-V5 antibody and subjected to Western blot analysis with either anti-E-cadherin or anti-V5 antibody. MCF7/pcDNA6 cell lysate was included in the experiment as control. No coimmunoprecipitation was observed, suggesting that E-cadherin and hepaCAM are not associated.

4.2.7.4 Transmembrane domain is essential for plasma membrane localization of hepaCAM

Deletion of the cytoplasmic domain did not affect plasma membrane localization of hepaCAM. Microscopic observation revealed that the cytoplasmic domain mutants of hepaCAM were clearly localized in the plasma membrane of MCF7/hCAM△320-GFP and MCF7/hCAM△263-GFP (Figure 4-36A) cells. Moreover, immunostaining of MCF7/hepaCAM-V5 and MCF7/hCAM△263-V5 cells (Figure 4-36B) with anti-

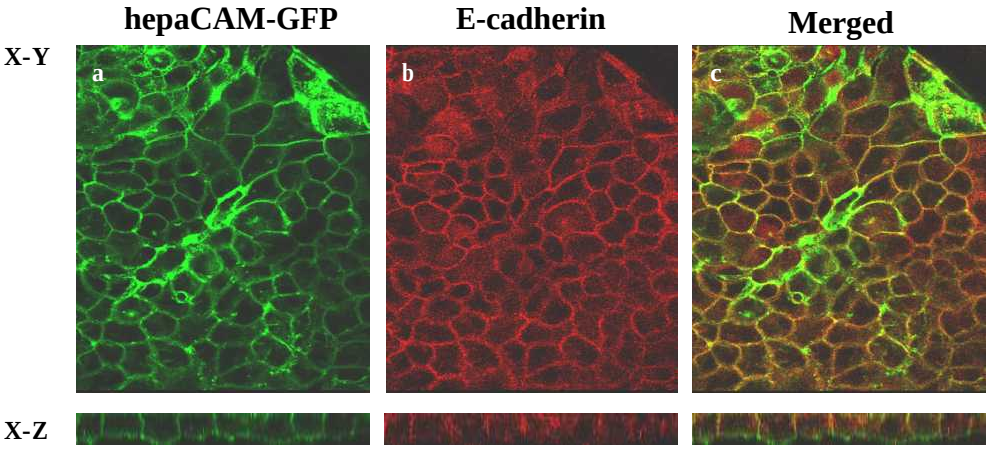

FIGURE 4-34 Colocalization of hepaCAM with E-cadherin. MCF7/hepaCAM-GFP cells grown to confluence on the Transwell filter unit were fixed, permeabilized, and immunostained with anti-E-cadherin. Laser scanning confocal microscopy was performed with a filter set suitable for fluorescein and rhodamine detection. The representative sets of X–Y and X–Z sections are indicated. a, hepaCAM-GFP stained green; b, E-cadherin stained red; c, confocal images of the hepaCAM-GFP and E-cadherin were merged to show regions of colocalization.

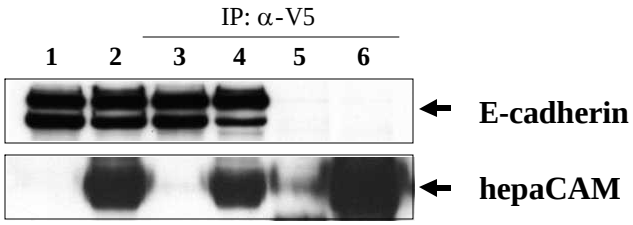

FIGURE 4-35 hepaCAM does not coimmunoprecipitate with E-cadherin. Equal amount of cell lysate prepared from MCF7/pcDNA6 or MCF7/hepaCAM-V5 cells was immunoprecipitated (IP) with anti-V5 antibody and analyzed by Western blotting using anti-E-cadherin (E-cadherin; top panel) or anti-V5 antibody (hepaCAM; bottom panel). The signals corresponding to E-cadherin and hepaCAM-V5 molecules are marked with arrowheads. Lane 1, cell lysate of MCF7/pcDNA6 before IP; Lane 2, cell lysate of MCF7/hepaCAM-V5 before IP; Lane 3, cell lysate of MCF7/pcDNA6 after IP; Lane 4, cell lysate of MCF7/hepaCAM-V5 after IP; Lane 5, precipitate of MCF7/pcDNA6; Lane 6, precipitate of MCF7/hepaCAM-V5.

A

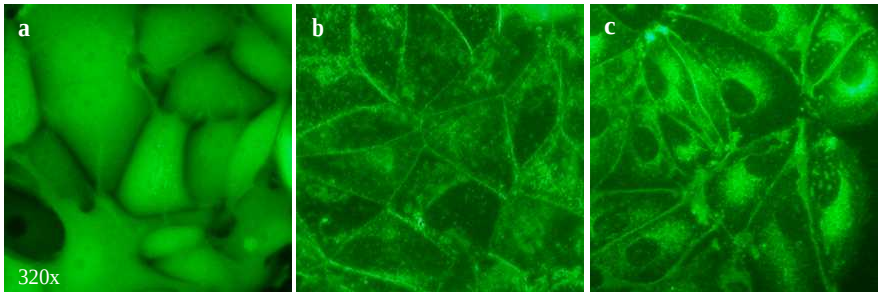

pEGFP-N2 hCAM△263 -GFP hCAM△320-GFP

B

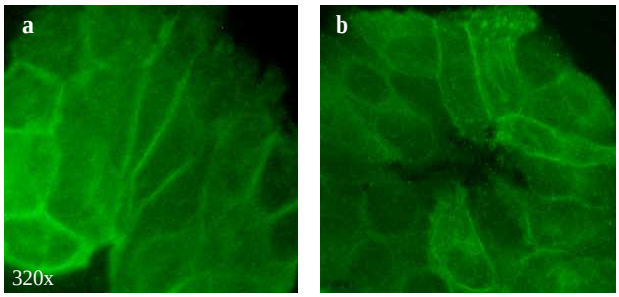

hepaCAM-V5 hCAM△263 -V5

FIGURE 4-36 Plasma membrane localization of hepaCAM is independent of its cytoplasmic domain. A, The expressions of pEGFP-N2 (a), hCAM△263-GFP (b) and hCAM△320-GFP (c) in stable MCF7 cells were detected by fluorescence microscopy. B, MCF7/hepaCAM-V5 (a) and MCF7/hCAM△263 -V5 (b) cells were immunostained with anti-V5 antibody. The localizations of hepaCAM and mutant were detected under a fluorescence microscope. 320x, magnification.

V5 antibody showed expression of wildtype and tailless hepaCAM on the plasma membrane, implicating that the extracellular/transmembrane domains hepaCAM may be responsible for its plasma membrane localization.

MCF7 cells were transfected with the extracellular/transmembrane mutants hCAMΔ1st Ig-V5, hCAMΔ2nd Ig-V5, hCAMΔIgs-V5, and hCAM_tail-V5 (Figure 4-37). Forty-eight hours post-transfection, the cells were immunostained with anti-V5 antibody and the localization of these proteins was visualized by fluorescence microscopy. hCAMΔ1st Ig-V5, hCAMΔ2nd Ig-V5, and hCAMΔIgs-V5 were distributed, with varying intensities, on the plasma membrane as well as to the punctuate structures in the cytoplasm of MCF7 cells. On the contrary, hCAM_tail-V5 was not distributed to the plasma membrane but localized in the cytoplasm in a punctuate pattern. The results suggested that the signal peptide and transmembrane domain of hepaCAM are essential for plasma membrane localization, although the extracellular Ig domains may participate in stabilizing the localization.

4.2.8 *N*-linked glycosylation of hepaCAM

Sequence analysis of hepaCAM predicted six *N*-linked glycosylation sites on its extracellular domain (Figure 4-16), indicating that hepaCAM protein might be glycosylated. To investigate if hepaCAM was indeed glycosylated, the cell lysate of MCF7/hepaCAM-GFP cells was enzymatically digested with PNGase F to cleave putative *N*-linked glycans (Figure 4-38A). An untreated sample was included as control. The molecular weight (MW) of hepaCAM-GFP was shown by Western blot analysis to be ~100 kDa. After deglycosylation, the MW shifted to ~75 kDa. Consistently, treatment of MCF7 cells transiently transfected with hepaCAM-GFP

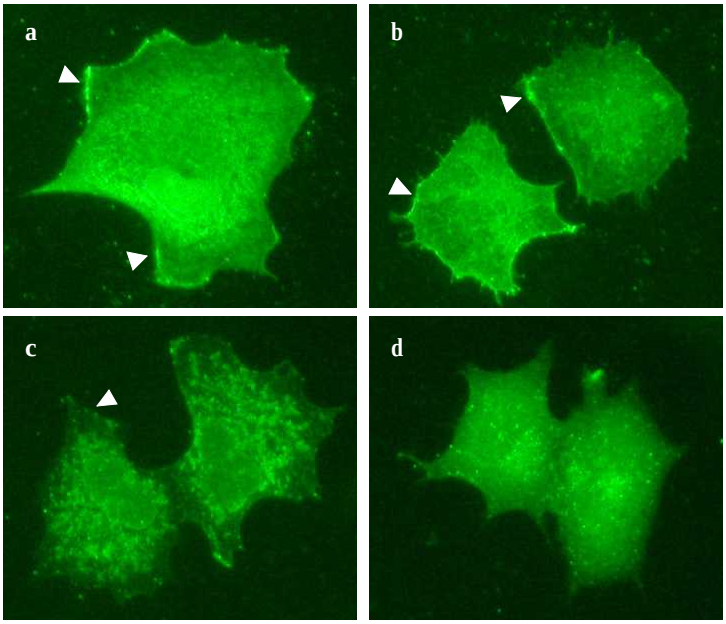

FIGURE 4-37 Subcellular localization of extracellular/ transmembrane domain mutants of hepaCAM in MCF7 cells. MCF7 cells transiently transfected with hCAMΔ1st Ig-V5(a), hCAMΔ2nd Ig-V5 (b), hCAMΔIgs-V5 (c), and hCAM_tail-V5 (d) were immunostained with anti-V5 antibody and visualized under a fluorescence microscope. Arrowheads show localization on plasma membrane. 320x, magnification.

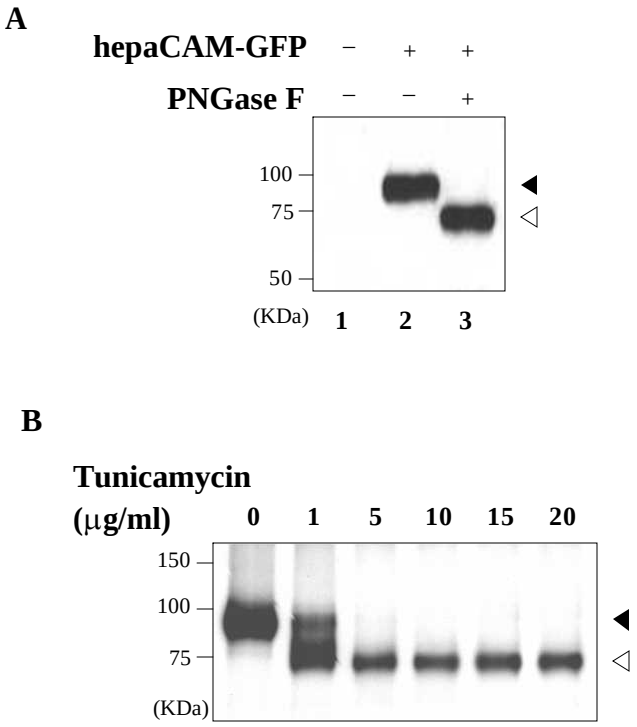

FIGURE 4-38 *N*-Linked glycosylation of hepaCAM. A, Cell lysate prepared from MCF7/hepaCAM-GFP cells (lanes 2 and 3) was treated without (-) or with (+) PNGase F. Cell lysate of untreated parental MCF7 cells (lane 1) was included as control. B, MCF7 cells transiently transfected with hepaCAM-GFP were treated with tunicamycin at the indicated concentrations for 24 hours before lysis. Protein samples were resolved by SDS-PAGE and analyzed by Western blotting using anti-GFP antibody. Solid and open arrowheads indicate signals for glycosylated and non-glycosylated proteins, respectively. Positions of the molecular size markers are shown on the left of each panel.

with different doses of tunicamycin (Figure 4-38B), an antibiotic that inhibits *N*-linked glycosylation, also gave rise to a band at ~75 kDa. The results verified that hepaCAM is a glycoprotein.

4.2.9 Homodimerization of hepaCAM occurs through *cis*-interaction on plasma membrane

4.2.9.1 Dimerization of hepaCAM on cell surface

The existing form of hepaCAM on cell surface was evaluated by incubating a monolayer of MCF7/hepaCAM-GFP cells with a noncleavable membrane-impermeable crosslinker BS3 (Figure 4-39A). An untreated sample served as control. The cells were lysed and analyzed by Western blotting using anti-GFP antibody. In the presence of BS3, a band of ~200 kDa which seemed to represent the dimerized form of hepaCAM-GFP appeared, accompanied with the disappearance of the hepaCAM monomers. Similarly, treatment of MCF7/hepaCAM-V5 cells with BS3 resulted in a loss of the ~75 kDa monomeric form of hepaCAM with a concomitant gain in the higher molecular weight species at ~150 kDa although no distinct band was noted (Figure 4-39B). It was possible that the anti-V5 antibody was unable to recognize the higher molecular weight species as efficiently as monomers.

4.2.9.2 Homodimerization of hepaCAM

To examine if hepaCAM could form homodimer on cell surface, MCF7/hepaCAM-GFP cells were treated with DTSSP, a reducible membrane-impermeable crosslinker. In the absence of the reducing agent DTT, a significant increase in the 200-kDa species was observed. However, when DTT was included into the sample buffer, the higher molecular weight species was reduced to the monomeric form to a level

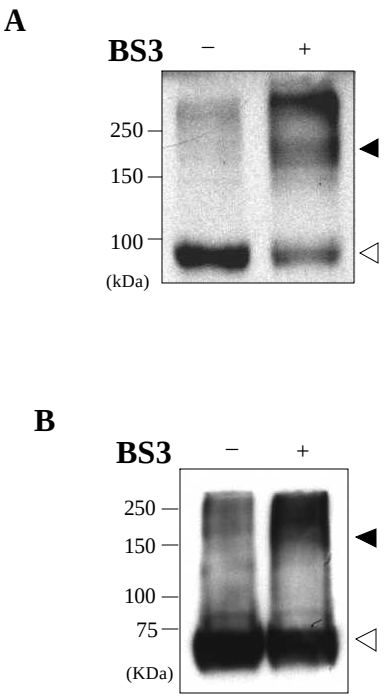

FIGURE 4-39 Dimerization of hepaCAM on plasma membrane. Crosslinking of hepaCAM-GFP (A) and hepaCAM-V5 (B) on cell surface. A monolayer of MCF7/hepaCAM-GFP or MCF7/hepaCAM-V5 cells was untreated (-) or treated (+) with 3 mM BS3 prior to cell lysate preparation using lysis buffer containing 10 mM iodoacetamide. Protein samples were subjected to Western blot analysis with anti-GFP or anti-V5 antibody, respectively. Solid and open arrowheads indicate signals for dimeric and monomeric proteins, respectively. The positions of the molecular size markers are shown on the left of each panel.

closely comparable to that of the untreated sample (Figure 4-40). Interestingly, protein species that seemed to represent the dimeric form of the proteins were noted in the untreated sample of hepaCAM-GFP. This phenomenon could be caused by the existence of strong covalent bonds between the dimers of hepaCAM-GFP.

A coimmunoprecipitation experiment further proved that hepaCAM homodimerized. An equal amount of cell lysate prepared from MCF7 cells transiently transfected with hepaCAM-GFP, hepaCAM-V5, or a combination of both was immunoprecipitated with anti-GFP antibody followed by Western blot analysis with anti-V5 or anti-GFP antibody. The result revealed coimmunoprecipitation of hepaCAM-V5 with hepaCAM-GFP (Figure 4-41), demonstrating that hepaCAM molecules dimerize through homophilic interaction.

4.2.9.3 *cis*-Dimerization of hepaCAM

To determine if hepaCAM-GFP formed *cis*- or *trans*-dimers on cell surface, an adherent monolayer and a single-cell suspension of MCF7/hepaCAM-GFP cells were treated with BS3 prior to Western blot analysis with anti-GFP antibody (Figure 4-42). The extent of dimerization was comparable in both adherent and suspension cells, suggesting that homodimerization of hepaCAM occurs predominantly through *cis*-interaction rather than *trans*-interaction within the plane of the membrane of individual cells.

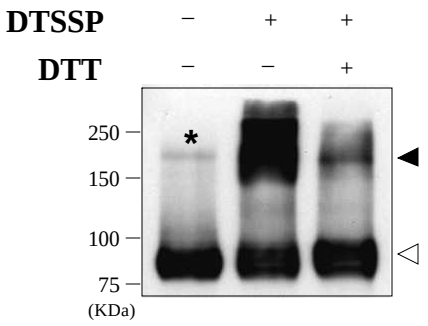

FIGURE 4-40 Homodimerization of hepaCAM on plasma membrane. A monolayer of MCF7/hepaCAM-GFP cells was untreated (-) or treated (+) with 3 mM DTSSP prior to cell lysis in lysis buffer containing 10 mM iodoacetamide. Protein samples were resuspended in Laemmli sample buffer in the presence (+) or absence (-) of 50 mM DTT, and analyzed by Western blotting using anti-GFP antibody. '*', dimer in un-crosslinked sample. Solid and open arrowheads indicate signals for dimeric and monomeric proteins, respectively. The positions of the molecular size markers are shown on the left panel.

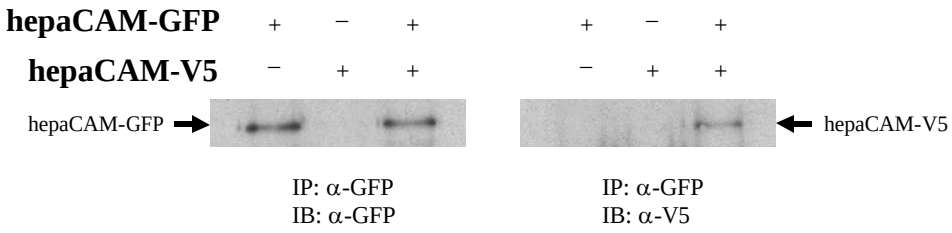

FIGURE 4-41 Coimmunoprecipitation of hepaCAM-GFP and hepaCAM-V5. MCF7 cells were transfected with hepaCAM-GFP, hepaCAM-V5, or both. Protein samples were prepared, immunoprecipitated (IP) with anti-GFP antibody and analyzed by Western blotting (IB) using either anti-GFP (left panel) or anti-V5 antibody (right panel). The signals corresponding to hepaCAM-GFP and hepaCAM-V5 molecules are marked with arrows.

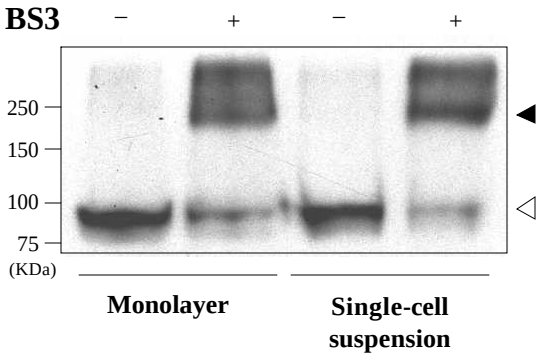

FIGURE 4-42 Dimerization of hepaCAM through *cis*-interaction. A monolayer or a single-cell suspension of MCF7/hepaCAM-GFP cells was incubated in the absence (-) or presence (+) of 3 mM BS3. Protein samples were subjected to Western blot analysis with anti-GFP antibody. Solid and open arrowheads indicate signals for dimeric and monomeric proteins, respectively. The positions of the molecular size markers are shown on the left panel.

4.2.9.4 Dimerization of hepaCAM is independent of its cytoplasmic domain

MCF7/hCAM△263-GFP cells were treated with BS3 to explore if the cytoplasmic domain of hepaCAM was essential for dimerization. After Western blot analysis with anti-GFP antibody, the result showed that the monomeric form of hCAM△263-GFP was diminished and its dimeric form was accumulated at ~125 kDa in the BS3-treated sample, indicating that dimerization of hepaCAM is independent of its cytoplasmic domain (Figure 4-43).

4.2.10 The cytoplasmic domain of hepaCAM is phosphorylated

A polyclonal antiserum that recognizes hepaCAM cytoplasmic domain, but only in its non-phosphorylated form, was generated. The antiserum was generated by immunization of rabbits with a recombinant bacterial His-tagged fusion protein expressing the cytoplasmic domain of hepaCAM. Western blot analysis showed that this anti-hepaCAM antiserum could specifically detect the bacterial fusion protein, otherwise undetectable by the preimmune serum. However, when the antiserum was tested on the cell lysate of MCF7 transfected with hepaCAM-V5, hepaCAM could not be detected. This observation led to the suspicion that the cytoplasmic domain of hepaCAM might be post-translationally modified by phosphorylation. Evaluation of the cytoplasmic sequence of hepaCAM by the NetPhos 2.0 server showed that the domain was highly phosphorylated. Twenty-eight potential serine, threonine or tyrosine phosphorylated residues were scattered along the cytoplasmic domain, with 20 of them giving a potential phosphorylation index above 0.5 (Figure 4-44A).

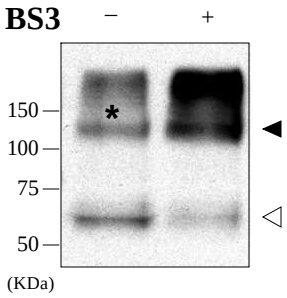

FIGURE 4-43 Dimerization of hepaCAM is independent of its cytoplasmic domain. A monolayer of MCF7/hCAM△263-GFP cells was untreated (-) or treated (+) with 3 mM BS3. Cell lysates prepared in lysis buffer containing 10 mM iodoacetamide were subjected to Western blot analysis with anti-GFP antibody. '*', dimer in un-crosslinked sample. Solid and open arrowheads indicate signals for dimeric and monomeric proteins, respectively. The positions of the molecular size markers are shown on the left panel.

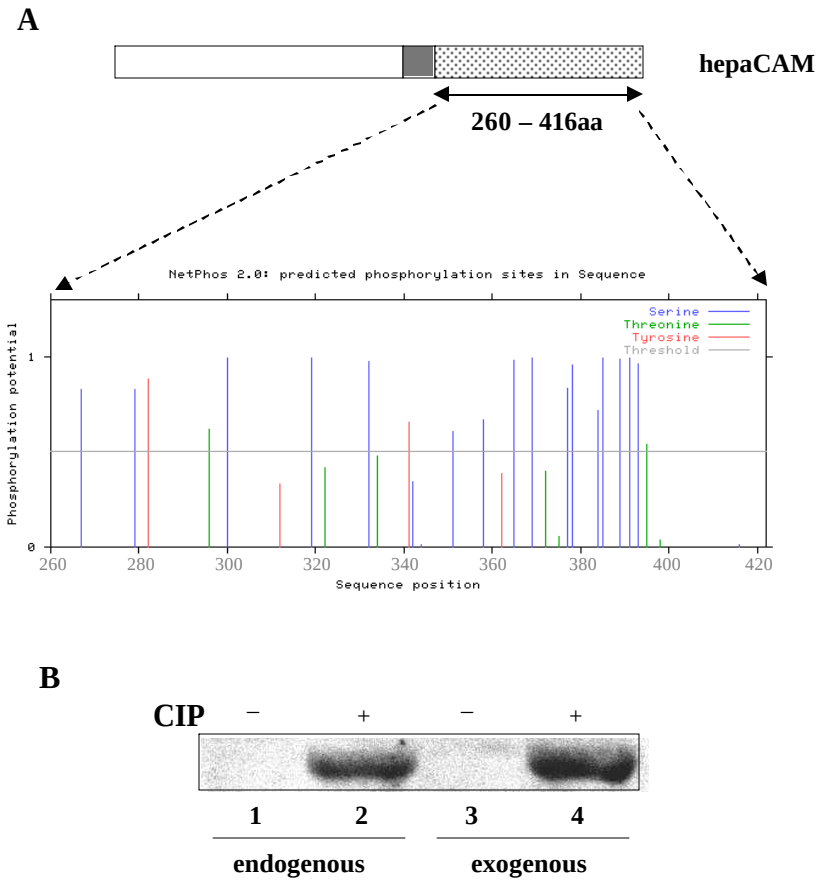

FIGURE 4-44 Phosphorylation of hepaCAM cytoplasmic domain. A, The cytoplasmic domain (residues 260-416) of hepaCAM was used to generate rabbit polyclonal anti-hepaCAM antiserum. Potential serine/threonine and tyrosine kinase phosphorylation sites in the cytoplasmic region were identified using NetPhos 2.0 software. aa, amino acids. B, Cell lysate prepared from C3A cells expressing endogenous hepaCAM (lanes 1 and 2) or MCF7/hepaCAM-V5 cells expressing exogenous hepaCAM (lanes 3 and 4) was either untreated (-) or treated (+) with calf intestinal alkaline phosphatase (CIP). After dephosphorylation, hepaCAM protein was detected by Western blot analysis with the rabbit anti-hepaCAM polyclonal antiserum.

Experimentally, cell lysates of C3A cells expressing endogenous hepaCAM and MCF7 cells expressing exogenous hepaCAM-V5 were dephosphorylated with calf intestinal alkaline phosphatase (CIP). Untreated cell lysates served as controls. As shown in Figure 4-44B, the CIP-treated endogenous and exogenous hepaCAM were detected by the rabbit anti-hepaCAM antiserum, confirming that the cytoplasmic domain of hepaCAM is phosphorylated.

4.2.11 Anti-proliferative effect of hepaCAM

The suppression of *hepaCAM* in a variety of human tumors implicated a possible involvement of hepaCAM in cell growth regulation. Therefore, colony formation was carried out while growth rate was determined in stable HepG2 clones to assess the anti-proliferative effect of hepaCAM. The results showed that the number of colonies formed after two weeks of blasticidin selection was reduced by 10-fold in the HepG2 cells transfected with hepaCAM-V5 ($P = 0.0022$, Figure 4-45), and the growth rate was decreased by 14-fold ($P < 0.001$, on day 5, Figure 4-46) in cells expressing hepaCAM (H1 and H3). No clear cell death was observed in the course of examining growth arrest, suggesting that hepaCAM inhibits cell growth through suppressing proliferation rather than inducing apoptosis.

4.2.12 hepaCAM induces p53 expression

The expression of tumor suppressor p53 was tested in the HepG2 clones transfected with vector alone (V1 and V2) and expressing hepaCAM-V5 (H1 and H3). Western blot analysis with anti-p53 antibody (Figure 4-47) showed that while p53 was undetectable in both vector clones, it was clearly activated in the cells expressing hepaCAM.

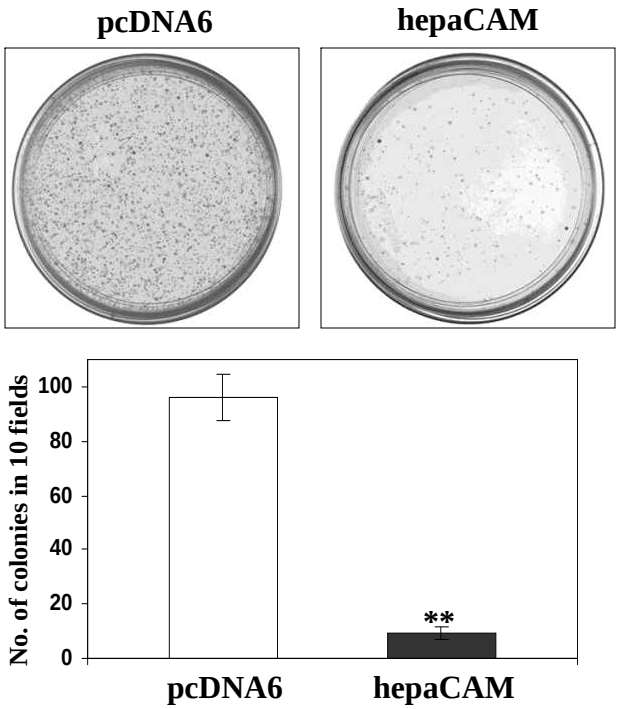

FIGURE 4-45 Inhibition of colony formation by hepaCAM. HepG2 cells transfected with pcDNA6B/V5-His vector (pcDNA6) or hepaCAM-V5 construct (hepaCAM) were selected with blasticidin for 2 weeks. The cell colonies formed at the end of the experiments were counted in 10 randomly selected fields and represented by the bar graph (means±SD, n = 6), ** P = 0.0022 as assessed by Mann-Whitney test.

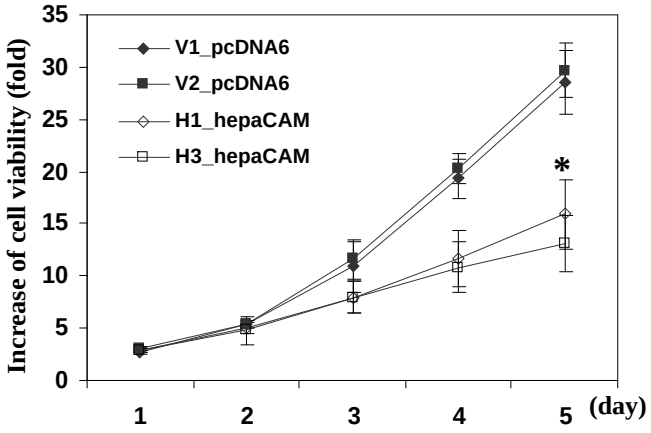

FIGURE 4-46 Suppression of cell growth by hepaCAM. The growth rate of the cells from HepG2 clones H1 and H3 (stably transfected with hepaCAM-V5) was compared to that of the cells from V1 and V2 (stably transfected with pcDNA6B/V5-His vector alone) for 5 days by MTT assay. Data represent means±SD (n = 6), * $P < 0.001$ (on day 5) as assessed by ANOVA.

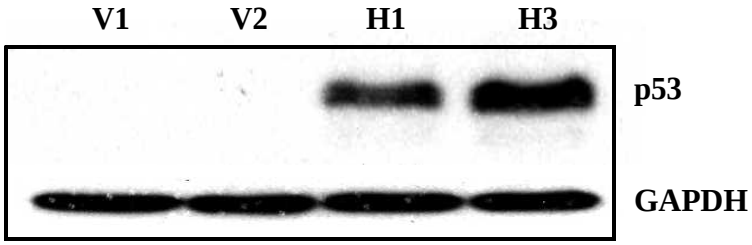

FIGURE 4-47 Effect of hepaCAM on tumor suppressor p53. The expression of p53 was detected in HepG2 clones transfected with pcDNA6B/V5-His vector alone (V1 and V2) and expressing hepaCAM-V5 (H1 and H3) by Western blot analysis with anti-p53 antibody. GAPDH, loading control.

4.2.13 Modulation of cell adhesion by hepaCAM

4.2.13.1 hepaCAM modulates cell-matrix interaction through its cytoplasmic domain

The adhesive properties of hepaCAM were evaluated on the stable HepG2 clones through cell aggregation and spreading assays. Although hepaCAM did not clearly change cell aggregation (Figure 4-48), it was capable of modulating cell-matrix adhesion significantly on fibronectin (Figure 4-49). About 50 and 90% of the cells from both clones H1 and H3 exhibited spread morphology at 30 min and 2 h of incubation, respectively. In contrast, the majorities of the cells from clones V1 and V2 remained round at the same time points. The number of cells showing spread morphology from clones H1 and H3 was about 5-fold higher than that from the control clones V1 and V2 ($P < 0.001$).

To investigate if the adhesive properties of hepaCAM were mediated through its cytoplasmic domain, MCF7 cells stably transfected with pcDNA6B/V5-His vector, hCAM△263-V5 (lacked cytoplasmic domain) and hepaCAM-V5 were used in cell spreading and detachment assays. Figure 4-50 showed that about 60% and 79% of the MCF7/hepaCAM-V5 cells exhibited spread morphology on fibronectin at 30 minutes and 2 hours of incubation, respectively, in contrast to 40.8% and 58.2% of the MCF7/hCAM△263-V5 cells, and 7.3% and 18% of the MCF7/pcDNA6 cells ($P < 0.001$). Similarly on matrigel, MCF7/hepaCAM-V5 cells showed the fastest spreading, followed by MCF7/hCAM△263-V5 cells, and then MCF7/pcDNA6 cells ($P < 0.001$). In cell detachment assay (Figure 4-51), MCF7/hepaCAM-V5 cells detached 18.9 times and 21.6 times slower than MCF7/pcDNA6 cells at 5 minutes and 15 minutes, respectively. MCF7/hCAM△263-V5 cells, on the other hand,

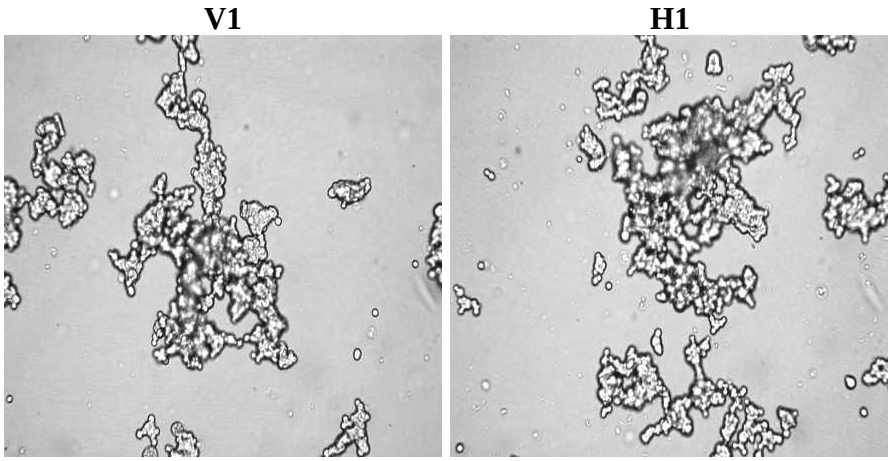

FIGURE 4-48 hepaCAM does not induce cell aggregation. Single cell suspension of HepG2 clones transfected with pcDNA6B/V5-His vector alone (V1) or expressing hepaCAM-V5 (H1) was incubated in HBSS for 1 hour on a rotary shaker at 37°C. The microscopic photos were taken under 200x-magnification. No apparent difference in cell aggregation was observed between V1 and H1.

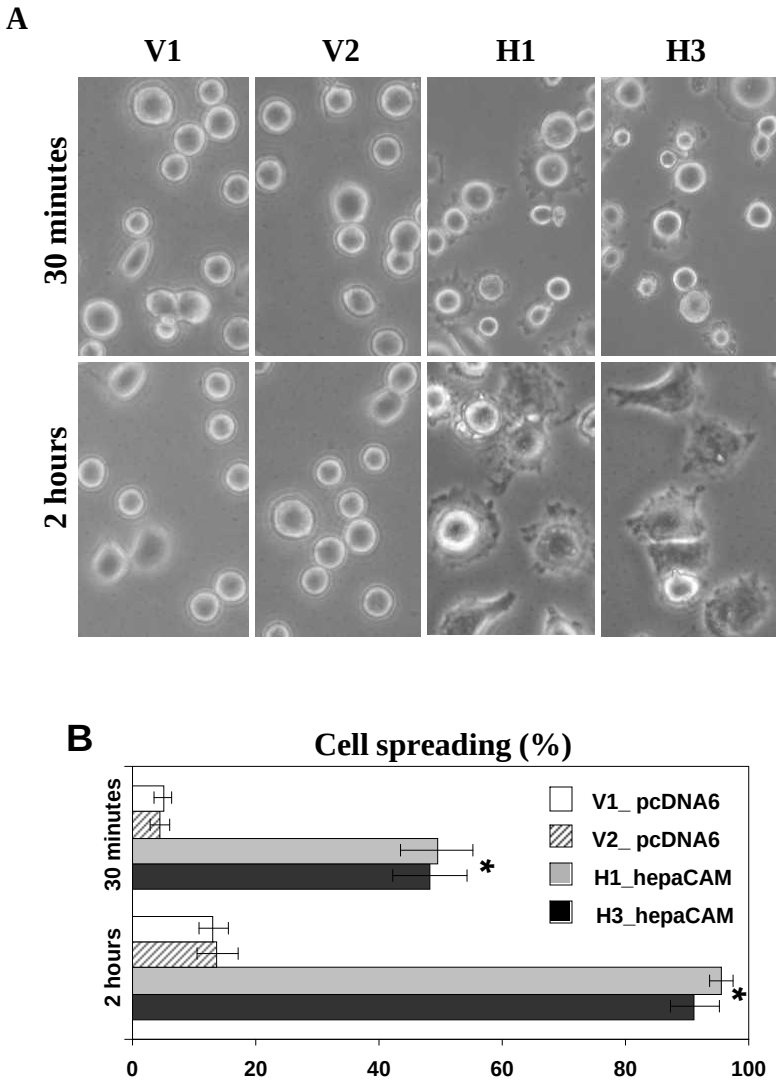

FIGURE 4-49 Modulation of cell-matrix adhesion by hepaCAM. A, Cell morphology. HepG2 clones transfected with pcDNA6B/V5-His vector alone (V1 and V2) and expressing hepaCAM-V5 (H1 and H3) were allowed to spread on fibronectin-coated plates for 30 min or 2 hours. The microscopic photos were taken under 200x-magnification. B, The percentage of cell spreading. At 30 min or 2 hours after plating, total number of cells and cells showing spread morphology were counted in ten randomly selected fields (>60 cell per field), and the percentage of cell spreading was then computed. The data represent means±SD (n = 6), * $P < 0.001$ as assessed by ANOVA.

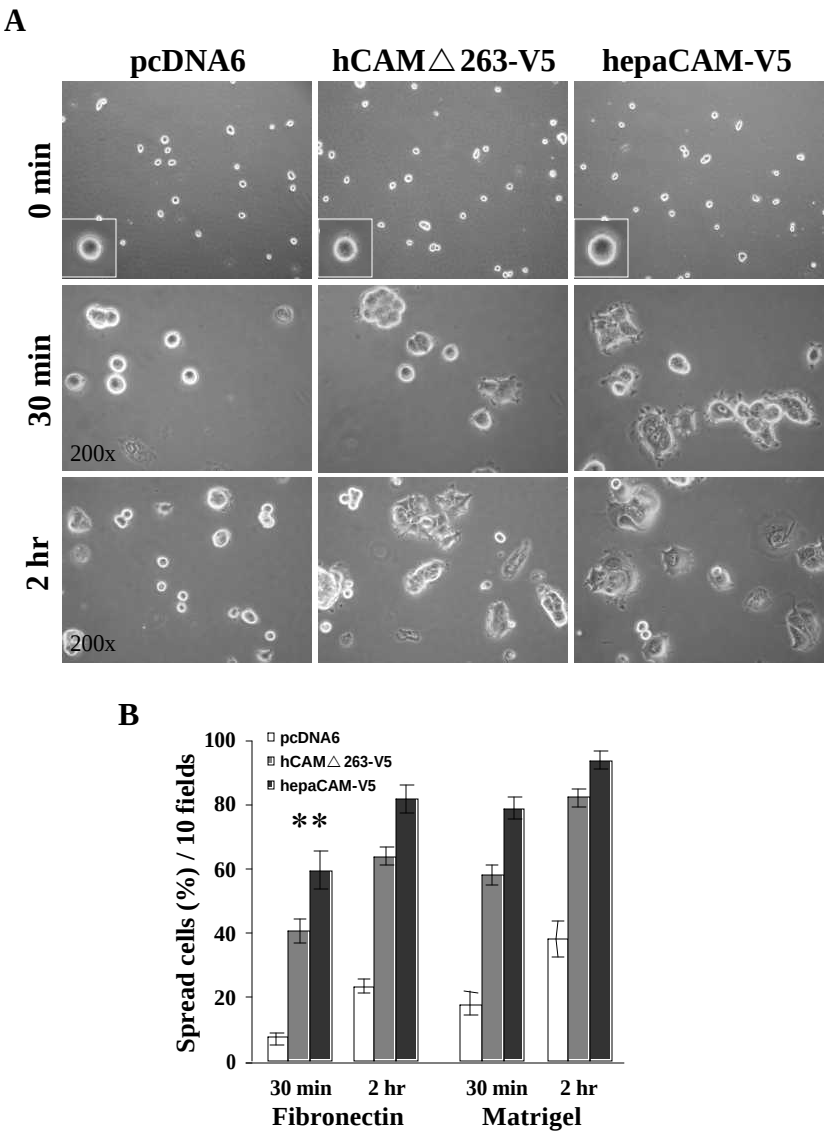

FIGURE 4-50 Cell spreading modulated by hepaCAM is dependent of its cytoplasmic domain. A, MCF7/pcDNA6 (left panel), MCF7/hCAM△263-V5 (middle panel) and MCF7/hepaCAM-V5 (right panel) cells were allowed to spread on matrigel-coated coverslips for 30 min or 2 hours. Inset, cell morphology before spreading. The microscopic photos were taken under 200x-magnification. B, The percentage of spread cells on fibronectin and matrigel. At 30 min or 2 hours after plating, total number of cells showing spread morphology were counted in ten randomly selected fields, and the percentage of cell spreading was then computed. The data represent means±SD (n = 6), ** $P < 0.001$ as assessed by ANOVA.

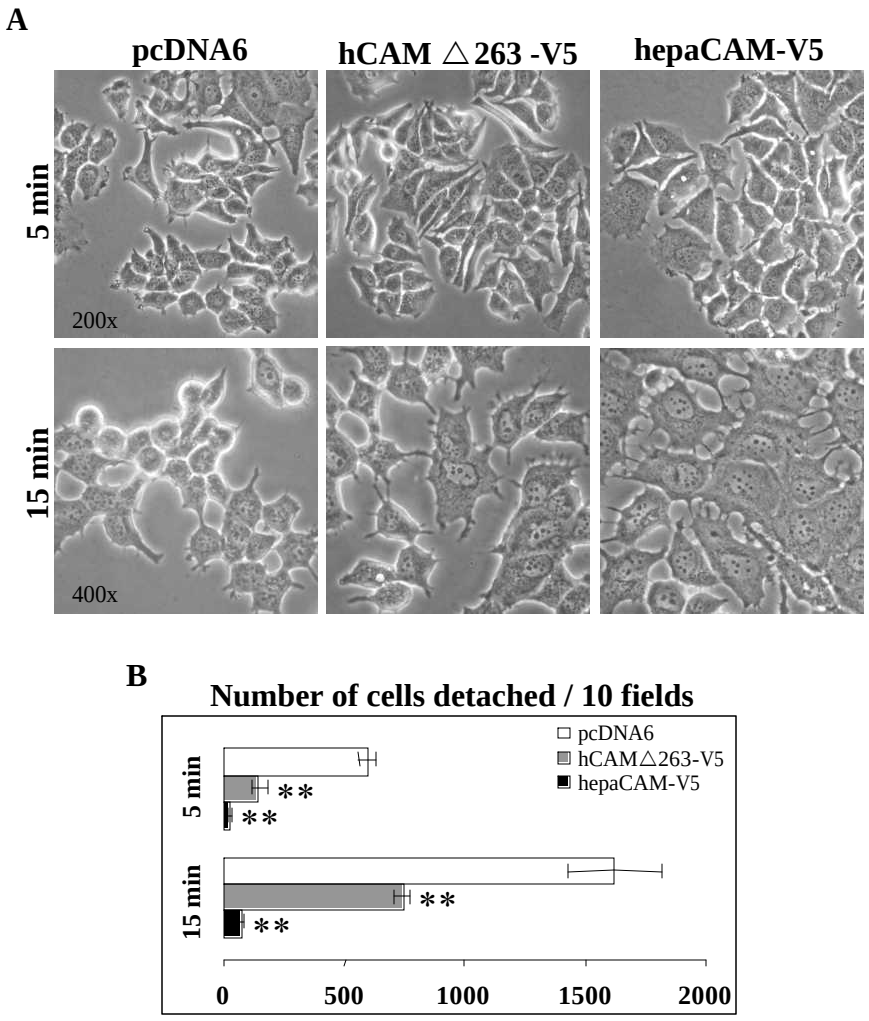

FIGURE 4-51 Cell detachment modulated by hepaCAM is dependent of its cytoplasmic domain. A, MCF7/pcDNA6 (left panel), MCF7/hCAM△263-V5 (middle panel) and MCF7/hepaCAM-V5 (right panel) cells were detached in 1 mM EDTA for 5 min or 15 minutes. The microscopic photos were taken under 200x- and 400x-magnifications. B, At 5 min or 15 min after incubation, total number of detached cells was counted in ten randomly selected fields, and the percentage of cell detachment was then computed. The data represent means±SD (n = 6), ** $P < 0.001$ as assessed by ANOVA.

detached approximately 4 times and 2.2 times slower than MCF7/pcDNA6 cells at time points 5 minutes and 15 minutes ($P < 0.001$). The results demonstrated that in addition to its extracellular and transmembrane domains, hepaCAM requires its cytoplasmic domain to mediate strong cell-matrix adhesion.

4.2.13.2 hepaCAM modulates cell motility essentially through its cytoplasmic domain

Assessment of cell motility of hepaCAM was carried out with the Boyden chamber and wound healing assays using HepG2 clones V1 (transfected with pcDNA6B/V5-His vector) and H1 (expressing hepaCAM-V5). Both Boyden chamber (Figure 4-52) and wound healing assays (Figure 4-53) showed that the motility of HepG2 cells was increased ($P = 0.0011$) when transfected with hepaCAM. These results indicated that hepaCAM increases cell motility.

Similar studies were performed on stable MCF7 cells transfected with pcDNA6B/V5-His vector, hepaCAM-V5, and hCAM△263-V5 (lacked cytoplasmic domain). Barely any of these cells migrated through the 8-μm transwell membrane. This observation could be explained by the poorly invasive nature of MCF7 cells. Moreover, MCF7/hepaCAM-V5 cells compared to the vector transfected cells appeared enlarged, therefore retarding migration. Nevertheless, wound healing assay (Figure 4-54) demonstrated that after 24 hours of incubation, MCF7/hepaCAM-V5 cells filled 59.3% of the scratched area ($P < 0.01$), compared to 36.3% by MCF7/hCAM△263-V5 cells ($P > 0.05$) and 33.1% by MCF7/pcDNA6 cells. After 48 hours, MCF7/hepaCAM-V5 cells closed 83.7% of the wound ($P < 0.01$), compared to 55.2% by MCF7/hCAM△263-V5 cells ($P > 0.05$) and 49.5% by MCF7/pcDNA6 cells.

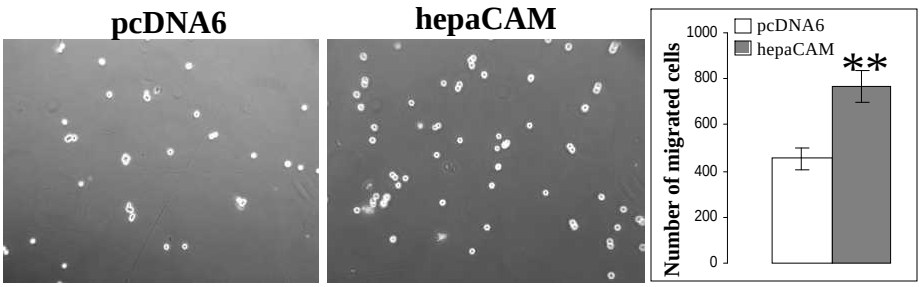

FIGURE 4-52 Induction of cell migration by hepaCAM. Cell migration was examined by using the transwell chambers with 8-μm pore size membranes coated with matrigel. HepG2 clones V1 (pcDNA6) and H1 (hepaCAM) were allowed to migrate through the membrane for 24 hours. The migrated cells were harvested into new 24-well plate and viewed by microscopy (100x-magnification). The migration was quantified by blind counting of the migrated cells in 10 randomly selected fields and represented as mean±SD (n = 6) by the bar graph. ** $P = 0.0011$ as assessed by Mann-Whitney test.

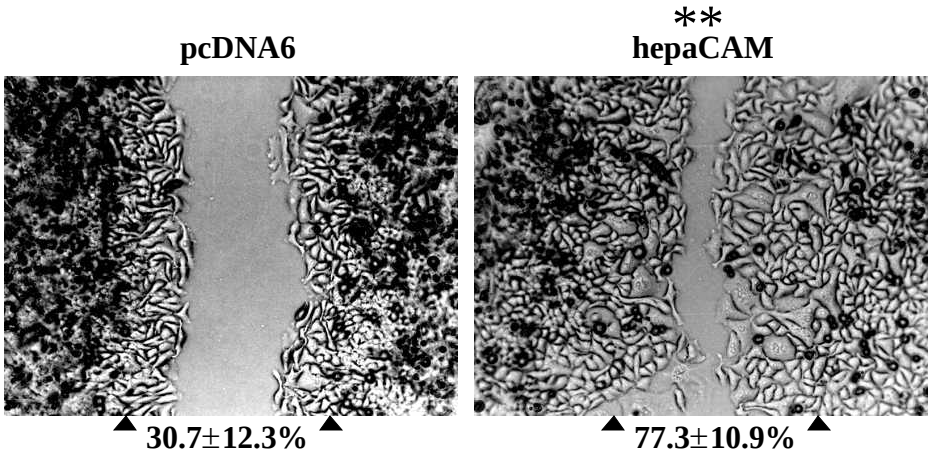

FIGURE 4-53 Promotion of wound healing by hepaCAM. Wounds were made by pipette tip on confluent HepG2 clones V1 (pcDNA6; left) and H1 (hepaCAM; right); and allowed to be healed by cell migration for 24 hours. The diameters of wounds were measured by microscopy (200x-magnification) at 0 hour and 24 hours after wounding. Arrowheads show the diameters of the initial wounds. Changes in diameter were computed into ratio (means±SD%, n = 6) to represent wound closure. ** P = 0.0011 as assessed by Mann-Whitney test.

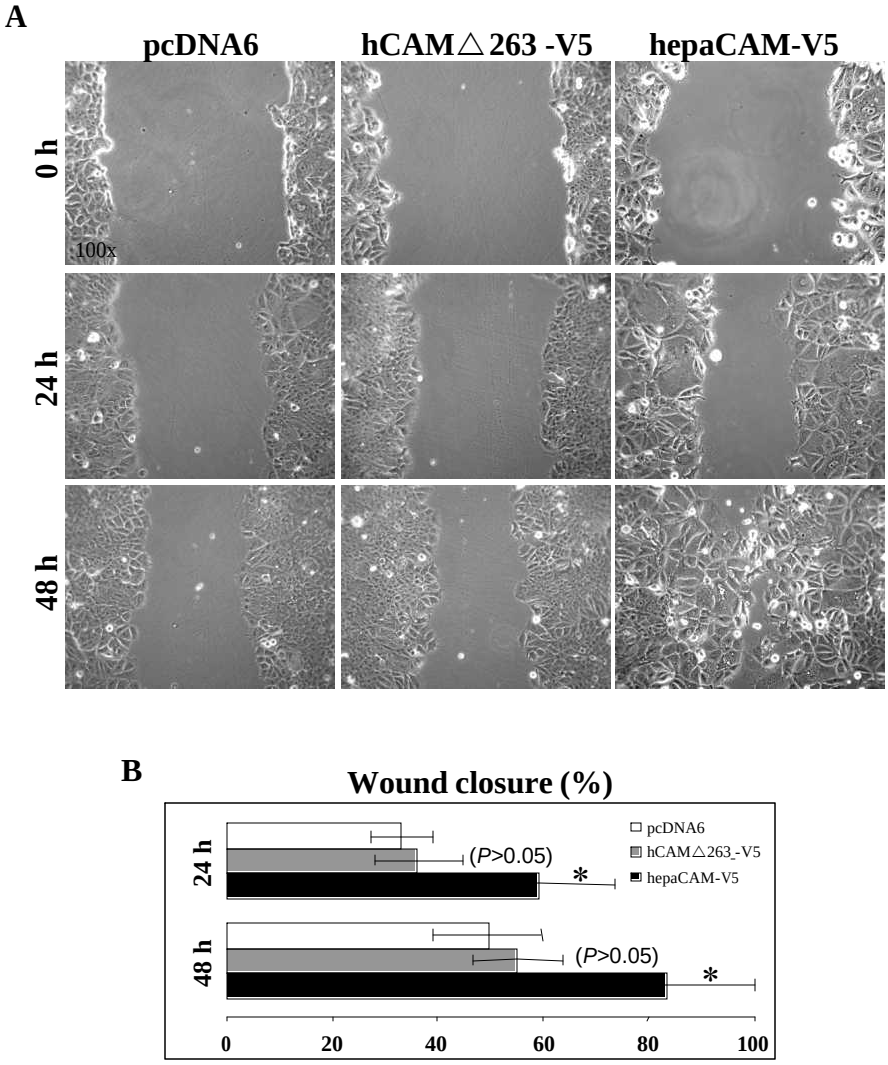

FIGURE 4-54 Wound healing modulated by hepaCAM is dependent of its cytoplasmic domain. A, Wounds were made by pipette tip on confluent MCF7/pcDNA6 (left panel), MCF7/hCAM△263-V5 (middle panel) and MCF7/hepaCAM-V5 (right panel) cells; and allowed to heal for 24 and 48 hours. The microscopic photos were taken under 100x-magnification. B, The diameters of wounds were measured on the microscopic photos at 0 hour, 24 hours and 48 hours after wounding. Changes in wound diameter were computed into percentage (means±SD%, n = 6) to represent wound closure. * $P < 0.01$ as assessed by ANOVA.

Hence, the cytoplasmic domain is important for cell motility modulated by hepaCAM.

4.2.14 Partial resistance of hepaCAM to Triton X-100 solubilization

Cell-matrix interactions are achieved by the coordinated interplay amongst cell adhesion molecules, actin cytoskeleton and lipid rafts. Detergent solubility assay is commonly used as a first step to study such interaction. Studies have shown that proteins that are interconnected to cytoskeletal proteins and lipid rafts are resistant to solubilization by non-ionic detergent e.g. Triton X-100, suggesting that proteins insoluble in non-ionic detergents interact with the cytoskeleton and/or lipid rafts (Simons and Ikonen, 1997; Tarone *et al*., 1984; Neame and Isacke, 1993; Stickney *et al*., 2004).

Detergent solubility assays were performed on C3A cells expressing endogenous hepaCAM and MCF7 cells transiently transfected with hepaCAM. The cells were extracted in 1% Triton X-100, and equal volumes of the detergent-soluble and -insoluble lysates were analyzed by Western blotting using anti-hepaCAM antiserum or anti-V5 antibody as indicated in Figure 4-55. In both C3A and transfected MCF7 cells, a fraction of hepaCAM remained resistant to Triton X-100 solubilization.

The distribution of hepaCAM-insoluble protein in MCF7 cells was shown in Figure 4-56. MCF7 cells transfected with hepaCAM-V5 construct were treated with 1% ice-cold Triton X-100 to remove the detergent-soluble proteins before fixation. The cells were subsequently immunostained with anti-V5 antibody. For a control, the transfected cells were fixed prior to permeabilization with 1% ice-cold Triton X-100. As visualized by fluorescence microscopy, detergent-insoluble hepaCAM was

FIGURE 4-55 Partial resistance of hepaCAM to Triton X-100 solubilization. The endogenous and exogenous hepaCAM proteins were extracted from C3A (left panel) and hepaCAM-V5-transfected MCF7 (right panel) cells, respectively. Equal volumes of Triton X-100-soluble (S) and -insoluble (I) lysates were analyzed by Western blotting (IB) using anti-hepaCAM antiserum or anti-V5 antibody as indicated.

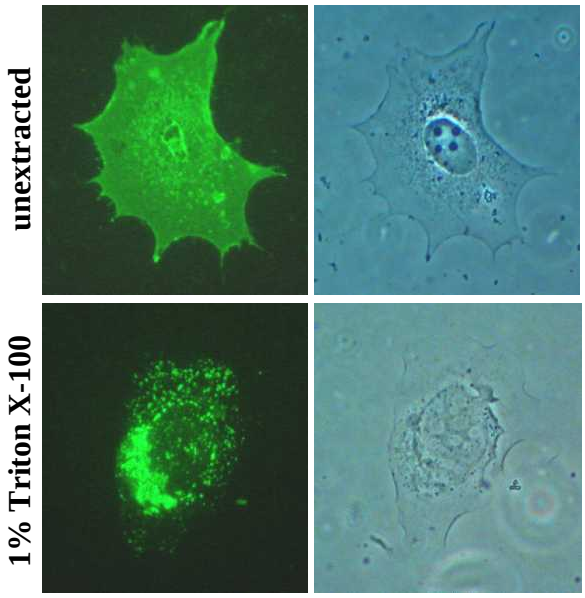

FIGURE 4-56 Subcellular localization of detergent-insoluble hepaCAM. MCF7 cells transiently transfected with hepaCAM-V5 were fixed either before (top panel) or after (bottom panel) extraction with ice-cold 1% Triton X-100, and immunostained with anti-V5 antibody. The cells were visualized by fluorescence (left panel) or phase contrast (right panel) microscopy. 320x, magnification.

localized predominantly to punctuate structures in the cytoplasm as well as weakly on the plasma membrane of MCF7 cells.

4.2.15 Residues located within 319-416 of the cytoplasmic domain of hepaCAM confers Triton X-100 insolubility

MCF7 and HeLa cells were transiently transfected with wildtype hepaCAM-V5 construct and cytoplasmic domain truncated constructs hCAM△318-V5, hCAM△290-V5, and hCAM△263-V5 for 48 hours. The cells were lysed in 1% Triton X-100, and equal volumes of the detergent-soluble and -insoluble lysates were subjected to Western blot analysis with anti-V5 antibody. In contrast to wildtype hepaCAM, truncations of hepaCAM cytoplasmic domain after residues 263, 290 and 318 completely abolished detergent insolubility of hepaCAM in MCF7 and HeLa cells (Figure 4-57). The results indicated that hepaCAM cytoplasmic domain, particularly residues located within 319-416, is responsible for conferring the detergent-resistant nature of the protein, implicating a critical role of the domain in interacting with the actin cytoskeleton and/or lipid rafts.

4.2.16 Interaction of hepaCAM with actin cytoskeleton

MCF7 cells transfected with hepaCAM-V5 were immunostained with anti-V5 antibody to detect hepaCAM as well as labeled with TRITC-conjugated phalloidin to stain F-actin. Colocalization of hepaCAM and F-actin was observed mainly on the plasma membrane and, to a lesser extent, to the punctuate structures in the cytoplasm (Figure 4-58). When the transfected MCF7 cells were treated with 10 μM cytochalasin B, an agent that disrupts the actin filament, not only was the actin cytoskeletal network disorganized but the distribution of hepaCAM on the plasma

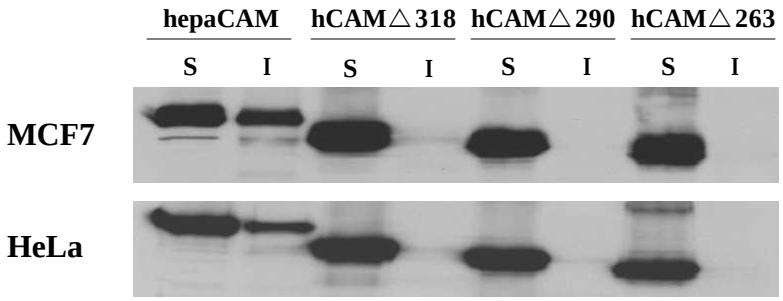

FIGURE 4-57 Detergent solubility of hepaCAM and its cytoplasmic domain mutants. MCF7 and HeLa cells were transiently transfected with V5-fused hepaCAM and its cytoplasmic domain deleted mutants for 48 hours. The cells were extracted in 1% Triton X-100 in PBS. Equal volumes of Triton X-100-soluble (S) and -insoluble (I) lysates were subjected to Western blot analysis with anti-V5 antibody.

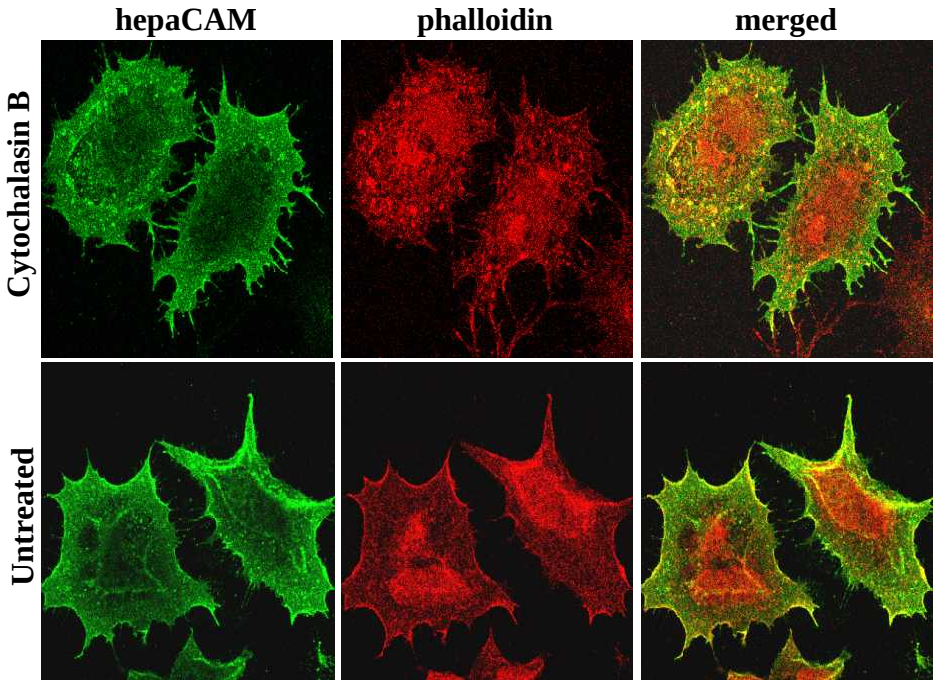

FIGURE 4-58 Colocalization of hepaCAM with F-actin. MCF7 cells transfected with hepaCAM-V5 were either treated (top panel) or untreated (bottom panel) with 10 μM cytochalasin B for 90 min to depolymerize F-actin. The cells were then immunostained with anti-V5 antibody (left panel). F-actin was labeled with TRITC-conjugated phalloidin (middle panel). Confocal images of hepaCAM and F-actin were merged to show regions of colocalization (right panel).

membrane was also affected — hepaCAM localized more dominantly to punctuate structures in the cytoplasm. Interestingly, translocated from the plasma membrane, both hepaCAM and actin appeared clustered in the cytoplasm.

Furthermore, P100 fractions containing cellular membranes and cytoskeletal elements were prepared from both MCF7 and HeLa cells transfected with hepaCAM-V5. These fractions were resuspended in buffer containing 1% Triton X-100 and separated into soluble and insoluble components (Figure 4-59). In accord with Figure 4-55, hepaCAM remained partially insoluble in 1% Triton X-100. Stickney *et al*. showed that disruption of the F-actin network with 1 M potassium iodide (KI) resulted in the solubilization of merlin in Triton X-100, implying the direct association of merlin with F-actin (Stickney *et al*., 2004). Similar experiments were performed. Depolymerization of F-actin resulted in a significant shift of hepaCAM from the insoluble fraction to the soluble one. Notably, a small amount of hepaCAM remained insoluble although F-actin was completely solubilized, indicating the presence of another Triton X-100-insoluble pool of hepaCAM not associated with F-actin.

4.2.17 Subcellular localization of hepaCAM affects its interaction with F-actin

The cytoplasmic domain of hepaCAM was essential for cell-matrix adhesion, cell motility and detergent insolubility, implicating a possible interaction of the cytoplasmic domain with F-actin. The subcellular distributions of several hepaCAM deletion mutants were determined to explore if the localization of the cytoplasmic

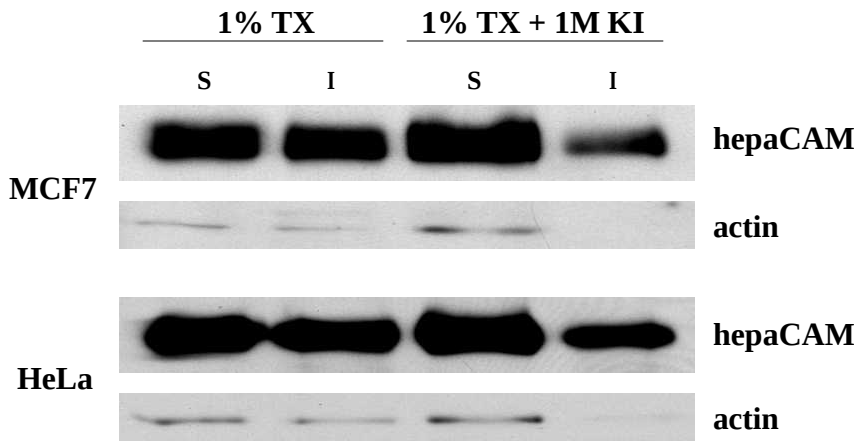

FIGURE 4-59 Depolymerization of F-actin affects detergent solubility of hepaCAM. P100 fractions of MCF7 and HeLa cells transfected with hepaCAM-V5 were extracted in PBS containing 1% Triton X-100 (TX) without or with 1 M potassium iodide (KI) to depolymerize F-actin. Equal volumes of soluble (S) and insoluble (I) lysates were subjected to Western blot analysis with anti-V5 (hepaCAM) or anti-actin (actin) antibody.

domain of hepaCAM affected its interaction with F-actin. The localizations of hepaCAM's extracellular/transmembrane mutants hCAMΔ1st Ig-V5, hCAMΔ2nd Ig-V5, hCAMΔIgs-V5 and hCAM_tail-V5 were shown in Figure 4-37. hCAMΔ1st Ig-V5, hCAMΔ2nd Ig-V5 and hCAMΔIgs-V5 were localized to the plasma membrane but hCAM_tail-V5 was localized to punctuate structures in the cytoplasm. MCF7 cells were transiently transfected with these mutants, and the P100 fractions harvested from these cells were extracted with 1% Triton X-100 in the absence or presence of 1M KI. Depolymerization of F-actin with KI showed an increased solubility of hCAMΔ1st Ig, hCAMΔ2nd Ig, and hCAMΔIgs proteins to 1% Triton X-100; however hCAM_tail remained unaffected (Figure 4-60), suggesting that the localization of hepaCAM cytoplasmic domain at the plasma membrane is necessary for its interaction with F-actin.

In addition to the observation in Figure 4-57 that the cytoplasmic domain of hepaCAM conferred its detergent-resistant nature, Figure 4-60 revealed that the extracellular Ig domains regulated the insolubility of plasma membrane-bound hepaCAM to 1% Triton X-100. Deletion of the 1st Ig domain of hepaCAM rendered the protein more soluble in 1% Triton X-100 (without KI). Conversely, removal of the 2nd Ig rendered the protein more insoluble in Triton X-100. In the absence of both Ig domains, an almost equivalent amount of hepaCAM was detected in both the soluble and insoluble fractions.

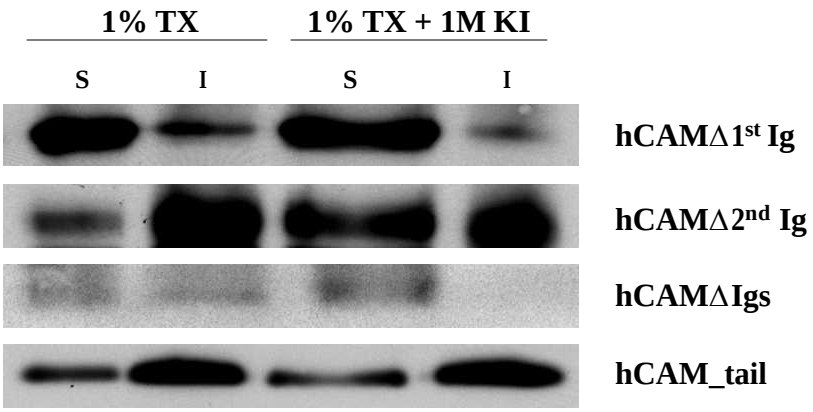

FIGURE 4-60 Relationship between hepaCAM structural domains and F-actin. P100 fractions of MCF7 cells transfected with hCAMΔ1st Ig-V5, hCAMΔ2nd Ig-V5, hCAMΔIgs-V5 and hCAM_tail-V5 for 48 hours were extracted in 1% Triton X-100 (TX) without or with 1 M potassium iodide (KI). Equal volumes of soluble (S) and insoluble (I) lysates were analyzed by Western blotting using anti-V5 antibody.

4.2.18 Recruitment of hepaCAM to lipid rafts

The fraction of hepaCAM that remained insoluble in Triton X-100 after depolymerization of F-actin with KI could be associated with lipid rafts or its derivative, caveolae. For convenience, both structures are here referred to as lipid rafts. Lipid rafts are cholesterol- and sphingolipid-enriched microdomains important for numerous signal transduction processes. Like the actin cytoskeleton, lipid rafts are insoluble in cold nonionic detergents. However, they can be differentiated from the cytoskeleton by their low buoyant density (Brown and London, 1998).

The putative connection between hepaCAM and the lipid rafts was examined by the detergent solubility assay. MCF7, HeLa, and NIH3T3 cells transiently transfected with hepaCAM-V5 for 48 hours were separated into cytosolic (S100) and membrane/cytoskeletal-bound (P100) fractions. The P100 pellet was further extracted into Triton X-100-soluble, n-OG (a detergent known to solubilize some lipid rafts)-soluble, and detergent-resistant (DRM) fractions. An equal volume of each fraction was subjected to Western blot analysis with anti-V5 antibody (Figure 4-61). Virtually no hepaCAM was detected in the cytosolic fraction. In the P100 fraction, the bulk of hepaCAM was extracted by Triton X-100, while the remaining was distributed between the n-OG-soluble and DRM fractions. Most hepaCAM was retained in the DRM of NIH3T3 cells, as compared to a lower concentration in HeLa cells, and the least in MCF7 cells.

NIH3T3 cells express a higher level of caveolin-1 than HeLa and MCF7 cells (Suzuki *et al*., 1998; Engelman *et al*., 1999). Caveolin-1 is commonly used as a marker for the

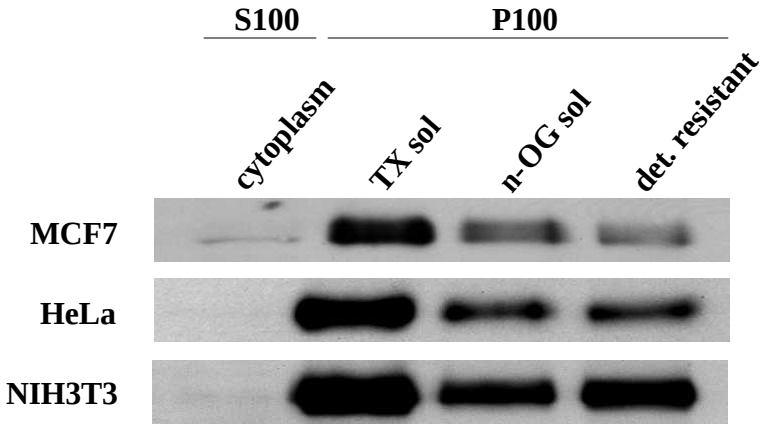

FIGURE 4-61 Association of hepaCAM with detergent-resistant membrane. MCF7, HeLa and NIH3T3 cells transfected with hepaCAM-V5 were fractionated into S100 (cytoplasm) and P100 fractions. The Triton X-100-soluble (TX sol) proteins from the P100 fraction were extracted, and the insoluble pellet was resuspended in *N*-octyl-β-D-glucopyranoside to solubilize some lipid raft components (n-OG sol). The insoluble material that remained after n-OG treatment was the DRM (det. resistant). An equal volume of each fraction was analyzed by Western blotting using anti-V5 antibody.

location of lipid rafts. Therefore, NIH3T3 cells were used to evaluate the relationship between hepaCAM and lipid rafts. The cells were transfected with hepaCAM-V5 and subjected to sucrose density gradient fractionation (Figure 4-62). Seven 0.5-ml fractions were subsequently collected and the proteins were concentrated by TCA/ethanol precipitation. An equal volume of the resuspended proteins in each fraction was subjected to Western blot analysis with anti-V5 (hepaCAM), anti-caveolin-1 (caveolin-1), or anti-actin (actin) antibody. The result showed that hepaCAM was present in the low-density lipid raft fractions and copartitioned with caveolin-1. In addition, hepaCAM also cofractionated with actin in the high-density fractions. Because lipid raft organization is dependent on the presence of cholesterol, the depletion of cholesterol with methyl-β-cyclodextrin (MCD) will cause the lipid raft-associated proteins to lose their buoyancy (Ilangumaran and Hoessli, 1998). MCD treatment of hepaCAM-transfected NIH3T3 cells (Figure 4-63) led to a modest diminishment of hepaCAM in fraction 2 accompanied with an accumulation of hepaCAM in fractions 3 and 4 of the density gradient, when compared to the untreated samples. This shift was similar to that observed in the control caveolin-1. These results indicated that hepaCAM is associated with the lipid rafts.

4.2.19 Colocalization of hepaCAM with lipid rafts and caveolae

Colocalization studies were performed to distinguish if hepaCAM resided in the caveolae, lipid rafts, or both. NIH3T3 cells transfected with hepaCAM-V5 for 48 hours were extracted with 0.5% ice-cold Triton X-100 prior to fixation and double-staining with anti-V5 antibody and caveolae marker caveolin-1 or lipid raft marker fyn (Figure 4-64). Confocal microscopy revealed that a proportion of Triton X-100-

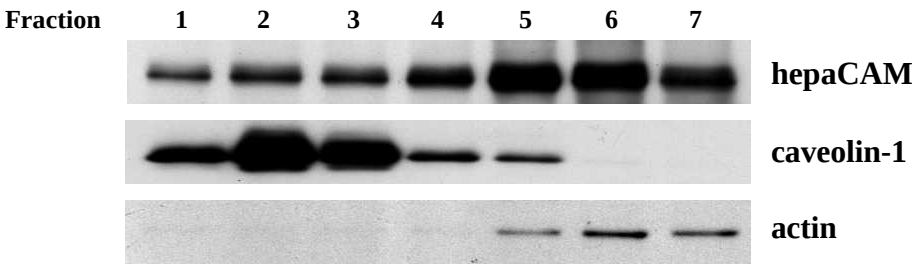

FIGURE 4-62 Partitioning of hepaCAM in lipid rafts. NIH3T3 cells were transfected with hepaCAM-V5 for 48 hours before assay. The cells were lysed in 1% Triton X-100 in TNE buffer and subjected to sucrose density gradient ultracentrifugation. Seven 0.5-ml fractions (numbered 1-7 from top to bottom) were collected, precipitated and analyzed by Western blotting using anti-V5 (hepaCAM), anti-caveolin-1 (caveolin-1) or anti-actin (actin) antibody. Caveolin-1 served as a positive control for low-density lipid raft-associated proteins. In contrast, actin was only detected in high-density fractions.

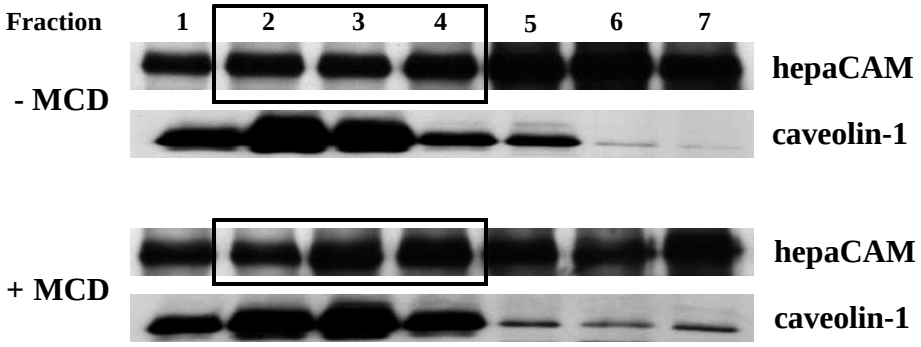

FIGURE 4-63 Disruption of cholesterol affects distribution of hepaCAM in lipid rafts. NIH3T3 cells transfected with hepaCAM-V5 were either untreated (- MCD; top panel) or treated (+ MCD; bottom panel) with 10 mM methyl-β-cyclodextrin (MCD) for 30 min to deplete membrane cholesterol. The cells were lysed in 1% Triton X-100 in TNE buffer and subjected to sucrose density gradient ultracentrifugation. Seven 0.5-ml fractions (numbered 1-7 from top to bottom) were collected, precipitated and analyzed by Western blotting using anti-V5 (hepaCAM) or anti-caveolin-1 (caveolin-1) antibody. Whereas comparable amount of hepaCAM resided in fractions 2, 3 and 4 of the untreated sample, a loss of hepaCAM in fraction 2 and an accumulation of hepaCAM in fractions 3 and 4 were noted in the MCD-treated sample. A similar trend of shift was observed in lipid raft control caveolin-1 in the MCD-treated sample.

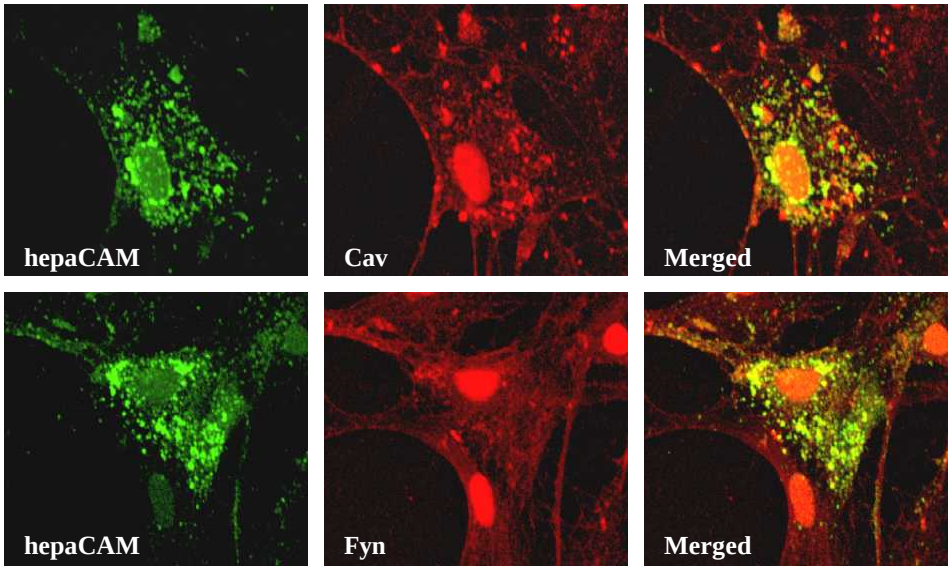

FIGURE 4-64 Colocalization of hepaCAM with lipid rafts and caveolae. NIH3T3 cells transfected with hepaCAM-V5 were detergent extracted with cold 0.5% Triton X-100 before fixing and immunostaining with anti-V5 antibody (left panel). Endogenous caveolin-1 (Cav) or fyn (Fyn) protein (middle panel) was also detected using either anti-caveolin-1 or anti-fyn antibody, respectively. Confocal images of the hepaCAM and caveolin-1 or fyn were merged to show regions of colocalization (right panel).

insoluble hepaCAM aligned with both caveolin-1 and fyn on the plasma membrane as well as in the punctuate structures in the cytoplasm, indicating that in addition to the lipid rafts, a part of hepaCAM is also recruited to the lipid raft derivative, caveolae.

4.2.20 Dimeric hepaCAM partitions to lipid rafts

NIH3T3 cells were transiently transfected with hepaCAM-V5. Forty-eight hours post-transfection, the cells were subjected to chemical crosslinking with BS3 prior to sucrose density gradient fractionation. An uncrosslinked sample was included as control. Seven 0.5-ml fractions were eventually collected and the proteins were concentrated by TCA/ethanol precipitation. An equal volume of the resuspended proteins in each fraction was analyzed by Western blotting using anti-V5 (hepaCAM) or anti-caveolin-1 (caveolin-1) antibody (Figure 4-65). The crosslinked dimeric hepaCAM was observed in fractions 1-4, demonstrating that the dimers are associated with the lipid rafts.

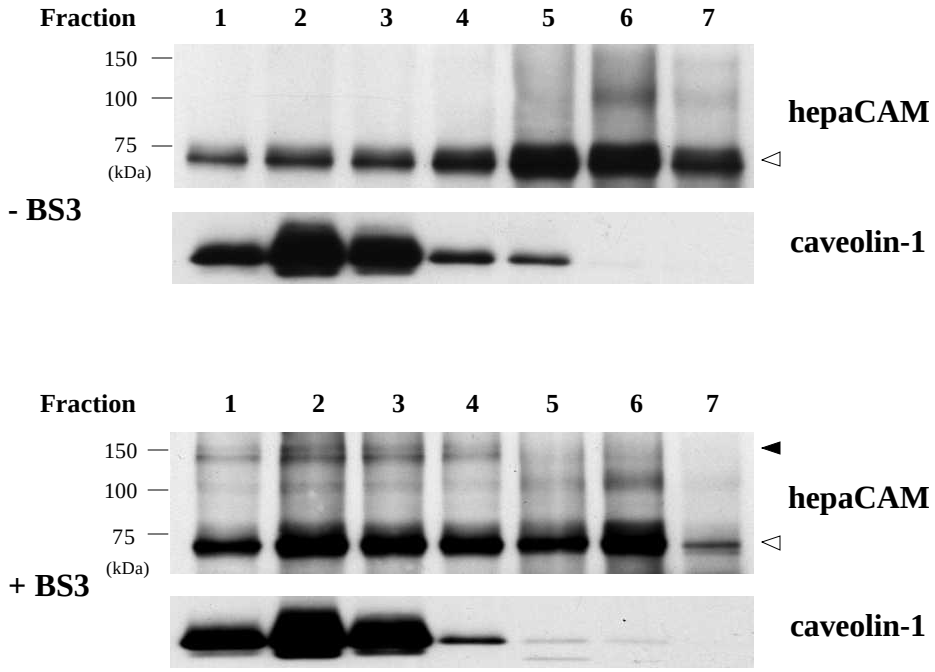

FIGURE 4-65 Partitioning of dimeric hepaCAM in lipid rafts. NIH3T3 cells were transfected with hepaCAM-V5 for 48 hours. Post-transfection, the cells were incubated in the absence (- BS3; top panel) or presence (+ BS3; bottom panel) of 3 mM BS3 prior to lysis in 1% Triton X-100 in TNE buffer. After sucrose density gradient ultracentrifugation, seven 0.5-ml fractions (numbered 1-7 from top to bottom) were collected, precipitated and analyzed by Western blotting using anti-V5 (hepaCAM) or anti-caveolin-1 (caveolin-1) antibody. Caveolin-1 served as a positive control for low-density lipid raft-associated proteins. Solid and open arrowheads indicate signals for dimeric and monomeric proteins, respectively. The positions of the molecular size markers are shown on the left of each panel.

4.3 Gene *HEPT3*

4.3.1 Upregulated expression of *HEPT3* in HCC

4.3.1.1 Expression of *HEPT3* in HCC patients

Suppression subtractive hybridization revealed that gene *HEPT3* was upregulated in HCC. The expression of *HEPT3* was examined in the matched liver samples of 23 HCC patients by semi-quantitative RT-PCR using gene-specific primers T3-F and T3-R. An elevated expression of *HEPT3* was observed in 87% of the HCC samples when evaluated against their adjacent non-tumorous liver tissues (Figure 4-66). Real-time RT-PCR was further performed on the same batch of liver specimens to quantitate the level of *HEPT3* expression (Figure 4-67). In addition to obtaining reproducible results pertaining to the frequency of *HEPT3* overexpression in HCC by both experimental approaches, real-time RT-PCR revealed a significant increase in the level of *HEPT3* expression in the tumor areas in comparison to the adjacent non-tumorous liver, which represented an average of 7-fold upregulation in mRNA expression, ($P < 0.0001$). The data showed that *HEPT3* overexpression was common in HCC tissues, suggesting its association with progression of tumorigenesis.

4.3.1.2 Expression of *HEPT3* in HCC cell lines

Furthermore, the expression of *HEPT3* was investigated in six liver cell lines by semi-quantitative RT-PCR using primers T3-F and T3-R (Figure 4-68). Chang liver is a HeLa-contaminated immortalized non-tumor liver cell line, while HepG2, C3A, Hep3B, Huh7 and SK-Hep1 are HCC cell lines. The result showed that *HEPT3* was expressed in all the six cell lines, but with a lower expression in Chang liver.

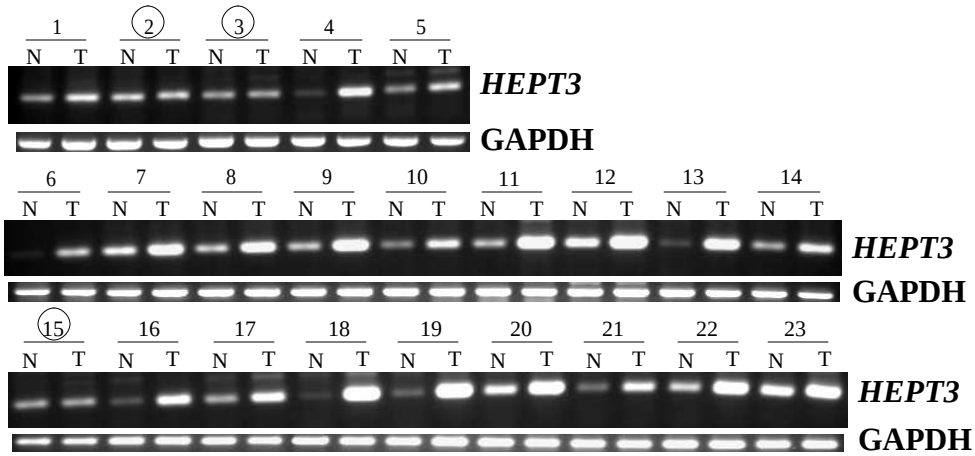

FIGURE 4-66 Expression of *HEPT3* transcript in 23 HCC patients by semi-quantitative RT-PCR. RT-PCR products of *HEPT3* generated by primers T3-F and T3-R were analyzed by gel electrophoresis. ◯ , sample that shows no clear difference in *HEPT3* expression; N, non-tumorous liver tissue; T, HCC liver tissue; GAPDH, internal control.

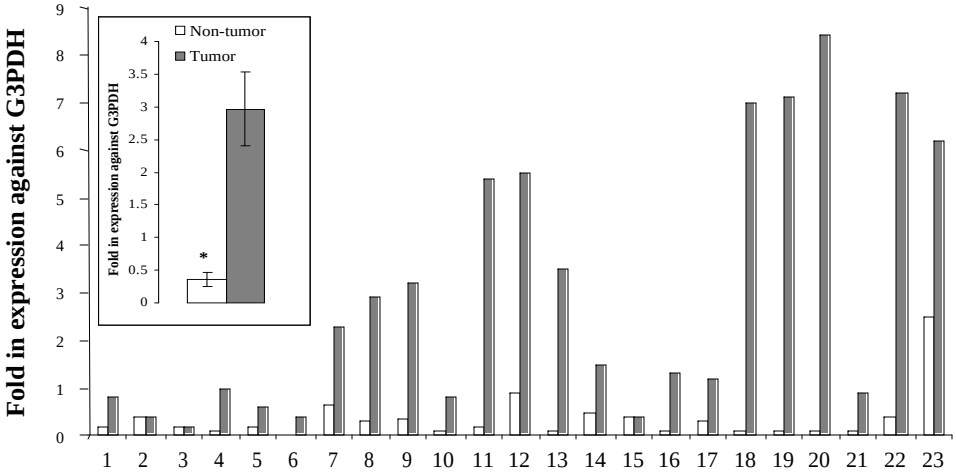

FIGURE 4-67 Expression of *HEPT3* transcript in 23 HCC patients by quantitative real-time RT-PCR. The expression level of *HEPT3* in each sample was determined by real-time RT-PCR. Results were normalized and converted into percentage against the expression level of GAPDH. The average level of expression (mean ± SD, n = 23) is represented in the left inset, * $P < 0.0001$. N, non-tumorous liver tissue; T, HCC liver tissue.

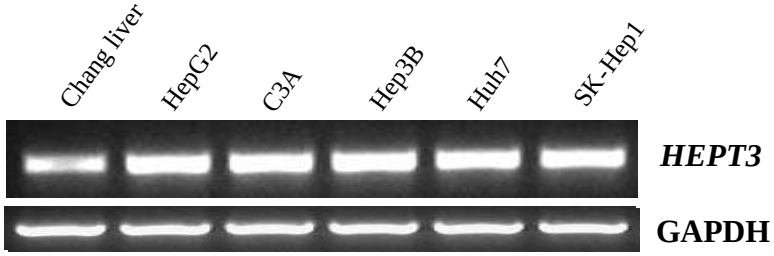

FIGURE 4-68 Expression of *HEPT3* transcript in 6 liver cell lines. Chang liver is a HeLa-contaminated immortalized non-tumor liver cell line, while HepG2, C3A, Hep3B, Huh7 and SK-Hep1 are HCC cell lines. Semi-quantitative RT-PCR was used to amplify *HEPT3* mRNA and GAPDH (an internal control). RT-PCR products were analyzed by gel electrophoresis.

4.3.2 Isolation of full-length *HEPT3* cDNA

5' and 3' RACE were employed to isolate the respective 5' and 3' ends of *HEPT3* cDNA from human normal liver cDNA library (Figure 4-69). Two successive rounds of 5' RACE using gene-specific primer T3-RACE-R and adaptor primer AP1 followed by nested primers T3-RACE-nR and AP2 yielded a band of ~1.7 kb. Concurrently, two consecutive rounds of 3' RACE using primers T3-RACE-F and T3-RACE-nF in combination with adaptor primers AP1 and AP2, respectively, generated a ~750 bp long 3' cDNA of *HEPT3*. The RACE fragments were cloned separately into the pGEM-T vector and sequenced. The overlapping sequences of the 5' and 3' RACE products were aligned together to obtain a composite sequence of 2839 bp, which represented the full-length cDNA of *HEPT3* (Figure 4-70). Based on this sequence, primers T3ful-F and T3ful-R corresponding to both ends of *HEPT3* cDNA were synthesized and used in end-to-end PCR to amplify the complete cDNA of *HEPT3*. The cDNA was cloned into the pGEM-T vector and sequenced for verification. This sequence was deposited into GenBank (Accession no. AY374441).

4.3.3 Genomic characteristics of *HEPT3*

4.3.3.1 Sequence analysis of *HEPT3* cDNA

The full-length cDNA of *HEPT3* contained a consensus polyadenylation signal, AATAAA, 23 bp upstream of the poly (A) tail at the 3' terminus (Figure 4-70). It also contained 13 copies of the mRNA destabilization motif, ATTTA.

A search of *HEPT3* cDNA against the NCBI database revealed no significant sequence homology to any characterized genes. Interestingly, two entries that seemed to represent the isoforms of *HEPT3* were identified (Figure 4-71). One of them was a

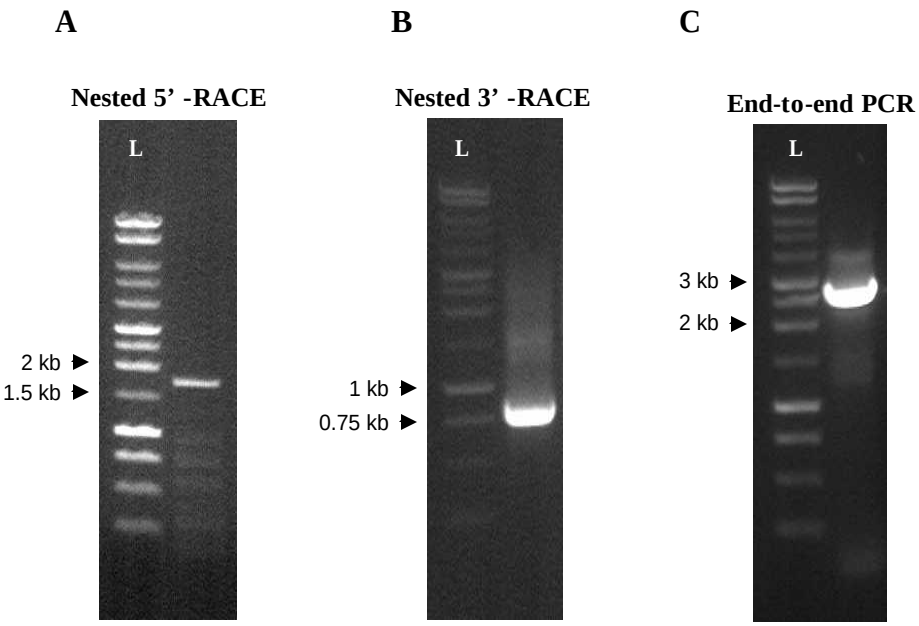

FIGURE 4-69 Isolation of *HEPT3* full-length cDNA by RACE. RACE-PCR products were analyzed by gel electrophoresis. A, Nested 5' RACE product was generated by primers T3-RACE-nR and AP2; B, Nested 3' RACE product was generated by primers T3-RACE-nF and AP2; C, Full-length *HEPT3* cDNA was amplified by end-to-end PCR using primers T3ful-F and T3ful-R. L, 1 kb DNA ladder.

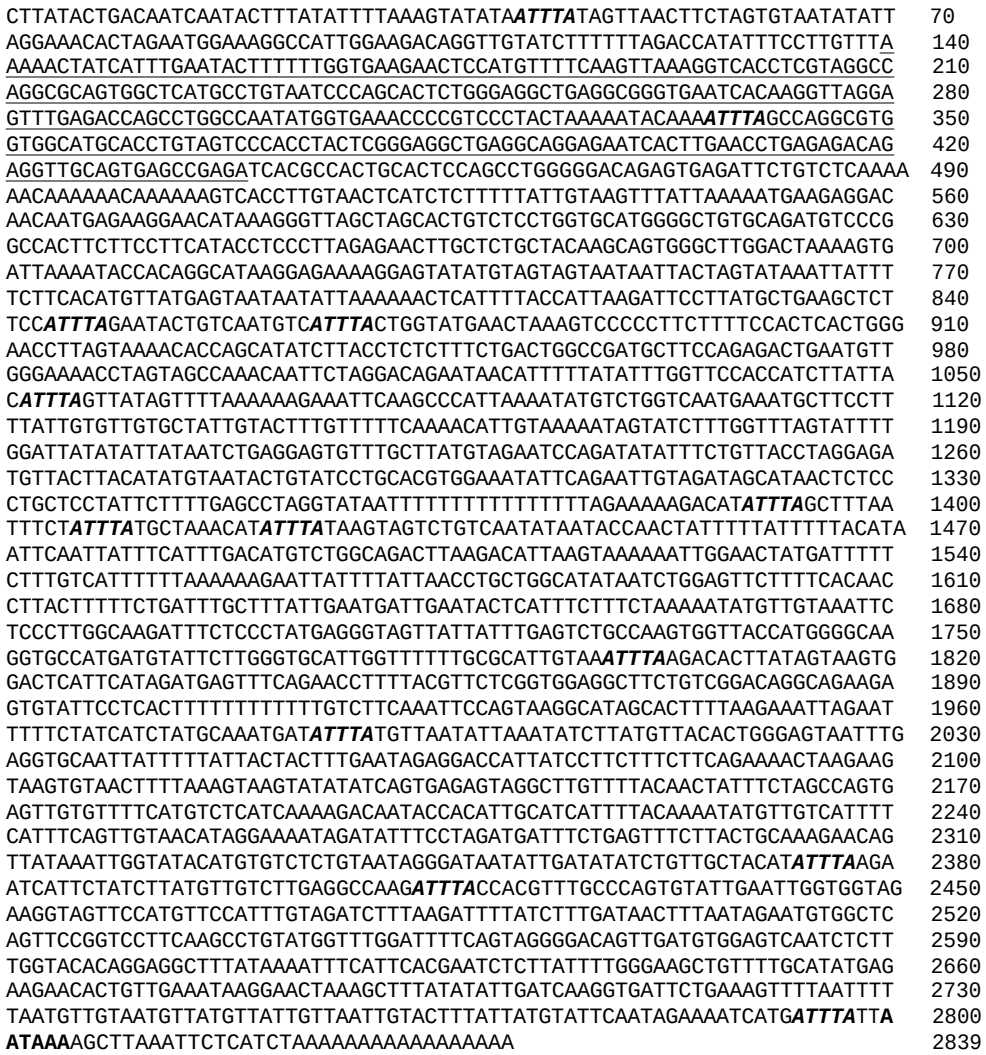

FIGURE 4-70 The full-length cDNA sequence of *HEPT3*. A polyadenylation signal (bold) was identified near the 3'-terminus. The mRNA destabilization motif, ATTTA, is in bold and italic. The ALU repetitive element is underlined. The sequence data for *HEPT3* is available in GenBank Accession no. AY374441.

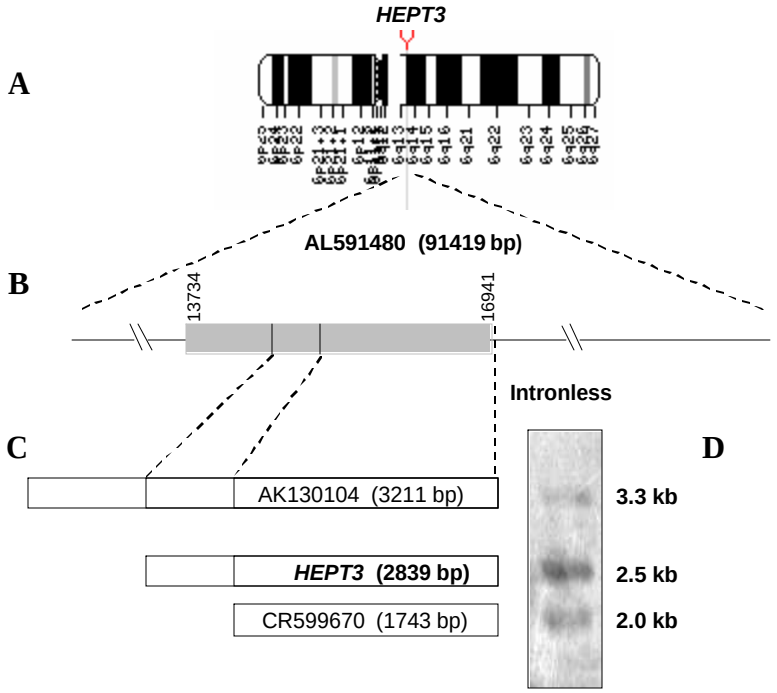

FIGURE 4-71 Genomic structure and isoforms of *HEPT3*. A, *HEPT3* is located on human chromosome 6q13-14. B, The genomic DNA of *HEPT3* (GenBank Accession no. AL591480) lacks intron. C, Isoforms of *HEPT3* retrieved from database. D, Northern blot analysis of *HEPT3*. Total RNA extracted from normal liver was separated on a 1% formaldehyde/MOPS gel, blotted onto membrane and probed with DIG-labeled *HEPT3* probe. Three transcripts with different sizes were detected.

3211 bp *Homo sapiens* cDNA FLJ26594 fis (GenBank Accession no. AK130104) that contained the entire *HEPT3* cDNA in its 3' region, and the other was a 1743 bp full-length cDNA clone CS0DF031YL13 of Fetal brain of *Homo sapiens* (GenBank Accession no. CR599670) that corresponded to the 3' end of *HEPT3* cDNA. Additionally, extensive homologies of *HEPT3* to a cluster of ESTs from various tissues were detected. The ESTs were derived from normal tissues of liver, lung, brain, uterus, prostate, adipose, and *etc*. More strikingly, ESTs were also identified in tumor tissues of kidney, bladder, breast, parathyroid, lung, testis, skin, and *etc*. These results indicated that *HEPT3* is widely expressed in diverse tissues, particularly high in tumors. It is noteworthy that gene *HEPT3* appeared to be exclusive to human because significant matches were not found between *HEPT3* and ESTs of other organisms.

The homologous ESTs revealed the presence of an Alu repetitive sequence in *HEPT3* cDNA. To confirm, the RepeatMasker program (Takeda *et al*., 1998) that screens DNA sequences for interspersed repetitive sequences was employed; and a 300 bp long Alu repetitive element located at nucleotides 140-439 of the *HEPT3* cDNA was identified.

The region on *HEPT3* cDNA that encompassed the Alu repetitive element, located at nucleotides 208-505, was shown by the BLAST program to be extensively complementary to multiple sites on the Alu-containing cDNA of the *AD7c-NTP* gene (GenBank Accession no. AAC08737). *AD7c-NTP* encoded a ~41 kDa neuronal thread protein that induced apoptosis and neuritic sprouting in transfected neuronal cells. The percentage of complementary base pairing between the two sequences ranged from

79-94% (Figure 4-72), suggesting a possible sense-antisense interaction between the two genes.

4.3.3.2 *HEPT3* lacks coding potential

A prominent feature of *HEPT3* cDNA sequence was the high density of stop codons in the three theoretical reading frames, causing a lack of extensive open reading frames (Figure 4-73), suggesting that *HEPT3* lacks coding capacity. Nevertheless, the possibility that *HEPT3* might encode a small protein could not be excluded. NCBI ORFinder analysis of *HEPT3* cDNA revealed multiple small open reading frames distributed throughout the gene. In the plus frames, the longest ATG-initiated ORF predicted was a 69 amino acid peptide which contained a protein kinase C phosphorylation site (residues 63-55). Other putative open reading frames included a 65 amino acid peptide that contained two putative protein kinase C phosphorylation sites (residues 7-9; 11-13) and a 62 amino acid peptide with no recognizable motifs. These predicted peptides shared no significant similarities with proteins and peptides deposited in the databases. In addition, the sequence surrounding the potential ATG start codon of each peptide did not contain a strong Kozak initiation sequence (Kozak, 1996).

Interestingly, the minus frame of *HEPT3* cDNA encoded a putative 103 amino acid protein, in which the entire protein had 55% identity to an unknown protein (GenBank Accession no. AAH01284), 94 of the 103 residues had 62% sequence match to an unnamed protein product (chromosome 9; GenBank Accession no. BAB15071), and ~70 of the 103 residues had about 60% homology to Alu subfamily sequence. Other matches included hypothetical protein FLJ20489 (GenBank Accession no.

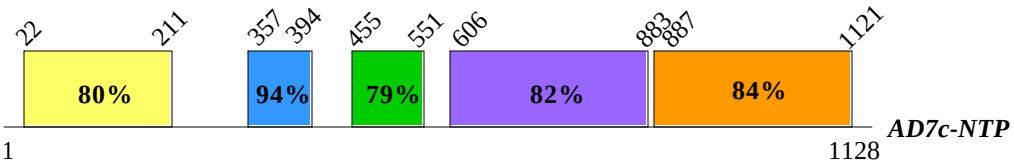

FIGURE 4-72 Possible sense-antisense interaction between *HEPT3* Alu element and *AD7c-NTP*. The full-length cDNA sequence of *AD7c-NTP* is 1128 bp long. As revealed by paired comparison between *HEPT3* and *AD7c-NTP* cDNA sequences, the ALU sequence of *HEPT3* is complementary to various regions on the *AD7c-NTP* cDNA. The location of each complementary site on *AD7c-NTP* is depicted by a box and the nucleotide positions are indicated above the box. The percentage of complementary is given in the boxes.

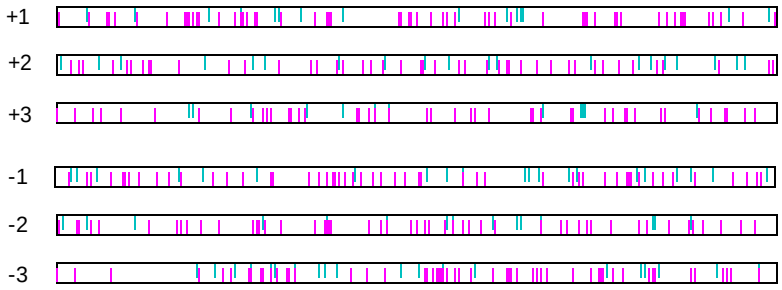

FIGURE 4-73 Coding potential of *HEPT3*. *HEPT3* cDNA sequence contains a high density of stop codons in the six reading frames and lacks extensive open reading frames. The location of each start codon is indicated by a green bar, and the location of each stop codon is indicated by a pink bar.

NP_060312), zinc finger protein HZF9 (GenBank Accession no. Accession no. NP_060312), zinc finger protein HZF9 (GenBank Accession no. XP_290171), neuronal thread protein (GenBank Accession no. NP_055301), topoisomerase II alpha-4 (GenBank Accession no. AAG13405), seven transmembrane helix receptor (GenBank Accession no. BAC05890), alpha-1A-adrenergic receptor isoform 2 (GenBank Accession no. NP_150646), seven transmembrane helix receptor (GenBank Accession no. BAC45260), and *etc*. Structural motifs identified by PROSITE algorithm included a *N*-glycosylation site (residues 34-37), two protein kinase C phosphorylation sites (residues 15-17; 38-40) and three *N*-myristoylation sites (residues 45-50; 69-74; 70-75).

4.3.3.3 Sequence analysis of *HEPT3* genomic DNA

A BLAST homology search was performed using the *HEPT3* full-length cDNA sequence against the human genome database of NCBI algorithm to determine the location of *HEPT3* on human chromosomes. *HEPT3* was mapped specifically to the human chromosome 6q13-14 (GenBank Accession no. AL591480; Figure 4-71). Comparative analysis revealed that *HEPT3* cDNA was collinear to the genomic sequence, indicating that gene *HEPT3* is intronless.

4.3.4 Northern blot analysis

Northern blot analysis was performed on total RNA extracted from normal liver to confirm that the isolated *HEPT3* cDNA was indeed full-length. The DIG-labeled *HEPT3* probe recognized three differently-sized transcripts — ~3.3 kb, ~2.5 kb and ~2 kb (Figure 4-71). The strongest ~2.5 kb signal appeared to correspond to the full-

length *HEPT3* product, while the 3.3 kb and 2 kb signals seemed to correspond to the two isoforms identified in the database.

4.3.5 Anti-proliferative effect of antisense *HEPT3*

An antisense approach was employed to examine the effect of *HEPT3* on HCC cell growth by inhibiting the expression of endogenous *HEPT3*. The antisense expression plasmid of *HEPT3* (HEPT3 (AS)-pcDNA3.1) was constructed by cloning a partial cDNA of *HEPT3* in the reverse orientation into vector pcDNA3.1 (Figure 4-74). Colony formation was carried out while growth rate was determined in stable C3A cells to assess the anti-proliferative effect of antisense *HEPT3*. In colony formation assay, HEPT3 (AS)-pcDNA3.1 was transfected into C3A cells and the cells were selected in 800 μg/ml of G418 for two weeks. Cells transfected with vector pcDNA3.1 served as control. As shown in Figure 4-75, antisense *HEPT3* significantly reduced the number of colonies formed as compared to the control. Moreover, the growth rate of the stable C3A cells expressing antisense *HEPT3* was 4-fold slower than cells transfected with empty vector (Figure 4-76). Semi-quantitative RT-PCR using the endogenous *HEPT3*-specific primer pair T3frag-f and T3frag-r demonstrated a moderately diminished expression of endogenous *HEPT3* in the C3A cells transfected with antisense *HEPT3* (Figure 4-77).

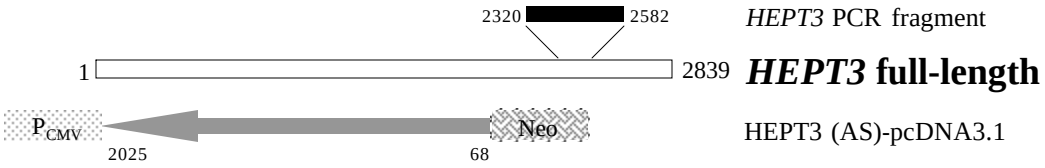

FIGURE 4-74 Schematic representation of *HEPT3* antisense construct. A cDNA fragment comprising of nucleotides 68-2025 of *HEPT3* cDNA was cloned in the reverse order into pcDNA3.1 vector to create the HEPT3 (AS)-pcDNA3.1 construct. Endogenous *HEPT3*-specific primers T3frag-f and T3frag-r were synthesized to amplify nucleotides 2320 to 2582 of endogenous *HEPT3*.

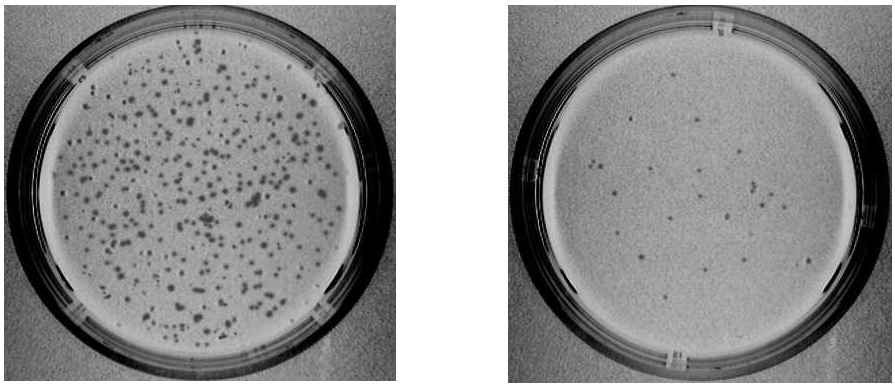

pcDNA3.1 **HEPT3 (AS)-pcDNA3.1**

FIGURE 4-75 Inhibition of colony formation by antisense *HEPT3*. C3A cells transfected with either antisense plasmid HEPT3 (AS)-pcDNA3.1 or pcDNA3.1 were cultured in the presence of 800 μg/ml of G418 for 2 weeks.

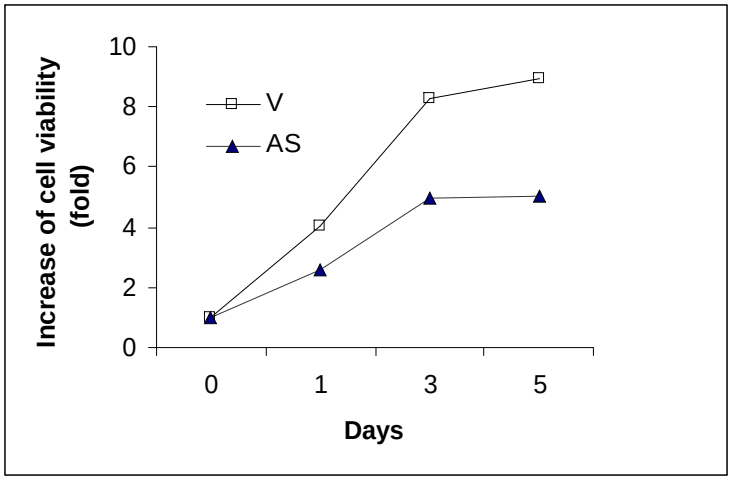

FIGURE 4-76 Inhibition of cell growth by antisense *HEPT3*. The growth rate of HEPT3 (AS)-pcDNA3.1-transfected C3A cells (AS) was compared to that of cells transfected with pcDNA3.1 alone (V) for 5 days by MTT assay.

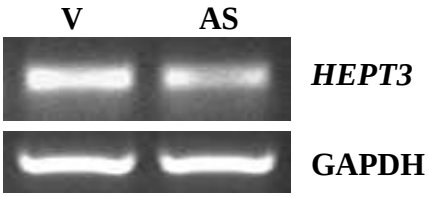

FIGURE 4-77 Suppression of endogenous *HEPT3* by antisense *HEPT3*. The expression levels of endogenous *HEPT3* in C3A cells stably transfected with HEPT3 (AS)-pcDNA3.1 (AS) and pcDNA3.1 alone (V) were examined by semi-quantitative RT-PCR using primers T3frag-f and T3frag-r. RT-PCR products were analyzed by gel electrophoresis. GAPDH, internal control.

CHAPTER 5 DISCUSSIONS

5.1 Gene *HEPN1*

5.1.1 Downregulation of *HEPN1* in HCC and other tumors

Gene *HEPN1*, downregulated in HCC, was identified in non-tumorous liver through the technique of suppression subtractive hybridization (SSH). Screening against 23 HCC patients, it was found that *HEPN1* mRNA was downregulated in 95.7% (22/23) of HCC and the average expression level was 5.7-fold lower in HCC tissues than that in non-tumorous liver tissues ($P < 0.0001$), suggesting that silencing of *HEPN1* is associated with carcinogenesis of hepatocytes. In addition, *HEPN1* was also significantly suppressed in 100% (4/4) of the HCC cell lines tested, further implying that loss of *HEPN1* expression is of generality in HCC of different etiologies. However, no correlation was identified between the loss of *HEPN1* expression and the events related to the development and progression of HCC, including hepatitis B viral infection, hepatitis C viral infection, liver cirrhosis, and the differentiation of HCC. This may be due to the ubiquitous downregulation of *HEPN1* in the HCC samples tested. The suppression of *HEPN1* seems to be applicable to diverse types of cancer. Evaluation of *HEPN1* expression in human cancer cell lines derived from blood, colon, breast, brain, and lung demonstrated a loss of expression in 83.3% (10/12) of the cell lines.

The mechanism responsible for the abrogation of *HEPN1* expression is still elusive. However, the reduced mRNA level in tumors implicates that silencing of *HEPN1* may be attributed to either deletion of *HEPN1* gene at the genomic DNA level such as

LOH (Largaespada, 2001; Cavenee *et al*., 1983) or transcriptional repression at the mRNA level such as epigenetic silencing through hypermethylation (Issa *et al*., 1994).

5.1.2 Genomic organization and characteristics of *HEPN1*

5.1.2.1 *HEPN1* encodes a protein of 88 amino acids

Gene *HEPN1* codes for a 1448 bp transcript. A probable functional TATA box resides upstream of the transcriptional start site at position -57. The predicted *HEPN1* product is a 10-kDa peptide consisting of 88 amino acids. The peptide neither has significant homology to any of the known proteins and peptides nor discloses substantial sequence and structural motifs in the available databases. The functionality of *HEPN1* gene is supported by the fact that *HEPN1* mRNA is translatable in transfected cells. Subcellular localization revealed that the encoded protein accumulated in the cytoplasm of HepG2 cells. It is certainly conceivable that small proteins that lack apparent functional domains may exert their effect primarily through interactions with other proteins. For example, *Brd* (Drosophila gene Bearded) encodes a novel small protein of 81 amino acids that interacts with and regulates genes of the Notch pathway (Leviten *et al*., 1997). Nevertheless, the novelty of *HEPN1* sequence led to the difficulty of understanding its biological role.

5.1.2.2 *HEPN1* is an intronless gene

A comparison between *HEPN1* cDNA sequence and the genomic sequence available in the database revealed a lack of intervening sequence in the genomic DNA, indicating that *HEPN1* is an intronless gene. In human, naturally intronless genes account for less than 6% of the genes in contrast to 96% in *S. cerevisiae* and 17% in *D. melanogaster* (Lewin, 2000). Since intronless genes do not require post-

transcriptional splicing, they can be transcribed more efficiently leading to a potentially faster rate of expression, greater abundance and higher fidelity. In essence, these intronless genes may react instantly to cellular signals. Families of intronless genes encode G-protein-coupled receptors and histones (Gentles and Karlin, 1999; Kedes, 1979). In the context of tumorigenesis, there are a few examples of intronless putative tumor suppressor genes. They include *TUSC1* (tumor suppressor candidate 1; Shan *et al*., 2004), *MORF4* (mortality factor 4; Bertram *et al*., 1999), and *BRCC2* (breast cancer cell 2; Broustas *et al*., 2004).

5.1.2.3 *HEPN1* maps to chromosome 11q24.2

HEPN1 is mapped to the human chromosome 11q24.2. Abnormalities of chromosome 11q including chromosome breakage, rearrangement, and loss on the long arm have been reported in a number of human tumors, including HCC (Walker *et al*., 1991; Wang and Rogler, 1988), colorectal cancer (Connolly *et al*., 1999), breast cancer (Gentile *et al*., 2001), melanoma (Goldberg *et al*., 2000), acute lymphoblastic leukemia (Mathew *et al*., 2001), and ovarian cancer (Launonen *et al*., 1998), signifying the presence of tumor suppressor genes in this region. The existence of important tumor suppressor genes is further supported by the observation that introduction of a normal chromosome 11 via microcell-mediated chromosome transfer can suppress tumorigenicity in Wilms' tumor, lung, rhabdomyosarcoma, ovarian, breast and melanoma cell lines (Weissman *et al*., 1987; Satoh *et al*., 1993; Loh *et al*., 1992; Stronach *et al*., 2003; Negrini *et al*., 1994; Robertson *et al*., 1996). Several tumor suppressor genes have been identified on 11q22-qter. They include the cell cycle regulatory and DNA repair genes, *ATM* at 11q23 (Rasio *et al*., 1995), and *CHK1* at 11q24 (Allinen *et al*., 2002), which are essential for the fidelity of DNA

replication and normal cell division. In response to DNA damage, ATM and ATR phosphorylate CHK1, which in turn inactivates Cdc25, and blocking the transition of the cell cycle. The p53 target genes, *PIG8* and *P53AIP1*, both involved in mediating p53-dependent apoptosis, are also located in 11q23 and 11q24, respectively (Gu *et al*., 2000; Matsuda *et al*., 2002).

5.1.3 HEPN1 inhibits cell growth and induces apoptosis

The frequent downregulation of *HEPN1* mRNA expression and its localization on chromosome 11 suggest a role of *HEPN1* in tumor suppression. To study its functional significance, *HEPN1* was expressed into a HEPN1-null HCC cell line, HepG2, in three phases. Firstly, transient transfection was performed on HepG2 cells. Forty-eight hours after transfection, the results showed that re-expression of HEPN1 inhibited cell growth by about 62.5±2.5% (P = 0.001). Secondly, colony formation was performed on cells transfected with the HEPN1-pEGFP construct and the pEGFP-N2 vector. The results showed that exogenous HEPN1 reduced both the number of colonies and the number of fluorescent cells. Furthermore, attempts to establish stable clones of HEPN1 from these colonies were unsuccessful; supporting that HEPN1 is indeed capable of suppressing cell growth in HepG2 cells. Finally, time-course transfection with GFP-fused HEPN1 visualized the dynamics of the distribution of HEPN1 and cell behaviour after transfection. Together with Annexin V assay, the results showed that HEPN1 promotes apoptosis in HepG2 cells. These data indicated that the *HEPN1* is a candidate tumor suppressor gene.

5.2 Gene *hepaCAM*

5.2.1 *hepaCAM* is antisense to *HEPN1*

A growing number of naturally occurring antisense RNAs has been identified in prokaryotes and eukaryotes over the last several years (Dolnick, 1997; Simons, 1988; Vanhee-Brossollet and Vaquero, 1998). Antisense transcripts are believed to constitute a general mechanism that regulates the expression of their sense target genes through transcription, nuclear processing, nuclear transport, translation, and mRNA stability (Green *et al*., 1986; Van der Krol *et al*., 1988). Numerous examples of antisense transcripts complementary to their sense counterparts have been documented. They include a native antisense RNA to *Hoxa11* (Chau *et al*., 2002), an antisense RNA to *Msx1* (Blin-Wakkach *et al*., 2001), and an antisense RNA to basic fibroblast growth factor (*bFGF*; Asa *et al*., 2001).

In this study, a previously unstudied gene antisense to *HEPN1* was identified. Containing the complete sequence of *HEPN1* in the reverse orientation in its 3' UTR, this gene was predicted to encode an incomplete ORF of 165 amino acids. Sequence extension by RACE revealed a 3244 bp long cDNA that contains a putative ORF of 416 amino acids. This novel gene was designated as *hepaCAM*. Gene *hepaCAM* is highly conserved in vertebrates. A search of the database revealed *hepaCAM* orthologues in chimpanzee, mouse and dog, with an overall 93-95% amino acid identity relative with the human sequence.

The fact that most of the antisense transcripts studied are non-translatable RNAs makes it difficult to establish if there might be a reciprocal relationship between the protein-encoding transcripts of *HEPN1* and *hepaCAM*. Nevertheless, based on the

similar transcriptional expression profiles of *HEPN1* and *hepaCAM* in tissues and cell lines of HCC and other tumors, it is least likely for *HEPN1* and *hepaCAM* to have repressive effects on each other.

5.2.2 Gene *hepaCAM* encodes a new member of the immunoglobulin superfamily

5.2.2.1 hepaCAM exhibits the typical sequence and structure of immunoglobulin-like cell adhesion molecule

Gene *hepaCAM* was predicted to encode a type I integral transmembrane immunoglobulin (Ig)-like cell adhesion molecule. The novel protein displays the typical structure of members of the immunoglobulin superfamily (IgSF), especially to JAM1, CAR and ESAM. Specifically, they contain an extracellular domain comprising of a membrane-distal V type Ig-domain and a membrane-proximal C2-type Ig-domain, a single transmembrane region, and a cytoplasmic tail. They also share a common feature of possessing conserved cysteine residues in the C2-type Ig domain that form intrachain disulfide bridges (Williams and Barclay, 1998). In addition, the extracellular domain of hepaCAM exhibits sequence homology to a cluster of cell adhesion molecules such as CEACAM3 and CAR. Collectively, these sequence and structural predictions suggest that *hepaCAM* may encode a new cell adhesion molecule belonging to the IgSF.

5.2.2.2 hepaCAM is localized predominantly on plasma membrane

Adhesion molecules such as TSLC1 (Masuda *et al*., 2002), CAR (Ashbourne Excoffon *et al*., 2003), and nectins (Satoh-Horikawa *et al*., 2000; Miyahara *et al*., 2000; Takahashi *et al*., 1999) commonly exhibit plasma membrane localization.

Similar characteristic pattern of distribution was also observed in hepaCAM. Analysis of the subcellular localization of hepaCAM revealed that the molecule was recruited predominantly to the plasma membrane, particularly in the areas of cell-cell contact when cells were confluent. Plasma membrane localization of many transmembrane proteins such as endothelial cell nitric oxide synthase (Sessa *et al*., 1993) has been attributed to myristoylation. Two putative myristoylation sites were recognized in hepaCAM.

In addition to its distribution to the plasma membrane, hepaCAM was also localized to the cytoplasm in a punctuate pattern. However, Western blot analysis of the membrane (P100) and cytosolic (S100) fractions revealed that hepaCAM was weakly present in the cytoplasm but abundant in the membrane. These findings imply that hepaCAM may reside in small membrane-bound vesicles in the cytoplasm. The identity of these structures has not been defined, but they are unlikely to be mitochondria because hepaCAM did not colocalize with mitochondria when examined in MCF7 cells.

In polarized cells, hepaCAM was accumulated at the basolateral plasma membranes, and lacking physical interaction, hepaCAM was shown to colocalize with E-cadherin at the lateral domain. Previous studies on adhesion molecules have defined a dileucine signal that functions in the basolateral targeting of the Lutheran glycoprotein (El Nemer *et al*., 1999) and E-cadherin (Miranda *et al*., 2001). Excluding those found in the signal peptide, hepaCAM contains 6 putative dileucine motifs — five in ectodomain and one in transmembrane domain. Although the exact functional dileucine motif has not been identified, these motifs may play a role in targeting

hepaCAM to the basolateral membrane. Dileucine signals that typically contain an acidic residue at the -4 position (D/E*XXX*LL) are also known to participate in endocytosis (Pond *et al*., 1995; Simonsen *et al*., 1998; Dietrich *et al*., 1997). Among the dileucine patterns in hepaCAM, three of them have the defined acidic residue in the -4 position. Therefore, it is possible that these sequences may also function as an endocytosis motif.

A potential GPI-binding site was identified near the COOH-terminal of hepaCAM. In contrast to the basolateral localization of hepaCAM in polarized cells, it has been reported that GPI-linked proteins are selectively sorted to the apical domain of many polarized epithelial cells, but preferentially excluded from the basolateral membrane. For example, a role of GPI in apical targeting has been demonstrated in Madin-Darby canine kidney (MDCK) cells and intestinal cells by attaching a GPI anchor to proteins not originally destined to the apical surface (Soole *et al*., 1985; Brown *et al*., 1989; Lisanti *et al*., 1989). Replacement of the GPI anchor of placental alkaline phosphatase with the transmembrane and cytoplasmic domains of vesicular stomatitis virus (VSV)-G switched its targeting from the apical to the basolateral surface (Brown *et al*., 1989). However, the role in apical targeting of the GPI-anchor has been challenged. It is now realized that GPI-anchored proteins may also contain basolateral-sorting signals. Clearly, in Fischer rat thyroid cells, six out of nine endogenously expressed GPI-linked proteins are directly delivered to the basolateral domain, the other three being apically disposed (Zurzolo *et al*., 1993). It was also observed that 50% of the native, GPI-anchored decay-accelerating factor (DAF) was localized to the basolateral domain. Moreover, fusion of the GPI-anchoring signal

sequence of DAF to the herpes simplex gD-1 protein exclusively targeted the molecule to the basolateral domain.

Deletion mutagenesis of hepaCAM revealed that the extracellular and transmembrane domains, but apparently not the cytoplasmic domain, are needed for plasma membrane localization of the molecule in mammalian cells. Nevertheless, it is to be clarified if the cytoplasmic domain of hepaCAM may play a role in the basolateral targeting of the protein. As exemplified by the two isoforms of adhesion molecule CEACAM1, both proteins are localized to the plasma membrane despite having different lengths of cytoplasmic domain. However, a recent study in polarized cells demonstrated that these isoforms, in fact, exhibit unequal plasma membrane localization. CEACAM1-S with the shorter cytoplasmic domain is exclusively distributed to the apical cell surface while CEACAM1-L is recruited to both the apical and lateral cell surfaces (Sundberg and Obrink, 2002). In addition, Neame and Isacke showed that the cytoplasmic tail of CD44 is required for its basolateral localization. Deletion of the domain resulted in the relocalization of the molecule onto the apical cell surface (Neame and Isacke, 1993).

5.2.2.3 hepaCAM is a glycoprotein

N-glycosylation in the endoplasmic reticulum (ER) is an essential protein modification critical for proper folding of the newly synthesized glycoproteins as they pass from one chaperone to another. In the ER, *N*-linked glycans attached to asparagines residues of newly synthesized glycoproteins provide binding sites for the lectin-like molecular chaperones, calreticulin and calnexin. The interactions between the glycoproteins and the ER chaperones provide a quality control system. Misfolded

or unassembled proteins are initially retained in the ER, after which, they are translocated to cytoplasm for ubiquitination and degradation by proteasomes (Parodi, 2000).

Like most membrane proteins, hepaCAM is also modified by *N*-linked glycosylation. In addition to the six predicted *N*-glycosylation sites on hepaCAM's extracellular domain, the observation of a difference between the calculated MW and the MW identified by Western blot analysis suggests that hepaCAM protein may be glycosylated. Enzymatic deglycosylation with PNGase and inhibition of glycosylation with tunicamycin confirmed that hepaCAM is a glycoprotein.

N-glycosylation has been reported to regulate the trafficking of proteins to the plasma membrane. Yan *et al*. showed that treatment of transfected podocyte and HEK-293 cells with tunicamycin led to the retention of non-glycosylated nephrin molecules in the ER. This result implies that nephrin depends on *N*-linked glycosylation for transport to the plasma membrane (Yan *et al*., 2002). Although it is still unclear if *N*-glycosylation affects the plasma membrane localization of hepaCAM, truncation of the extracellular domain of hepaCAM, which contains the *N*-glycosylation sites, clearly decreased the distribution of hepaCAM to the plasma membrane.

5.2.3 hepaCAM modulates cell-matrix adhesion

Cell adhesion is essential in all aspects of cell growth, cell migration and cell differentiation. It is mediated by cell adhesion molecules that are responsible for adhesion of cells to neighbouring cells or to the ECM components in the extracellular environment (Okegawa *et al*., 2004; Cohen *et al*., 1997). These molecules have been

implicated in a wide variety of processes including organogenesis, cell growth, immunity, wound healing, and signal transduction.

In polarized cells, hepaCAM was distributed to the basal membrane, suggesting an interaction of the molecule with the substratum. In favour of this notion, cell adhesion assays demonstrated that hepaCAM increased cell spreading on matrices fibronectin and matrigel, and delayed cell detachment. Deletion of the cytoplasmic domain reduced, but did not completely inhibit hepaCAM-mediated cell-matrix adhesion, implicating that, to a considerable extent, the extracellular and transmembrane domains may be needed to initiate and strengthen adhesion. Interestingly, hepaCAM was predicted to contain binding sites for Cdk5. Negash *et al*. demonstrated that Cdk5 promotes cell-matrix adhesion in lens epithelial cells when overexpressed (Negash *et al*., 2002).

The accelerated cell-matrix adhesion mediated by hepaCAM raises the possibility that loss of hepaCAM may ultimately lead to the disruption of tissue architecture by the loss of a tumor cell's ability to communicate with its extracellular environment.

5.2.4 *hepaCAM* is a candidate tumor suppressor gene

5.2.4.1 *hepaCAM* is frequently downregulated in tumors

It is evident that alterations in the adhesive properties play a vital role in the development and progression of cancer. Perturbation of cell adhesion to the ECM or to neighboring cells is a prominent feature of cancer cells. It allows malignant cells to escape from their site of origin, degrade the ECM, gain a more motile and invasion phenotype, and eventually, invade and metastasize (Okegawa *et al*., 2004). In the

context of IgSF adhesion molecules such as *CEACAM1* that is normally widely expressed in epithelia, vessel endothelia, and leukocytes (Odin *et al*., 1988), a loss of expression had been observed in numerous malignancies in humans including HCC (Tanaka *et al*., 1997), colon (Neumaier *et al*., 1993; Nollau *et al*., 1997), endometrial (Bamberger *et al*., 1998), breast (Huang *et al*., 1998), and prostate (Hsieh *et al*., 1995) cancers. Likewise, *hepaCAM* was expressed in a wide variety of normal human tissues, but frequently suppressed in tissues and cell lines of HCC and tumors derived brain, breast, lung, kidney, stomach, colon, rectum, prostate, uterus, ovary, skin and blood.

The mode of *hepaCAM* suppression in tumors is unelucidated. It may be inactivated by genetic modifications such as LOH (Largaespada, 2001; Cavenee *et al*., 1983) or epigenetic silencing through CpG methylation (Issa *et al*., 1994). Two potential CpG sites were recognized in the coding region and 3' UTR of *hepaCAM* transcript. Whether these sequences participate in the silencing of *hepaCAM* is unknown. Riggs and Jones proposed that methylation of the coding regions, introns or untranslated regions is relatively insignificant as compared to methylation of the promoter regions. Methylation of the promoter region could be the primary switching mechanism while methylation of the other regions could provide only fine-tuning (Riggs and Jones, 1983). Nevertheless, Malumbres *et al*. demonstrated that CpG methylation of the cell cycle inhibitor $p15^{INK4b}$ at the 3' UTR decreases its transcription in primary lymphomas (Malumbres *et al*., 1999).

5.2.4.2 *hepaCAM* is localized on chromosome 11 in a region where other adhesion molecules/tumor suppressors exist

Gene *hepaCAM* is mapped to the human chromosome 11q24.2. Molecular genetic and cytogenetic studies have indicated that the long arm of chromosome 11 is one of the most common targets for chromosomal aberrations during the progression of human malignancies. Several tumor suppressor genes encoding cell adhesion molecules of the IgSF have been identified on 11q22-qter. An Ig-like adhesion molecule *TSLC1* is a tumor suppressor at 11q23 and its downregulated expression through promoter hypermethylation has been reported in the development of many human cancers such as cancers of the lung, cervix, breast and prostate (Pletcher *et al*., 2001). Truncation of the cytoplasmic domain of TSLC1 in a primary NSCLC tumor suggests that this domain is important for tumor suppression activity (Kuramochi *et al*., 2001). Another example is the *OPCML* in 11q25, which is a member of the IgLON family of Ig domain-containing GPI-anchored cell adhesion molecules. The gene is frequently somatically silenced in epithelial ovarian carcinoma by allele loss and by CpG island methylation (Sellar *et al*., 2003).

5.2.4.3 hepaCAM inhibits cell proliferation

Importantly, transfection studies revealed that hepaCAM reduced cell colony formation and inhibited cell growth in HCC cell line HepG2 through suppression of cell proliferation. The frequent loss of hepaCAM expression in HCC and other tumors together with its anti-proliferative effect meets the most important criteria widely used to define tumor suppressor.

5.2.4.4 Possible mechanism of cell growth regulation by *hepaCAM*

Several interesting motifs identified in the sequence of *hepaCAM* allowed us to deduce a possible pathway in which *hepaCAM* may exert cell growth control in response to DNA damage. Three putative DNA binding sites for the tumor suppressor p53 were detected in the genomic DNA of *hepaCAM*, indicating that *hepaCAM* may be a p53-responsive gene. Some of the common targets of p53 are $p21^{waf1/cip1}$, *Bax*, *gadd45*, and *14-3-3*σ genes whose overexpression induces cell growth arrest and/or apoptosis (Kaghad *et al*., 1997; Jost *et al*., 1997; Yang *et al*., 1998; Zhu *et al*., 1998). Strikingly, an elevated expression of p53 protein was observed in HepG2 cells expressing hepaCAM. Cell cycle regulatory motifs were also recognized on hepaCAM protein. They include binding sites for ATM kinase, 14-3-3, Cdk5 and Cdc2.

It is attractive to speculate that upon DNA damage, *hepaCAM* may be activated through two pathways. p53 may act as a transcription factor that binds to *hepaCAM* genomic DNA to drive the expression of gene. In response, the gene product of *hepaCAM* may further stimulate the activity of p53. Alternatively, the existing hepaCAM protein may be activated through phosphorylation by ATM kinase. The activated hepaCAM molecule may, in turn, induce 14-3-3 that can subsequently sequester cyclin-dependent kinases such as Cdc2 and Cdk5 in the cytoplasm, causing cell cycle arrest. Otherwise, hepaCAM may directly interact with the cyclin-dependent kinases and block their cell cycle progression activities.

5.2.5 hepaCAM modulates cell motility

Cell-matrix adhesion is a key aspect of cell migration. Cell migration is a complex and integrated phenomenon that plays a central role in normal physiological processes such as embryonic development, wound healing, regeneration and immune surveillance, as well as in pathological processes such as angiogenesis, tumor invasion and metastasis (Gilbert, 2003; Ridley *et al*., 2003). To assess if hepaCAM is capable of modulating cell motility, Boyden chamber and wound healing assays were employed. Cells expressing hepaCAM exhibited increased motility through the transwell membrane. Furthermore, the cells had an increased ability to migrate into the mechanical scratch wound. The migratory effect of hepaCAM was almost completely abolished when lacking the cytoplasmic domain, indicating that hepaCAM modulates cell motility mainly via its cytopasmic domain.

hepaCAM was predicted to contain binding sites for Cdc2. It is of interest that Cdc2 is capable of promoting cell migration through $\alpha_v\beta_3$ integrin (Manes *et al*., 2003). In addition, the accumulation of p53 in hepaCAM-expressing cells further supports hepaCAM's ability to mediate cell migration since a loss of p53 activity was shown to decrease cell motility under physiological conditions (Sablina *et al*., 2003).

Adhesion molecules that stimulate cell migration have been associated with tumor spreading. A classic example is integrin which is the well established mediator of cell migration (Hynes, 1999). The $\alpha_v\beta_3$ integrin is predominantly, although not exclusively, found in cancer cells and neovessels (Byzova *et al*., 1998; Seftor *et al*., 1999). Overexpression of $\alpha_v\beta_3$ integrin in tumor cells alters cell-ECM interactions and causes increased tumorigenicity and tumor cell invasion (Felding-Habermann *et al*.,

1992). $\alpha_v\beta_3$ integrin has been shown to contribute to the establishment and growth of pulmonary metastatic melanoma lesions (Filardo *et al*., 1995). Additionally, it increases invasiveness of melanomas from the epidermis to the dermis (Hsu *et al*., 1998) and of human breast cancer cells in nude mice (Felding-Habermann *et al*., 2001).

Gene *hepaCAM* is widely expressed in normal tissues. Therefore, it is believed that, in physiology, hepaCAM-mediated cell migration stimulates tissue remodeling and wound healing. Nevertheless, it remains in question if hepaCAM, in contrast to its tumor suppressor activity, plays a role in promoting tumor invasion and metastasis in pathology. The notion of two opposing roles for a protein is not uncommon. A recent study showed that fibroblasts deficient of $p27^{Kip1}$ exhibit a dramatic decrease in cell motility as compared to the wildtype cells. Gene $p27^{Kip1}$ is a well characterized tumor suppressor and is frequently inactivated in malignancies. However, in subsets of tumors, high $p27^{Kip1}$ levels correlate with high tumor grade and increased metastasis. Besson *et al*. proposed that the overexpression of $p27^{Kip1}$ in these tumors might result in a switch of role from a cell cycle-inhibitor to an inducer of tumor progression and metastasis (Besson *et al*., 2004).

5.2.6 hepaCAM – a signal transducer?

5.2.6.1 hepaCAM resides in the lipid rafts and caveolae

Interaction of cell adhesion molecules with ECM components allows the transmission of signals directly or indirectly to second messengers that in turn unravel a cascade of events leading to the coordinated expression of a variety of genes involved in cell adhesion, migration, proliferation, differentiation and death.

Lipid rafts and its derivative, caveolae, are platforms for signal transduction. They are most abundant on the plasma membrane, but can also be found in intracellular membrane compartments, such as the endocytotic pathway or the Golgi apparatus; and are formed by the dynamic assemblies of cholesterol and sphingolipids. There is ample evidence suggesting that association of transmembrane receptors and signaling molecules with the lipid rafts provides a cellular mechanism for the concentration of receptor and signaling proteins to the microdomains of the cell surface (Simons and Ikonen, 1997; Brown and London, 1998; Jacobson and Dietrich, 1999). For example, ephrinB1, which is involved in embryonic patterning, is localized in lipid rafts where it recruits and interacts with signaling molecules such as the glutamate receptor-interacting protein (GRIP). Stimulation of ephrinB1 with its ligand causes the formation of large raft patches that contain GRIP and induces serine/threonine kinase activity (Bruckner *et al*., 1999).

Several lines of evidence demonstrate that hepaCAM is associated with both lipid rafts and caveolae. Firstly, the membrane-spanning domain of hepaCAM contains a membrane lipoprotein lipid attachment site and two potential palmitoylation sites. It has been shown that disruption of the palmitoylation sites of NCAM140 by mutation destroys its raft association (Niethammer *et al*., 2002). In addition, the dileucine signals of hepaCAM that may serve as endocytosis motifs implicate an interaction with lipid rafts/caveolae in the endocytotic pathway. Furthermore, hepaCAM was predicted to be a GPI-anchored protein and such proteins are found abundantly in the lipid rafts (Simons and Ikonen, 1997). Experimentally, a pool of insoluble hepaCAM remained after Triton X-100 solubilization and F-actin depolymerization, indicating that hepaCAM resides, at least partially, in the lipid rafts/caveolae. Detergent

solubility assays performed on MCF7, HeLa and NIH3T3 cells unmasked a possible association between hepaCAM and caveolae. Caveolin-1, the essential structural component of caveolae, is known to be highly expressed in NIH3T3 cells but lowly expressed in HeLa cells and deficient in MCF7 cells (Suzuki *et al*., 1998; Engelman *et al*., 1999). The level of caveolin-1 expression correlated with the level of hepaCAM in the detergent-resistant membranes (DRMs) of these three cell lines. The retention of hepaCAM was the highest in the DRM of NIH3T3, followed by HeLa, and then MCF7 cells. Furthermore, sucrose density gradient ultracentrifugation partitioned hepaCAM to the lipid rafts/caveolae fractions, and this buoyant density of hepaCAM could be altered by cholesterol dispersion. Finally, colocalization studies of hepaCAM with caveolae marker caveolin-1 and lipid raft marker fyn showed that hepaCAM colocalized in part with caveolae as well as lipid rafts.

A substantial amount of hepaCAM also resides in the high density fractions, suggesting that hepaCAM molecules either do not all reside in lipid rafts or shift between raft-associated and -unassociated states. A number of proteins are known to be functionally modified by a partial association with lipid rafts. For example, GRIP variably associates with lipid rafts via its interaction with ephrinB (Bruckner *et al*., 1999). A similar phenomenon may occur via binding to a linker protein that is variably associated with rafts. As demonstrated in CD44, the adhesion molecule associates with rafts through its interaction with annexin II, which partitions into the rafts in a calcium-dependent manner. In addition, disruption of the actin cytoskeleton results in the flotation of CD44-containing-lipid rafts, indicating that the interaction of CD44 with the heavy cytoskeleton restricts the buoyancy of raft-associated CD44 (Oliferenko *et al*., 1999; Bruses *et al*., 2001).

5.2.6.2 hepaCAM forms *cis*-homodimers on cell surface

Dimerization is fundamental to the activation of transmembrane receptors. It is common that signaling through cell surface receptor proteins containing a single transmembrane domain is transduced by dimerization of the proteins in response to ligand binding (Schlessinger, 2000; Heldin, 1995). It has also been postulated that oligomerization of transmembrane proteins may regulate their association with lipid rafts (Simons and Toomre, 2000).

The role of leucine zipper in mediating homo- or heterodimer formation is well established. Dimerization within the family or with other leucine zipper proteins is considered to mediate DNA binding specificity (Kouzarides and Ziff, 1988; Vinson *et al*., 1989). Protein analysis of hepaCAM revealed a leucine zipper on its extracellular domain, implicating that hepaCAM may dimerize through its ectodomain. As demonstrated by chemical crosslinking, hepaCAM is capable of forming *cis*-homodimers on the cell surface. Deletion of the cytoplasmic domain did not interfere with dimer formation, indicating that dimerization of hepaCAM is mediated by the extracellular and/or transmembrane domains independent of the cytoplasmic domain. This finding concurs with reports indicating that the ectodomains of N- and E-cadherins support their lateral interactions (Nagar *et al*., 1996; Pertz *et al*., 1999; Shapiro *et al*., 1995; Tamura *et al*., 1998; Tomschy *et al*., 1996). Moreover, sucrose density gradient ultracentrifugation of crosslinked hepaCAM showed that dimeric hepaCAM partitioned exclusively in the lipid rafts/caveolae, suggesting that dimerization regulates the association of hepaCAM with lipid rafts/caveolae as well as emphasizing the role of dimeric hepaCAM in cell signaling.

Notably, crosslinking of hepaCAM or its cytoplasmic domain deleted mutant showed the presence of high molecular weight proteins, indicating that hepaCAM may form large complexes with other endogenously expressed cellular proteins through its extracellular and/or transmembrane domains. Alternatively, it may represent higher order homo-oliogomers of hepaCAM or its mutant. Growing evidences indicate that most adhesion molecules transduce signaling by associating with other adhesion molecules and/or receptors for a soluble ligand (Kamiguchi and Lemmon, 2000; Aplin *et al*., 1999; Yamada and Geiger, 1997). Hence, identification of hetero-interacting partners for hepaCAM may lead to finding novel signaling pathways underlying its biological functions. It is interesting to observe the seemingly dimeric form of hepaCAM and its mutant in their respective un-crosslinked samples. Although the mechanism resulting in such interaction is unknown to us, Hunter *et al*. (Hunter *et al*., 1996) and others (Greenberg *et al*., 1991) have observed a similar phenomenon in CEACAM and raised the possibility that CEACAM dimers become covalently linked, perhaps through the action of transglutaminase, an enzyme which catalyzes the formation of γ-glutamyl-ε-lysine bonds in a restricted number of cellular proteins.

5.2.6.3 Cytoplasmic domain of hepaCAM is phosphorylated

Dimerization of extracellular domains results in the juxtaposition of the cytoplasmic domains which may lead to subsequent autophosphorylation on residues such as tyrosine in the cytoplasmic domains. These phosphorylated residues either trigger the intrinsic catalytic activity of the receptor or serve as recruitment sites for downstream signaling proteins (Klemm *et al*., 1998; Plotnikov *et al*., 1999).

Investigations need to be carried out to determine if the cytoplasmic domain of hepaCAM is capable of undergoing autophosphorylation upon dimerization. Nevertheless, the cytoplasmic domain of hepaCAM was predicted to contain potential serine/threonine and tyrosine kinase phosphorylation sites. Enzymatic dephosphorylation of hepaCAM revealed that the intracellular domain of hepaCAM is indeed phosphorylated. Although the sites of phosphorylation have not been identified, the results obtained suggest an important role of hepaCAM cytoplasmic domain in signal transduction.

Furthermore, sequence analyses showed that the cytoplasmic domain of hepaCAM contains phosphorylation sites for casein kinase II and protein kinase C, suggesting that hepaCAM may be a substrate for casein kinase II and/or protein kinase C. Additionally, the cytoplasmic domain also contains a proline-rich region with 6 SH3-binding domains. The amino acids of the proline-rich region may be capable of forming a polyproline type II helix and mediating interactions with SH3 binding domains (Pawson, 1995). Some adapter proteins containing SH3 domains may associate with the cytoplasmic domain of hepaCAM and induce intracellular signaling. Recently, the CD2-interacting adapter protein CD2AP was shown to bind to the proline-rich cytoplasmic sequence of CD2 and induce clustering of CD2 as well as cytoskeletal polarization (Dustin *et al*., 1998).

5.2.6.4 hepaCAM interacts with F-actin

Cell adhesion and migration require the coordinated interactions amongst the plasma membrane, cell adhesion molecules and actin cytoskeleton. These interactions are regulated by signaling complexes formed by the assembly of transmembrane,

cytosolic proteins and membrane lipids. The signaling complexes are thought to participate in the polymerization of actin filaments leading to the formation of membrane protrusions, or in the contraction of the actomyosin network leading to membrane retraction (Pollard and Borisy, 2003; Gumbiner, 1996). Many adhesion molecules interact with the actin cytoskeleton, some directly, such as beta-dystroglycan (Chen *et al*., 2003), and others indirectly, such as Ep-CAM that interacts with the actin cytoskeleton via α-actinin (Balzar *et al*., 1998).

Detergent solubility is a widely accepted technique that is routinely used in the analysis of actin cytoskeleton and lipid microdomains. Cold Triton X-100 extraction of endogenous and exogenous hepaCAM showed a portion of hepaCAM to be resistant to detergent solubilization. Extensive deletion mutagenesis of hepaCAM revealed that while the cytoplasmic domain, specifically residues located within 319-416, confers the detergent-resistant nature of the molecule, the extracellular Ig domains regulate the insolubility. Notably, further truncations of hepaCAM within residues 319-416 were not feasible because of the high GC content that restricted suitable primer design as well as the lack of unique restriction enzyme sites in the cDNA sequence.

In addition to the detergent solubility assay, the interaction between hepaCAM and the actin cytoskeleton was evidenced by the distribution of hepaCAM to the high density sucrose gradient where the actin cytoskeleton resides. Disassembly of F-actin by potassium iodide resulted in an increased solubility of hepaCAM. Moreover, the subcellular localization of hepaCAM seemed to be mediated by interaction with the actin network. Treatment of the hepaCAM-expressing MCF7 cells with cytochalasin

B, a filamentous actin-disrupting agent, not only affected the actin cytoskeleton, but also disorganized the subcellular localization of hepaCAM. Intriguingly, hepaCAM protein, previously localized on cell periphery, was redistributed into clusters containing the polymerized actin. These findings indicate that the subcellular localization of hepaCAM is influenced by the integrity of F-actin.

Furthermore, the localization of hepaCAM on plasma membrane seemed necessary to establish an interaction with F-actin. When the cytoplasmic domain of hepaCAM was cloned and transfected into cells, the protein was no longer localized on the plasma membrane, and its solubility could not be affected by F-actin depolymerization. Whether variations in post-translational modifications of the mutant, if any, influence the interaction with F-actin requires further investigation. The cytoplasmic domain of hepaCAM does not contain any consensus actin-binding sites such as the LKXXES/T motif (Prekeris *et al*., 1996; Howard *et al*., 1998) and I/LWEQ module (McCann and Craig, 1997), indicating that the interaction with the actin cytoskeleton may be indirect or mediated by cytoskeleton-associated proteins.

5.3 Gene *HEPT3*

5.3.1 *HEPT3* is upregulated in HCC

HEPT3 was identified by SSH as a novel gene that was upregulated in HCC. RT-PCR revealed an average 7-fold increase in the expression of *HEPT3* in 87% (20/23) of the HCC patients. In addition, the expression of *HEPT3* was elevated in 100% (5/5) of the HCC cell lines tested. The frequent transcriptional activation of *HEPT3* indicates a gain in function favoring liver cell proliferation/survival. Although the expression profile of *HEPT3* in other tumors has not been established, it is noteworthy that a cluster of *HEPT3*-homologous ESTs derived from a variety of human tumors can be retrieved from the public databases.

5.3.2 Genomic organization and characteristics of *HEPT3*

5.3.2.1 *HEPT3* is localized on chromosome 6q13-14

The full-length cDNA of *HEPT3* was isolated by RACE and constitutes 2839 bp. *HEPT3* is mapped to the long arm of human chromosome 6 at q13-14. Chromosome 6 is best recognized for the Major Histocompatibility Complex (MHC) that is critical to the human immune response. Additionally, it was documented to carry genes related to genetic diseases such as arthritis (Jawaheer *et al*., 2003), diabetes (Metz *et al*., 2002), schizophrenia (Lindholm *et al*., 1999), cancers, and *etc*. Abnormalities in chromosome 6 have been implicated in a wide spectrum of human neoplasms including melanoma (Trent *et al*., 1990; Das *et al*., 2000), ovarian cancer (Wan *et al*., 1999) and breast cancer (Rodriguez *et al*., 2000), with allelic deletions in the long arm being a commonplace. Microcell-mediated transfer of normal chromosome 6 into melanoma (Trent *et al*., 1990) and ovarian (Wan *et al*, 1999) cell lines was demonstrated to suppress tumorigenicity. Gains in chromosome 6 have also been

reported in HCC (Zimmermann *et al*., 1997), gastric, (Cavalho *et al*., 2001) and breast cancers (Rodriguez *et al*., 2000). Overall, these genetic aberrations highlight the importance of chromosome 6 in controlling the progressive transformation of normal cells into malignant derivatives.

5.3.2.2 *HEPT3* and isoforms are encoded by an intronless gene

Further molecular characterization revealed several unusual characteristics of gene *HEPT3*. Firstly, *HEPT3* represents an intronless gene. The cDNA of *HEPT3* was found to be collinear to its genomic DNA. In human, naturally intronless genes account for less than 6% of the genes in contrast to 96% in *S. cerevisiae* and 17% in *D. melanogaster* (Lewin, 2000). Since intronless genes do not require post-transcriptional splicing, they can be transcribed more efficiently leading to a potentially faster rate of expression, greater abundance and higher fidelity. In essence, these intronless genes may react immediately to cellular signals. Families of intronless genes encode G-protein-coupled receptors and histones (Gentles and Karlin, 1999; Kedes, 1979). There are also examples of proto-oncogenes that are intronless, the classic being *myc* (Sugiyama *et al*., 1999) and *c-jun* (Hattori *et al*., 1988) genes, and a recent addition, the human pituitary tumor transforming gene (PTTG) homologs (Prezant *et al*., 1999).

The lack of intron/exon boundaries in the genomic sequence implies that alternative splicing of *HEPT3* is unlikely to occur. Surprisingly, Northern blot analysis revealed three differently sized signals of approximately 3.3 kb, 2.5 kb and 2.0 kb, suggesting that *HEPT3* has isoforms. Indeed, database analysis revealed two uncharacterized full-length cDNAs that match *HEPT3* in sequence and in chromosomal location. One

is a ~3.2 kb long transcript obtained from human lung and the other is a ~1.7 kb transcript derived from human fetal brain. Like *HEPT3*, both transcripts are synthesized by intronless genomic DNA. These findings indicate that *HEPT3* and its 'alternatively spliced' variants are transcribed from the same genomic DNA. However, the mechanism of generating these differently sized transcripts by the DNA machinery remains puzzling.

5.3.2.3 *HEPT3* may encode a natural noncoding RNA

Another striking feature of *HEPT3* is the high density of stop codons in all the reading frames. The lack of extensive open reading frames suggests that *HEPT3* may be an example of noncoding RNA (ncRNA) termed as "riboregulator" which may function solely through its RNA. The theory of central dogma defines that DNA that carries the genetic information is transcribed to RNA and subsequently translated to protein; and proteins have been perceived as the functional outputs of genes. However, there is a growing class of ncRNA genes, which constitute about 98% of the transcriptional output of the human genome, that do not conform to this well-accepted paradigm of post-translational function. Rather, they produce functional transcripts that directly regulate important processes such as gene splicing nucleotide modification, protein transport, cell cycle progression, gene expression, protein degradation, and translocation through mechanisms such as RNA-RNA base pairing, RNA-protein interactions and intrinsic RNA activity (Mattick, 2001; 2003). Consequently, identification of ncRNAs is important. However, conventional protein gene-finding softwares such as Genscan are not designed to support the detection of ncRNAs, thus making the search difficult.

The identification of an Alu repetitive element in the *HEPT3* transcript portrayed another characteristic of ncRNA, in which the presence of short interspersed repetitive sequences (SINEs) and other repeats is a frequent event (Michel, 2002), but rare in translated transcripts (Yulug *et al*., 1995). Alu sequences are short interspersed repetitive DNA elements distributed throughout the genomes of primates (Singer, 1982), and have been implicated to be involved in recombination and evolution of the genome as well as contribute to about 0.1% of human genetic diseases (Deininger and Batzer, 1999). Although Alu sequences were initially thought to be 'junk DNA', evidence suggests that Alu repeats have a function. A study by Norris *et al*. demonstrated that Alu sequences possess the ability to function as estrogen receptor-dependent enhancers (Norris *et al*., 1995).

The polyadenylated transcript of *HEPT3* contains 13 copies of the mRNA destabilization motif, AUUUA. Such motifs have been reported in lymphokines, cytokines and proto-oncogene mRNAs; and have been proposed to interact with the AU-binding factor that destabilizes mRNA. Therefore, the RNA levels of *HEPT3* may be regulated by mechanisms involving RNA stability (Shaw and Kamen, 1986). Collectively, the atypical structural features of the cDNA suggest that *HEPT3* may function as a noncoding RNA.

Two examples of relatively well-studied mammalian genes that act at the RNA level are *XIST* (X (inactive)-specific transcript) and H19 (Szymanski *et al*., 2003; Askew and Xu, 1999). *XIST* gene produces a 17-kb noncoding, spliced, polyadenylated transcript exclusively expressed from the inactivated X chromosome (Avner and Heard, 2001; Marahrens *et al*., 1998). The *XIST* transcript, localized in the nucleus,

randomly coats one of the two chromosome X in female, resulting in transcriptional silencing of the chromosome in order to achieve dosage compensation. This process of X inactivation is critical for the maintenance of equivalent levels of X-linked gene expression in XX females and XY males. *H19* is implicated in imprinting of the insulin-like growth factor 2 (*IGF-II*) gene (Okamoto *et al*., 1997). The silencing of *H19* by methylation results in a loss of *IGF-II*/*H19* imprinting, leading to biallelic expression of both paternal and maternal *IGF-II*, and predisposing individuals to Wilms tumor and other embryonal tumors. Restoration of *H19* into embryonal tumor cell lines suppressed cell growth and induced morphological changes. Furthermore, clonogenicity in soft agar and tumorigenicity in nude mice were inhibited, indicating that *H19* may function as a tumor suppressor RNA (Hao *et al*., 1993).

5.3.3 *HEPT3* promotes tumorigenesis

To determine if *HEPT3* mRNA is involved in cell growth regulation of liver cells, an antisense inhibition approach was employed to interfere with the biological function of *HEPT3*. A plasmid that expressed a partial cDNA of *HEPT3* in the antisense orientation was constructed. The introduction of the antisense plasmid into C3A cells led to a modest suppression of endogenous *HEPT3* mRNA level. Colony formation assay showed that antisense *HEPT3* reduced the incidence of colonies that were resistant to antibiotic selection as compared to cells transfected with vector alone. In addition, C3A cells stably expressing antisense *HEPT3* displayed a 4-fold decrease in the rate of cell proliferation. These results demonstrated that antisense *HEPT3* exerts anti-proliferative effect on the liver cells that express endogenous *HEPT3* gene, implying that transcriptional activation of the *HEPT3* gene may stimulate the oncogenic pathway that induces cell proliferation.

5.3.4 Possible sense-antisense interaction between *HEPT3* and *AD7c-NTP*

Sequence analysis revealed that the region encompassing the Alu repetitive sequence of *HEPT3* is remarkably complementary to multiple sites on the Alu-containing cDNA of the *AD7c-NTP* gene. *AD7c-NTP* encodes a ~41 kDa neuronal thread protein that induces apoptosis and neuritic sprouting in transfected neuronal cells (Monte *et al*., 1997). This observation suggests a possible sense-antisense relationship between *HEPT3* and *AD7c-NTP*. Interestingly, *HEPT3* (chromosome 6q13-14) and *AD7c-NTP* (chromosome 1p36) are localized on different chromosomes.

Antisense RNAs may regulate expression of the corresponding sense genes, at the nuclear, transcriptional, post-transcriptional, or translational level. Gene regulation by naturally occurring antisense RNA has been initially documented in prokaryotes (Simons, 1988; Wagner and Simons, 1994), which later progresses to eukaryotes (Kumar and Carmichael, 1998; Vanhee-Brossollet and Vaquero, 1998) like plants (Terryn and Rouze, 2000) and animals (Erdmann *et al*., 2001). A recent study by Chen *et al*. predicted 22% of natural sense-antisense transcripts in the human genome (Chen *et al*., 2004). Endogenous antisense RNAs in eukaryotes may be grouped into *cis*-encoded antisense molecules that are transcribed from the opposite strand of the same genomic locus as the sense RNA and form a long or perfect RNA duplexes with the sense transcript; and *trans*-encoded antisense molecules that are transcribed from the genomic locus different from the sense RNA and form short or imperfect RNA duplexes with the sense transcript. The presence of highly repetitive sequences within the genome provides the potential for transcripts from different strands to yield RNAs that might anneal (Kumar and Carmichael, 1998). It is apparent that although many

examples of naturally occurring transcripts have been reported to date, no general rule of antisense RNA in the regulation of gene expression has been verified. Potentially, *HEPT3* RNA and *AD7c-NTP* transcript may form *trans*-RNA duplexes and degrade through double-stranded RNA formation, thus impeding the gene function. However, further investigations need to be conducted to establish this hypothesis.

CHAPTER 6 CONCLUSION

6.1 Conclusion

The present study embraces three novel genes, *HEPN1*, *hepaCAM* and *HEPT3* that are genetically altered in human hepatocellular carcinoma (HCC). Aiming to characterize these three novel genes, in this study, their full-length cDNAs were cloned and their expression and biological functions were investigated in HCC and other malignant cells.

Gene *HEPN1* is frequently silenced in HCC and in cell lines derived from various tumor types. *HEPN1* maps to human chromosome 11q24.2; and its gene product, a 10-kDa peptide, is distributed predominantly in the cytoplasm. Exogenous *HEPN1* is capable of suppressing cell growth and inducing apoptosis of HepG2 cells. The data suggest that silencing of *HEPN1* may be associated with carcinogenesis of hepatocytes.

Gene *hepaCAM* is expressed in a wide variety of normal human tissues, but frequently silenced in HCC and in other human tumors. Gene *hepaCAM* maps to human chromosome 11q24.2 and contains 7 exons; and the gene product of 416 amino acids encodes a cell adhesion molecule of the immunoglobulin superfamily. The hepaCAM protein is glycosylated, phosphorylated and forms *cis*-homodimers on cell surface. The molecule is distributed predominantly to the plasma membrane and is recruited to the basolateral membrane of polarized cells. The extracellular/transmembrane domains of hepaCAM are important for its dimerization and localization on plasma membrane. Ectopic expression of hepaCAM exerts anti-

proliferative effect on cell growth and activates tumor suppressor p53. In addition, hepaCAM modulates cell-matrix adhesion and cell motility mainly through its cytoplasmic domain. The detergent-resistance nature of hepaCAM is conferred by residues located within 319-416 of the cytoplasmic domain and regulated by the extracellular immunoglobulin domains. hepaCAM interacts with the actin cytoskeleton and resides in the lipid rafts. Taken together, hepaCAM is a new immunoglobulin-like cell adhesion molecule that plays important roles in cell growth regulation, cell-matrix interaction, and signal transduction.

Gene *HEPT3* exhibits a frequent upregulated expression in HCC tumors and cell lines. *HEPT3* maps to chromosome 6q13-14 and its transcript contains sequence characteristics typical of the emerging class of noncoding RNA including the lack of extensive ORF and the presence of an Alu sequence. Antisense studies revealed that HCC cell growth was significantly suppressed when *HEPT3* expression level was reduced. The data indicate that *HEPT3* may function as a noncoding RNA and may participate in the malignant transformation of hepatocytes.

In conclusion, the data presented to date indicate that *HEPN1*, *hepaCAM* and *HEPT3* may serve as promising markers for the early diagnosis of HCC and other malignancies. Understanding the molecular mechanisms of tumor suppression by *HEPN1* and *hepaCAM* as well as tumor promotion by *HEPT3* will provide insight into the applications of these molecules in prevention and treatment of human cancers.

6.2 Future work

The work presented in this thesis has laid the foundation for further studies. Along with the particularly interesting findings obtained for hepaCAM, several lines of research may be pursued.

Firstly, the frequent downregulation of hepaCAM in diverse human tumors and its ability to negatively regulate cell growth suggested an important role for hepaCAM in carcinogenesis. To date, the mode of silencing, the events leading to hepaCAM expression and its mechanism of regulation remain to be elucidated. The putative binding sites for cell cycle regulatory proteins on hepaCAM may provide a clue to the pathway(s) in which the molecule may exert anti-proliferative effects on cells. Identification of the functional domain of hepaCAM responsible and sufficient for tumor suppression may allow the synthesis of a peptide for use in cancer therapy.

Secondly, through *in vitro* studies, hepaCAM was shown to modulate cell-matrix adhesion and cell migration. It will be worthwhile to explore the *in vivo* role of hepaCAM in cell adhesion and migration in development, physiology and pathology. It is not uncommon for tumor suppressor genes to promote metastasis and invasion, depending on the stage of tumor progression and level of gene expression. Profiling the expression of hepaCAM in tumors of different grades may reveal if the molecule plays contrasting roles.

Last but not least, signaling through cell adhesion molecules are critical for the regulation of many cellular processes including embryonic development, homeostasis, immune responses, wound healing, and malignant transformation. The cytoplasm

domain of hepaCAM was shown to be phosphorylated. Although the sites of phosphorylation have not been identified, hepaCAM may be the substrate of kinases such as casein kinase II and protein kinase C. Recent experiments confirmed the physical interactions of hepaCAM with actin and the structural protein of caveolae, caveolin-1. Delineating the signaling pathways of actin and caveolin-1 may unravel the mechanisms of hepaCAM-mediated cell adhesion, cell migration, and tumor suppression. Furthermore, microarray- and proteomics-based technologies may be applied to provide a more complete picture of the network of genes altered by hepaCAM.

REFERENCES

Aberle H., Schwartz, H., and Kelmer, R. (1996) Cadherin-catenin complex: Protein interactions and their implications for cadherin function. *J. Cell. Biochem.* **61**, 514-523

Ahmadian M. R., Wittinghofer, A., and Schmidt, G. (2002) The actin filament architecture: tightly regulated by the cells, manipulated by pathogens. *EMBO reports* **3**, 214-218

Allinen, M., Peri, L., Kujala, S., Lahti-Domenici, J., Outila, K., Karppinen, S. M., Launonen, V., and Winqvist, R. (2002) Analysis of 11q21-24 loss of heterozygosity candidate target genes in breast cancer: indications of TSLC1 promoter hypermethylation. *Genes Chromosomes Cancer* **34**, 384-389

Amati, B., Alevizopoulos, K., and Vlach, J. (1998) Myc and the cell cycle. *Front. Biosci.* **3**, d250-d268

Aplin, A. E., Howe, A. K., and Juliano, R. L. (1999) Cell adhesion molecules, signal transduction and cell growth. *Curr. Opin. Cell. Biol.* **11**, 737-744

Arthur, M. J. (2000) Fibrogenesis II. Metalloproteinases and their inhibitors in liver fibrosis. *Am. J. Gastrointest. Liver Physiol.* **279**, 245-249

Asa, S. L., Ramyar, L., Murphy, P. R., Li, A. W., and Ezzat, S. (2001) The endogenous fibroblast growth factor-2 antisense gene product regulates pituitary cell growth and hormone production. *Mol. Endocrinol.* **15**, 589-599

Ashbourne Excoffon, K. J., Moninger, T., and Zabner, J. (2003) The coxsackie B virus and adenovirus receptor resides in a distinct membrane microdomain. *J. Virol.* **77**, 2559-2567

Askew, D. S., and Xu, F. (1999) New insights into the function of noncoding RNA and its potential role in disease pathogenesis. *Histol. Histopathol.* **14**, 235-241

Avner, P., and Heard, E. (2001) X-chromosome inactivation: counting, choice and initiation. *Nat. Rev. Genet.* **2**, 59-67

Balagurumoorthy, P., Sakamoto, H., Lewis, M. S., Zambrano, N., Clore, G. M., Gronenborn, A. M., Appella, E., and Harrington, R. E. (1995) Four p53 DNA-binding domain peptides bind natural p53-response elements and bend the DNA. *Proc. Natl. Acad. Sci. USA* **92**, 8591-8595

Ballestrem, C., Hinz, B., Imhof, B. A., and Wehrle-Haller, B. (2001) Marching at the front and dragging behind: differential alphaVbeta3-integrin turnover regulates focal adhesion behavior. *J. Cell Biol.* **155**, 1319-1332

Balzar, M., Bakker, H. A., Briaire-de-Bruijn, I. H., Fleuren, G. J., Warnaar, S. O., and Litvinov, S. V. (1998) Cytoplasmic tail regulates the intercellular adhesion function of the epithelial cell adhesion molecule. *Mol. Cell. Biol.* **18**, 4833-4843

Bamberger, A. M., Riethdorf, L., Nollau, P., Naumann, M., Erdmann, I., Götze, J., Brümmer, J., Schulte, H. M., Wagener, C., and Löning, T. (1998) Dysregulated expression of CD66a (BGP, C-CAM), an adhesion molecule of the CEA family, in endometrial cancer. *Am. J. Pathol.* **152**, 1401-1406

Barry, S. T., Flinn, H. M., Humphries, M. J., Critchley, D. R., and Ridley, A. J. (1997) Requirement for Rho in integrin signaling. *Cell. Adhes. Commun.* **4**, 387-398

Bazzoni, G., Martinez-Estrada, O. M., Orsenigo, F., Cordenonsi, M., Citi, S., and Dejana, E. (2000) Interaction of junctional adhesion molecule with the tight junction components ZO-1, cingulin, and occludin. *J. Biol. Chem.* **275**, 20520-20526

Beaugrand, M., N'kontchou, G., Seror, O., Ganne, N., and Trinchet, J. C. (2005) Local/regional and systemic treatments of hepatocellular carcinoma. *Semin. Liver Dis.* **25**, 201-211

Becker, K. F., Atkinson, M. J., Reich, U., Becker, I., Nekarda, H., Siewert, J. R., and Hofler, H. (1994) E-cadherin gene mutations provide clues to diffuse type gastric carcinomas. *Cancer Res.* **54**, 3845-3852

Beckerle, M. C., Burridge, K., DeMartino, G. N., and Croall, D. E. (1987) Colocalization of calcium-dependent protease II and one of its substrates at sites of cell adhesion. *Cell* **51**, 569-577

Beckman, G., and Bork, P. (1993) An adhesive domain detected in functionally diverse receptors. Trends *Biochem. Sci.* **18**, 40-41

Befeler, A. S., and Di Bisceglie, A. M. (2002) Hepatocellular carcinoma: Diagnosis and treatment. *Gastroenterology* **122**, 1609-1619

Behrens, J., Vakaet, L., Friis, R., Winterhager, E., Van Roy, F., Mareel, M. M., and Birchmeier, W. (1993) Loss of epithelial differentiation and gain of invasiveness correlates with tyrosine phosphorylation of the E-cadherin/β-catenin complex in cells transformed with a temperature-sensitive *v-SRC* gene. *J. Cell Biol.* **120**, 757-766

Behrens, J., von Kries, J. P., Kuhl, M., Bruhn, L., Wedlich, D., Grosschedl, R., and Birchmeier, W. (1996) Fuctional interaction of beta-catenin with the transcription factor LEF-1. *Nature* **382**, 638-642

Benn, J., and Schneider, R. J. (1994) Hepatitis B virus HBx protein activates ras-GTP complex formation and establishes a ras, raf, MAP kinase signaling cascade. *Proc. Natl. Acad. Sci. USA* **91**, 10350-10354

Benn, J., Su, F., Doria, M., and Schneider, R. J. (1996) Hepatitis B virus HBx protein induces transcription factor AP-1 by activation of extracellular signal-related and c-jun N-terminal mitogen-activated protein kinases. *J. Virol.* **70**, 4978-4985

Bertram, M. J., Berube, N. G., Hang-Swanson, X., Ran, Q., Leung, J. K., Bryce, S., Spurgers, K., Bick, R. J., Baldini, A., Ning, Y., Clark, L. J., Parkinson, E. K., Barrett, J. C., Smith, J. R., and Pereira-Smith, O. M. (1999) Identification of a gene that reverses the immortal phenotype of a subset of cells and is a member of a novel family of transcription factor-like genes. *Mol. Cell. Biol.* **19**, 1479-1485

Berx, G., Cleton-Jansen, A. M., Nollet, F., de Leeuw, W. J., van de Vijver, M., Cornelisse, C., and van Roy, F. (1995) E-cadherin is a tumour invasion suppressor gene mutated in human lobular breast cancers. *EMBO J.* **14**, 6107-6115

Besson, A., Gurian-West, M., Schmidt, A., Hall, A., and Roberts, J. M. (2004) p27Kip1 modulates cell migration through the regulation of RhoA activation. *Genes Dev.* **18**, 862-876

Birchmeier, W., and Behrens, J. (1994) Cadherin expression in carcinomas: role in the formation of cell junctions and the prevention of invasiveness. *Biochim. Biophys. Acta* **1198**, 11-26

Blin-Wakkach, C., Lezot, F., Ghoul-Mazgar, S., Hotton, D., Monteiro, S., Teillaud, C., Pibouin, L., Orestes-Cardoso, S., Papagerakis, P., Macdougall, M., Robert, B., and Berdal, A. (2001) Endogenous Msx1 antisense transcript: in vivo and in vitro evidences, structure, and potential involvement in skeleton development in mammals. *Proc. Natl. Acad. Sci. USA* **98**, 7336-7341

Blum, H. E. (2005) Treatment of hepatocellular carcinoma. *Best Pract. Res. Clin. Gastroenterol.* **19**, 129-145

Born, T. L., Frost, J. A., Schonthal, A., Prendergast, G. C., and Feramisco, J. R. (1994) c-Myc cooperates with activated Ras to induce the cdc2 promoter. *Mol. Cell. Biol.* **14**, 5710-5718

Bosch, F. X., and Ribes, J. In Tabor, E. (Ed) Viruses and Liver Cancer. (1st Ed). Elsevier Science. 2002, pp. 1-16

Bosch, F. X., Ribes, J., and Borras, J. (1999) Epidemiology of primary liver cancer. *Semin. Liver Dis.* **19**, 271-285

Bouchard, C., Thieke, K., Maier, A., Saffrich, R., Hanley-Hyde, J., Ansorge, W., Reed, S., Sicinski, P., Bartek, J., and Eilers, M. (1999) Direct induction of cyclin D2 by Myc contributes to cell cycle progression and sequestration of p27. *EMBO J.* **18**, 5321-5333

Brady-Kalnay, S. M., Mourton, T., Nixon, J. P., Pietz, G., Kinch, M., Chen, H., Brackenbury, R., Rimm, D. L., Del Vecchio, R. L., and Tonks, N. K. (1998) Dynamic interaction of PTPμ with multiple cadherins in vivo. *J. Cell Biol.* **141**, 287-296

Broustas, C. G., Gokhale, P. C., Rahman, A., Dritschilo, A., Ahmad, I., and Kasid, U. (2004) BRCC2, a novel BH3-like domain-containing protein, induces apoptosis in a caspase-dependent manner. *J. Biol. Chem.* **279**, 26780-26788

Brown, D. A., Crise, B., and Rose, J. K. (1989) Mechanism of membrane anchoring affects polarized expression of two proteins in MDCK cells, *Science* **245**, 1499-1501

Brown, D. A., and London, E. (1998) Structure and origin of ordered lipid domains in biological membranes. *J. Membr. Biol.* **164**, 103-114

Brown, D. A., and London, E. (2000) Structure and function of sphingolipid - and cholesterol-rich membrane rafts. *J. Biol. Chem.* **275**, 17221-17224

Brown, D. A., and Rose, J. K. (1992) Sorting of GPI-anchored proteins to glycolipid-enriched membrane subdomains during transport to the apical cell surface. *Cell* **68**, 533-544

Bruckner, K., Labrador, J. P., Scheiffele, P., Herb, A., Seeburg, P. H., and Klein, R. (1999) EphrinB ligands recruit GRIP family PDZ adaptor proteins into raft membrane microdomains. *Neuron* **22**, 511-524

Bruses J. L., Chauvet, N., and Rutishauser, U. (2001) Membrane lipid rafts are necessary for the maintenance of the α7 nicotinic acetylcholine receptor in somatic spines of ciliary neurons. *J. Neurosci.* **21**, 504-512

Burridge, K., and Chrzanowska-Wodnicka, M. (1996) Focal adhesions, contractility, and signaling. *Annu. Rev. Cell Dev. Biol.* **12**, 463-518

Busby, W. F. Jr., and Wogan, G. N. Aflatoxins. In Searle CE (Ed): Chemical Carcinogens. (2nd Ed). Vol 12. American Chemical Society. 1984, pp. 945-1136

Buxton, R. S., Cowin, P., Franke, W. W., Garrod, D. R., Green, K. J., King, I. A., Koch, P. J., Magee, A. I., Rees, D. A., Stanley, J. R., and Steinberg, M. S. (1993) Nomenclature of the desmosomal cadherins. *J. Cell Biol.* **121**, 481-483

Byzova, T. V., Rabbani, R., D'Souza, S. E., and Plow, E. F. (1998) Role of integrin alpha(v)beta3 in vascular biology. *Thromb. Haemost.* **80**, 726-734

Campbell, K. P. (1995) Three muscular dystrophies: loss of cytoskeleton-extracellular matrix linkage. *Cell* **80**, 675-679

Carr, B. I. (2004) Hepatocellular carcinoma: current management and future trends. *Gastroenterology* **127**, S218-S224

Carvalho, B., van der Veen, A., Gartner, F., Carneiro, F., Seruca, R., Buys, C. H., and Kok, K. (2001) Allelic gains and losses in distinct regions of chromosome 6 in gastric carcinoma. *Cancer Genet. Cytogenet.* **131**, 54-59

Cavenee, W. K., Dryja, T. P., Phillips, R. A., Benedict, W. F., Godbout, R., Gallie, B. L., Murphree, A. L., Strong, L. C., and White, R. L. (1983) Expression of recessive alleles by chromosomal mechanisms in retinoblastoma. *Nature* **305**, 779-784

Cepek, K. L., Shaw, S. K., Parker, C. M., Russell, G. J., Morrow, J. S., Rimm, D. L., and Brenner, M. B. (1994) Adhesion between epithelial cells and T lymphocytes mediated by E-cadherin and the alpha E beta 7 integrin. *Nature* **372**, 190-193

Cha, C. H., Ruo, L., Fong, Y., Jarnagin, W. R., Shia, J., Blumgart, L. H., and DeMatteo, R. P. (2003) Resection of hepatocellular carcinoma in patients otherwise eligible for transplantation. *Ann. Surg.* **238**, 315-321

Cha, M. Y., Kim, C. M., Park, Y. M., and Ryu, W. S. (2004) Hepatitis B virus X protein is essential for the activation of Wnt/β-catenin signaling in hepatoma cells. *Hepatology* **39**, 1683-1693

Chau, Y. M., Pando, S., and Taylor, H. S. (2002) HOXA11 silencing and endogenous HOXA11 antisense ribonucleic acid in the uterine endometrium. *J. Clin. Endocrinol. Metab.* **87**, 2674-2680

Chen, J., Sun, M., Kent, W. J., Huang, X., Xie, H., Wang, W., Zhou, G., Shi, R. Z., and Rowley, J. D. (2004) Over 20% of human transcripts might form sense-antisense pairs. *Nucleic Acids Res.* **32**, 4812-4820

Chen, W. Y., Grant, M. E., Schor, A. M., and Schor, S. L. (1989) Differences between adult and fetal fibroblasts in the regulation of hyaluronate synthesis: correlation with migratory activity. *J. Cell Sci.* **94**, 577-584

Chen, Y. J., Spence, H. J., Cameron, J. M., Jess, T., Ilsley, J. L., and Winder, S. J. (2003) Direct interaction of beta-dystroglycan with F-actin. *Biochem. J.* **375**, 329-337

Chung, Y. L., Sheu, M. L., and Yen, S. H. (2003) Hepatitis C virus NS5A as a potential viral Bcl-2 homologue interacts with Bax and inhibits apoptosis in hepatocellular carcinoma. *Int. J. Cancer* **107**, 65-73

Citi, S., Sabanay, H., Jakes, R., Geiger, B., and Kendrick-Jones, J. (1988) Cingulin, a new peripheral component of tight junctions. *Nature* **333**, 272-275

Clark, E. A., King, W. G., Brugge, J. S., Symons, M., and Hynes, R. O. (1998) Integrin-mediated signals regulated by members of the Rho family of GTPases. *J. Cell Biol.* **142**, 573-586

Clark, H. P., Carson, W. F., Kavanagh, P. V., Ho, C. P., Shen, P., and Zagoria, R. J. (2005) Staging and current treatment of hepatocellular carcinoma. *Radiographics* **Suppl1**, S3-S23

Cohen, M. B., Griebling, T. L., Ahaghotu, C. A., Rokhlin, O. W., and Ross, J. S. (1997) Cellular adhesion molecules in urologic malignancies. *Am. J. Clin. Pathol.* **107**, 56-63

Coleman, W. B. (2003) Mechanisms of human hepatocarcinogenesis. *Curr. Mol. Med.* **3**, 573-588

Colombo, M., and Sangiovanni, A. (2004) The strategic role of staging in the treatment of HCC. *Hepatology* **39**, 552-553

Connolly, K. C., Gabra, H., Millwater, C. J., Taylor, K. J., Rabiasz, G. J., Watson, J. E., Smyth, J. F., Wyllie, A. H., and Jodrell, D. I. (1999) Identification of a region of frequent loss of heterozygosity at 11q24 in colorectal cancer. *Cancer Res*. **59**, 2806-2809

Das, S., Lese, C. M., Song, M., Jensen, J. L., Wells, L. A., Barnoski, B. L., Roseberry, J. A., Camacho, J. M., Ledbetter, D. H., and Schnur, R. E. (2000) Partial paternal uniparental disomy of chromosome 6 in an infant with neonatal diabetes, macroglossia, and craniofacial abnormalities. *Am*. *J*. *Hum*. *Genet*. **67**, 1586-1591

Deane, N. G., Parker, M. A., Aramandla, R., Diehl, L., Lee, W. J., Washington, M. K., Nanney, L. B., Shyr, Y., and Beauchamp, R. D. (2001) Hepatocellular carcinoma results from chronic cyclin D1 overexpression in transgenic mice. *Cancer Res*. **61**, 5389-5395

Dehner, L. P., Snover, D. C., Sharp, H. L., Ascher, N., Nakhleh, R., and Day, D. L. (1989) Hereditary tyrosinemia type I (chronic form): pathologic findings in the liver. *Hum*. *Pathol*. **20**, 149-158

Deininger, P. L., and Batzer, M. A. (1999) Alu repeats and human disease. *Mol*. *Genet*. *Metab*. **67**, 183-193

Deuffic, S., Poynard, T., Buffat, L., and Valleron, A. J. (1998) Trends in primary liver cancer. *Lancet* **351**, 214-215

Deugnier, Y., and Turlin, B. In Okuda, K., and Tabor, E (Eds) Liver Cancer. Churchill Livingstone. 1997, pp. 97-110

Dexter, D. L., and Leith, J. T. (1986) Tumor heterogeneity and drug resistance. *J*. *Clin*. *Oncol*. **4**, 244-257

Dietrich, J., Kastrup, J., Nielsen, B. L., Odum, N., and Geisler, C. (1997) Regulation and function of the CD3 DxxxLL motif: a binding site for adaptor protein-1 and adaptor protein-2 in vitro. *J*. *Cell Biol*. **138**, 271-281

Dolnick, B. J. (1997) Naturally occurring antisense RNA. *Pharmacol*. *Ther*. **75**, 179-184

Dourakis, S. P., and Tolis, G. (1998) Sex hormonal preparations and the liver. *Eur*. *J*. *Contracept*. *Reprod*. *Health Care* **3**, 7-16

Dustin, M. L., Olszowy, M. W., Holdorf, A. D., Li, J., Bromley, S., Desai, N., Widder, P., Rosenberger, F., van der Merwe, P. A., Allen, P. M., and Shaw, A. S. (1998) A novel adaptor protein orchestrates receptor patterning and cytoskeletal polarity in T-cell contacts. *Cell* **94**, 667-677

Ebnet, K., Schulz, C. U., Meyer Zu Brickwedde, M. K., Pendl, G. G., and Vestweber, D. (2000) Junctional Adhesion Molecule Interacts with the PDZ Domain-containing Proteins AF-6 and ZO-1. *J. Biol. Chem.* **275**, 27979-27988

Ebnet, K., Suzuki, A., Ohno, S., and Vestweber, D. (2004) Junctional adhesion molecules (JAMs): more molecules with dual functions? *J. Cell Sci.* **117**, 19-29

El Nemer, W., Colin, Y., Bauvy, C., Codogno, P., Fraser, R. H., Cartron, J. P., and Le Van Kim, C. L. (1999) Isoforms of the lutheran/basal cell adhesion molecule glycoprotein are differentially delivered in polarized epithelial cells. *J. Biol. Chem.* **274**, 31903-31908

El-Serag, H. B., and Mason, A. C. (1999) Rising incidence of hepatocellular carcinoma in the United States. *N. Engl. J. Med.* **340**, 745-750

Endo, K., Ueda, T., Ueyama, J., Ohta, T., and Terada, T. (2000) Immunoreactive E-cadherin, alpha-catenin, beta-catenin, and gamma-catenin proteins in hepatocellular carcinoma: relationships with tumor grade, clinicopathologic parameters, and patients' survival. *Hum. Pathol.* **31**, 558-565

Engelman, J. A., Zhang, X. L., and Lisanti, M. P. (1999) Sequence and detailed organization of the human caveolin-1 and -2 genes located near the D7S522 locus (7q31.1). Methylation of a CpG island in the 5' promoter region of the caveolin-1 gene in human breast cancer cell lines. *FEBS Lett.* **448**, 221-230

Engqvist-Goldstein, A. E., and Drubin, D. G. (2003) Actin assembly and endocytosis: from yeast to mammals. *Annu. Rev. Cell Dev. Biol.* **19**, 287-332

Erdmann, V. A., Barciszewska, M. Z., Hochberg, A., de Groot, N., and Barciszewski, J. (2001) Regulatory RNAs. *Cell Mol. Life Sci.* **58**, 960-977

Eriksson, S., Carlson, J., and Velez, R. (1986) Risk of cirrhosis and primary liver cancer in alpha 1-antitrypsin deficiency. *N. Engl. J. Med.* **314**, 736-739

Fais, S., and Malorni, W. (2003) Leukocyte uropod formation and membrane/cytoskeleton linkage in immune interactions. *J. Leukoc. Biol.* **73**, 556-563

Fanning, A. S., Jameson, B. J., Jesaitis, L. A., and Anderson, J. M. (1998) The tight junction protein ZO-1 establishes a link between the transmembrane protein occludin and the actin cytoskeleton. *J. Biol. Chem.* **273**, 29745-29753

Fausto, N., Laird A. D., and Webber, E. M. (1995) Liver regeneration. 2. Role of growth factors and cytokines in hepatic regeneration. *FASEB J.* **9**, 1527-1536

Feitelson, M. A. (2006) Parallel epigenetic and genetic changes in the pathogenesis of hepatitis virus-associated hepatocellular carcinoma. *Cancer Lett.* **239**, 10-20

Felding-Habermann, B., Mueller, B. M., Romerdahl, C. A., and Cheresh, D. A. (1992) Involvement of integrin alpha V gene expression in human melanoma tumorigenicity. *J. Clin. Invest.* **89**, 2018-2022

Felding-Habermann, B., O'Toole, T. E., Smith, J. W., Fransvea, E., Ruggeri, Z. M., Ginsberg, M. H., Hughes, P. E., Pampori, N., Shattil, S. J., Saven, A., and Mueller, B. M. (2001) Integrin activation controls metastasis in human breast cancer. *Proc. Natl. Acad. Sci. USA* **98**, 1853-1858

Felding-Habermann, B., Silletti, S., Mei, F., Siu, C., Yip, P. M., Brooks, P. C., Cheresh, D. A., O'Toole, T. E., Ginsberg, M. H., and Montgomery, A. M. P. (1997) A Single Immunoglobulin-like Domain of the Human Neural Cell Adhesion Molecule L1 Supports Adhesion by Multiple Vascular and Platelet Integrins. *J. Cell. Biol.* **139**, 1567-1581

Felsher, D. W. (2004) MYC inactivation uncovers pluripotent differentiation and tumour dormancy in hepatocellular cancer. *Nature* **431**, 1112-1117

Ferlay, J., Bray, F., Pisani, P., and Parkin, D. M. J. Globocan 2000: cancer incidence, mortality and prevalence worldwide. IARC CancerBase No. 5. Lyon, France. IARC Press. 2001

Filardo, E. J., Brooks, P. C., Deming, S. L., Damsky, C., and Cheresh, D. A. (1995) Requirement of the NPXY motif in the integrin beta 3 subunit cytoplasmic tail for melanoma cell migration in vitro and in vivo. *J. Cell Biol.* **130**, 441-450

Freemont, A. J. (1998) Adhesion molecules. *J. Clin. Pathol.: Mol. Pathol.* **51**, 175-184

Freemont, A. J., and Hoyland, J. A. (1996) Cell adhesion molecules. *Clin. Mol. Pathol.* **49**, M321-M330

Fukuda-Taira, S. (1981) Hepatic induction in the avian embryo: specificity of reactive endoderm and inductive mesoderm. *J. Embryol. Exp. Morphol.* **63**, 111-25

Fukutomi, T., Zhou, Y., Kawai, S., Eguchi, H., Wands, J. R., and Li, J. (2005) Hepatitis C virus core protein stimulates hepatocyte growth: correlation with upregulation of wnt-1 expression. *Hepatology* **41**, 1096-1105

Furuse, M., Fujita, K., Hiiragi, T., Fujimoto, K., and Tsukita, S. (1998) Claudin-1 and -2, novel integral membrane proteins localizing at tight junctions with no sequence similarity to occludin. *J. Cell Biol.* **141**, 1539-1550

Furuse, M., Hirase, T., Itoh, M., Nagafuchi, A., Yonemura, S., Tsukita, S., and Tsukita, S. (1993) Occludin: a novel integral membrane protein localizing at tight junctions. *J. Cell Biol.* **123**, 1777-1788

Furuse, M., Itoh, M., Hirase, T., Nagafuchi, A., Yonemura, S., Tsukita, S., and Tsukita, S. (1994) Direct association of occludin with ZO-1 and its possible involvement in the localization of occludin at tight junctions. *J. Cell Biol.* **127**, 1617-1626

Garrod, D. R. (1993) Desmosomes and hemidesmosomes. *Curr. Opin. Cell. Biol.* **5**, 30-40

Geiger, B., and Ginsberg, D. (1991) The cytoplasmic domain of adherens-type junctions. *Cell. Motil. Cytoskeleton* **20**, 1-6

Gentile, M., Wiman, A., Thorstenson, S., Loman, N., Borg, A., and Wingren, S. (2001) Deletion mapping of chromosome segment 11q24-q25, exhibiting extensive allelic loss in early onset breast cancer. *Int. J. Cancer* **92**, 208-213

Gentles, A. J., and Karlin, S. (1999) Why are human G-protein-coupled receptors predominantly intronless? *Trends Genet.* **15**, 47-49

Gilbert, S. F. *Developmental Biology*. (7th Ed). Sinauer Associates, Sunderland, MA. 2003.

Gkantiragas, I., Brugger, B., Stuven, E., Kaloyanova, D., Li, X. Y., Lohr, K., Lottspeich, F., Wieland, F. T., and Helms, J. B. (2001) Sphingomyelin-enriched microdomains at the Golgi complex. *Mol. Biol. Cell* **12**, 1819-1833

Goldberg, E. K., Glendening, J. M., Karanjawala, Z., Sridhar, A., Walker, G. J., Hayward, N. K., Rice, A. J., Kurera, D., Tebha, Y., and Fountain, J. W. (2000) Localisation of multiple melanoma tumour-suppressor genes on chromosome 11 by use of homozygosity mapping-of-deletions analysis. *Am. J. Hum. Genet.* **67**, 417-431

Green, K. J., and Jones, J. C. (1996) Desmosomes and hemidesmosomes: structure and function of molecular components. *FASEB J.* **10**, 871-881

Green, P. J., Pines, O., and Inouye, M. (1986) The role of antisense RNA in gene regulation. *Annu. Rev. Biochem.* **55**, 569-597

Greenberg, C. S., Birckbichler, P. J., and Rice, R. H. (1991) Transglutaminases: multifunctional cross-linking enzymes that stabilize tissues. *FASEB J.* **5**, 3071-3077

Gressner, A. M., Lahme, B., Mannherz, H. G., and Polzar, B. (1997) TGF-beta-mediated hepatocellular apoptosis by rat and human hepatoma cells and primary rat hepatocytes. *J. Hepatol.* **26**, 1079-1092

Gressner, A. M., Weiskirchen, R., Breitkopf, K., and Dooley, S. (2002) Roles of TGF-beta in hepatic fibrosis. *Front. Biosci.* **7**, d793-d807

Grieco, A., Pompili, M., Caminiti, G., Miele, L., Covino, M., Alfei, B., Rapaccini, G. L., and Gasbarrini, G. (2005) Prognostic factors for survival in patients with early-intermediate hepatocellular carcinoma undergoing non-surgical therapy: comparison of Okuda, CLIP, and BCLC staging systems in a single Italian centre. *Gut* **54**, 411-418

Groopman, J. D., Donahue, P. R., Zhu, J. Q., Chen, J. S., and Wogan, G. N. (1985) Aflatoxin metabolism in humans: detection of metabolites and nucleic acid adducts in urine by affinity chromatography. *Proc. Natl. Acad. Sci. USA* **82**, 6492-6496

Grunwald, G. B., Bromberg, R. E., Crowley, N. J., and Lilien, J. (1981) Enzymatic dissection of embryonic cell adhesive mechanisms. II. Developmental regulation of an endogenous adhesive system in the chick neural retina. *Dev*. *Biol*. **86**, 327-338

Gu, Z., Gilbert, D. J., Valentine, V. A., Jenkins, N. A., Copeland, N. G., and Zambetti, G. P. (2000) The p53-inducible gene EI24/PIG8 localizes to human chromosome 11q23 and the proximal region of mouse chromosome 9. *Cytogenet*. *Cell Genet*. **89**, 230-233

Gualdi, R., Bossard, P., Zheng, M., Hamada, Y., Coleman, J. R., and Zaret, K. S. (1996) Hepatic specification of the gut endoderm in vitro: cell signaling and transcriptional control. *Genes Dev*. **10**, 1670-1682

Gumbiner, B. M. (1996) Cell adhesion: The molecular basis of tissue architecture and morphogenesis. *Cell* **84**, 345-357

Gumucio, J. J. (1983) Functional and anatomic heterogeneity in the liver acinus: impact on transport. *Am*. *J*. *Physiol*. **244**, G578-G582

Haas, T. A., and Plow, E. F. (1994) Integrin-ligand interactions: a year in review. *Curr*. *Opin*. *Cell Biol*. **6**, 656-662

Hall, A. (1994) Small GTP-binding proteins and the regulation of the actin cytoskeleton. *Annu*. *Rev*. *Cell Biol*. **10**, 31-54

Hanahan, D., and Weinberg, R. A. (2000) The hallmarks of cancer. *Cell* **100**, 57-70

Hao, Y., Crenshaw, T., Moulton, T., Newcomb, E., and Tycko, B. (1993) Tumor suppressor activity of *H19* RNA. *Nature* **365**, 764-767

Harder, K. W., Moller, N. P., Peacock, J. W., and Jirik, F. R. (1998) Protein-tyrosine phosphatase alpha regulates Src family kinases and alters cell-substratum adhesion. *J*. *Biol*. *Chem*. **273**, 31890-31900

Haskins, J., Gu, L., Wittchen, E. S., Hibbard, J., and Stevenson, B. R. (1998) ZO-3, a novel member of the MAGUK protein family found at the tight junction, interacts with ZO-1 and occludin. *J*. *Cell Biol*. **141**, 199-208

Hassan, M. M., Frome, A., Patt, Y. Z., and El-Serag, H. B. (2002) Rising prevalence of hepatitis C virus infection among patients recently diagnosed with hepatocellular carcinoma in the United States. *J*. *Clin*. *Gastroenterol*. **35**, 266-269

Hattori, K., Angel, P., Le Beau, M. M., and Karin, M. (1988) Structure and chromosomal localization of the functional intronless human JUN protooncogene. *Proc*. *Natl*. *Acad*. *Sci*. *USA* **85**, 9148-9152

Heinze, T., Jonas, S., Karsten, A., and Neuhaus, P. (1999) Determination of the oncogenes p53 and C-erb B2 in the tumour cytosols of advanced hepatocellular carcinoma (HCC) and correlation to survival time. *Anticancer Res*. **19**, 2501-2503

Heldin, C. H. (1995) Dimerization of cell surface receptors in signal transduction. *Cell* **80**, 213-223

Hendriks, H. F., Verhoofstad, W., Brouwer, A., De Leeuw, A., and Knnok, D. L. (1985) Perisinusoidal fat-storing cells are the main vitamin A storage sites in the liver. *Exp*. *Cell Res*. **160**, 138-149

Higashitsuji, H., Itoh, K., Nagao, T., Dawson, S., Nonoguchi, K., Kido, T., Mayer, R. J., Arii, S., and Fujita, J. (2000) Reduced stability of retinoblastoma protein by gankyrin, an oncogenic ankyrin-repeat protein overexpressed in hepatomas. *Nat*. *Med*. **6**, 96-99

Hoschuetzky, H., Aberle, H., and Kemler, R. (1994) β-catenin mediates the interaction of the cadherin-catenin complex with epidermal growth factor receptor. *J*. *Cell Biol*. **127**, 1375-1380

Howard, P. L., Klamut, H. J., and Ray, P. N. (1998) Identification of a novel actin binding site within the Dp71 dystrophin isoform. *FEBS Lett*. **441**, 337-341

Hsia, C. C., Di Bisceglie, A. M., Kleiner, D. E. Jr., Farshid, M., and Tabor, E. (1994) RB tumor suppressor gene expression in hepatocellular carcinoma from patients infected with the hepatitis B virus. *J*. *Med*. *Virol*. **44**, 67-73

Hsieh, J. T., Luo, W., Song, W., Wang, Y., Kleinerman, D. I., Van, N. T., and Lin, S. H. (1995) Tumor suppressive role of an androgen-regulated epithelial cell adhesion molecule (C-CAM) in prostate carcinoma cell revealed by sense and antisense approaches. *Cancer Res*. **55**, 190-197

Hsu, M. Y., Shih, D. T., Meier, F. E., Van Belle, P., Hsu, J. Y., Elder, D. E., Buck, C. A., and Herlyn, M. (1998) Adenoviral gene transfer of beta3 integrin subunit induces conversion from radial to vertical growth phase in primary human melanoma. *Am*. *J*. *Pathol*. **153**, 1435-1442

Huang, C. C., Wu, M. C., Xu, G. W., Li, D. Z., Cheng, H., Tu, Z. X., Jiang, H. Q., and Gu, J. R. (1992) Overexpression of the MDR1 gene and P-glycoprotein in human hepatocellular carcinoma. *J*. *Natl*. *Cancer Inst*. **84**, 262-264

Huang, J., Simpson, J. F., Glackin, C., Riethorf, L., Wagener, C., and Shively, J. E. (1998) Expression of biliary glycoprotein (CD66a) in normal and malignant breast epithelial cells. *Anticancer Res*. **18**, 3203-3212

Hughes, R. C., and Stamatoglou, S. C. (1987) Adhesive interactions and the metabolic activity of hepatocytes. *J*. *Cell Sci*. **Suppl. 8**, 273-291

Hunter, I., Sawa, H., Edlund, M., and Obrink, B. (1996) Evidence for regulated dimerization of cell-cell adhesion molecule (C-CAM) in epithelial cells. *Biochem*. *J*. **320**, 847-853

Hyafil, F., Babinet, C., and Jacob, F. (1981) Cell-cell interactions in early embryogenesis: a molecular approach to the role of calcium. *Cell* **26**, 447-454

Hynes, R. O. (1987) Integrins: a family of cell surface receptors. *Cell* **48**, 549-550

Hynes, R. O. (1999) Cell adhesion: old and new questions. *Trends Cell Biol*. **9**, M33-M37

Ilangumaran, S., and Hoessli, D. C. (1998) Effects of cholesterol depletion by cyclodextrin on the sphingolipid microdomains of the plasma membrane. *Biochem. J*. **335**, 433-440

International Union Against Cancer (UICC). In Sobin, L. H., and Wittekind, C. H. (Eds): TMN classification of malignant tumours. (5th Ed). New York: Wiley-Liss. 1997, pp. 74-77

Issa, J. P., Ottaviano, Y. L., Celano, P., Hamilton, S. R., Davidson, N. E., and Baylin, S. B. (1994) Methylation of the oestrogen receptor CpG island links ageing and neoplasia in human colon. *Nat. Genet*. **7**, 536-540

Itoh, M., Furuse, M., Morita, K., Kubota, K., Saitou, M., and Tsukita, S. (1999) Direct binding of three tight junction-associated MAGUKs, ZO-1, ZO-2, and ZO-3, with the COOH termini of claudins. *J. Cell Biol*. **147**, 1351-1363

Ivorra, C., Samyn, H., Edo, M. D., Castro, C., Sanz-Gonzalez, S. M., Deez-Juan, A., and Andres, V. (2003) Inhibiting cyclin-dependent kinase/cyclin activity for the treatment of cancer and cardiovascular disease. *Curr. Pharm. Biotechnol*. **4**, 21-37

Jacobson, K., and Dietrich, C. (1999) Looking at lipid rafts? *Trends Cell Biol*. **9**, 87-91

Jaken, S., Leach, K., and Klauck, T. (1989) Association of type 3 protein kinase C with focal contacts in rat embryo fibroblasts. *J. Cell. Biol*. **109**, 697-704

Jakubczak, J. L., Chisari, F. V., and Merlino, G. (1997) Synergy between transforming growth factor alpha and hepatitis B virus surface antigen in hepatocellular proliferation and carcinogenesis. *Cancer Res*. **57**, 3606-3611

Jawaheer, D., Seldin, M. F., Amos, C. I., Chen, W. V., Shigeta, R., Etzel, C., Damle, A., Xiao, X., Chen, D., Lum, R. F., Monteiro, J., Kern, M., Criswell, L. A., Albani, S., Nelson, J. L., Clegg, D. O., Pope, R., Schroeder, H. W. Jr., Bridges, S. L. Jr., Pisetsky, D. S., Ward, R., Kastner, D. L., Wilder, R. L., Pincus, T., Callahan, L. F., Flemming, D., Wener, M. H., and Gregersen, P. K. (2003) North American Rheumatoid Arthritis Consortium. Screening the genome for rheumatoid arthritis susceptibility genes: a replication study and combined analysis of 512 multicase families. *Arthritis. Rheum*. **48**, 906-916

Jesaitis, L. A., and Goodenough, D. A. (1994) Molecular characterization and tissue distribution of ZO-2, a tight junction protein homologous to ZO-1 and the *Drosophila* discs-large tumor suppressor protein. *J. Cell Biol*. **124**, 949-961

Jockusch, B. M., Bubeck, P., Giehl, K., Kroemker, M., Moschner, J., Rothkegel, M., Rudiger, M., Schluter, K., Stanke, G., and Winkler, J. (1995) The molecular architecture of focal adhesions. *Annu. Rev. Cell Dev. Biol.* **11**, 379-416

Jost, C. A., Marin, M. C., and Kaelin, W. G. Jr. (1997) p73 is a simian [correction of human] p53-related protein that can induce apoptosis. *Nature* **389**, 191-194

Juliano, R. L. (2002) Signal transduction by cell adhesion receptors and the cytoskeleton: functions of integrins, cadherins, selectins, and immunoglobulin-superfamily members. *Annu. Rev. Pharmacol. Toxicol.* **42**, 283-323

Kaghad, M., Bonnet, H., Yang, A., Creancier, L., Biscan, J. C., Valent, A., Minty, A., Chalon, P., Lelias, J. M., Dumont, X., Ferrara, P., McKeon, F., and Caput, D. (1997) Monoallelically expressed gene related to p53 at 1p36, a region frequently deleted in neuroblastoma and other human cancers. *Cell* **90**, 809-819

Kamiguchi, H., and Lemmon, V. (2000) Recycling of the cell adhesion molecule L1 in axonal growth cones. *J. Neurosci.* **20**, 3676-3686

Kanai, Y., Ushijima, S., Hui, A. M., Ochiai, A., Tsuda, H., Sakamoto, M., and Hirohashi, S. (1997) The E-cadherin gene is silenced by CpG methylation in human hepatocellular carcinomas. *Int. J. Cancer* **71**, 355-359

Kao, C. F., Chen, S. Y., Chen, J. Y., and Wu Lee, Y. H. (2004) Modulation of p53 transcription regulatory activity and post-translational modification by hepatitis C virus core protein. *Oncogene* **23**, 2472-2483

Kaplan, K. B., Bibbins, K. B., Swedlow, J. R., Arnaud, M., Morgan, D. O., and Varmus, H. E. (1994) Association of the amino-terminal half of c-Src with focal adhesions alters their properties and is regulated by phosphorylation of tyrosine 527. *EMBO J.* **13**, 4745-4756

Kawakatsu, T., Shimizu, K., Honda, T., Fukuhara, T., Hoshino, T., and Takai, Y. (2002) Trans-interactions of nectins induce formation of filopodia and lamellipodia through the respective activation of Cdc42 and Rac small G proteins. *J. Biol. Chem.* **277**, 50749-50755

Kedes, L. H. (1979) Histone genes and histone messengers. *Annu. Rev. Biochem.* **48**, 837-870

Kekule, A. S., Lauer, U., Weiss, L., Luber, B., and Hofschneider, P. H. (1993) Hepatitis B virus transactivator HBx uses a tumour promoter signalling pathway. *Nature* **361**, 742-745

Kew, M. C. (2003) Synergistic interaction between aflatoxin B1 and hepatitis B virus in hepatocarcinogenesis. *Liver Int.* **23**, 405-409

Kinch, M. S., Clark, G. J., Der, C. J., and Burridge, K. (1995) Tyrosine phosphorylation regulates the adhesions of *ras*-transformed breast epithelia. *J. Cell Biol.* **130**, 461-471

Kira, S., Nakanishi, T., Suemori, S., Kitamoto, M., Watanabe, Y., and Kajiyama, G. (1997) Expression of transforming growth factor alpha and epidermal growth factor receptor in human hepatocellular carcinoma. *Liver* **17**, 177-182

Kishida, S., Yamamoto, H., Ikeda, S., Kishida, M., Sakamoto, I., Koyama, S., and Kikuchi, A. (1998) Axin, a negative regulator of the Wnt signaling pathway, directly interacts with adenomatous polyposis coli, and regulates the stabilization of beta-catenin. *J. Biol. Chem.* **273**, 10823-10826

Kiyosawa, K., and Tanaka, E. (2002) Characteristics of hepatocellular carcinoma in Japan. *Oncology* **62**, 5-7

Klein, E. S., Asculai, S. S., and Ben-Ari, G. Y. (1996) Effects of hyaluronic acid on fibroblast behavior in peritoneal injury. *J. Surg. Res.* **61**, 473-476

Klemke, R. K., Cai, S., Giannini, A. L., Gallagher, P. J., de Lanerolle, P., and Cheresh, D. A. (1997) Regulation of cell motility by mitogen-activated protein kinase. *J. Cell Biol.* **137**, 481-492

Klemm, J. D., Schreiber, S. L., and Crabtree, G. R. (1998) Dimerization as a regulatory mechanism in signal transduction. *Annu. Rev. Immunol.* **16**, 569-592

Knudson, A. G. Jr., Hethcote, H. W., and Brown, B. W. (1975) Mutation and childhood cancer: A probabilistic model for the incidence of retinoblastoma. *Proc. Natl. Acad. Sci. USA* **72**, 5116-5120

Kouzarides, T., and Ziff, E. (1988) The role of the leucine zipper in the fos-jun interaction. *Nature* **336**, 646-651

Kozak, M. (1990) Downstream secondary structure facilitates recognition of initiator codons by eukaryotic ribosomes. *Proc. Natl. Acad. Sci. USA* **87**, 8301-8305

Kozma, R., Ahmed, S., Best, A., and Lim, L. (1995) The ras-related protein cdc42Hs and bradykinin promote formation of peripheral actin microspikes and filopodia in Swiss 373 fibroblasts. *Mol. Cell. Biol.* **15**, 1942-1952

Kudo, M., Chung, H., and Osaki, Y. (2003) Prognostic staging system for hepatocellular carcinoma (CLIP score): its value and limitations, and a proposal for a new staging system, the Japan Integrated Staging Score (JIS score). *J. Gastroenterol.* **38**, 207-215

Kumar, M., and Carmichael, G. G. (1998) Antisense RNA: function and fate of duplex RNA in cells of higher eukaryotes. *Microbiol. Mol. Biol. Rev.* **62**, 1415-1434

Kumar, N. M., and Gilula, N. B. (1996) The gap junction communication channel. *Cell* **84**, 381-388

Kuramochi, M., Fukuhara, H., Nobukuni, T., Kanbe, T., Maruyama, T., Ghosh, H. P., Pletcher, M., Isomura, M., Onizuka, M., Kitamura, T., Sekiya, T., Reeves, R. H., and

Murakami, Y. (2001) TSLC1 is a tumor-suppressor gene in human non-small-cell lung cancer. *Nat. Genet.* **27**, 427-430

Lagenaur, C., and Lemmon, V. (1987) An L1-like molecule, the 8D9 antigen, is a potent substrate for neurite extension. *Proc. Natl. Acad. Sci. USA* **84**, 7753-7757

Lai, E. C., Choi, T. K., Cheng, C. H., Mok, F. P., Fan, S. T., Tan, E. S., and Wong, J. (1990) Doxorubicin for unresectable hepatocellular carcinoma. A prospective study on the addition of verapamil. *Cancer* **66**, 1685-1687

Lalor, P. F., and Adams, D. H. (2002) The liver: a model of organ-specific lymphocyte recruitment. *Expert. Rev. Mol. Med.* 1-16

Lammers, R., Lerch, M. M., and Ullrich, A. (2000) The carboxy-terminal tyrosine residue of protein-tyrosine phosphatase α mediates association with focal adhesion plaques. *J. Biol. Chem.* **275**, 3391-3396

Largaespada, D. A. (2001) Haploinsufficiency for tumor suppression: the hazards of being single and living a long time. *J. Exp. Med.* **193**, F15-F18

Lasky, T., and Magder, L. (1997) Hepatocellular carcinoma p53 G > T transversions at codon 249: the fingerprint of aflatoxin exposure? *Environ. Health Perspect.* **105**, 392-397

Lauffenburger, D. A., and Horwitz, A. F. (1996) Cell migration: a physically integrated molecular process. *Cell* **84**, 359-369

Launonen, V., Stenback, F., Puistola, U., Bloigu, R., Huusko, P., Kytola, S., Kauppila, A., and Winqvist, R. (1998) Chromosome 11q22.3-q25 LOH in ovarian cancer: association with a more aggressive disease course and involved subregions. *Gynecol. Oncol.* **71**, 299-304

Laure, L., Ohsugi, M., Hirchenhain, J., and Kemler, R. (1994) E-cadherin null mutant embryos fail to form a trophectoderm epithelium. *Proc. Natl. Acad. Sci. USA* **91**, 8263-8267

Le Douarin, N. M. (1975) An experimental analysis of liver development. *Med. Biol.* **53**, 427-455

Lee, Y. H., and Yun, Y. (1998) HBx protein of hepatitis B virus activates Jak1-STAT signaling. *J. Biol. Chem.* **273**, 25510-25515

Levine, A. J. (1997) *p53*, the cellular gatekeeper for growth and division. *Cell* **88**, 323-331

Leviten, M. W., Lai, E. C., and Posakony, J. W. (1997) The Drosophila gene Bearded encodes a novel small protein and shares 3' UTR sequence motifs with multiple Enhancer of split complex genes. *Development* **124**, 4039-4051

Levy, L., Renard, C. A., Wei, Y., and Buendia, M. A. (2002) Genetic alterations and oncogenic pathways in hepatocellular carcinoma. *Ann. N. Y. Acad. Sci.* **963**, 21-36

Lewin, B. Genes VII. Oxford University Press, New York. 2000, pp. 37-65

Lin, S. Y., Xia, W., Wang, J. C., Kwong, K. Y., Spohn, B., Wen, Y., Pestell, R. G., and Hung, M. C. (2000) Beta-catenin, a novel prognostic marker for breast cancer: its roles in cyclin D1 expression and cancer progression. *Proc. Natl. Acad. Sci. USA* **97**, 4262-4266

Lindholm, E., Ekholm, B., Balciuniene, J., Johansson, G., Castensson, A., Koisti, M., Nylander, P. O., Pettersson, U., Adolfsson, R., and Jazin, E. (1999) Linkage analysis of a large Swedish kindred provides further support for a susceptibility locus for schizophrenia on chromosome 6p23. *Am. J. Med. Genet.* **88**, 369-377

Lindner, J., Rathjen, F. G., and Schachner, M. (1983) L1 mono- and polyclonal antibodies modify cell migration in early postnatal mouse cerebellum. *Nature* **305**, 427-430

Lisanti, M. P., Caras, I. W., Davitz, M. A., and Rodriguez-Boulan, E. (1989) A glycophospholipid membrane anchor acts as an apical targeting signal in polarized epithelial cells. *J. Cell Biol.* **109**, 2145-2156

Liu, S., Calderwood, D. A., and Ginsberg, M. H. (2000) Integrin cytoplasmic domain-binding proteins. *J. Cell Sci.* **113**, 3563-3571

Llovet, J. M. (2005) Updated treatment approach to hepatocellular carcinoma. *J. Gastroenterol.* **40**, 225-235

Llovet, J. M., Bru, C., and Bruix, J. (1999) Prognosis of hepatocellular carcinoma: the BCLC staging classification. *Semin. Liver Dis.* **19**, 329-338

Loh, W. E. Jr., Scrable, H. J., Livanos, E., Arboleda, M. J., Cavenee, W. K., Oshimura, M., and Weissman, B. E. (1992) Human Chromosome 11 Contains Two Different Growth Suppressor Genes for Embryonal Rhabdomyosarcoma. *Proc. Natl. Acad. Sci. USA* **89**, 1755-1759

Luo, D. Z., Vermijlen, D., Ahishali, B., Triantis, V., Plakoutsi, G., Braet, F., Vanderkerken, K., and Wisse, E. (2000) On the cell biology of pit cells, the liver-specific NK cells. *World J. Gastroenterol.* **6**, 1-11

Macdonald, G. A., Greenson, J. K., Saito, K., Cherian, S. P., Appelman, H. D., and Boland, C. R. (1998) Microsatellite instability and loss of heterozygosity at DNA mismatch repair gene loci occurs during hepatic carcinogenesis. *Hepatology* **28**, 90-97

Malumbres, M., Perez de Castro, I., Santos, J., Fernandez Piqueras, J., and Pellicer, A. (1999) Hypermethylation of the cell cycle inhibitor p15INK4b 3'-untranslated region interferes with its transcriptional regulation in primary lymphomas. *Oncogene* **18**, 385-396

Manes, T., Zheng, D. Q., Tognin, S., Woodard, A. S., Marchisio, P. C., and Languino, L. R. (2003) Alpha(v)beta3 integrin expression up-regulates cdc2, which modulates cell migration. *J. Cell Biol*. **161**, 817-826

Marahrens, Y., Loring, J., and Jaenisch, R. (1998) Role of the Xist gene in X chromosome choosing. *Cell* **92**, 657-664

Martin-Padura, I., Lostaglio, S., Schneemann, M., Williams, L., Romano, M., Fruscella, P., Panzeri, C., Stoppacciaro, A., Ruco, L., Villa, A., Simmons, D., and Dejana, E. (1998) Junctional adhesion molecule, a novel member of the immunoglobulin superfamily that distributes at intercellular junctions and modulates monocyte transmigration. *J. Cell Biol*. **142**, 117-127

Mast, B. A., Diegelmann, R. F., Krummel, T. M., and Cohen, I. K. (1993) Hyaluronic acid modulates proliferation, collagen and protein synthesis of cultured fetal fibroblasts. *Matrix* **13**, 441-446

Masuda, M., Yageta, M., Fukuhara, H., Kuramochi, M., Maruyama, T., Nomoto, A., and Murakami, Y. (2002) The tumor suppressor protein TSLC1 is involved in cell-cell adhesion. *J. Biol. Chem*. **277**, 31014-31019

Mathew, S., Shurtleff, S. A., and Raimondi, S. C. (2001) Novel cryptic, complex rearrangements involving ETV6-CBFA2 (TEL-AML1) genes identified by fluorescence in situ hybridisation in pediatric patients with acute lymphoblastic leukemia. *Genes Chromosomes Cancer* **32**, 188-193

Matsuda, K., Yoshida, K., Taya, Y., Nakamura, K., Nakamura, Y., and Arakawa, H. (2002) p53AIP1 regulates the mitochondrial apoptotic pathway. *Cancer Res*. **62**, 2883-2889

Matsumura, T., Makino, R., and Mitamura, K. (2001) Frequent down-regulation of E-cadherin by genetic and epigenetic changes in the malignant progression of hepatocellular carcinomas. *Clin. Cancer Res*. **7**, 594-599

Mattick, J. S. (2001) Non-coding RNAs: the architects of eukaryotic complexity. *EMBO Reports* **2**, 986-991

Mattick, J. S. (2003) Challenging the dogma: the hidden layer of non-protein-coding RNAs in complex organisms. *BioEssays* **25**, 930-939

McCann, R. O., and Craig, S. W. (1997) The I/LWEQ module: a conserved sequence that signifies F-actin binding in functionally diverse proteins from yeast to mammals. *Proc. Natl. Acad. Sci. USA* **94**, 5679-5684

Metz, C., Cave, H., Bertrand, A. M., Deffert, C., Gueguen-Giroux, B., Czernichow, P., and Polak, M. (2002) NDM French Study Group. Neonatal diabetes mellitus. Neonatal diabetes mellitus: chromosomal analysis in transient and permanent cases. *J. Pediatr*. **141**, 483-489

Michalopoulos, G. K., and DeFrances, M. C. (1997) Liver regeneration. *Science* **276**, 60-66

Michel, U. (2002) Non-coding ribonucleic acids--a class of their own? *Int. Rev. Cytol.* **218**, 143-219

Miranda, K. C., Khromykh, T., Christy, P., Le, T. L., Gottardi, C. J., Yap, A. S., Stow, J. L., and Teasdale, R. D. (2001) A dileucine motif targets E-cadherin to the basolateral cell surface in Madin-Darby canine kidney and LLC-PK1 epithelial cells. *J. Biol. Chem.* **276**, 22565-22572

Mitchison, T. J., and Cramer, L. P. (1996) Actin-based cell motility and cell locomotion. *Cell* **84**, 371-379

Miyahara, M., Nakanishi, H., Takahashi, K., Satoh-Horikawa, K., Tachibana, K., and Takai, Y. (2000) Interaction of nectin with afadin is necessary for its clustering at cell-cell contact sites but not for its cis dimerization or trans interaction. *J. Biol. Chem.* **275**, 613-618

Miyashita, T., and Reed, J. C. (1995) Tumor suppressor p53 is a direct transcriptional activator of the human bax gene. *Cell* **80**, 293-299

Miyoshi, Y., Iwao, K., Nagasawa, Y., Aihara, T., Sasaki, Y., Imaoka, S., Murata, M., Shimano, T., and Nakamura, Y. (1998) Activation of the beta-catenin gene in primary hepatocellular carcinomas by somatic alterations involving exon 3. *Cancer Res.* **58**, 2524-2547

Monte, S. M., Ghanbari, K., Frey, W. H., Beheshti, I., Averback, P., Hauser, S. L., Ghanbari, H. A., and Wands, J. R. (1997) Characterization of the AD7C-NTP cDNA expression in Alzheimer's disease and measurement of a 41-kD protein in cerebrospinal fluid. *J. Clin. Invest.* **100**, 3093-3104

Moroni, M. C., Hickman, E. S., Lazzerini Denchi, E., Caprara, G., Colli, E., Cecconi, F., Muller, H., and Helin, K. (2001) Apaf-1 is a transcriptional target for E2F and p53. *Nat. Cell Biol.* **3**, 552-558

Murakami, H., Sanderson, N. D., Nagy, P., Marino, P. A., Merlino, G., and Thorgeirsson, S. S. (1993) Transgenic mouse model for synergistic effects of nuclear oncogenes and growth factors in tumorigenesis: interaction of c-myc and transforming growth factor alpha in hepatic oncogenesis. *Cancer Res.* **53**, 1719-1723

Murakami, Y., Hayashi, K., Hirohashi, S., and Sekiya, T. (1991) Aberrations of the tumor suppressor p53 and retinoblastoma genes in human hepatocellular carcinomas. *Cancer Res.* **51**, 5520-5525

Nagar, B., Overduin, M., Ikura, M., and Rini, J. M. (1996) Structural basis of calcium-induced E-cadherin rigidification and dimerization. *Nature* **380**, 360-364

Nagy, P., Evarts, R. P., McMahon, J. B., and Thorgeirsson, S. S. (1989) Role of TGF-beta in normal differentiation and oncogenesis in rat liver. *Mol. Carcinog.* **2**, 345-354

Neame, S. J., and Isacke, C. M. (1993) The cytoplasmic tail of CD44 is required for basolateral localization in epithelial MDCK cells but does not mediate association with the detergent-insoluble cytoskeleton of fibroblasts. *J. Cell Biol*. **121**, 1299-1310

Negash, S., Wang, H. S., Gao, C., Ledee1, D., and Zelenka1, P. (2002) Cdk5 regulates cell-matrix and cell-cell adhesion in lens epithelial cells. *J. Cell Sci*. **115**, 2109-2117

Negrini, M., Sabbioni, S., Possati, L., Rattan, S., Corallini, A., Barbanti-Brodano, G., and Croce, C. M. (1994) Suppression of tumorigenicity of breast cancer cells by microcell-mediated chromosome transfer: studies on chromosomes 6 and 11. *Cancer Res*. **54**, 1331-1336

Neumaier, M., Paululat, S., Chan, A., Matthaes, P., and Wagener, C. (1993) Biliary glycoprotein, a potential human cell adhesion molecule, is down-regulated in colorectal carcinomas. *Proc*. *Natl*. *Acad*. *Sci*. *USA* **90**, 10744-10748

Niethammer, P., Delling, M., Sytnyk, V., Dityatev, A., Fukami, K., and Schachner, M. (2002) Cosignaling of NCAM via lipid rafts and the FGF receptor is required for neuritogenesis. *J. Cell Biol*. **157**, 521-532

Nishida, N., Fukuda, Y., Kokuryu, H., Toguchida, J., Yandell, D. W., Ikenega, M., Imura, H., and Ishizaki, K. (1993) Role and mutational heterogeneity of the p53 gene in hepatocellular carcinoma. *Cancer Res*. **53**, 368-372

Nishida, N., Fukuda, Y., Komeda, T., Kita, R., Sando, T., Furukawa, M., Amenomori, M., Shibagaki, I., Nakao, K., and Ikenaga, M. (1994) Amplification and overexpression of the cyclin D1 gene in aggressive human hepatocellular carcinoma. *Cancer Res*. **54**, 3107-3110

Nishida, T., Nakamura, M., Mishima, H., and Otori, T. (1991) Hyaluronan stimulates corneal epithelial migration. *Exp*. *Eye Res*. **53**, 753-758

Nobes, C. D., and Hall, A. (1995) Rho, rac, and cdc42 GTPases regulate the assembly of multimolecular focal complexes associated with actin stress fibers, lamellipodia, and filopodia. *Cell* **81**, 53-62

Nojima, Y., Tachibana, K., Sato, T., Schlosman, S. F., and Morimoto, C. (1995) Focal adhesion kinase (pp125FAK) is tyrosine phosphorylated after engagement of alpha 4 beta 1 and alpha 5 beta 1 integrins on human T-lymphoblastic cells. *Cell Immunol*. **161**, 8-13

Nollau, P., Scheller, H., Kona-Horstmann, M., Rohde, S., Hagenmuller, F., Wagener, C., and Neumaier, M. (1997) Expression of CD66a (human C-CAM) and other members of the carcinoembryonic antigen family of adhesion molecules in human colorectal adenomas. *Cancer Res*. **57**, 2354-2357

Norris, J., Fan, D., Aleman, C., Marks, J. R., Futreal, P. A., Wiseman, R. W., Iglehart, J. D., Deininger, P. L., and McDonnell, D. P. (1995) Identification of a new subclass

of Alu DNA repeats which can function as estrogen receptor-dependent transcriptional enhancers. *J. Biol. Chem.* **270**, 22777-22782

Odin, P., Asplund, M., Busch, C., and Obrink, B. (1988) Immunohistochemical localization of cell-CAM 105 in rat tissues. Appearance in epithelia, platelets and granulocytes. *J. Histochem. Cytochem.* **36**, 729-739

Ohnishi, K., Iida, S., Iwama, S., Goto, N., Nomura, F., Takashi, M., Mishima, A., Kono, K., Kimura, K., Musha, H., Kotota, K., and Okuda, K. (1982) The effect of chronic habitual alcohol intake on the development of liver cirrhosis and hepatocellular carcinoma: relation to hepatitis B surface antigen carriage. *Cancer* **49**, 672-677

Oka, K., Nagano-Fujii, M., Yoshida, I., Hidajat, R., Deng, L., Akutsu, M., and Hotta, H. (2003) Hepatitis C virus core protein selectively inhibits synthesis and accumulation of p21/Waf1 and certain nuclear proteins. *Microbiol. Immunol.* **47**, 429-438

Okamoto, K., Morison, I. M., Taniguchi, T., and Reeve, A. E. (1997) Epigenetic changes at the insulin-like growth factor II/H19 locus in developing kidney is an early event in Wilms tumorigenesis. *Proc. Natl. Acad. Sci. USA* **94**, 5367-5371

Okegawa, T., Pong, R. C., Li, Y., and Hsieh, J. T. (2004) The role of cell adhesion molecule in cancer progression and its application in cancer therapy. *Acta Biochim. Pol.* **51**, 445-457

Okuda, K., Nakashima, T., Sakamoto, K., Ikari, T., Hidaka, H., Kubo, Y., Sakuma, K., Motoike, Y., Okuda, H., and Obata, H. (1982) Hepatocellular carcinoma arising in noncirrhotic and highly cirrhotic livers: a comparative study of histopathology and frequency of hepatitis B markers. *Cancer* **49**, 450-455

Okuda, K., and Ohnishi, K. The role of viral infections in alcoholic liver disease. In Alcoholic Liver Disease: Pathology and Pathogenesis. (2nd Ed). Edward Arnold. 1994, pp. 147-159

Okuda, K., Ohtsuki, T., Obata, H., Tomimatsu, M., Okazaki, N., Hasegawa, H., Nakajima, Y., and Ohnishi, K. (1985) Natural history of hepatocellular carcinoma and prognosis in relation to treatment. Study of 850 patients. *Cancer* **56**, 918-928

Oliferenko, S., Paiha, K., Harder, T., Gerke, V., Schwarzler, C., Schwarz, H., Beug, H., Gunthert U., and Huber L. A. (1999) Analysis of CD44-containing lipid rafts: recruitment of annexin II and stabilization by the actin cytoskeleton. *J. Cell Biol.* **146**, 843-854

Orford, K., Crockett, C., Jensen, J. P., Weissman, A. M., and Byers, S. W. (1997) Serine phosphorylation-regulated ubiquitination and degradation of beta-catenin. *J. Biol. Chem.* **272**, 24735-24738

Oster, S. K., Ho, C. S., Soucie, E. L., and Penn, L. Z. (2002) The myc oncogene: MarvelouslY Complex. *Adv. Cancer Res.* **84**, 81-154

Parkin, D. M., Bray, F. I., and Devesa, S. S. (2001) Cancer burden in the year 2000. The global picture. *Eur. J. Cancer* **37**, S4-S66

Parodi, A. J. (2000) Protein glucosylation and its role in protein folding. *Annu. Rev. Biochem.* **69**, 69-93

Pascale, R. M., Simile, M. M., and Feo, F. (1993) Genomic abnormalities in hepatocarcinogenesis: Implications for a chemopreventive strategy. *Anticancer Res.* **13**, 1341-1356

Pavletich, N. P., Chambers, K. A., and Pabo, C. O. (1993) The DNA-binding domain of p53 contains the four conserved regions and the major mutation hot spots. *Genes Dev.* **7**, 2556-2564

Pawson, T. (1995) Protein modules and signalling networks. *Nature* **373**, 573-580

Peach, R. J., Hollenbaugh, D., Stamenkovic, I., and Aruffo, A. (1993) Identification of hyaluronic acid binding sites in the extracellular domain of CD44. *J. Cell Biol.* **122**, 257-264

Pece, S., and Gutkind, J. S. (2000) Signaling from E-cadherins to the MAPK pathway by the recruitment and activation of epidermal growth factor receptors upon cell-cell contact formation. *J. Biol. Chem.* **275**, 41227-41233

Perez-Roger, I., Kim, S. H., Griffiths, B., Sewing, A., and Land, H. (1999) Cyclins D1 and D2 mediate myc-induced proliferation via sequestration of p27(Kip1) and p21(Cip1). *EMBO J.* **18**, 5310-5320

Pertz, O., Bozic, D., Koch, A. W., Fauser, C., Brancaccio, A., and Engel, J. (1999) A new crystal structure, Ca2+ dependence and mutational analysis reveal molecular details of E-cadherin homoassociation. *EMBO J.* **18**, 1738-1747

Pletcher, M. T., Nobukuni, T., Fukuhara, H., Kuramochi, M., Maruyama, T., Sekiya, T., Sussan, T., Isomura, M., Murakami, Y., and Reeves, R. H. (2001) Identification of tumor suppressor candidate genes by physical and sequence mapping of the TSLC1 region of human chromosome 11q23. *Gene* **273**, 181-189

Plotnikov, A. N., Schlessinger, J., Hubbard, S. R., and Mohammadi, M. (1999) Structural basis for FGF receptor dimerization and activation. *Cell* **98**, 641-650

Pollard, T. D., and Borisy, G. G. (2003) Cellular motility driven by assembly and disassembly of actin filaments. *Cell* **112**, 453-465

Pond, L., Kuhn, L. A., Teyton, L., Schutze, M. P., Tainer, J. A., Jackson, M. R., and Peterson, P. A. (1995) A role for acidic residues in di-leucine motif-based targeting to the endocytic pathway. *J. Biol. Chem.* **270**, 19989-19997

Powell, L. W., Bassett, M. L., and Halliday, J. W. (1980) Hemochromatosis: 1980 update. *Gastroenterology* **78**, 374-381

Prekeris, R., Mayhew, M. W., Cooper, J. B., and Terrian, D. M. (1996) Identification and localization of an actin-binding motif that is unique to the epsilon isoform of protein kinase C and participates in the regulation of synaptic function. *J. Cell Biol.* **132**, 77-90

Prezant, T. R., Kadioglu, P., and Melmed, S. (1999) An intronless homolog of human proto-oncogene hPTTG is expressed in pituitary tumors: evidence for hPTTG family. *J. Clin. Endocrinol. Metab.* **84**, 1149-1152

Price, L. S., Leng, J., Schwartz, M. A., and Bokoch, G. M. (1998) Activation of Rac and Cdc42 by integrins mediates cell spreading. *Mol. Biol. Cell* **9**, 1863-1871

Pugh, R. N., Murray-Lyon, I. M., Dawson, J. L., Pietroni, M. C., and Williams, R. (1973) Transection of the oesophagus for bleeding oesophageal varices. *Br. J. Surg.* **60**, 646-649

Quest, A. F. G., Leyton, L., and Parraga, M. (2004) Caveolins, caveolae, and lipid rafts in cellular transport, signaling, and disease. *Biochem. Cell Biol.* **82**, 129-144

Rasio, D., Negrini, M., and Croce, C. M. (1995) Genomic organization of the ATM locus involved in ataxia-telangiectasia. *Cancer Res.* **55**, 6053-6057

Ray, B. B., Steele, R., Meyer, K., and Ray, R. (1997) Transcriptional repression of p53 promoter by hepatitis C virus core protein. *J. Biol. Chem.* **272**, 10983-10986

Rebollo, A., and Martínez-A, C. (1999) Ras Proteins: Recent Advances and New Functions. *Blood* **94**, 2971-2980

Regev, A., and Jeffers, L. J. (1999) Hepatitis C and alcohol. *Alcohol Clin. Exp. Res.* **23**, 1543-1551

Richardson, A., Malik, R. K., Hildebrand, J. D., and Parsons, J. T. (1997) Inhibition of cell spreading by expression of the C-terminal domain of focal adhesion kinase (FAK) is rescued by coexpression of Src or catalytically inactive FAK: a role for paxillin tyrosine phosphorylation. *Mol. Cell. Biol.* **17**, 6906-6914

Ridley, A., and Hall, A. (1992) The small GTP-binding protein rho regulates the assembly of focal adhesions and actin stress fibers in response to growth factors. *Cell* **70**, 389-399

Ridley, A., Paterson, H., Johnston, C., Diekmann, D., and Hall, A. (1992) The small GTP-binding protein rac regultes growth factor-induced membrane ruffling. *Cell* **70**, 401-410

Ridley, A. J., Schwartz, M. A., Burridge, K., Firtel, R., Ginsberg, M., Borisy, G., Parsons, J. T., and Horwitz, A. F. (2003) Cell migration: Integrating signals from front to back. *Science* **302**, 1704-1709

Riggs, A. D., and Jones, P. A. (1983) 5-methylcytosine, gene regulation, and cancer. *Adv. Cancer Res.* **40**, 1-30

Robertson, G., Coleman, A., and Lugo, T. G. (1996) A malignant melanoma tumor suppressor on human chromosome 11. *Cancer Res.* **56**, 4487-4492

Rodriguez, C., Causse, A., Ursule, E., and Theillet, C. (2000) At least five regions of imbalance on 6q in breast tumors, combining losses and gains. *Genes Chromosomes Cancer* **27**, 76-84

Roepstorff, K., Thomsen, P., Sandvig, K., and van Deurs, B. (2002) Sequestration of epidermal growth factor receptors in non-caveolar lipid rafts inhibits ligand binding. *J. Biol. Chem.* **277**, 18954-18960

Sablina, A. A., Chumakov, P. M., and Kopnin, B. P. (2003) Tumor suppressor p53 and its homologue p73alpha affect cell migration. *J. Biol. Chem.* **278**, 27362-27371

Safran, M., Chalifa-Caspi, V., Shmueli, O., Olender, T., Lapidot, M., Rosen, N., Shmoish, M., Peter, Y., Glusman, G., Feldmesser, E., Adato, A., Peter, I., Khen, M., Atarot, T., Groner, Y., and Lancet, D. (2003) Human Gene-Centric Databases at the Weizmann Institute of Science: GeneCards, UDB, CroW 21 and HORDE. *Nucleic Acids Res.* **31**, 142-146

Sala, M., Forner, A., Varela, M., and Bruix, J. (2005) Prognostic prediction in patients with hepatocellular carcinoma. *Semin. Liver Dis.* **25**, 171-180

Salvucci, M., Lemoine, A., Saffroy, R., Azoulay, D., Lepere, B., Gaillard, S., Bismuth, H., Reynes, M., and Debuire, B. (1999) Microsatellite instability in European hepatocellular carcinoma. *Oncogene* **18**, 181-187

Sandgren, E. P., Quaife, C. J., Pinkert, C. A., Palmiter, R. D., and Brinster, R. L. (1989) Oncogene-induced liver neoplasia in transgenic mice. *Oncogene* **4**, 715-724

Sastry, S. K., and Burridge, K. (2000) Focal adhesions: a nexus for intracellular signaling and cytoskeletal dynamics. *Exp. Cell Res.* **261**, 25-36

Satoh, H., Lamb, P. W., Dong, J. T., Everitt, J., Boreiko, C., Oshimura, M., and Barrett, J. C. (1993) Suppression of tumorigenicity of A549 lung adenocarcinoma cells by human chromosomes 3 and 11 introduced via microcell-mediated chromosome transfer. *Mol. Carcinog.* **7**, 157-164

Satoh, S., Daigo, Y., Furukawa, Y., Kato, T., Miwa, N., Nishiwaki, T., Kawasoe, T., Ishiguro, H., Fujita, M., Tokino, T., Sasaki, Y., Imaoka, S., Murata, M., Shimano, T., Yamaoka, Y., and Nakamura, Y. (2000) AXIN1 mutations in hepatocellular carcinomas, and growth suppression in cancer cells by virus-mediated transfer of AXIN1. *Nat. Genet.* **24**, 245-250

Satoh-Horikawa, K., Nakanishi, H., Takahashi, K., Miyahara, M., Nishimura, M., Tachibana, K., Mizoguchi, A., and Takai, Y. (2000) Nectin-3, a New member of

immunoglobulin-like cell adhesion molecules that shows homophilic and heterophilic cell-cell adhesion activities. *J. Biol. Chem.* **275**, 10291-10299

Savani, R. C., Cao, G., Pooler, P. M., Zaman, A., Zhou, Z., and DeLisser, H. M. (2001) Differential involvement of the hyaluronan (HA) receptors CD44 and receptor for HA-mediated motility in endothelial cell function and angiogenesis. *J. Biol. Chem.* **276**, 36770-36778

Schlessinger, J. (2000) Cell signaling by receptor tyrosine kinases. *Cell* **103**, 211-225

Schwarz, M. A., Owaribe, K., Kartenbeck, J., and Franke, W. W. (1990) Desmosomes and hemidesmosomes: constitutive molecular components. *Annu. Rev. Cell Biol.* **6**, 461-491

Sechi, A. S., and Wehland, J. (2000) The actin cytoskeleton and plasma membrane connection: PtdIns(4,5)P(2) influences cytoskeletal protein activity at the plasma membrane. *J. Cell Sci.* **113**, 3685-3695

Seftor, R. E., Seftor, E. A., and Hendrix, M. J. (1999) Molecular role(s) for integrins in human melanoma invasion. *Cancer Metastasis Rev.* **18**, 359-375

Sellar, G. C., Watt, K. P., Rabiasz, G. J., Stronach, E. A., Li, L., Miller, E. P., Massie, C. E., Miller, J., Contreras-Moreira, B., Scott, D., Brown, I., Williams, A. R., Bates, P. A., Smyth, J. F., and Gabra, H. (2003) OPCML at 11q25 is epigenetically inactivated and has tumor-suppressor function in epithelial ovarian cancer. *Nat. Genet.* **34**, 337-343

Seow, A., Koh, W. P., Chia, K. S., Shi, L. M., Lee, H. P., and Shanmugaratnam K. (2004) Trends in cancer incidence in Singapore 1968-2002. Singapore Cancer Registry Report No. 6.

Sessa, W. C., Barber, C. M., and Lynch, K. R. (1993) Mutation of N-myristoylation site converts endothelial cell nitric oxide synthase from a membrane to a cytosolic protein. *Circ. Res.* **72**, 921-924

Shachaf, C. M., Kopelman, A. M., Arvanitis, C., Karlsson, A., Beer, S., Mandl, S., Bachmann, M. H., Borowsky, A. D., Ruebner, B., Cardiff, R. D., Yang, Q., Bishop, J. M., Contag, C. H., and Harada, K., Shiota, G., and Kawasaki, H. (1999) Transforming growth factor-alpha and epidermal growth factor receptor in chronic liver disease and hepatocellular carcinoma. *Liver* **19**, 318-325

Shafritz, D. A., Shouval, D., Sherman, H. I., Hadziyannis, S. J., and Kew, M. C. (1981) Integration of hepatitis B virus DNA into the genome of liver cells in chronic liver disease and hepatocellular carcinoma. Studies in percutaneous liver biopsies and post-mortem tissue specimens. *N. Engl. J. Med.* **305**, 1067-1073

Shan, Z., Parker, T., and Wiest, J. S. (2004) Identifying novel homozygous deletions by microsatellite analysis and characterization of tumor suppressor candidate 1 gene, TUSC1, on chromosome 9p in human lung cancer. *Oncogene* **23**, 6612-6620

Shapiro, L., Fannon, A. M., Kwong, P. D., Thompson, A., Lehmann, M. S., Grübel, G., Legrand, J. F., Als-Nielsen, J., Colman, D. R., and Hendrickson, W. A. (1995) Structural basis for cell-cell adhesion by cadherins. *Nature* **374**, 327-336

Shaw, G., and Kamen, R. (1986) A conserved AU sequence from the 3' untranslated region of GM-CSF mRNA mediates selective mRNA degradation. *Cell* **46**, 659-667

Sheen, I. S., Liaw, Y. F., Lin, D. Y., and Chu, C. M. (1994) Role of hepatitis C and delta virus in the termination of chronic hepatitis B surface antigen carrier state: a multivariate analysis in a longitudinal follow-up study. *J. Infect. Dis.* **170**, 358-361

Shen, L., Fang, J., Qiu, D., Zhang, T., Yang, J., Chen, S., and Xiao, S. (1998) Correlation between DNA methylation and pathological changes in human hepatocellular carcinoma. *Hepatogastroenterology* **45**, 1753-1759

Sheu, J. C., Huang, G. T., Lee, P. H., Chung, J. C., Chou, H. C., Lai, M. Y., Wang, J. T., Lee, H. S., Shih, L. N., and Yang, P. M. (1992) Mutation of p53 gene in hepatocellular carcinoma in Taiwan. *Cancer Res.* **52**, 6098-6100

Shih, W. L., Kuo, M. L., Chuang, S. E., Cheng, A. L., and Doong, S. L. (2000) Hepatitis B virus X protein inhibits transforming growth factor-β-induced apoptosis through the activation of phosphatidylinositol 3-kinase pathway. *J. Biol. Chem.* **275**, 25858-25864

Shtutman, M., Zhurinsky, J., Simcha, I., Albanese, C., D'Amico, M., Pestell, R., and Ben-Ze'ev, A. (1999) The cyclin D1 gene is a target of the beta-catenin/LEF-1 pathway. *Proc. Natl. Acad. Sci. USA* **96**, 5522-5527

Simile, M. M., De Miglio, M. R., Muroni, M. R., Frau, M., Asara, G., Serra, S., Muntoni, M. D., Seddaiu, M. A., Daino, L., Feo, F., and Pascale, R. M. (2004) Down-regulation of c-myc and Cyclin D1 genes by antisense oligodeoxy nucleotides inhibits the expression of E2F1 and in vitro growth of HepG2 and Morris 5123 liver cancer cells. *Carcinogenesis* **25**, 333-341

Simons, R. W. (1988) Naturally occurring antisense RNA control: a brief review. *Gene* **72**, 35-44

Simons, K., and Ikonen, E. (1997) Functional rafts in cell membranes. *Nature* **387**, 569-572

Simons, K., and Toomre, D. (2000) Lipid rafts and signal transduction. *Nat. Rev. Mol. Cell. Biol.* **1**, 31-39

Simonsen, A., Bremnes, B., Nordeng, T. W., and Bakke, O. (1998) The leucine-based motif DDQxxLI is recognized both for internalization and basolateral sorting of invariant chain in MDCK cells. *Eur. J. Cell Biol.* **76**, 25-32

Singer, M. F. (1982) SINEs and LINEs: highly repeated short and long interspersed sequences in mammalian genomes. *Cell* **28**, 433-434

Singer, S. J., and Nicolson, G. L. (1972) The fluid mosaic model of the structure of cell membranes. *Science* **175**, 720-731

Soole, K. L., Jepson, M. A., Hazlewood, G. P., Gilbert, H. J., and Hirst, B. H. (1985) Epithelial sorting of a glycosylphosphatidylinositol-anchored bacterial protein expressed in polarized renal MDCK and intestinal Caco-2 cells, *J. Cell Sci*. **108**, 369-377

Stamatoglou, S. C., and Hughes, R. C. (1994) Cell adhesion molecules in liver function and pattern formation. *FASEB J*. **8**, 420-427

Stevenson, B. R., Siciliano, J. D., Mooseker, M. S., and Goodenough, D. A. (1986) Identification of ZO-1: A high molecular weight polypeptide associated with the tight junction (zonula occludens) in a variety of epithelia. *J. Cell Biol*. **103**, 755-766

Stickney J. T., Bacon, W. C., Rojas, M., Ratner, N., and Ip, W. (2004) Activation of the tumor suppressor merlin modulates its interaction with lipid rafts. *Cancer Res*. **64**, 2717-2724

Stronach, E. A., Sellar, G. C., Blenkiron, C., Rabiasz, G. J., Taylor, K. J., Miller, E. P., Massie, C. E., Al-Nafussi, A., Smyth, J. F., Porteous, D. J., and Gabra, H. (2003) Identification of clinically relevant genes on chromosome 11 in a functional model of ovarian cancer tumor suppression. *Cancer Res*. **63**, 8648-8655

Su, F., and Schneider, R. J. (1996) Hepatitis B virus HBx protein activates transcription factor NF-κB by acting on multiple cytoplasmic inhibitors of rel-related proteins. *J. Virol*. **70**, 4558-4566

Su, J., Muranjan, M., and Sap, J. (1999) Receptor protein tyrosine phosphatase alpha activates Src-family kinases and controls integrin-mediated responses in fibroblasts. *Curr. Biol*. **9**, 505-511

Su, L. K., Abdalla, E. K., Law, C. H., Kohlmann, W., Rashid, A., and Vauthey, J. N. (2001) Biallelic inactivation of the APC gene is associated with hepatocellular carcinoma in familial adenomatous polyposis coli. *Cancer* **92**, 332-339

Sugiyama, A., Noguchi, K., Kitanaka, C., Katou, N., Tashiro, F., Ono, T., Yoshida, M. C., and Kuchino, Y. (1999) Molecular cloning and chromosomal mapping of mouse intronless *myc* gene acting as a potent apoptosis inducer. *Gene* **226**, 273-283

Sun, Z., Lu, P., Gail, M. H., Pee, D., Zhang, Q., Ming, L., Wang, J., Wu, Y., Liu, G., Wu, Y., and Zhu, Y. (1999) Increased risk of hepatocellular carcinoma in male hepatitis B surface antigen carriers with chronic hepatitis who have detectable urinary aflatoxin metabolite M1. *Hepatology* **30**, 379-383

Sundberg, U., and Obrink, B. (2002) CEACAM1 isoforms with different cytoplasmic domains show different localization, organization and adhesive properties in polarized epithelial cells. *J. Cell Sci*. **115**, 1273-1284

Suzuki, T., Suzuki, Y., Hanada, K., Hashimoto, A., Redpath, J. L., Stanbridge, E. J., Nishijima, M., and Kitagawa, T. (1998) Reduction of caveolin-1 expression in tumorigenic human cell hybrids. *J. Biochem*. **124**, 383-388

Szymanski, M., Barciszewska, M. Z., Zywicki, M., and Barciszewski, J. (2003) Noncoding RNA transcripts. *J. Appl. Genet*. **44**, 1-19

Takahashi, K., Nakanishi, H., Miyahara, M., Mandai, K., Satoh, K., Satoh, A., Nishioka, H., Aoki, J., Nomoto, A., Mizoguchi, A., and Takai, Y. (1999) Nectin/PRR: an immunoglobulin-like cell adhesion molecule recruited to cadherin-based adherens junctions through interaction with afadin, a PDZ domain-containing protein. *J. Cell Biol*. **145**, 539-549

Takeda, K., Ichijo, H., Fujii, M., Mochida, Y., Saitoh, M., Nishitoh, H., Sampath, T. K., and Miyazono, K. (1998) Identification of a novel bone morphogenetic protein-responsive gene that may function as a noncoding RNA. *J. Biol. Chem*. **273**, 17079-17085

Takeichi, M. (1977) Functional correlation between cell adhesive properties and some cell surface proteins. *J. Cell Biol*. **75**, 464-474

Takeichi, M. (1988) The cadherins: cell-cell adhesion molecules controlling animal morphogenesis. *Development* **102**, 639-655

Takeichi, M. (1993) Cadherins in cancer: implications for invasion and metastasis. *Curr. Opin. Cell Biol*. **5**, 806-811

Takekuni, K., Ikeda, W., Fujito, T., Morimoto, K., Takeuchi, M., Monden, M., and Takai, Y. (2003) Direct binding of cell polarity protein PAR-3 to cell-cell adhesion molecule nectin at neuroepithelial cells of developing mouse. *J. Biol. Chem*. **278**, 5497-5500

Tamura, K., Shan, W. S., Hendrickson, W. A., Colman, D. R., and Shapiro, L. (1998) Structure-function analysis of cell adhesion by neural (N-) cadherin. *Neuron* **20**, 1153-1163

Tanaka, K., Hinoda, Y., Takahashi, H., Sakamoto, H., Nakajima, Y., and Imai, K. (1997) Decreased expression of biliary glycoprotein in hepatocellular carcinomas. *Int. J. Canc*er **74**, 15-19

Tarone, G., Ferracini, R., Galetto, G., and Comoglio, P. (1984) A cell surface integral membrane glycoprotein of 85,000 mol wt (gp85) associated with triton X-100-insoluble cell skeleton. *J. Cell Biol*. **99**, 512-519

Taylor-Robinson, S. D., Foster, G. R., Arora, S., Hargreaves, S., and Thomas, H. C. (1997) Increase in primary liver cancer in the UK, 1979-1994. *Lancet* **350**, 1142-1143

Tedder, T. F., Steeber, D. A., Chen, A., and Engel, P. (1995) The selectins: vascular adhesion molecules. *FASEB J*. **9**, 866-873

Terryn, N., and Rouze, P. (2000) The sense of naturally transcribed antisense RNAs in plants. *Trends Plant Sci*. **5**, 394-396

Tetsu, O., and McCormick, F. (1999) Beta-catenin regulates expression of cyclin D1 in colon carcinoma cells. *Nature* **398**, 422-426

Thomas, M. B. (2005) Hepatocellular carcinoma: The need for progress. *J. Clin. Oncol*. **23**, 2892-2899

Thorgeirsson, S. S., and Grisham, J. W. (2002) Molecular pathogenesis of human hepatocellular carcinoma. *Nat. Genet*. **31**, 339-346

Tomschy, A., Fauser, C., Landwehr, R., and Engel, J. (1996) Homophilic adhesion of E-cadherin occurs by a co-operative two-step interaction of N-terminal domains. *EMBO J*. **15**, 3507-3514

Tonks, N. K. (1993) Protein tyrosine phosphates. *Semin. Cell Biol*. **4**, 373-453

Toole, B. P. (2002) Hyaluronan promotes the malignant phenotype. *Glycobiology* **12**, 37R-42R

Trent, J. M., Stanbridge, E. J., McBride, H. L., Meese, E. U., Casey, G., Araujo, D. E., Witkowski, C. M., and Nagle, R. B. (1990) Tumorigenicity in human melanoma cell lines controlled by introduction of human chromosome 6. *Science* **247**, 568-571

Truant, R., Antunovic, J., Greenblatt, J., Prives, C., and Cromlish, J. A. (1995) Direct interaction of the hepatitis B virus HBx protein with p53 leads to inhibition by HBx of p53 response element-directed transactivation. *J. Virol*. **69**, 1851-1859

Tsukita, S., Furuse, M., and Itoh, M. (1999) Structural and signalling molecules come together at tight junctions. *Curr. Opin. Cell. Biol*. **11**, 628-633

Ueta, T., Ikeguchi, M., Hirooka, Y., Kaibara, N., and Terada, T. (2002) β-catenin and cyclin D1 expression in human hepatocellular carcinoma. *Oncol. Rep*. **9**, 1197-1203

Van der Krol, A. R., Mol, J. N. M., and Stuitje, A. R. (1988) Regulation of eukaryotic gene expression by complementary RNA or DNA sequences. *Biotechniques* **6**, 958-976

Van Nhieu, J. T., Renard, C. A., Wei, Y., Cherqui, D., Zafrani, E. S., and Buendia, M. A. (1999) Nuclear accumulation of mutated beta-catenin in hepatocellular carcinoma is associated with increased cell proliferation. *Am. J. Pathol*. **155**, 703-710

Vanhee-Brossollet, C., and Vaquero, C. (1998) Do natural antisense transcripts make sense in eukaryotes? *Gene* **211**, 1-9

Vinson, C. R., Sigler, P. B., and McKnight, S. L. (1989) Scissors-grip model for DNA recognition by a family of leucine zipper proteins. *Science* **246**, 911-916

von Weizsacker, F., Maedi, E., Brown, N. V., Poynard, T., Galun, E., Labeit, S., Caput, J. C., Arima, T., Blum, H., and Wands, J. R. (1995) Hepatitis B and C virus infection in HBsAg-negative alcoholics without iv drug abuse or previous blood transfusions. *Int. Hepatol. Commun.* **4**, 80-87

Wagner, E. G., and Simons, R. W. (1994) Antisense RNA control in bacteria, phages, and plasmids. *Annu. Rev. Microbiol.* **48**, 713-742

Wake, K. (1980) Perisinusoidal stellate cells (fat storing cells, interstitial cells, lipocytes), they related structural in and around the liver sinusoids, and vitamin A-storing cells in extrahepatic organs. *Int. Rev. Cytol.* **66**, 303-353

Walker, G. J., Hayward, N. K., Falvey, S., and Cooksley, W. G. E. (1991) Loss of somatic heterozygosity in hepatocellular carcinoma. *Cancer Res.* **51**, 4367- 4370

Wan, M., Sun, T., Vyas, R., Zheng, J., Granada, E., and Dubeau, L. (1999) Suppression of tumorigenicity in human ovarian cancer cell lines is controlled by a 2 cM fragment in chromosomal region 6q24-q25. *Oncogene* **18**, 1545-1551

Wang, H. P., and Rogler, C. E. (1988) Deletions in human chromosome arms 11p and 13q in primary hepatocellular carcinoma. *Cytogenet. Cell Genet.* **48**, 72-78

Wang, X. W., Forrester, K., Yeh, H., Feitelson, M. A., Gu, J. R., and Harris, C. C. (1994) Hepatitis B virus X protein inhibits p53 sequence-specific DNA binding, transcriptional activity, and association with transcription factor ERCC3. *Proc. Natl. Acad. Sci. USA* **91**, 2230-2234

Webb, D. J., Parsons, J. T., and Horwitz, A. F. (2002) Adhesion assembly, disassembly and turnover in migrating cells – Over and over and over again. *Nat. Cell Biol.* **4**, E97-E100

Weber, H. O., Samuel, T., Rauch, P., and Funk, J. O. (2002) Human p14(ARF)-mediated cell cycle arrest strictly depends on intact p53 signaling pathways. *Oncogene* **21**, 3207-3212

Weiler-Normann, C., and Rehermann, B. (2004) The liver as an immunological organ. *J. Gastroenterol. Hepatol.* **19**, S279-S283

Weissman, B. E., Saxon, P. J., Pasquale, S. R., Jones, G. R., Geiser, A. G., and Stanbridge, E. J. (1987) Introduction of a normal human chromosome 11 into a Wilms' tumor cell line controls its tumorigenic expression. *Science* **236**, 175-180

Welch, M. D., and Mullins, R. D. (2002) Cellular control of actin nucleation. *Annu. Rev. Cell Dev. Biol.* **18**, 247-288

Wells, J. M., and Melton, D. A. (1999) Vertebrate endoderm development. *Annu. Rev. Cell Dev. Biol.* **15**, 393-410

Wheelock, M. J., and Johnson, K. R. (2003) Cadherins as modulators of cellular phenotype. *Annu. Rev. Cell Dev. Biol.* **19**, 207-235

Wiig, M., Abrahamsson, S. O., and Lundborg, G. (1996) Effects of hyaluronan on cell proliferation and collagen synthesis: a study of rabbit flexor tendons in vitro. *J. Hand Surg. Am.* **21**, 599-604

Williams, A. F., and Barclay, A. N. (1998) The immunoglobulin superfamily – domains for cell surface recognition. *Annu. Rev. Immunol.* **6**, 381-405

Wisse, E., Braet, F., Luo, D., De Zanger, R., Jans, D., Crabbe, E., and Vermoesen, A. (1996) Structure and function of sinusoidal lining cells in the liver. *Toxicol. Pathol.* **24**, 100-111

Wollenberg, G. K., Semple, E., Quinn, B. A., and Hayes, M. A. (1987) Inhibition of proliferation of normal, preneoplastic, and neoplastic rat hepatocytes by transforming growth factor-beta. *Cancer Res.* **47**, 6595-6599

Wu, Y., Renard, C. A., Apiou, F., Huerre, M., Tiollais, P., Dutrillaux, B., and Buendia, M. A. (2002) Recurrent allelic deletions at mouse chromosomes 4 and 14 in Myc-induced liver tumors. *Oncogene* **21**, 1518-1526

Yamada, K. M., and Geiger, B. (1997) Molecular interactions in cell adhesion complexes. *Curr. Opin. Cell. Biol.* **9**, 76-85

Yan, K., Khoshnoodi, J., Ruotsalainen, V., and Tryggvason, K. (2002) N-linked glycosylation is critical for the plasma membrane localization of nephrin. *J. Am. Soc. Nephrol.* **13**, 1385-1389

Yang, A., Kaghad, M., Wang, Y., Gillett, E., Fleming, M. D., Dotsch, V., Andrews, N. C., Caput, D., and McKeon, F. (1998) p63, a p53 homolog at 3q27-29, encodes multiple products with transactivating, death-inducing, and dominant-negative activities. *Mol. Cell* **2**, 305-316

Yang, B., Zahang, L., and Turley, E. A. (1993) Identification of two hyaluronan-binding domains in the hyaluronan receptor RHAMM. *J. Biol. Chem.* **268**, 8617-8623

Yeh, F. S., Yu, M. C., Mo, C. C., Luo, S., Tong, M. J., and Henderson, B. E. (1989) Hepatitis B virus, aflatoxins, and hepatocellular carcinoma in southern Guangxi, China. *Cancer Res.* **49**, 2506-2509

Yoshida, C., and Takeichi, M. (1982) Teratocarcinoma cell adhesion: identification of a cell-surface protein involved in calcium-dependent cell aggregation. *Cell* **28**, 217-224

Yulug, I. G., Yulug, A., and Fisher, E. M. (1995) The frequency and position of Alu repeats in cDNAs, as determined by database searching. *Genomics* **27**, 544-548

Zamir, E., and Geiger, B. (2001) Molecular compexity and dynamics of cell-matrix adhesions. *J. Cell Sci.* **114**, 3583-3590

Zaret, K. S. (2002) Regulatory phases of early liver development: paradigms of organogenesis. *Nat. Rev. Genet.* **3**, 499-512

Zhang, Y. J. Jiang, W., Chen, C. J., Lee, C. S., Kahn, S. M., Santella, R. M., and Weinstein, I. B. (1993) Amplification and overexpression of cyclin D1 in human hepatocellular carcinoma. *Biochem. Biophys. Res. Commun.* **196**, 1010-1016

Zhu, J., Jiang, J., Zhou, W., and Chen, X. (1998) The potential tumor suppressor p73 differentially regulates cellular p53 target genes. *Cancer Res.* **58**, 5061-5065

Zimmermann, U., Feneux, D., Mathey, G., Gayral, F., Franco, D., and Bedossa, P. (1997) Chromosomal aberrations in hepatocellular carcinomas: relationship with pathological features. *Hepatology* **26**, 1492-1498

Zurzolo, C., Lisanti, M. P., Caras, I. W., Nitsch, L., and Rodriguez-Boulan, E. (1993) Glycosylphosphatidylinositol-anchored proteins are preferentially targeted to the basolateral surface in Fischer rat thyroid epithelial cells. *J. Cell Biol.* **121**, 1031-1039

APPENDICES

Antibiotic solutions

Antibiotics	Concentration
Ampicillin	100 mg/ml in H_2O
Kanamycin	30 mg/ml in H_2O
Blasticidin	10 mg/ml in H_2O

All water-soluble antibiotics were filter-sterilized.

Solutions for preparation of competent cells and bacterial cultivation

Solution	Concentration
LB medium	1% Tryptone 0.5g Yeast Extract 1% NaCl
LB agar	1% Tryptone 0.5g Yeast Extract 1% NaCl 1.5% Agar
$CaCl_2$ solution	60 mM $CaCl_2$, 15% Glycerol 10 mM PIPES [piperazine-*N*,*N*'-bis(2-hydroxypropane-sulfonic acid)] Adjust pH to 7.0
0.1 M IPTG	1.2 g IPTG (isopropyl-beta-D-thiogalactopyranoside) in 50 ml of H_2O
X-gal (2 ml)	100 mg X-Gal (5-bromo-4-chloro-3-indolyl-β-D-galactoside) in 2 ml of *N*,*N*'-dimethyl-formamide

Solutions for Northern/Dot blot

Solution	Concentration
DEPC-treated solutions	Add 1 ml of DEPC (diethylpyrocarbonate) per liter of solution. Shake vigorously and leave overnight at room temperature. Autoclave at 121°C for 15 min
10X MOPS buffer	200 mM MOPS (3-[N-Morpholino] propanesulfonic acid) 50 mM Sodium acetate 20 mM EDTA Adjust pH to 7.0

1% Formaldehyde/MOPS gel (50 ml)	Melt 0.5 g of agarose in 47.3 ml of 1X MOPS buffer, and add 2.7 ml of 37% formaldehyde and 2.5 µl of ethidium bromide.
Running buffer	Dilute 10X MOPS to 1X with DEPC-treated H_2O
Loading buffer (500 µl)	250 µl 100% formamide, 83 µl 37% formaldehyde, 50 µl of 10X MOPS, 50 µl 100% glycerol, 10 µl 2.5% bromophenol blue, 57 µl DEPC-treated H_2O
20X SSC	3M NaCl 0.3 M Sodium citrate Adjust pH to 7.2
Low Stringeny buffer	2X SSC containing 0.1% SDS
High Stringency buffer	0.1X SSC containing 0.1% SDS
Maleic Acid buffer	0.1 M Maleic acid 0.15 M NaCl Adjust pH to 7.5
Blocking solution	Dilute 10X Blocking solution to 1X with Maleic Acid buffer
Washing buffer	Dissolve 0.3% (v/v) Tween-20 in Maleic Acid buffer
Antibody solution	Dilute Anti-Digoxigenin-AP 1:10,000 in Blocking solution
Detection buffer	0.1 M Tris-HCl 0.1 M NaCl Adjust pH to 9.5
Wash solution 1	2X SSC, 1% SDS
Wash solution 2	0.1X SSC, 0.5% SDS

Solutions for agarose gel electrophoresis and DNA purification from gel

Solution	Concentration
1X TAE buffer	40 mM Tris 20 mM Acetic acid 1 mM EDTA Adjust pH to 7.8
6X Loading dye	0.25% (w/v) Xylene Cyanol FF 15% (w/v) Ficoll 400 0.25% (w/v) Bromophenol Blue
3 M sodium acetate	Dissolve 123g of sodium acetate in 500 ml of H_2O Adjust pH to 5.2 with acetic acid

Solutions for immunocytochemistry

Solution	Concentration
1X PBS (1 liter)	8 g NaCl, 0.2 g KCl, 1.44 g $Na_2HPO_4 \cdot 7H_2O$, 0.24 g KH_2PO_4 Adjust pH to 7.2
3.7% Paraformaldehyde (50 ml)	Add 1.85 g of paraformaldehyde into 40 ml of 1X PBS. Warm to dissolve. Add 5M NaOH dropwise until solution clears. Adjust pH to 7.4 and increase volume to 50 ml. Filter-sterilize and aliquot. Store at -20°C

Solutions for cell extraction

Solution	Concentration
Hypotonic buffer	20 mM Tris-HCl, pH 7.4 1 mM EDTA 0.01% β-mercaptoethanol
RIPA buffer	50 mM Tris pH8.0 150 mM NaCl 1% Triton X-100 0.5% NaDOC 0.1% SDS

Solutions for sucrose density gradient ultracentrifugation

Solution	Concentration
Lysis buffer	25 mM Tris-HCl, pH 7.5 150 mM NaCl 5 mM EDTA 1% Triton X-100
TNE buffer	25 mM Tris-HCl, pH 7.5 150 mM NaCl 5 mM EDTA
80% (w/v) sucrose (50 ml)	Add 40 g of sucrose into 40 ml of TNE buffer. Warm to dissolve and increase volume to 50 ml
30% (w/v) sucrose (10 ml)	Dilute 3.75 ml of 80% sucrose in 6.25 ml of TNE buffer
10% (w/v) sucrose (10 ml)	Dilute 1.25 ml of 80% sucrose in 8.75 ml of TNE buffer

Solutions for Western blot

Solution	Concentration
2X Laemmli sample buffer	125 mM Tris-HCl pH6.8 4% SDS 1.8% β-mercaptoethanol 10% glycerol 0.01% bromophenol blue
5X Laemmli sample buffer	62.5 mM Tris-HCl pH6.8 2% SDS 5% β-mercaptoethanol 10% Glycerol 0.05% Bromophenol blue
10% separating gel (10 ml)	2.72 ml H_2O, 3.75 ml Tris-HCl pH 8.8, 3.33 ml 30% acrylamide/bis solution (29:1; Biorad), 100 µl 10% SDS, 100 µl 10% APS (ammonium persulfate), 4 µl TEMED
4% stacking gel (4 ml)	2.75 ml H_2O, 0.5 ml Tris-HCl pH 6.8, 0.67 ml 30% acrylamide/bis solution, 40 µl 10% SDS, 40 µl 10% APS, 4 µl TEMED
1X SDS-PAGE running buffer	25 mM Tris-HCl 0.2 M Glycine 0.1% SDS Adjust pH to 8.3
Stripping buffer	25 mM Glycine Adjust pH to 2.0 1% SDS
Towbin transfer buffer	25 mM Tris 192 mM Glycine 20% v/v Methanol Adjust pH to 8.3
10X TBS	0.2M Tris base 1.37M NaCl Adjust pH to 7.6
1X TBS	20 mM Tris base 137 mM NaCl Adjust pH to 7.6
1X TBS-T	0.1% Tween-20 in 1X TBS
Blocking buffer	Dissolve 5% non-fat milk powder (Anlene) in 1X TBS buffer

ELSEVIER

Journal of Hepatology 39 (2003) 580–586

Journal of Hepatology

www.elsevier.com/locate/jhep

HEPN1, a novel gene that is frequently down-regulated in hepatocellular carcinoma, suppresses cell growth and induces apoptosis in HepG2 cells

Mei Chung Moh[1], Lay Hoon Lee[1], Xiaodong Yang[2], Shali Shen[1,*]

[1]*Department of Physiology, Faculty of Medicine, National University of Singapore, 2 Medical Drive, Singapore 117597, Singapore*
[2]*Department of Surgery, No. 3 Hospital of Chongqing, Chongqing, China*

***Background/Aims*: Examining genes associated with human hepatocellular carcinoma (HCC) by subtractive hybridisation, we identified a novel transcript, designated as *HEPN1*, in non-tumorous liver. In this study, we aimed to evaluate *HEPN1* gene expression in HCC patients, to characterise and to explore the functional significance of *HEPN1* in vitro.**

***Methods*: One-step reverse transcription-polymerase chain reaction (RT-PCR) and real-time RT-PCR were employed to determine *HEPN1* expression in 23 paired (HCC and the adjacent non-HCC) liver specimens. Sequence analyses were performed by bioinformatics. Transfection studies were carried out by expressing HEPN1, V5-fused HEPN1, and green fluorescent protein-fused HEPN1, individually, in HepG2 cells.**

***Results*: Significant downregulation of *HEPN1* ($P < 0.0001$) was detected in 22/23 of HCC patients tested. Gene *HEPN1* maps to chromosome 11q24.2; and the predicted gene product, a 10-kDa peptide with 88 amino acids, has no homology to known proteins. When transfected into HepG2 cells, *HEPN1* reduced cell viability to 37.5 ± 2.5% ($P = 0.001$), and induced apoptosis with typical morphological changes as demonstrated by microscopy and Annexin V assay.**

***Conclusions*: Our data show that *HEPN1* is frequently silenced in HCC, and that exogenous *HEPN1* exhibits antiproliferative effect on HepG2 cells, suggesting that silencing of *HEPN1* may be associated with carcinogenesis of hepatocytes.**

***Keywords*: Novel gene; Hepatocellular carcinoma; HepG2; Apoptosis; Growth inhibition**

1. Introduction

Hepatocellular carcinoma (HCC) is one of the most common malignancies worldwide, with significantly higher incidence rates in Africa, Southeast Asia and China. Despite a few improvements made in diagnosis and treatment, prognosis of HCC remains extremely poor leading to almost one million deaths annually [1]. The causes of HCC have been associated with chronic liver diseases due to hepatitis virus infections [2,3] and/or aflatoxin exposure [4]. Although it has been shown that genetic changes occur in hepatocytes following exposure to various viral or chemical carcinogens [5], the underlying mechanisms of the hepatocarcinogenesis are still largely unknown.

Genetic alterations have been defined as the hallmark of cancers. A widely accepted approach to study genetic instability is to identify cancer-related genes, in particular, the two major groups of growth regulatory genes – oncogenes and tumour suppressor genes. Noticeably, studies on genetic alterations in HCC have recently increased, reporting genes that are either up- or down-regulated or lost in hepatocellular carcinoma [6–11]. Among genes that are down-regulated in HCC, *DRH1* [11] is one of the few genes that have directly been linked to carcinogenesis and progression of hepatocellular carcinoma; however, its biological role in cell growth/death of hepatocytes remains to be examined.

Received 9 January 2003; received in revised form 10 April 2003; accepted 7 July 2003

* Corresponding author. Tel.: +65-6874-6406; fax: +65-6778-8161.
E-mail address: phsssl@nus.edu.sg (S. Shen).

0168-8278/$30.00
doi:10.1016/S0168-8278(03)00359-3

To explore genes associated with HCC, we compared the gene expression between HCC and its adjacent non-tumorous liver using the technique of suppression subtractive hybridisation. With this approach, we identified a novel transcript, *HEPN1*, which was suppressed in HCC liver tissue. In this report, we demonstrate the frequency of *HEPN1* downregulation in human hepatocellular carcinoma, the characteristics and the functional significance of this gene in HepG2, a cell line derived from HCC.

2. Materials and methods

2.1. Isolation of HEPN1 full-length cDNA

A fragment about 400 bp of *HEPN1* was identified by subtractive hybridisation. Based on the known sequence, gene-specific primers 1 and 2 were generated. The full-length cDNA of *HEPN1* was obtained by the technique of rapid amplification of cDNA ends (RACE). RACE reactions were prepared using the SMART™ RACE cDNA Amplification Kit (Clontech, Palo Alto, CA, USA) and total RNA extracted from normal liver tissue. To confirm the sequence information, RACE was repeated using the Human Liver Marathon-Ready™ cDNA (Clontech, Palo Alto, CA, USA). Briefly, the gene-specific primer 1 (GSP1, 5′CTC CTA AAC TCC AGC TCT GAT 3′) was used in combination with the adapter primer to amplify the 5′-end of the gene. PCR amplification was performed for 35 cycles of 94°C for 30 s and 68°C for 4 min with a reaction volume of 50 μl. Similarly, the gene-specific primer 2 (GSP2, 5′ATC CAA GTC CTG CTG CCT CTT 3′) was used together with the adaptor primer to generate the 3′-end. The overlap between 5′- and 3′-RACE products was about 300 bp. RACE products were cloned into the pGEM-T system (Promega, Madison, WI, USA) and sequenced by ABI PRISM 377 DNA sequencer (Applied Biosystems, Foster City, CA, USA). Two primers at 5′- and 3′-end were then designed to isolate the full-length *HEPN1* cDNA by PCR. The full-length cDNA was cloned into pGEM-T and sequenced.

2.2. Liver specimens and cell culture

A total of 23 liver specimens (Table 1) were collected from the No. 3 Hospital of Chongqing in China. Each sample was snap-frozen and stored in liquid nitrogen before experiment. The final diagnosis of HCC was confirmed by histological examination. Four HCC cell lines, HepG2, Hep3B, Huh7 and SK-Hep1 were maintained in the recommended media and culture conditions.

2.3. RNA purification and reverse transcription-polymerase chain reaction (RT-PCR)

RT-PCR was performed to screen the expression of *HEPN1* in 23 HCC patients and in four HCC cell lines. Total RNA was extracted from either liver tissues or cells by the RNeasy Kit (Qiagen, Hilden, Germany) and treated with DNase I (Promega, Madison, WI, USA). RT-PCR reactions were prepared by using the OneStep RT-PCR kit (Qiagen, Hilden, Germany) and 0.2 μg of total RNA. Primers GSP1 and GSP2 were used in the reactions to generate a *HEPN1* fragment about 300 bp. Beta-actin or GAPDH was included as an internal control. The One-step RT-PCR conditions were: (1) 50°C for 30 min (RT); (2) 95°C for 15 min (inactivation of reverse transcriptase); and (3) for PCR amplification, 35 cycles of 30 s at 94°C, 30 s at 55°C, and 1 min at 72°C; and ended with 10 min at 72°C. RT-PCR products were analysed by electrophoresis on 1% agarose gels.

2.4. Real-time RT-PCR

The expression level of *HEPN1* in HCC patients, as well as in transfected HepG2 cells, was quantitated by Real-time RT-PCR with LightCycler (Roche, Basel, Switzerland). Each product was amplified from 0.2 μg of total RNA. Reactions were prepared in 20-μl volumes using the LightCycler RNA Amplification Kit SYBR Green I (Roche, Basel, Switzerland) in thin-walled glass capillaries. The Real-time RT-PCR conditions were programmed as follows: 55°C for 10 min for RT followed by PCR initial denaturation at 95°C for 10 s and 45 cycles of 5 s at 95°C, 10 s at 55°C, and 12 s at 72°C. Primers GSP1 and GSP2 were used in quantitative RT-PCR. RT-PCR products were evaluated on agarose gels to ascertain the specificity of the experiments. The results were normalised and presented as percentage against the expression level of the internal control *GAPDH*.

Table 1
Clinical data of 23 patients with HCC

Case	Sex	Age (years)	HBsAg	HCV Ab	Cirrhosis	Grade
1	M	67	+	−	+	3
2	F	66	−	−	+	2
3	M	46	+	−	−	2
4	M	36	+	−	+	3
5	M	55	+	−	+	2
6	M	69	+	−	+	1
7	M	63	−	−	+	1
8	F	72	−	−	−	2
9	F	73	+	+	+	2
10	M	24	+	−	−	3
11	M	39	+	−	+	3
12	M	69	+	−	+	2
13	M	32	+	−	+	3
14	M	68	+	−	+	1
15	M	70	+	−	+	2
16	M	58	+	−	+	2
17	M	56	+	−	+	2
18	M	64	−	+	+	2
19	F	75	−	−	−	2
20	M	60	+	−	+	2
21	F	66	+	−	+	2
22	M	48	+	−	+	2
23	M	33	+	+	+	3

HBsAg, hepatitis B virus surface antigen in serum; HCV Ab, anti-hepatitis C virus antibodies in serum; Cirrhosis, HCC accompanied by liver cirrhosis; +, positive; −, negative. Grade, histological differentiation of HCC: 1, well; 2, moderate; and 3, poor.

2.5. Plasmid constructs

The open reading frame (ORF) of *HEPN1* was generated by PCR and cloned into three types of expression vectors, including: (1) pcDNA3.1/+ (Invitrogen, Carlsbad, CA, USA) promoting high level expression of HEPN1; (2) pcDNA6/V5-His (Invitrogen, Carlsbad, CA, USA) allowing HEPN1 to be fused with V5/His for detection by anti-V5 or anti-His antibody; and (3) pEGFP-N2 (Clontech, Palo Alto, CA, USA) allowing HEPN1 to be fused with the green fluorescent protein (GFP) for visualisation. The constructed plasmids were named as HEPN1-pcDNA, HEPN1-V5, and HEPN1-EGFP, respectively. The empty vectors were used as controls in the respective experiments.

2.6. Transfection studies

Monolayers of exponentially growing HepG2 cells were transfected with desired plasmids using Lipofectamine Plus (Invitrogen, Carlsbad, CA, USA) according to the manufacturer's instructions. Transfection efficiency, approximately 40% in this study, was detected by transfecting HepG2 cells with the pEGFP-N2 vector and calculated based on the number of fluorescent cells against the total number of cells in the test. For transient transfection, HepG2 cells were transfected with either HEPN1-pcDNA or pcDNA3.1 vector alone and analysed by microscopy, MTT (3-[4,5-dimethylthiazol-2-yl]-2,5-diphenyltetrazolium bromide) assay, and real-time RT-PCR at 48 h after transfection. Transient transfections were performed in triplicates and repeated four times. For colony formation,

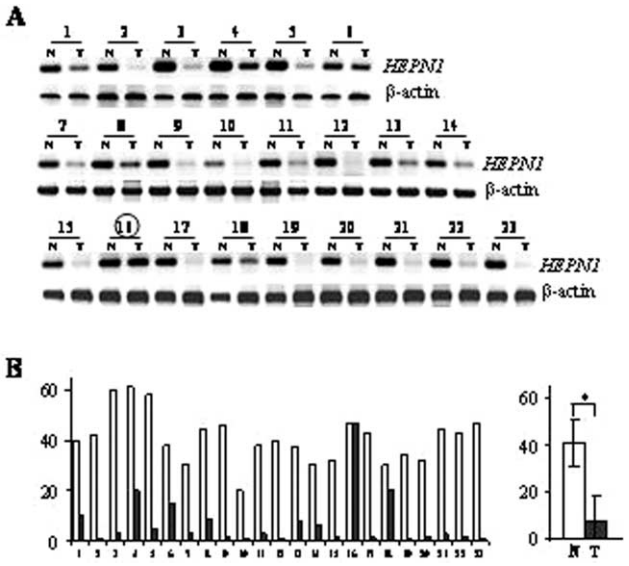

Fig. 1. Expression of *HEPN1* in 23 HCC patients. (A) One-step RT-PCR products were analysed by gel electrophoresis. (B) The expression level of *HEPN1* in each sample was determined by Real-time RT-PCR. Results were normalised and converted into percentage against the expression level of GAPDH. The average level of expression (mean ± SD, $n = 23$) is represented on the right, *$P < 0.0001$. N, non-tumorous liver tissue; T, HCC liver tissue; and β-actin, internal control.

HepG2 cells had been transfected with either HEPN1-EGFP or vector pEGFP-N2 and selected in medium with 800 μg/ml of G418 for 2 weeks before colonies were counted and cells were analysed by confocal microscopy. For transfections with time-course, HepG2 cells were transfected with either HEPN1-EGFP or vector pEGFP-N2 and examined by fluorescent microscopy between 8 and 24 h after transfection with 2-h interval.

2.7. Cell behaviour analyses

2.7.1. MTT assay

Cell viability was assessed by MTT dye conversion. At 48 h after transfection in six-well culture plate, a volume of 100 μl MTT (5 mg/ml in phosphate buffered saline) was added into each well. After 3 h of incubation at 37°C, cells were lysed and formazan crystals were dissolved in 1 ml of isopropanol with 0.4 N HCl. Optical density (OD) was read at 570 nm. Cell viability (CV) was computed by the following equation:

$$\mathrm{CV}(\%) = \left(1 - \frac{\mathrm{ODc} - \mathrm{ODe}}{\mathrm{TE} \times \mathrm{ODc}}\right) \times 100\%$$

where TE = transfection efficiency, i.e. 40% in this study; ODe = OD reading of experiment; ODc = OD reading of control. Cell viability of control was regarded as 100%.

2.7.2. Light microscopy

Cells were observed under an inverted microscope (Carl Zeiss, Germany) to examine cell density and morphology. Cell behaviour was recorded by microscopic photography with magnifications 100× and 400×.

2.7.3. Fluorescent or confocal microscopy

Cells were cultured on cover slips and transfected with either HEPN1-EGFP or pEGFP-N2 alone. At desired times, cells were fixed in 3.7% paraformaldehyde at 37°C for 10 min, and then examined by either Leica DM RXA2 fluorescent microscopy (Heerbrugg, Switzerland) or Confocal Laser Scanning Microscope LSM 510 (Carl Zeiss, Germany).

2.8. Detection of V5-fused HEPN1 protein

Anti-V5 antibody was purchased from Invitrogen (Carlsbad, CA, USA) and the secondary antibody (biotin-conjugated goat anti-mouse IgG) was from Santa Cruz Biotechnology (Santa Cruz, CA, USA). The experimental protocols provided by the manufacturers were therefore combined. Briefly, HepG2 cells were cultured on coverslips and transfected with either HEPN1-V5 construct or the empty vector pcDNA6/V5-His. At 12 h after transfection, cells were fixed in − 10°C methanol for 5 min and incubated in succession with blocking serum (for 20 min), primary antibody (anti-V5, 1:200 dilution, for 60 min), secondary antibody (3 μg/ml, for 45 min), and streptavidin-fluorescein (15 μg/ml, for 15 min in dark). Finally, the coverslips were mounted onto slides and cells were examined by fluorescent microscopy.

2.9. Detection of apoptosis by Annexin V

ApoAlert® Annexin V (Clontech, Palo Alto, CA, USA) was used to detect changes in the position of phosphatidylserine (PS) in the cell membrane. HepG2 cells cultured on cover slips were transfected with either HEPN1-pcDNA or vector pcDNA3.1 alone. At 16 h after transfection, cells were rinsed with binding buffer, incubated with 5 μl of Annexin V for 10 min and observed under a fluorescent microscope using a filter for FITC (fluorescein isothiocyanate).

2.10. Bioinformatics and statistics

Database searches were carried out using BLAST and Swiss-Prot. Motif searches were performed with PROSITE program. Statistics was performed by paired *t*-test and Mann–Whitney test for *HEPN1* expression in liver tissues and the reduction of cell viability in transfection studies, respectively. Software InStat 3.0 (GraphPad, San Diego, CA, USA) was employed and $P < 0.05$ was considered as significant.

3. Results

3.1. Identification of HEPN1 and isolation of its full-length cDNA

Using the technique of subtractive hybridisation, we compared mRNA populations of HCC and its adjacent non-tumorous liver tissue obtained from a randomly chosen HCC patient (No. 15 in Fig. 1). With this approach, we identified 272 genes that were either up- or down-regulated in HCC. Several novel genes were screened against a panel of HCC patients by RT-PCR. A novel transcript, designated as *HEPN1*, was chosen for further studies as it appeared to be constantly down-regulated in HCC.

The full-length cDNA of *HEPN1* was isolated from normal liver tissue by the technique of RACE (Rapid Amplification of cDNA Ends). The complete length and sequence information were confirmed by the second set of RACE reactions performed on the full-length cDNA of normal liver from Clontech.

3.2. Loss of HEPN1 expression in human hepatocellular carcinoma

To determine the frequency of its suppression in liver cancer, we examined the expression of *HEPN1* against 23

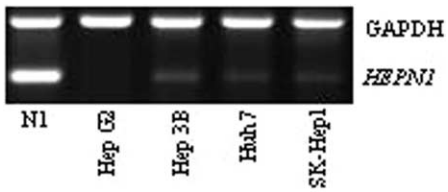

Fig. 2. Expression of *HEPN1* in four HCC cell lines. One-step RT-PCR was used to amplify *HEPN1* mRNA and GAPDH (an internal control). The expression of *HEPN1* in four HCC cell lines, HepG2, Hep3B, Huh7 and SK-Hep1, was compared to that in the non-tumorous liver tissue from patient number one (N1).

HCC patients using both RT-PCR and real-time RT-PCR. RT-PCR results (Fig. 1A) showed that *HEPN1* was ubiquitously expressed in 23 non-tumorous liver tissues, but either down-regulated or lost in 22 HCC tissues (except for sample 16), demonstrating suppression of *HEPN1* in 95.7% of 23 HCC samples tested. Real-time RT-PCR (Fig. 1B) detected a significant reduction of *HEPN1* expression in 22 of 23 HCC and the average expression level in HCC (7.2 ± 10.4) was 5.7 folds lower than that in non-tumorous liver tissues (40.8 ± 10.0), $P < 0.0001$.

Furthermore, in four HCC cell lines tested, RT-PCR showed that the expression of *HEPN1* was significantly suppressed in Hep3B, Huh7 and SK-Hep1, and completely lost in HepG2 cells as compared to a non-tumorous liver tissue (Fig. 2). However, silencing of *HEPN1* in HepG2 cells was not resulted from gene mutation as direct sequencing failed to reveal any alterations in *HEPN1* genomic DNA.

3.3. Characteristics of HEPN1

The full-length cDNA of *HEPN1* (Fig. 3A) is approximately 1.4 kb long containing an ORF of 267 base pairs. The start codon ATG, the stop codon TGA, and the Kozak sequence [12] were identified (GenBank Accession No. AY275431). Searching *HEPN1* against human EST (expressed sequence tag) databases yielded a number of aligned fragments identified mainly in the brain. The predicted HEPN1 peptide consisted of 88 amino acids with a molecular weight about 10 kDa. The peptide had no significant homology in the available databases of proteins and peptides. BLAST search against the human genome database revealed that *HEPN1* was mapped to human chromosome 11 at q24.2 (Fig. 3B); however, the promoter region remained to be identified. To localise *HEPN1* gene product in living cells, the construct expressing HEPN1-V5 fusion protein was transfected into HepG2 cells. Fluorescent microscopy showed that HEPN1 peptide was predominately distributed in the cytoplasm (Fig. 3C).

3.4. Growth suppression in HepG2 cells by HEPN1

To determine the biological role of *HEPN1*, we expressed *HEPN1* in a HEPN1-null HCC cell line, HepG2. The construct HEPN1-pcDNA was transiently transfected into HepG2 cells. Cells transfected with pcDNA3.1 vector served as control. At 48 h after transfection, cells were subjected to light microscopy, MTT assay, and real-time RT-PCR analysis. As shown in

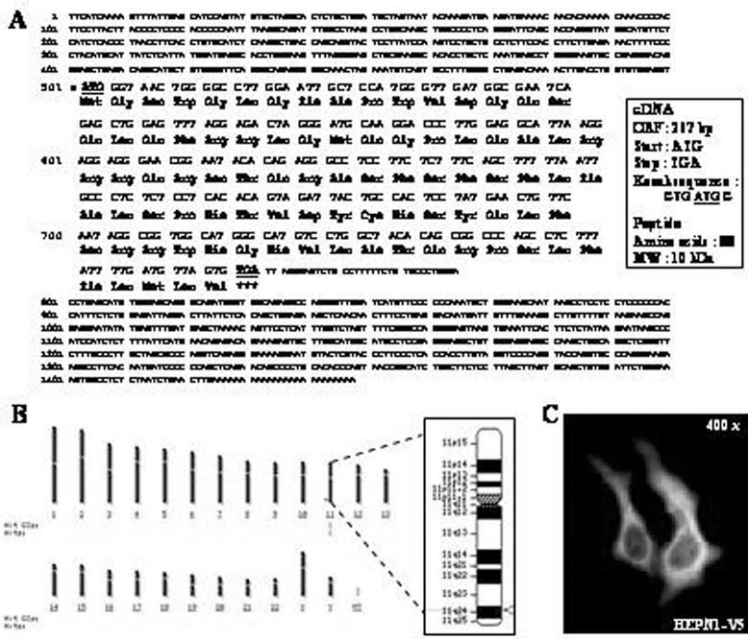

Fig. 3. Characteristics of *HEPN1*. (A) Sequences of *HEPN1* cDNA and the predicted amino acid (GenBank Accession No. AY275431). The full-length cDNA of *HEPN1* is approximately 1.4 kb long. The ORF, start codon, stop codon, and the Kozak sequence are highlighted. The predicted peptide has 88 amino acids with molecular weight about 10 kDa. (B) Localisation of *HEPN1* in human genome. *HEPN1* is mapped to chromosome 11q24.2. (C) Subcellular localisation of HEPN1 in HepG2 cells. HepG2 cells transfected with HEPN1-V5 construct. Anti-V5 immunostaining visualised that HEPN1 is predominantly distributed in the cytoplasm.

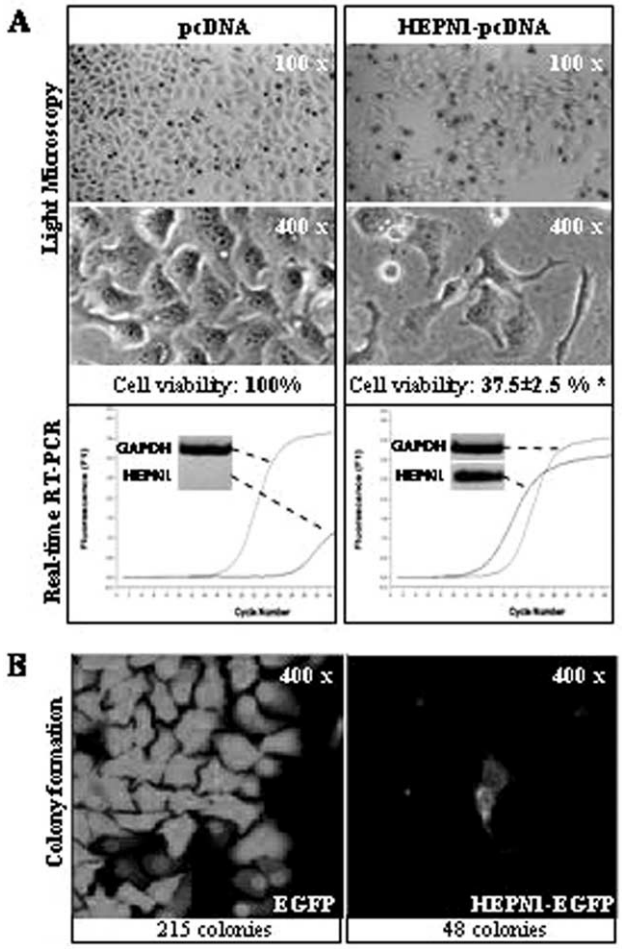

Fig. 4. Growth inhibition of HepG2 cells by *HEPN1*. (A) Transient transfection for 48 h. Light microscopic photographs demonstrate the density (100 ×) and morphology (400 ×) of HepG2 cells transfected with HEPN1-pcDNA (right) in contrast to the control, cells transfected with pcDNA3.1 vector alone (left). Cell viability (mean ± SD, $n = 12$) was detected by MTT assay and computed into percentage against the control; *$P = 0.001$. Real-time RT-PCR results show the expression level of *HEPN1* in the transfected HepG2 cells. GAPDH was used as control. The RT-PCR products were analysed by gel electrophoresis to verify the specificity. (B) Colony formation. HepG2 cells transfected with the plasmid HEPN1-EGFP (right) and pEGFP-N2 vector (left) were cultured in the presence of 800 μg/ml of G418 for 2 weeks before confocal microscopy. The density and morphology of cells in a colony were visualised by green fluorescence. The number of colonies presented at the bottom of each picture was counted manually.

Fig. 4A, re-expression of HEPN1 (real-time RT-PCR) decreased cell density, changed cell morphology (light microscopy), and reduced cell viability to 37.5 ± 2.5% ($P = 0.001$).

Colony formation was performed to confirm the inhibitory effect of *HEPN1* on cell growth. HepG2 cells transfected with HEPN1-EGFP were compared with those transfected with pEGFP-N2 vector alone. Green fluorescent protein facilitated the visualisation of cells in each colony. The results showed (Fig. 4B) that, in addition to the significant reduction of the number of colonies formed, the number of fluorescent cells in the cells transfected with HEPN1-EGFP was extremely low compared to that in the cells transfected with pEGFP-N2 vector alone.

3.5. Apoptosis induction in HepG2 cells by HEPN1

To explore if *HEPN1* could promote cell death, we transfected HepG2 cells with either HEPN1-EGFP construct or pEGFP-N2 vector alone. Between 8 and 24 h post-transfection, cells were analysed by fluorescent microscopy at every 2 h. Fig. 5 shows the cell behaviour of HepG2 cells transfected with *HEPN1* in contrast with the control cells. After transfection: (1) at hour 8, HEPN1 started being expressed predominately in cytoplasm; (2) at hour 10, the expression level was increased and concentrated in granules; (3) at hour 12, HEPN1 was distributed more in the perinuclear region; and (4) at hour 14, HEPN1 started translocating into cell nuclei; and from hour 16 onwards, typical apoptotic morphology including cytoplasm shrinking (16 h), cell blebbing (18 h), and nuclear fragmentation (20 and 22 h) was observed. At hour 24, the number of cells transfected with HEPN1-EGFP was considerably reduced compared to that at hour 12 presented in the inset. The control cells transfected with pEGFP-N2 vector alone remained unchanged throughout.

Annexin V was used to determine if cells were indeed undergoing apoptosis. Since Annexin V detects changes in the position of PS in the cell membrane, one of the earliest changes of apoptotic cells, HepG2 cells were examined at 16 h after transfection. As shown in Fig. 6, positive Annexin V-PS binding on the cell membrane was observed in cells transfected with HEPN1-pcDNA but not in the cells transfected with pcDNA3.1 vector alone.

4. Discussion

We report here the characterisation of a novel gene, *HEPN1*, and its functional significance in HepG2 cells. Gene *HEPN1*, suppressed in HCC, was identified in non-tumorous liver through the technique of subtractive hybridisation. Screening against 23 hepatocellular carcinoma patients, we found that *HEPN1* was down-regulated in 95.7% (22/23) of HCC and the average expression level was 5.7 folds lower in HCC tissues than that in non-tumorous liver tissues, suggesting that silencing of *HEPN1* is associated with carcinogenesis of hepatocytes ($P < 0.0001$). Additionally, *HEPN1* is also significantly suppressed in all the HCC cell lines tested, further implying that loss of *HEPN1* expression is of generality in HCC. However, we failed to identify any correlation between the loss of *HEPN1* expression and the events related to the development and progression of HCC, including hepatitis B viral infection, hepatitis C viral infection, liver cirrhosis, and the differentiation of HCC. This may be due to the ubiquitous downregulation of *HEPN1* in the HCC samples tested.

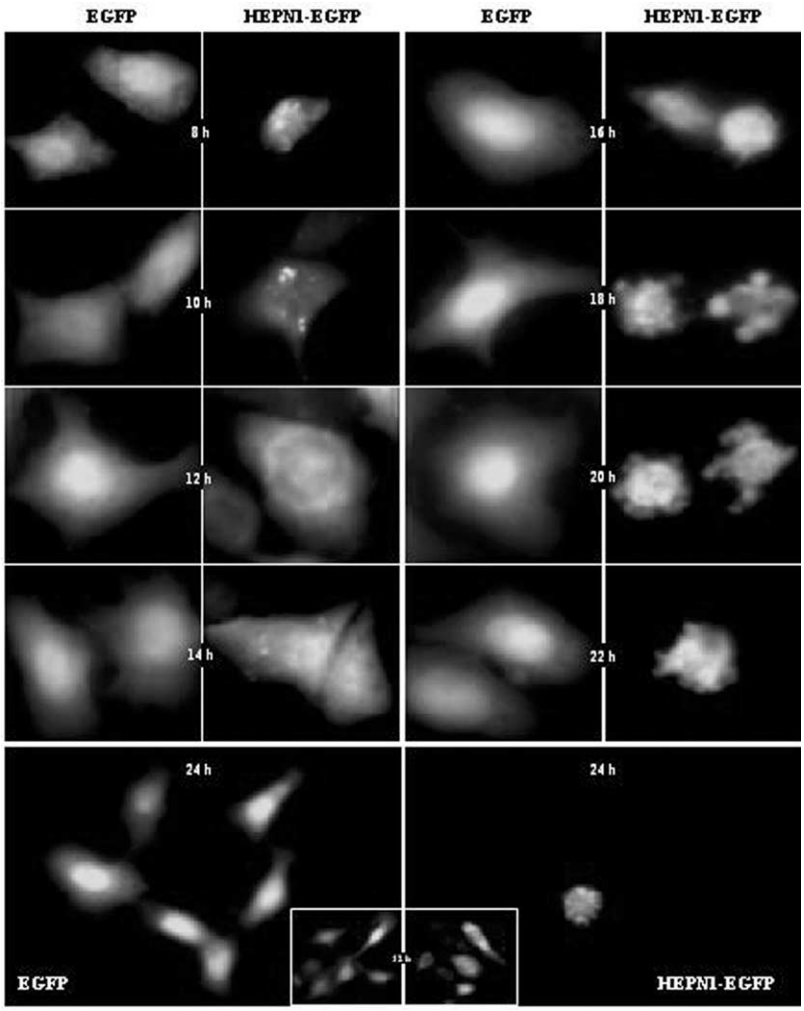

Fig. 5. Induction of apoptosis in HepG2 cells by *HEPN1*. HepG2 cells were transfected with either pEGFP-N2 vector alone (labeled as EGFP) or HEPN1-EGFP construct. Between 8 and 24 h after transfection, cells were analysed by fluorescent microscopy at every 2 h. Green fluorescence visualised cell number, cell morphology and distribution of HEPN1. Microphotographs are presented at each time point and indicated as 8, 10, 12, 14, 16, 18, 20, 22, and 24 h, respectively. An entire microscopic view at 24 h is compared to that at 12 h (inset), showing the reduction of cell number when *HEPN1* was re-expressed.

HEPN1 is mapped to the human chromosome 11q24. Abnormalities of chromosome 11q including chromosome breakage, rearrangement and loss on the long arm have been reported in a number of human tumours, such as, colorectal cancer [13], breast cancer [14], melanoma [15], acute lymphoblastic leukemia [16], and ovarian cancer [17], signifying the presence of tumour suppressor genes in this region. However, *HEPN1* does not resemble any of the tumour suppressor genes identified to date; and, moreover, no known alterations of chromosome 11q24 have been found in HCC. Therefore, the mechanisms that suppress the expression of *HEPN1* in HCC remain to be explored.

The predicted *HEPN1* product is a 10-kDa peptide (p10) consisting of 88 amino acids. The peptide neither has significant homology to any of the known proteins and peptides nor discloses substantial sequence motifs in the available databases. Unlike gene *PTEN*, whose structure provided important clues to the function of the protein when it was first discovered [18], the novelty of *HEPN1* sequence led to the difficulty of understanding its biological role.

To study its functional significance, we expressed *HEPN1* into a HEPN1-null HCC cell line, HepG2, in

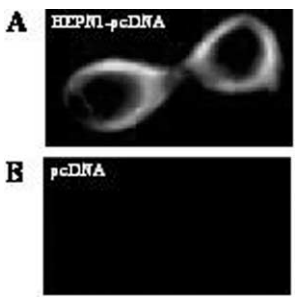

Fig. 6. Results of Annexin V assay. The fluorescent rings represent positive binding of Annexin V with PS in the cell membrane, an early indication of apoptosis. (A) HepG2 cells transfected with HEPN1-pcDNA construct; and (B) HepG2 cells transfected with the empty vector pcDNA3.1.

three phases. Firstly, transient transfection was performed on HepG2 cells. Forty-eight hours after transfection, the results showed that re-expression of HEPN1 inhibited cell growth by about 62.5 ± 2.5% ($P = 0.001$). Secondly, colony formation was performed on cells transfected with the HEPN1-pEGFP construct and the EGFP-N2 vector. The results showed that exogenous HEPN1 reduced both the number of colonies and the number of fluorescent cells, supporting that *HEPN1* is indeed capable of suppressing cell growth in HepG2 cells. Finally, time-course transfection with GFP-fused HEPN1 visualised the dynamics of the distribution of HEPN1 and cell behaviour after transfection. Together with Annexin V assay, the results showed that *HEPN1* promotes apoptosis in HepG2 cells. These data indicate that the predicted HEPN1 peptide does exhibit biological functions.

In conclusion, gene *HEPN1* is frequently silenced in hepatocellular carcinoma. *HEPN1* maps to chromosome 11q24.2; and its product, a 10-kDa peptide, is distributed predominantly in the cytoplasm. Exogenous *HEPN1* is capable of suppressing cell growth and inducing apoptosis in HepG2 cells. Our data suggest that *HEPN1* is involved in the growth control of hepatocytes; however, the mechanisms of its antiproliferative effect are to be determined.

Acknowledgements

This research project is supported by the National Medical Research Council of Singapore (Grant No.: NMRC/0598/2001). We thank Miss Asha Reka Das for her unconditional assistance wherever needed.

References

[1] Akriviadis EA, Llovet JM, Efremidis SC, Shouval D, Canelo R, Ringe B, et al. Hepatocellular carcinoma. Br J Surg 1998;85: 1319–1331.

[2] Blumberg BS, Larouze B, London WT, Werner B, Hesser JE, Millman I, et al. The relation of infection with hepatitis B agent to primary hepatic carcinoma. Am J Pathol 1975;81: 669–682.

[3] Mor E, Kaspa RT, Sheiner P, Schwartz M. Treatment of hepatocellular carcinoma associated with cirrhosis in the era of liver transplantation. Ann Intern Med 1998;129:643–653.

[4] Alpert ME, Hutt MS, Wogan GN, Davidson CS. Association between aflatoxin content of food and hepatoma frequency in Uganda. Cancer 1971;28:253–260.

[5] Montesano R, Hainaut P, Wild CP. Hepatocellular carcinoma: from gene to public health. J Natl Cancer Inst 1997;89:1844–1851.

[6] Kondoh N, Wakatsuki T, Ryo A, Hada A, Aihara T, Horiuchi S, et al. Identification and characterisation of genes associated with human hepatocellular carcinogenesis. Cancer Res 1999;59:4990–4996.

[7] Ng IO, Liang ZD, Cao L, Lee TK. DLC-1 is deleted in primary hepatocellular carcinoma and exerts inhibitory effects on the proliferation of hepatoma cell lines with deleted DLC-1. Cancer Res 2000;60:6581–6584.

[8] Zhao X, Li J, He Y, Lan F, Guo J, Zhao R, et al. A novel growth suppressor gene on chromosome 17p13.3 with a high frequency of mutation in human hepatocellular carcinoma. Cancer Res 2001;61: 7383–7387.

[9] Yamashita T, Kaneko S, Hashimoto S, Sato T, Nagai S, Toyoda N, et al. Serial analysis of gene expression in chronic hepatitis C and hepatocellular carcinoma. Biochem Biophys Res Commun 2001;282: 647–654.

[10] Ricketts SL, Garcia NF, Betz BL, Coleman WB. Identification of candidate liver tumour suppressor genes from human 11p11.2–p12. Genes Chromosomes Cancer 2002;33:47–59.

[11] Yamamoto Y, Sakamoto M, Fujii G, Kanetaka K, Asaka M, Hirohashi S. Cloning and characterisation of a novel gene, DRH1, down-regulated in advanced human hepatocellular carcinoma. Clin Cancer Res 2001;7:297–303.

[12] Kozak M. Downstream secondary structure facilitates recognition of initiator codons by eukaryotic ribosomes. Proc Natl Acad Sci 1990; 87:8301–8305.

[13] Connolly KC, Gabra H, Millwater CJ, Taylor KJ, Rabiasz GJ, Watson JE, et al. Identification of a region of frequent loss of heterozygosity at 11q24 in colorectal cancer. Cancer Res 1999;59: 2806–2809.

[14] Gentile M, Wiman A, Thorstenson S, Loman N, Borg A, Wingren S. Deletion mapping of chromosome segment 11q24–q25, exhibiting extensive allelic loss in early onset breast cancer. Int J Cancer 2001; 92:208–213.

[15] Goldberg EK, Glendening JM, Karanjawala Z, Sridhar A, Walker GJ, Hayward NK, et al. Localisation of multiple melanoma tumour-suppressor genes on chromosome 11 by use of homozygosity mapping-of-deletions analysis. Am J Hum Genet 2000;67: 417–431.

[16] Mathew S, Shurtleff SA, Raimondi SC. Novel cryptic, complex rearrangements involving ETV6-CBFA2 (TEL-AML1) genes identified by fluorescence in situ hybridisation in pediatric patients with acute lymphoblastic leukemia. Genes Chromosomes Cancer 2001;32: 188–193.

[17] Launonen V, Stenback F, Puistola U, Bloigu R, Huusko P, Kytola S, et al. Chromosome 11q22.3–q25 LOH in ovarian cancer: association with a more aggressive disease course and involved subregions. Gynecol Oncol 1998;71:299–304.

[18] Li J, Yen C, Liaw D, Podsypanina K, Bose S, Wang SI, et al. PTEN, a putative protein tyrosine phosphatase gene mutated in human brain, breast, and prostate cancer. Science 1997;275:1943–1947.

ELSEVIER

Journal of Hepatology 42 (2005) 833–841

Journal of Hepatology

www.elsevier.com/locate/jhep

Cloning and characterization of hepaCAM, a novel Ig-like cell adhesion molecule suppressed in human hepatocellular carcinoma

Mei Chung Moh, Lay Hoon Lee, Shali Shen*

Laboratory of Hepato-Oncogenetics, Department of Physiology, Faculty of Medicine, National University of Singapore, 2 Medical Drive, Singapore 117597

***Background/Aims*: Previously, we reported on gene HEPN1 that was silenced in hepatocellular carcinoma (HCC) and its capability of arresting cell growth. In this study, we identified another novel gene hepaCAM from the liver, which contains the full-length HEPN1 on its antisense strand in the 3′-noncoding region, and assessed its expression, characteristics and functions in HCC.**

***Methods*: Full-length hepaCAM cDNA was isolated by rapid amplification of cDNA ends. The gene expression was examined by semi-quantitative RT-PCR in 23 paired HCC liver specimens and 5 HCC cell lines. Transfection studies, coupled with immunocytochemistry, cellular interaction analyses, colony formation and microtetrazolium assay, were employed to elucidate the localization and functions of hepaCAM.**

***Results*: The expression of hepaCAM decreased in 20/23 of HCC samples and was undetectable in 5 HCC cell lines tested. The gene product consisting of 416 amino acids displayed the typical structure of Ig-like cell adhesion molecules. The protein was glycosylated and predominantly localized on the cytoplasmic membrane. When re-expressed in HepG2, hepaCAM accelerated cell spreading ($P < 0.001$), increased cell motility ($P = 0.0011$), reduced colony formation ($P = 0.0022$), and inhibited cell growth ($P < 0.001$).**

***Conclusions*: Gene hepaCAM, frequently silenced in HCC, encodes an Ig-like transmembrane glycoprotein and is involved in cell adhesion and growth control.**

***Keywords*: Hepatocellular carcinoma; hepaCAM; Ig-like cell adhesion molecule; Cell growth arrest; Cell–matrix interaction; HEPN1**

1. Introduction

Cell adhesion is crucial not only for the formation and maintenance of cellular architecture but also for the normal biological processes including adhesion, migration, proliferation and survival [1]. Such specialized recognition and adhesion are mediated by cell adhesion molecules (CAMs) expressed on the cell surface. Generally classified into cadherins [2,3], selectins [4], integrins [5], and immunoglobulin superfamily (IgSF) [6], these glycoproteins recognize and interact either with other cell adhesion molecules on the adjacent cell surface or with proteins deposited in the extracellular matrix. In addition to the adhesive properties of these molecules, an exciting concept that has emerged from recent cell biological research is that cell adhesion complexes are not simply static architectural entities. Rather, they are dynamic units that are critical in modulating cytoplasmic signaling cascades by capturing and integrating signals from the extracellular environment [2].

Cell organization and tissue architecture of the liver are well defined. Approximately, 80% of the adult liver consists of hepatocytes that are arranged as single-cell annastomosing plates extending from the portal region of the liver lobule towards the central vein [7]. Proper liver architecture is crucial for hepatic function [8] and is commonly disrupted in disease/injury state, including hepatitis, cirrhosis [9] and hepatocellular carcinoma [10]. Disruption of normal cell–cell adhesion in transformed cells may contribute to tumor cells' enhanced

Received 24 September 2004; received in revised form 6 January 2005; accepted 15 January 2005; available online 7 April 2005

* Corresponding author. Tel.: +65 6874 6406; fax: +65 6778 8161.
E-mail address: phsssl@nus.edu.sg (S. Shen).

0168-8278/$30.00 © 2005 European Association for the Study of the Liver. Published by Elsevier B.V. All rights reserved.
doi:10.1016/j.jhep.2005.01.025

migration and proliferation, leading to invasion and metastasis. Although the underlying mechanism of how these phenotypes are resulted remains elusive, such disruption has been related to inactivation of cadherin, or the catenin family members, and activation of signaling pathways that prevent the assembly of adherens junctions [11].

Extensive studies have shown that the disruption of cell adhesion plays a causal role in tumor progression and metastasis [12]. Alterations of several IgSF tumor suppressors have been implicated in tumor malignancies. One such intriguing Ig-containing protein is the neural cell adhesion molecule (NCAM), a cell surface sialoglycoprotein, which is involved in neural development, signal transduction and synaptic plasticity and is downregulated during tumorigenesis [13–17]. A correlation between reduced NCAM expression and poor prognosis has been reported in several cancer types, including gastrointestinal neoplasia, colorectal cancer, and pancreatic cancer [18–20]. Another IgSF adhesion protein implicated in carcinogenesis is the carcinoembryonic antigen cell adhesion molecule-1 (CEACAM1), an epithelial cell adhesion molecule, which is frequently downregulated in liver, colorectal and prostate cancers [21–24]. Consistently, ectopic restoration of its expression in colorectal and prostate carcinoma cells significantly suppressed their tumorigenicity in vitro and in vivo [24–26], suggesting that CEACAM1 functions as a tumor suppressor gene. Moreover, CEACAM1 is an angiogenic factor and an effector of vascular endothelial growth factor in endothelial cells; and has been implicated in cell invasion and metastasis [27,28].

In our previous study, examining genes associated with human hepatocellular carcinoma (HCC) by suppression subtractive hybridization, we identified a novel gene, HEPN1, frequently silenced in HCC [29]. Interestingly, an updated BLAST search revealed that an mRNA sequence in the database (GenBank AL834419), encoding a partial open reading frame (ORF) at the 5′ terminus, contained the entire antisense strand of HEPN1 in its 3′ noncoding region. This finding led us to isolate a new gene with a full-length cDNA approximately 3.2 kb. The gene encodes a putative Ig-like cell adhesion molecule with 416 amino acids, designated as hepaCAM. In this report, we demonstrate the expression, characteristics and functions of hepaCAM in hepatocellular carcinoma.

2. Materials and methods

2.1. Isolation of hepaCAM full-length cDNA

Rapid amplification of cDNA ends was performed with the Human Liver Marathon-Ready™ cDNA Kit (Clontech) according to the manufacturer's instructions. The gene-specific primer (GSP, 5′-GCTAGGCACTCTGCTGGATGCTAGTA-3′) designed at the 5′-end on the antisense strand of HEPN1 was used with the adapter primer 1 (provided) to amplify the full-length cDNA of hepaCAM. The cDNA was cloned and sequenced.

2.2. Liver specimens and cell lines

A total of 23 paired liver specimens and 6 normal liver tissues were surgically collected at the No. 3 Hospital of Chongqing in China through Dr Yang Xiaodong. The final diagnosis of HCC was confirmed and classified by histological examination. Five human HCC cell lines, HepG2, Hep3B, Huh7, SK-Hep1 and PLC-5, were maintained in the recommended conditions.

2.3. RT-PCR

Semi-quantitative RT-PCR reactions were performed with the OneStep RT-PCR kit (Qiagen) while real-time RT-PCR was performed with the LightCycler RNA Amplification Kit SYBR Green I (Roche). A forward primer (5′-TGTACAGCTGCATGGTGGAGA-3′) and a reverse primer (5′-TCTGGTTTCAGGCGGTCATCA-3′) were used to generate a hepaCAM fragment of 235 bp from 0.2 μg of DNase-treated total RNA. Beta-actin or GAPDH was included as control.

2.4. Plasmid construct

The open reading frame of hepaCAM was generated by PCR from the full-length cDNA with the forward primer 5′-GAAGCTT(*Hind*III)-CAAAATGGAGAGAGAAAGGGGAGCC-3′ and the reverse primer 5′-AGGATCC(*Bam*HI)-GGCCCAGGCGCTGATCTCCACC-3′. The PCR product was cloned into the *Hind*III/*Bam*HI restriction sites of pcDNA6/V5-His (Invitrogen). The construct, namely hepaCAM-V5, facilitated the expression of hepaCAM-V5 fusion protein and the detection by anti-V5 antibody.

2.5. Transfection

Transient transfections were carried out with Lipofectamine Plus (Invitrogen). Hep3B and HepG2 cells grown on coverslips were transfected with either hepaCAM-V5 or pcDNA6/V5-His (pcDNA6) vector for 48 h before immunocytochemistry. Stable transfections were performed on HepG2 cells. Transfected cells were selected in the presence of 10 μg/ml of blasticidin (Invitrogen) for 3 weeks and then cloned.

2.6. Immunocytochemistry

Cells cultured on coverslips were washed with PBS, fixed with 2% paraformaldehyde, and permeabilized with 0.2% Triton-X 100. Nonspecific sites were blocked in 10% normal goat serum (Santa Cruz). Protein expression of hepaCAM was detected using mouse anti-V5 antibody (Invitrogen) diluted at 1:200, biotin-conjugated goat anti-mouse IgG antibody (3 μg/ml), and subsequently streptavidin-fluorescein (15 μg/ml). Fluorescence was visualized by Fluorescence Microscope and Confocal Microscope LSM 510 (Carl Zeiss).

2.7. Western analysis

Total protein (50 μg) from HepG2 or liver tissue was resolved by SDS-PAGE, transblotted onto membrane, and detected by either rabbit anti-hepaCAM polyclonal antibody (generated following the procedure described in the Current Protocol) or mouse anti-V5 monoclonal antibody. The membranes were stripped and reprobed with mouse anti-GAPDH antibody (Chemicon) to assess loading quantity.

2.8. Deglycosylation

Cell lysate was deglycosylated with peptide *N*-glycosidase F (PNGase F) (New England Biolabs) according to the manufacturer's instructions. Equal amount of cell lysate without PNGase F treatment served as control. These samples were then subjected to western analysis.

2.9. Cell spreading

Cells were seeded in plates coated with 10 μg/ml-fibronectin (Santa Cruz) and incubated under standard conditions. Cell morphology was observed by microscopy (Carl Zeiss). Unspread cells were defined as round cells, while spread cells were defined as cells with extended processes [30]. The percentage of cells demonstrating spread morphology was quantified in 10 randomly selected fields (>60 cells/field).

2.10. Matrigel invasion assay

Cell migration was assessed using the transwell chambers with 8-μm pore size membranes coated with matrigel (BD Biosciences) in 24-well plates. Cells (5×10^4) were loaded into the upper volume of the chambers and allowed to migrate through the membrane for 24 h. Non-migrated cells were removed with a cotton swab, and the migrated cells were harvested by trypsinizing the lower surface of the membrane and collected into new 24-well plate. The migration activity was quantified by blind counting of the migrated cells in 10 randomly selected microscopic fields (>40 cells/field).

2.11. Wound closure assay

Cell motility was also assessed by the wound healing experiment on monolayer cells. Cells were seeded in 35-mm culture plates at high density and allowed to form monolayers overnight. Wounds were made by pipette tip on confluent cells and allowed to be healed by cell migration for 24 h. The changes in diameter (D) of each wound were measured by microscopy and computed into ratio ($D_{24\ h}/D_{initial}\times100\%$) to represent wound closure.

2.12. Colony formation

HepG2 cells transfected with either hepaCAM-V5 or vector pcDNA6 were selected in 10 μg/ml of blasticidin (Invitrogen) for 3 weeks without trypsinization while medium was refreshed every 2 days. The cell colonies formed at the end of experiment were visible, and the size and thickness of the colonies were analyzed by microscopy. The number of colonies was counted in 10 randomly selected fields.

2.13. Growth curve

The growth rate of HepG2 stable cell lines were monitored for 5 days. Cells were seeded in triplicates and cultured under standard conditions. At every 24 h, cell viability was determined by MTT assay. The growth rate of each cell line was presented as folds of increase in cell viability against the respective base line obtained on the day of seeding cells.

2.14. Bioinformatics and statistical analysis

Sequence analyses were carried out through database searches (facilitated by the NCBI, Ensembl and ExPASy). Mann–Whitney test was performed to compare two means of samples with small sample size ($n=6$). Fisher's exact test was used to assess the correlation between two parameters. Nonparametric ANOVA was performed to compare the differences between more than two means. Software InStat 3.0 (GraphPad) was employed and $P<0.05$ was considered as significant.

3. Results

3.1. Identification of hepaCAM

As illustrated in Fig. 1, the cDNA sequence AL834419 (GenBank) containing the antisense strand of HEPN1 in its 3′-noncoding region was deficient in the 5′-noncoding region. The gene specific primer (GSP) at the 5′-end of HEPN1 antisense strand and the adaptor primer (AP1) enabled us to isolate a new gene, hepaCAM, from a human normal liver cDNA library. Gene hepaCAM was mapped to human chromosome 11q24 and its genomic DNA sequence contained 7 exons ranging in sizes from 71 to 2252 bp. The full-length cDNA sequence of hepaCAM (3244 bp) has been submitted to the GenBank (AY047587).

3.2. Suppression of hepaCAM in HCC

Semi-quantitative RT-PCR revealed that hepaCAM was expressed at a similar level in all the normal liver tissues tested (Fig. 2A). To evaluate if hepaCAM expression was downregulated in HCC, we examined hepaCAM mRNA levels in 23 paired liver samples from HCC patients using a pair of hepaCAM specific primers that were not associated with the HEPN1 sequence. The results showed that hepaCAM was reduced in 87% (20/23) of HCC tissues (Fig. 2B). The expression of hepaCAM was not detectable when evaluated in 5 human HCC cell lines HepG2, Hep3B,

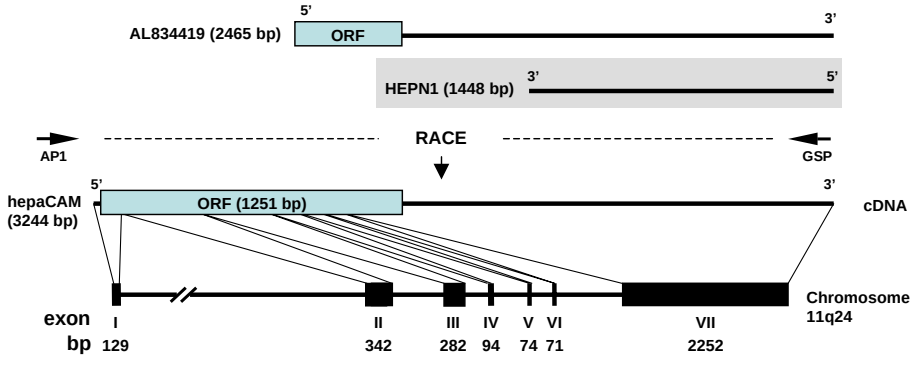

Fig. 1. Molecular cloning of hepaCAM. (A) Reconstitution scheme of hepaCAM. The full-length cDNA of hepaCAM was isolated from normal human liver cDNA library by RACE. A forward primer on the adaptor (AP1) and a gene specific primer (GSP, the reverse primer) at the 5′-end of HEPN1 antisense strand were used in the RACE reaction. The cDNA lengths of hepaCAM, HEPN1 and sequence AL834419 are given in the brackets. The indications of 5′ and 3′ correspond to the orientations of the cDNAs. The genomic DNA of hepaCAM mapped to human chromosome 11q24 contains 7 exons indicated as I–VII and accompanied by their respective length in base pairs (bp). [This figure appears in colour on the web.]

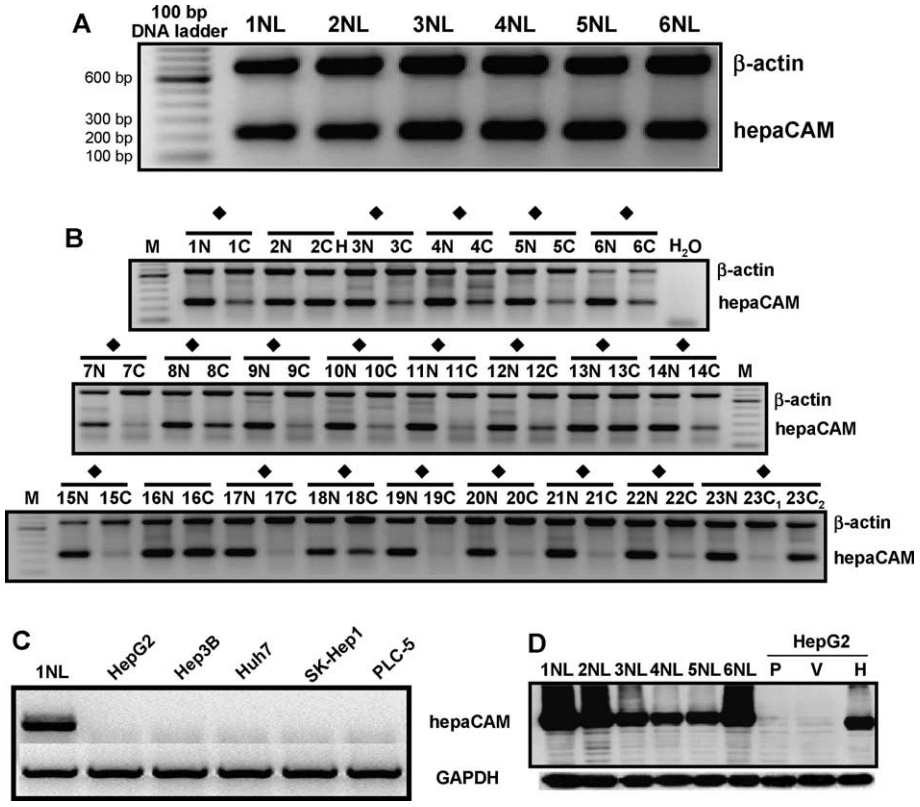

Fig. 2. Expression of hepaCAM in liver specimens and HCC cell lines. (A) Expression of hepaCAM in normal liver tissues. Semi-quantitative RT-PCR was performed to determine the mRNA expression of hepaCAM in 6 normal liver tissues obtained from 6 individuals. Two pairs of gene specific primers were included in one RT-PCR reaction to generate the fragments of genes β-actin (720 bp, as the internal control) and hepaCAM (235 bp), respectively. The samples are labeled from 1 to 6; NL, normal liver. (B) Expression of hepaCAM in 23 HCC patients. Semi-quantitative RT-PCR products were analyzed by gel electrophoresis. ♦, samples that show clear differences in hepaCAM expression; N, non-tumor liver tissue; C, HCC liver tissue; β-actin, internal control. Patient 23 had two HCC nodules (C_1 and C_2) in the liver. (C) Expression of hepaCAM in five hepatic cell lines. Semi-quantitative RT-PCR was used to amplify hepaCAM mRNA and GAPDH mRNA (internal control). The expression level of hepaCAM in 5 HCC cell lines, HepG2, Hep3B, Huh7, SK-Hep1 and PLC-5, was compared to that in the normal liver tissue 1NL. (D) Protein levels of hepaCAM in normal liver tissues and HepG2 cells. Western analysis with rabbit anti-hepaCAM polyclonal antibody revealed the endogenous hepaCAM protein levels in 6 normal liver tissues and the exogenous protein in hepaCAM-transfected HepG2 cells (H). No hepaCAM protein was detectable in both the parental (P) and the vector-transfected (V) HepG2 cells. GAPDH protein level indicates the loading quantity.

Huh7, SK-Hep1 and PLC-5 (Fig. 2C). Furthermore, western analysis with anti-hepaCAM polyclonal antibody confirmed the protein expression of hepaCAM in all the normal liver tissues, as well as in HepG2 cells transfected with hepaCAM, but neither in the parental HepG2 cells nor in the cells transfected with vector alone (Fig. 2D). These data implied the association between the loss of hepaCAM and hepatocarcinogenesis. No correlations between hepaCAM and the clinicopathologic parameters could be detected. This could be due to the high rate of hepaCAM suppression in the HCC samples tested (Table 1).

3.3. Characterization of hepaCAM protein sequence

Gene hepaCAM encoded a 46-kDa protein of 416 amino acids consisting of an extracellular region, a transmembrane segment, and a cytoplasmic tail (Fig. 3A). The extracellular region comprised a signal

Table 1
Correlation between hepaCAM suppression and the clinicopathologic parameters in 23 HCC patients

Parameters	hepaCAM suppression	Unchanged hepaCAM	Suppression rate (%)	*P*
Total number	20	3	87	
Sex				
Male	16	2	89	NS
Female	4	1	80	NS
Grade				
Well	3	0	100	NS
Moderate	12	2	86	NS
Poor	5	1	83	NS
Cirrhosis	16	3	84	NS
Hepatitis virus				
HBV	18	2	90	NS
HCV	3	0	100	NS
HBV + HCV	2	0	100	NS

Grade, histological differentiation of HCC; NS, not significant; *P* was revealed by the Fisher's exact test.

peptide and 2 Ig domains (Ig-like and C2 domains) as predicted by SignalP [31] and SMART [32], respectively. Two cysteine residues flanking the C2 domain contributed to the formation of intrachain disulfide-linked loop. Six *N*-glycosylation sites were identified in the extracellular region, which may contribute to the glycosylation of hepaCAM protein. The transmembrane segment was found to contain a prokaryotic membrane lipoprotein lipid attachment site (LLVTLVTVCAC). At the cytoplasmic tail, two potential class III PDZ domain-binding motifs were predicted. Overall, the structure of hepaCAM closely resembles Ig-like cell adhesion molecules.

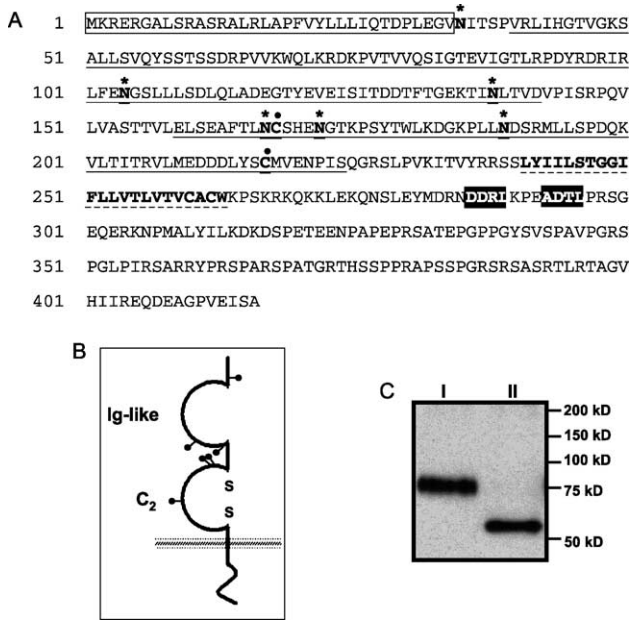

Fig. 3. The characteristics of hepaCAM protein sequence. (A) Predicted amino acid sequence of human hepaCAM. The fragment highlighted in the box is the putative signal peptide (34 amino acids). The regions underlined with solid lines are the two immunoglobulin-like (Ig-like) domains (103 and 66 amino acids, respectively) while the one underlined with dashed line is the transmembrane domain (23 amino acids). Two cysteine residues (marked underneath the '●') are identified in the second Ig-like domain, which may be needed for the formation of the disulfide bond in the domain. Six asparagines (marked underneath the '*') are in the extracellular region, which represent the potential *N*-linked glycosylation sites. The class III PDZ domain binding motifs (in the inverted shades) are present in the cytoplasmic region. (B) Illustration of the secondary structure of hepaCAM protein. hepaCAM owns the typical structure of proteins in the immunoglobulin superfamily, including an extracellular segment consisting of an *N*-terminal-proximal Ig-like domain and a membrane-proximal C_2-type Ig-domain with a disulfide bond formed between two cysteine residues (S S), a transmembrane region, and a cytoplasmic tail. The six putative *N*-linked glycosylation sites are indicated by the signs of '🍴'. (C) Deglycosylation of hepaCAM. HepG2 cells transfected with hepaCAM were lysed and treated with (lane II) or without (lane I) peptide *N*-glycosidase F. The cell lysates were resolved by SDS-PAGE and subjected to western blotting with anti-V5 antibody.

3.4. Deglycosylation of hepaCAM protein

The molecular weight of the epitope-tagged hepaCAM shown by western analysis was approximately 75 kDa, larger than the predicted size (46 kDa). The six *N*-glycosylation sites identified on hepaCAM protein within the extracellular region (Fig. 3B) implied that hepaCAM protein might be glycosylated. The cleavage of *N*-linked glycans on hepaCAM by PNGase F indeed shifted the molecular weight from 75 to 60 kDa (Fig. 3C), indicating hepaCAM a glycoprotein. Noticeably, the molecular weight of the deglycosylated protein was still higher than the predicted one, suggesting the involvement of additional post-translational modifications.

3.5. Cellular localization of hepaCAM

Two hepatic cell lines Hep3B and HepG2, in which hepaCAM was undetectable (Fig. 2C), were transiently transfected with hepaCAM-V5. Immunofluorescence staining with anti-V5 antibody showed that hepaCAM was scattered in the cytoplasm, absent in the nucleus and predominantly localized on the plasma membrane of both Hep3B and HepG2 cells (Fig. 4A). Interestingly, the cellular localization of hepaCAM appeared to be cell density-dependent in HepG2 with stable transfection. In well-spread cells (Fig. 4B upper), hepaCAM was distributed in the cytoplasm and at the cell surface protrusions that were about to make cell contacts. In confluent cells (Fig. 4B lower), hepaCAM was predominantly localized on the cytoplasmic membrane, particularly in the areas of cell–cell contacts.

3.6. Evaluation of stable transfection

Two clones stably transfected with vector (V1 and V2) and 3 clones with hepaCAM-V5 (H1, H2 and H3) were screened. Western analysis showed that hepaCAM was absent in the vector clones V1 and V2, and expressed in 2 (among 3) hepaCAM clones H1 and H3 (Fig. 5A). Real-time RT-PCR showed that hepaCAM was expressed in clones H1 and H3 but not overexpressed when compared to the normal liver tissues, and was expectedly absent in clones V1, V2 and H2 (Fig. 5B). Immunofluorescence staining and confocal microscopy confirmed the establishment of cell clones (Fig. 5C). Clones V1, V2, H1 and H3 were therefore selected for the downstream functional exploration of hepaCAM.

3.7. Cell–matrix interaction and cell motility modulated by hepaCAM

As hepaCAM displayed the typical structure of cell adhesion molecules, we evaluated the adhesive properties of hepaCAM on the stable HepG2 clones through cell aggregation and spreading assays. Although hepaCAM did not clearly change cell aggregation (data not shown), it was

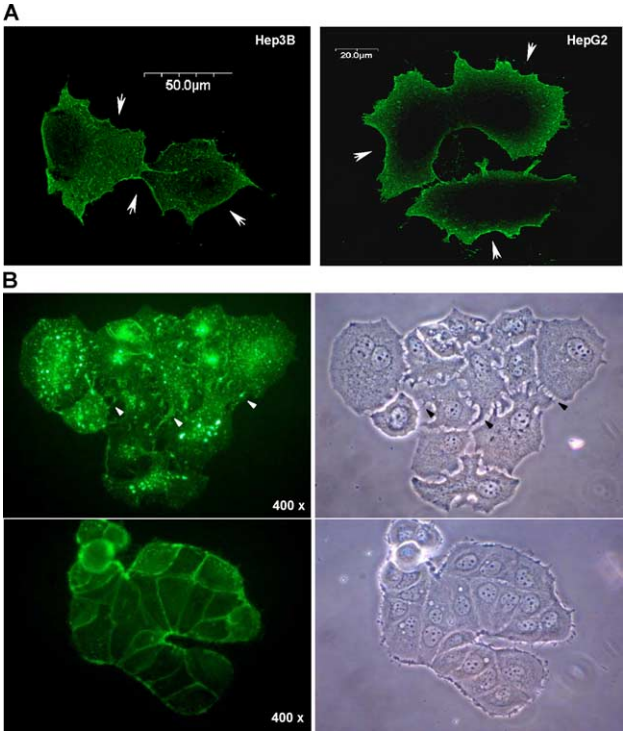

Fig. 4. Cellular localization of hepaCAM. (A) Through transient transfection and immunocytochemistry, hepaCAM protein was localized in 2 HCC cell lines. Fused with V5 in vector pcDNA6/V5-His, hepaCAM was transfected into Hep3B and HepG2 cells. Anti-V5 antibody was used for immunostaining to detect the expression and localization of hepaCAM. Confocal microscopy revealed that hepaCAM was scattered in the cytoplasm and predominantly localized on the cell membrane (arrows). (B) The localization of hepaCAM in HepG2 cells with stable transfection was cell density-dependent. Upper panel, well-spread cells with surface protrusions (arrow heads); lower panel, confluent cells with clear cell-cell contacts. [This figure appears in colour on the web.]

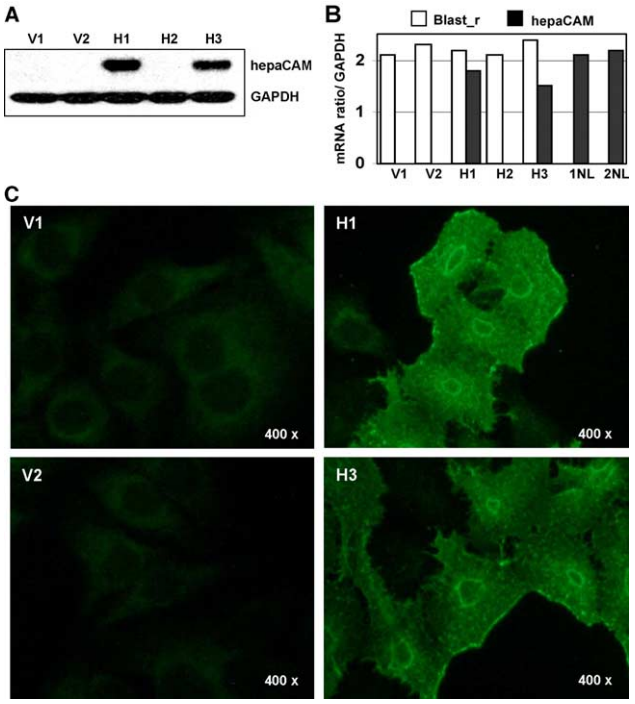

Fig. 5. Stable transfection of hepaCAM in HepG2. HepG2 cells stably transfected with vector or hepaCAM-V5 construct were cloned. (A) Western analysis. Anti-V5 antibody was used in the western analysis to evaluate the protein levels of hepaCAM in two clones transfected with vector alone (V1 and V2) and three clones transfected with hepaCAM-V5 (H1, H2, and H3). The membrane was stripped and reprobed with anti-GAPDH antibody for loading control. (B) Real-time RT-PCR analysis. The mRNA levels of blasticidin resistant gene (Blast_r) and hepaCAM were determined in all the clones and two normal liver tissues (1NL and 2NL), and converted into ratio against GAPDH mRNA levels. (C) Confocal microscopy. Immunofluorescence staining through anti-V5 antibody was used to visualize hepaCAM protein in both cells from the control clones V1 and V2 and cells from the clones expressing hepaCAM (H1 and H3). 400×, magnification. [This figure appears in colour on the web.]

capable of modulating cell–matrix adhesion significantly (Fig. 6A). About 50% and 90% of the cells from both clones H1 and H3 exhibited spread morphology at 30 min and 2 h of incubation, respectively (Fig. 6B). In contrast, the majorities of the cells from clones V1 and V2 remained round at the same time points. The number of cells showing spread morphology from clones H1 and H3 was about 5 folds higher than that from the control clones V1 and V2 ($P<0.001$). Furthermore, HepG2 cell motility was increased ($P=0.0011$) when transfected with hepaCAM as determined by matrigel invasion (Fig. 7A) and wound healing assays in culture dish (Fig. 7B). These results indicate that hepaCAM may be involved in cell and extracellular matrix interactions.

3.8. Antiproliferative effect of hepaCAM

Many Ig-like adhesion molecules, such as NCAM-1 [14], TSLC-1 [33], and OPCML [34], are known as tumor suppressors exhibiting antiproliferative effects. To examine the involvement of hepaCAM in cell growth control, colony formation was carried out while growth rate was determined in stable HepG2 clones. The results showed that the number of colonies was reduced by 10 folds in the cells transfected with hepaCAM ($P=0.0022$, Fig. 8A), and the growth rate was decreased by 14 folds ($P<0.001$, on day 5, Fig. 8B) in cells expressing hepaCAM (H1 and H3). No clear cell death was observed in the course of examining growth arrest, suggesting that hepaCAM inhibits cell growth through suppressing proliferation rather than inducing apoptosis.

4. Discussion

We have identified hepaCAM as a new Ig-like adhesion molecule. The novel protein displays the typical structure of the adhesion molecules in immunoglobulin superfamily (IgSF), including two extracellular Ig-like domains, a single transmembrane region, and a cytoplasmic tail [6].

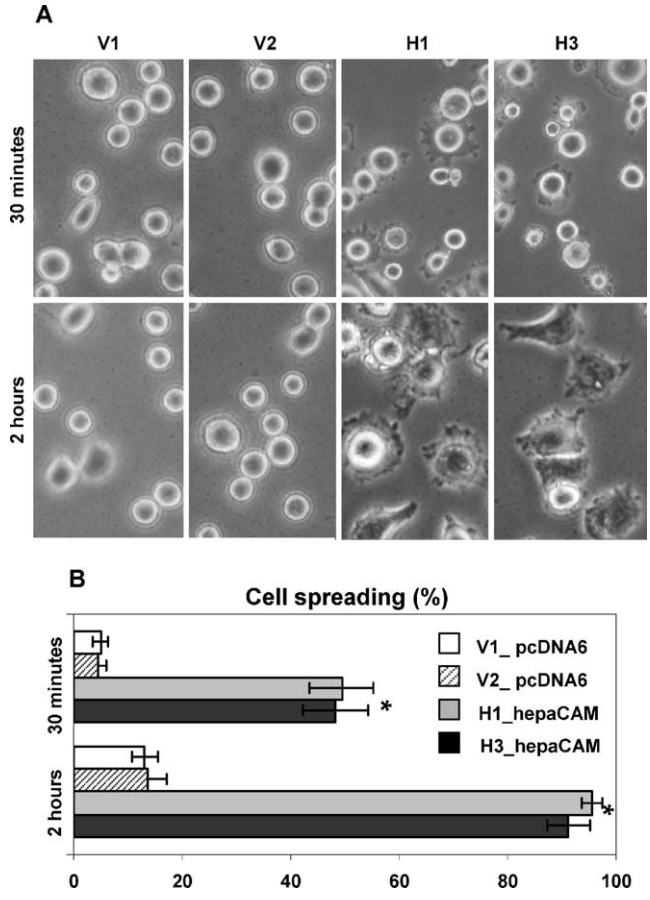

Fig. 6. Modulation of cell-matrix adhesion by hepaCAM. (A) Cell morphology. HepG2 clones transfected with vector alone (V1 and V2) and expressing hepaCAM-V5 (H1 and H3) were allowed to spread on fibronectin-coated plates for 30 min or 2 h. The microscopic photos were taken under 200×-magnification. (B) The percentage of cell spreading. At 30 min or 2 h after plating, total number of cells and cells showing spread morphology were counted in ten randomly selected fields (>60 cells per field), and the percentage of cell spreading was then computed. The data represent means±SD ($n=6$), *$P<0.001$ as assessed by ANOVA.

The structure of hepaCAM is similar to that of adhesion molecules JAMs, CAR, and ESAM, which are known to be involved in cellular interactions. Experimentally, we have demonstrated that hepaCAM protein is glycosylated and predominantly localized on plasma membrane, particularly in the areas of cell–cell contacts when cells are confluent. Such distribution is also shown with JAMs, CAR, and ESAM. Moreover, revealed by cell spreading and motility assays, hepaCAM is capable of modulating cell–matrix interactions, further supporting hepaCAM to be an adhesion molecule.

Intriguingly, our data suggest that hepaCAM may be a tumor suppressor in human hepatocellular carcinoma. Firstly, we show that hepaCAM is expressed in all normal and non-tumorous liver tissues, but suppressed in 87% (20/23) of HCC patients and 100% (5/5) of HCC cell lines, i.e. when hepatocytes have become cancerous, indicating that loss of hepaCAM expression is associated

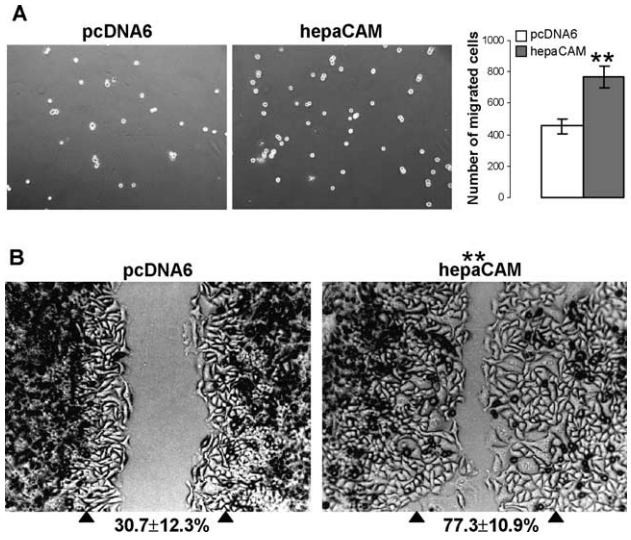

Fig. 7. Modulation of cell motility by hepaCAM. (A) Matrigel invasion assay. Cell migration was examined by using the transwell chambers with 8-μm pore size membranes coated with matrigel. HepG2 cells stably transfected with either pcDNA6 vector or hepaCAM-V5 were allowed to migrate through the membrane for 24 h. The migrated cells were harvested into new 24-well plate and viewed by microscopy (100×). The migration was quantified by blind counting of the migrated cells in 10 randomly selected fields and represented as mean±SD ($n=6$) by the bar graph. (B) In vitro wound healing assay. Wounds were made by pipette tip on confluent HepG2 cells stably transfected with either pcDNA6 vector alone (left) or hepaCAM-V5 (right) and allowed to be healed by cell migration for 24 h. The diameters of wounds were measured by microscopy (200×) at 0 h and 24 h after wounding. Arrow heads show the diameters of the initial wounds. Changes in diameter were computed into ratio (means±SD%, $n=6$) to represent wound closure. ** $P=0.0011$ as assessed by Mann–Whitney test.

with hepatocarcinogenesis. Secondly, the accelerated cell–-matrix adhesion mediated by hepaCAM raises the possibility that loss of hepaCAM may ultimately lead to the disruption of liver tissue architecture by the loss of a tumor cell's ability to communicate with its extracellular environment. Thirdly, transfection studies revealed that hepaCAM reduced cell colony formation and inhibited cell growth in HCC cell line HepG2 through suppression of cell proliferation. The frequent loss of hepaCAM expression in HCC together with the antiproliferative effect of hepaCAM meets the most important criteria widely used to define tumor suppressor.

In addition, hepaCAM is mapped to the human chromosome 11q24. Molecular genetic and cytogenetic studies have indicated that the long arm of chromosome 11 is one of the most common targets for chromosomal aberrations during the progression of human malignancies. Tumor suppressor genes encoding cell adhesion molecules of the Ig superfamily have been identified on 11q22-qter. An Ig-like adhesion molecule TSLC1 is a tumor suppressor at 11q23 and its expression through promoter hypermethylation has been reported in the development of many human cancers such as cancers of the lung, cervix, breast and prostate [35]. However, no studies have reported

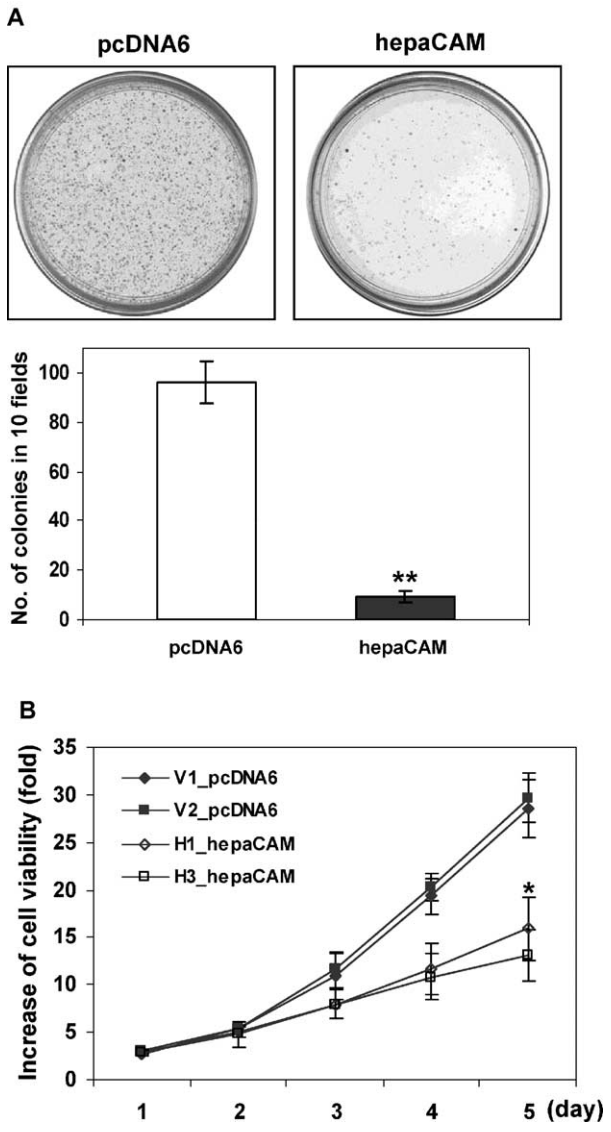

Fig. 8. Inhibition of cell growth by hepaCAM. (A) Colony formation. HepG2 cells transfected with vector (pcDNA6) or hepaCAM-V5 construct (hepaCAM) were selected with blasticidin for 3 weeks. The cell colonies formed at the end of the experiments were visible (upper panel) and the size and the thickness of the colonies were observed by microscopy. The number of colonies was counted in 10 randomly selected fields and represented by the bar graph (means ± SD, $n = 6$), $^{**}P = 0.0022$ as assessed by Mann–Whitney test. (B) Cell growth curve. The growth rate of the cells from clones H1 and H3 (stably transfected with hepaCAM-V5) was compared to that of the cells from V1 and V2 (stably transfected with vector alone) for 5 days by microtetrazolium (MTT) assay. Data represent means ± SD ($n = 6$), $^{*}P < 0.001$ (on day 5) as assessed by ANOVA.

the loss of heterozygosity (LOH) of chromosome 11q in HCC and the mode of hepaCAM gene silencing is yet to be understood.

In conclusion, we have identified a novel gene hepaCAM that encodes an Ig-like cell adhesion molecule. Gene hepaCAM is found frequently silenced in human hepatocellular carcinoma and the gene product is shown to be a transmembrane glycoprotein. When re-expressed in HepG2, hepaCAM is capable of mediating cell-matrix adhesion and cell motility, and exhibits antiproliferative effect. This study suggests that hepaCAM is a new Ig-like cell adhesion molecule which may play roles in cell–matrix interaction and cell growth regulation.

Acknowledgements

The study was supported by the National Medical Research Council (NMRC/0598/2001) and the Biomedical Research Council (Project No. 01/1/21/19/162) of Singapore. We thank Miss Asha Reka Das for her assistance whenever and wherever needed.

References

[1] Edelman GM. Cell adhesion molecules in the regulation of animal form and tissue pattern. Annu Rev Cell Biol 1986;2:81–116.
[2] Rosales C, O'Brien V, Kornberg L, Juliano R. Signal transduction by cell adhesion receptors. Biochim Biophys Acta 1995;1242:77–98.
[3] Wesseling J, van der Valk SW, Hilkens J. A mechanism for inhibition of E-cadherin-mediated cell–cell adhesion by the membrane-associated mucin episialin/MUC1. Mol Biol Cell 1996;7:565–577.
[4] Tedder TF, Steeber DA, Pizcueta P. L-selectin-deficient mice have impaired leukocyte recruitment into inflammatory sites. J Exp Med 1995;181:2259–2264.
[5] Hynes RO. Targeted mutations in cell adhesion genes: what have we learned from them? Dev Biol 1996;180:402–412.
[6] Williams AF, Barclay AN. The immunoglobulin superfamily—domains for cell surface recognition. Annu Rev Immunol 1998;6:381–405.
[7] Ross M, Kaye GI, Pawlina W. Digestive System III: Liver, Gallbladder, and Pancreas. In: Histology: a text and atlas. 532. Baltimore: Lippincott Williams and Wilkins; 2002 p. 532–47.
[8] Kmiec Z. Cooperation of liver cells in health and disease. Adv Anat Embryol Cell Biol 2001;161:1–151.
[9] Sherlock S, Dooley J. Hepatic cirrhosis. In: Diseases of liver and biliary system. Oxford: Blackwell Science; 1997 p. 371–82.
[10] Yoshidome S, Tanabe G, Yoshida A, Ueno S, Hamanoue M, Mitue S, et al. Risk prediction using histology of noncancerous liver before hepatic resection for hepatocellular carcinoma. Hepatogastroenterology 2001;48:518–522.
[11] Ben-Ze'ev A, Geiger B. Differential molecular interactions of β-catenin and plakoglobin in adhesion, signaling and cancer. Curr Opin Cell Biol 1998;10:629–639.
[12] Hirohasi S. Inactivation of the E-Cadherin-mediated cell adhesion system in human cancers. Am J Pathol 1998;153:333–339.
[13] Williams EJ, Furness J, Walsh FS, Doherty P. Characterisation of the second messenger pathway underlying neurite outgrowth stimulated by FGF. Development 1994;120:1685–1693.
[14] Krushel LA, Tai MH, Cunningham BA, Edelman GM, Crossin KL. Neural cell adhesion molecule (N-CAM) domains and intracellular signaling pathways involved in the inhibition of astrocyte proliferation. Proc Natl Acad Sci USA 1998;95:2592–2596.
[15] Beggs HE, Soriano P, Maness PF. NCAM-dependent neurite outgrowth is inhibited in neurons from Fyn-minus mice. J Cell Biol 1994;127:825–833.
[16] Beggs HE, Baragona SC, Hemperly JJ, Maness PF. NCAM140 interacts with the focal adhesion kinase p125(fak) and the SRC-related tyrosine kinase p59(fyn). J Biol Chem 1997;272:8310–8319.

[17] Ronn LC, Berezin V, Bock E. The neural cell adhesion molecule in synaptic plasticity and ageing. Int J Dev Neurosci 2000;18:193–199.
[18] Fogar P, Basso D, Pasquali C, De Paoli M, Sperti C, Roveroni G, et al. Neural cell adhesion molecule (N-CAM) in gastrointestinal neoplasias. Anticancer Res 1997;17:1227–1230.
[19] Roesler J, Srivatsan E, Moatamed F, Peters J, Livingston EH. Tumor suppressor activity of neural cell adhesion molecule in colon carcinoma. Am J Surg 1997;174:251–257.
[20] Tezel E, Kawase Y, Takeda S, Oshima K, Nakao A. Expression of neural cell adhesion molecule in pancreatic cancer. Pancreas 2001;22: 122–125.
[21] Tanaka K, Hinoda Y, Takahashi H, Sakamoto H, Nakajima Y, Imai K. Decreased expression of biliary glycoprotein in hepatocellular carcinomas. Int J Cancer 1997;74:15–19.
[22] Kleinerman DI, Troncoso P, Lin SH, Pisters LL, Sherwood ER, Brooks T, et al. Consistent expression of an epithelial cell adhesion molecule (C-CAM) during human prostate development and loss of expression in prostate cancer: implication as a tumor suppressor gene. Cancer Res 1995;55:1215–1220.
[23] Neumaier M, Paululat S, Chan A, Matthaes P, Wagener C. Biliary glycoprotein, a potential human cell adhesion molecule, is down-regulated in colorectal carcinomas. Proc Natl Acad Sci USA 1993;90: 10744–10748.
[24] Hsieh JT, Luo W, Song W, Wang Y, Kleinerman DI, Van NT, et al. Tumor suppressive role of an androgen-regulated epithelial cell adhesion molecule (C-CAM) in prostate carcinoma cell revealed by sense and antisense approaches. Cancer Res 1995;55:190–197.
[25] Hsieh JT, Earley K, Pong RC, Wang Y, Van NT, Lin SH. Structural analysis of the C-CAM1 molecule for its tumor suppression function in human prostate cancer. Prostate 1999;41:31–38.
[26] Kunath T, Ordonez-garcia C, Turbide C, Beauchemin N. Inhibition of colonic tumor cell growth by biliary glycoprotein. Oncogene 1995;11: 2375–2382.
[27] Ergun S, Kilik N, Ziegeler G, Hansen A, Nollau P, Gotze J, et al. CEA-related cell adhesion molecule 1: a potent angiogenic factor and a major effector of vascular endothelial growth factor. Mol Cell 2000; 5:311–320.
[28] Brummer J, Ebrahimnejad A, Flayeh R, Schumacher U, Loning T, Bamberger AM, et al. cis Interaction of the cell adhesion molecule CEACAM1 with integrin beta(3). Am J Pathol 2001;159:537–546.
[29] Moh MC, Lee LH, Yang X, Shen S. HEPN1, a novel gene that is frequently down-regulated in hepatocellular carcinoma, suppresses cell growth and induces apoptosis in HepG2 cells. J Hepatol 2003;39: 580–586.
[30] Richardson A, Malik RK, Hildebrand JD, Parsons JT. Inhibition of cell spreading by expression of the C-terminal domain of focal adhesion kinase (FAK) is rescued by coexpression of Src or catalytically inactive FAK: a role for paxillin tyrosine phosphorylation. Mol Cell Biol 1997;17:6906–6914.
[31] Nielsen H, Engelbrecht J, Brunak S, von Heijne G. Identification of prokaryotic and eukaryotic signal peptides and prediction of their cleavage sites. Protein Eng 1997;10:1–6.
[32] Letunic I, Goodstadt L, Dickens NJ, Doerks T, Schultz J, Mott R, et al. Recent improvements to the SMART domain-based sequence annotation resource. Nucleic Acids Res 2002;30:242–244.
[33] Masuda M, Yageta M, Fukuhara H, Kuramochi M, Maruyama T, Nomoto A, et al. The tumor suppressor protein TSLC1 is involved in cell–cell adhesion. J Biol Chem 2002;277:31014–31019.
[34] Sellar GC, Watt KP, Rabiasz GJ, Stronach EA, Li L, Miller EP, et al. OPCML at 11q25 is epigenetically inactivated and has tumor-suppressor function in epithelial ovarian cancer. Nat Genet 2003;34: 337–343.
[35] Pletcher MT, Nobukuni T, Fukuhara H, Kuramochi M, Maruyama T, Sekiya T, et al. Identification of tumor suppressor candidate genes by physical and sequence mapping of the TSLC1 region of human chromosome 11q23. Gene 2001;273:181–189.

THE JOURNAL OF BIOLOGICAL CHEMISTRY
Vol. 280, No. 29, Issue of July 22, pp. 27366–27374, 2005

Printed in U.S.A.

Structural and Functional Analyses of a Novel Ig-like Cell Adhesion Molecule, hepaCAM, in the Human Breast Carcinoma MCF7 Cells*

Received for publication, January 24, 2005, and in revised form, May 24, 2005
Published, JBC Papers in Press, May 25, 2005, DOI 10.1074/jbc.M500852200

Mei Chung Moh‡, Chunli Zhang‡, Chunli Luo§, Lay Hoon Lee‡, and Shali Shen‡¶

From the ‡Department of Physiology, Faculty of Medicine, National University of Singapore, 2 Medical Drive, Singapore 117597, Republic of Singapore and §Department of Laboratory Diagnosis, Chongqing Medical University, Chongqing 400016, China

We have recently identified a novel gene, *hepaCAM*, in liver that encodes a cell adhesion molecule of the immunoglobulin superfamily. In this study, we examined the characteristics of hepaCAM protein and the relationship between its structure and function, in particular its adhesive properties. The wild-type and the cytoplasmic domain-truncated mutants of *hepaCAM* were transfected into the human breast carcinoma MCF7 cells, and the physiological and biological properties were assessed. Biochemical analyses revealed that hepaCAM is an *N*-linked glycoprotein phosphorylated in the cytoplasmic domain and that it forms homodimers through *cis*-interaction on the cell surface. The subcellular localization of hepaCAM appears density-dependent; in well spread cells, hepaCAM is distributed to cell protrusions, whereas in confluent cells, hepaCAM is predominantly accumulated at the sites of cell-cell contacts on the cell membrane. In polarized cells, hepaCAM is recruited to the lateral and basal membranes, and lacking physical interaction, hepaCAM is shown to co-localize with E-cadherin at the lateral membrane. Cell adhesion and motility assays demonstrated that hepaCAM increased cell spreading on the matrices fibronectin and matrigel, delayed cell detachment, and enhanced wound healing. Furthermore, when the cytoplasmic domain was deleted, hepaCAM mutants did not affect cell surface localization and dimer formation. Cell-matrix adhesion, however, was less significantly increased, and cell motility was almost unchanged when compared with the effect of the wild-type hepaCAM. Taken together, the cytoplasmic domain of hepaCAM is essential to its function on cell-matrix interaction and cell motility.

Cell adhesion is a dynamic process essential for the normal development and maintenance of tissues and organs in multicellular organisms. Cell-cell and cell-matrix interactions are mediated by a large and complex number of cell adhesion molecules expressed on the cell surface that interact with each other in a spatially and temporally regulated manner. According to their structural and functional features, cell adhesion molecules are generally classified into at least four major families: the cadherins, integrins, selectins, and members of the immunoglobulin superfamily (1–5). Apart from linking cells to each other or to components of the extracellular matrix, an exciting concept that has emerged from recent cell biological research is that cell adhesion molecules function also as receptors critical in modulating signal transduction (6). Such interactions are vital for the regulation of cellular adhesion, proliferation, apoptosis, migration, and differentiation.

We have recently reported the identification of a novel gene in liver, designated as *hepaCAM* (GenBank™ AY047587), which was differentially expressed in human hepatocellular carcinoma. Located on human chromosome 11q24 and spanning 7 exons, *hepaCAM* encodes a novel member of the immunoglobulin superfamily. The predicted protein of 416 amino acids displays a typical structure of Ig-like adhesion molecules, including two extracellular Ig-like domains, a transmembrane segment, and a cytoplasmic tail. In addition, when exogenously expressed in the human hepatocellular carcinoma cell line HepG2, hepaCAM accelerates cell spreading and increases cell motility (7).

The mechanism of hepaCAM in mediating cell-matrix interaction is unknown. However, transfection studies with mutant and chimeric constructs of other adhesion molecules have suggested that the structural features of adhesion molecules play important roles in mediating their physiological and biological roles. Structure and function study of E-cadherin reveals that the formation of *cis*-dimer is fundamental for cell adhesion, and inhibition of *cis*-dimer formation is correlated with the lack of cell-cell interaction (8). For CEACAM1, it has been proposed that both the first extracellular Ig domain and cytoplasmic domain are required for its adhesion function (9). Thus, defining the molecular organization of hepaCAM may help to elucidate the functional roles of hepaCAM.

In this study, we aimed to characterize the physiological and biological properties of hepaCAM and to investigate the importance of the cytoplasmic domain on hepaCAM functions in the hepaCAM-deficient MCF7 cells. We showed that hepaCAM is a phosphorylated glycoprotein that forms *cis*-homodimers on the cell surface and mediates cell-matrix interaction. In addition, the cytoplasmic domain is required for cell-matrix modulation but dispensable in subcellular localization and surface dimerization.

EXPERIMENTAL PROCEDURES

Plasmid Construction—The complete coding sequence of *hepaCAM* and its mutants with truncated cytoplasmic domain were generated by PCR amplification. The cDNAs of *hepaCAM* residues 1–416 (wild-type), residues 1–320, or residues 1–263 were cloned into pEGFP-N2 vector (Clontech, Palo Alto, CA) or pcDNA6/V5-His vector (Invitrogen), at the HindIII/BamHI restriction sites. For polyclonal antibody generation, hepaCAM (residues 260–416) was cloned into the BglII/SalI restriction sites of the pQE40 vector (Qiagen). The sequences of the recombinant plasmids were verified by sequencing.

Cell Culture and Transfection—The MCF7 breast carcinoma cell line obtained from American Type Culture Collection (Manassas, VA) was maintained in the recommended conditions. Transfections of MCF7

* This study was supported by the Biomedical Research Council of Singapore (Project No. 01/1/21/19/162). The costs of publication of this article were defrayed in part by the payment of page charges. This article must therefore be hereby marked "*advertisement*" in accordance with 18 U.S.C. Section 1734 solely to indicate this fact.

¶ To whom correspondence should be addressed: Dept. of Physiology, Faculty of Medicine, National University of Singapore, 2 Medical Dr., Singapore 117597, Republic of Singapore. Tel.: 65-68746406; Fax: 65-67788161; E-mail: phsssl@nus.edu.sg.

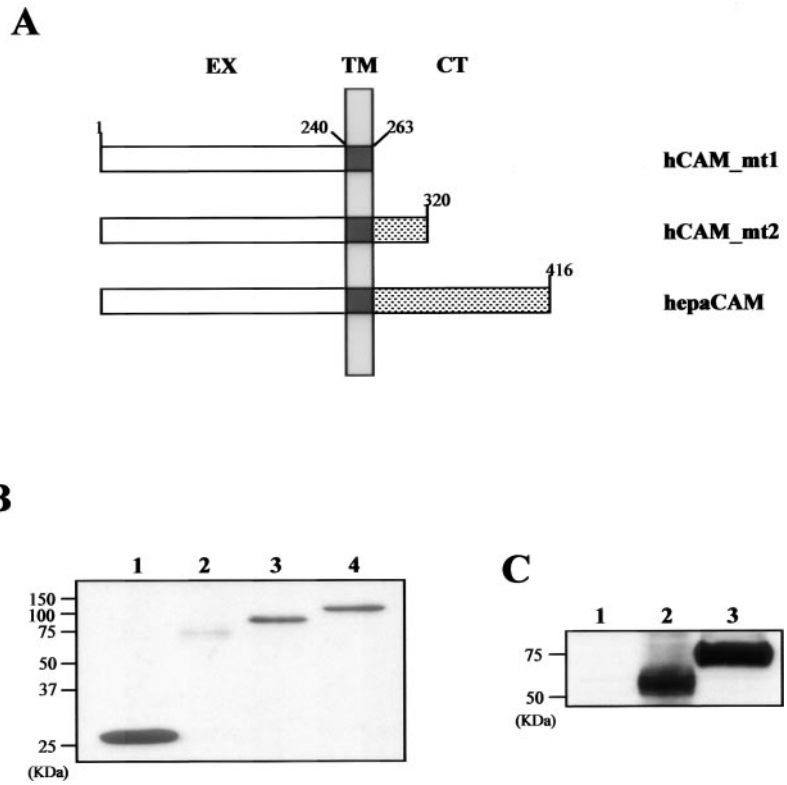

FIG. 1. **Schematic representation and expression of wild-type and cytoplasmic domain mutants of hepaCAM.** *A*, the wild-type and cytoplasmic domain mutants of *hepaCAM* were cloned into the eukaryotic expression vectors pEGFP-N2 and pCDNA6/V5-His and transfected into the breast carcinoma cell line MCF7. *EX*, extracellular domain (*white box*); *TM*, transmembrane domain (*gray box*); *CT*, cytoplasmic domain (*dotted box*). *B*, protein expression of pEGFPN2 vector and GFP-fused wild-type and mutant *hepaCAM* in MCF7 cells was detected by Western blotting using anti-GFP antibody. *Lane 1*, MCF7/pEGFPN2; *lane 2*, MCF7/hCAM_mt1-GFP; *lane 3*, MCF7/hCAM_mt2-GFP; *lane 4*, MCF7/hepaCAM-GFP. *C*, protein expression of pcDNA6/V5-His vector and V5-fused wild-type and mutant *hepaCAM* in MCF7 cells was detected by Western blotting using anti-V5 antibody. *Lane 1*, MCF7/pcDNA6; *lane 2*, MCF7/hCAM_mt1-V5; *lane 3*, MCF7/hepaCAM-V5. Positions of the molecular size markers are shown on the *left* of each panel.

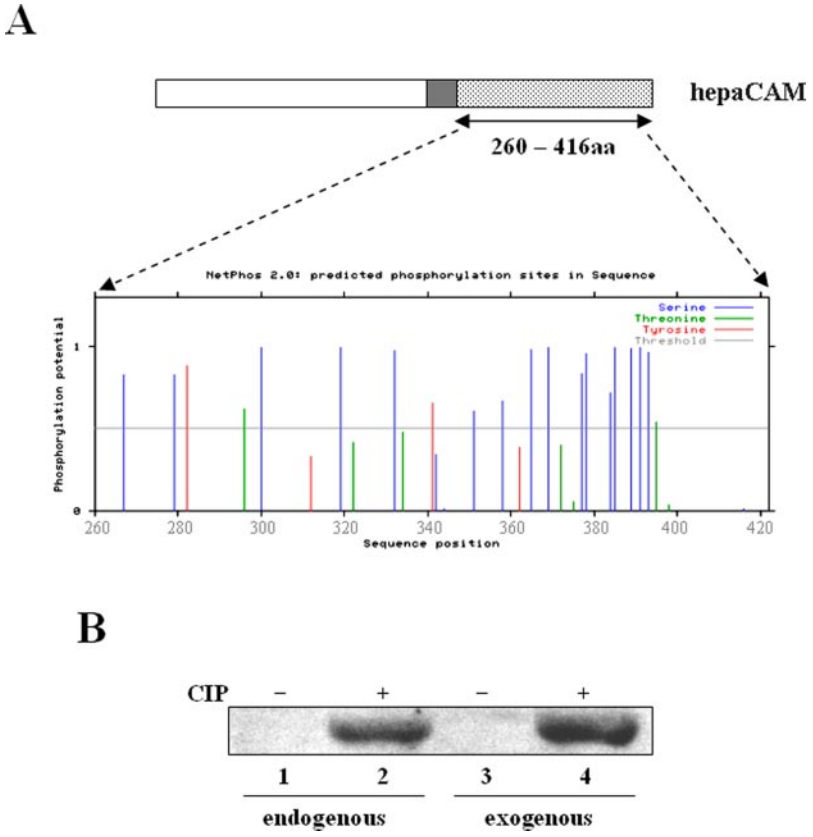

FIG. 2. **Phosphorylation of hepaCAM cytoplasmic domain.** *A*, residues 260–416 of hepaCAM was used to generate rabbit polyclonal antibody. Potential serine/threonine and tyrosine kinase phosphorylation sites in the cytoplasmic region were identified using NetPhos version 2.0 software. *aa*, amino acids. *B*, cell lysate prepared from C3A cells expressing endogenous hepaCAM (*lanes 1* and *2*) or MCF7/hepaCAM-V5 cells expressing exogenous hepaCAM (*lanes 3* and *4*) was either untreated (−) or treated (+) with calf intestinal alkaline phosphatase (*CIP*), as described under "Experimental Procedures." After dephosphorylation, hepaCAM protein was detected by Western blotting using the rabbit anti-hepaCAM polyclonal antiserum.

cells were carried out using the reagent Lipofectamine Plus (Invitrogen) according to the manufacturer's instructions. Transfected cells were selected for 4 weeks, either in the presence of 600 μg/ml G418 or 10 μg/ml blasticidin, and cloned.

Western Blot Analysis—Cells were lysed in radioimmunoprecipitation assay buffer to extract the total cell lysate. Immunoprecipitation was carried out by incubating the precleared cell lysate with the appropriate mouse monoclonal antibody and horseradish peroxidase-rec-protein G (Zymed Laboratories Inc., San Francisco, CA) overnight at 4 °C. Protein was resolved by SDS-PAGE, transblotted onto membrane, and detected by either rabbit anti-hepaCAM polyclonal antiserum, mouse anti-V5 antibody (Invitrogen), mouse anti-GFP antibody (Santa Cruz Biotechnology, Santa Cruz, CA), or mouse anti-E-cadherin (Zymed Laboratories Inc.).

Alkaline Phosphatase Treatment—Cell lysate was incubated in de-

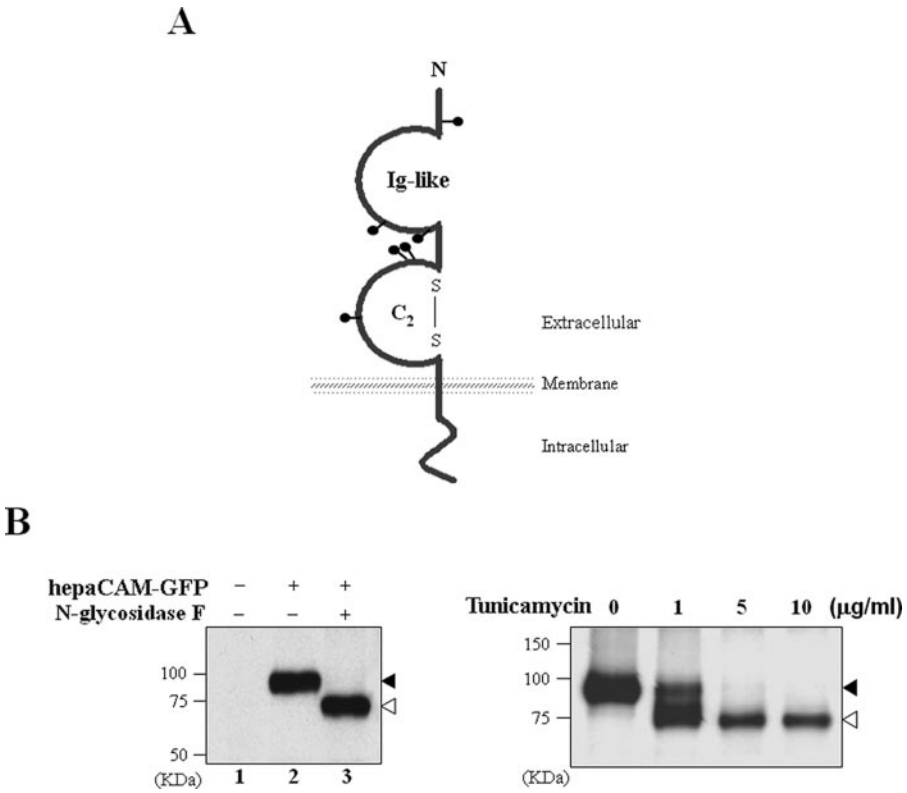

FIG. 3. ***N*-Linked glycosylation of hepaCAM-GFP.** *A*, illustration of the secondary structure of hepaCAM protein. hepaCAM owns the typical structure of proteins in the immunoglobulin superfamily, including an extracellular segment consisting of an NH_2-terminal-proximal Ig-like domain and a membrane-proximal C_2-type Ig domain with a disulfide bond formed between two cysteine residues (S—S), a transmembrane region, and a cytoplasmic tail. The six putative *N*-linked glycosylation sites are indicated by the symbol •. *B*, *left panel*, cell lysate was prepared from MCF7/hepaCAM-GFP (*lanes 2* and *3*) treated without (−) or with (+) *N*-glycosidase F. Untreated parental MCF7 cells (*lane 1*) were included as the control. *Right panel*, MCF7 cells transfected with hepaCAM-GFP were treated with tunicamycin at the indicated concentrations for 24 h before lysis. Protein samples were resolved by SDS-PAGE and subjected to Western blotting with anti-GFP antibody. *Solid* and *open arrowheads* indicate signals for glycosylated and deglycosylated proteins, respectively. Positions of the molecular size markers are shown on the *left*.

phosphorylation buffer for 10 min at 30 °C. Calf intestinal alkaline phosphatase (Roche Applied Science) was added and incubated for a further 15 min prior to Western analysis.

N-Linked Glycosylation Analysis—For inhibiting *N*-linked glycosylation, MCF7 cells were transiently transfected with hepaCAM-GFP and subsequently exposed to tunicamycin (Sigma) at the indicated concentrations for 24 h before lysis. For enzymatic digestion of *N*-linked oligosaccharides, the cell lysate of MCF7/hepaCAM-V5 was treated with peptide *N*-glycosidase F (New England Biolabs) according to the manufacturer's instructions. The samples were then subjected to Western analysis.

Chemical Cross-linking—A monolayer or a single suspension of cells was incubated in phosphate-buffered saline containing 3 mM BS3[1] (Pierce) or DTSSP (Pierce) at room temperature for 30 min. The reaction was quenched with the addition of 20 mM Tris-HCl, pH 7.5, for 15 min. Single cell suspension was assured by microscopic observation before and after chemical cross-linking reaction. DTSSP-cross-linked proteins were resuspended in Laemmli sample buffer without 50 mM dithiothreitol, unless indicated. Cell lysate was prepared in radioimmunoprecipitation assay buffer containing 10 mM iodoacetamide (10).

Immunocytochemistry—Cells cultured on coverslips were fixed with 2% paraformaldehyde and permeabilized with 0.2% Triton X-100. Nonspecific sites were blocked in 10% normal goat serum (Santa Cruz Biotechnology). Protein expression of V5-tagged hepaCAM was detected using mouse anti-V5 antibody, biotin-conjugated goat anti-mouse IgG antibody, and subsequently streptavidin-fluorescein. For co-localization experiments, cells were grown to confluence on 0.4-μm Transwell filters (Costar, Cambridge, MA). Protein expression of E-cadherin was detected using mouse anti-E-cadherin antibody, biotin-conjugated goat anti-mouse IgG antibody, and subsequently avidin-TRITC conjugate (Sigma). Fluorescence was visualized by fluorescence microscope (Carl Zeiss) or confocal microscope LSM 510 (Carl Zeiss) with sectioning performed at 0.5 μm.

Cell Spreading—Cells were seeded onto coverslips coated with 40 μg of matrigel basement membrane matrix (Clontech) or 10 μg/ml fibronectin (Santa Cruz Biotechnology) and incubated under standard culture conditions. Cell morphology was observed by microscopy. Unspread cells were defined as round cells, whereas spread cells were defined as cells with extended processes (11). The percentage of cells demonstrating spread morphology was quantified in 10 randomly selected fields.

Cell Detachment—A confluent monolayer of cells was detached in 1 mM EDTA in phosphate-buffered saline at 37 °C. Cell detachment was evaluated under the inverted microscope at 5 and 15 min of incubation. Concurrently, the dissociated cells were harvested and counted in 10 randomly selected fields.

Wound-healing Assay—A confluent monolayer of cells was wounded with a sterile plastic 200-μl micropipette tip. The wound was observed microscopically at 24 and 48 h. The percentage of wound filling was calculated by measuring the remaining gap space on the pictures.

Bioinformatics and Statistical Analysis—The protein sequence of hepaCAM was analyzed using the NetPhos version 2.0 and Prosite programs. Nonparametric analysis of variance was performed to compare the difference among more than two means. Software InStat version 3.0 (GraphPad) was employed, and $p < 0.01$ was considered significant.

RESULTS

Wild-type and COOH-terminal Mutants of hepaCAM—The wild-type *hepaCAM* encodes a transmembrane Ig-like adhesion molecule of 416 amino acids. To assess the importance of hepaCAM cytoplasmic domain in its physiological and biological functions, we constructed two deletion mutants of *hepaCAM*. hCAM_mt1, lacking the entire cytoplasmic tail, was constructed by truncating residues 264–416 of hepaCAM. hCAM_mt2 was constructed by deleting residues 321–416 of hepaCAM to obtain a partial cleavage of the cytoplasmic tail (Fig. 1*A*). Wild-type *hepaCAM*, hCAM_mt1, and hCAM_mt2 were fused in-frame at the NH_2-terminal of the green fluorescent protein (GFP) gene of the expression vector pEGFP-N2, and the resulting plasmids were named hepaCAM-GFP, hCAM_mt1-GFP, and hCAM_mt2-GFP, respectively. In addition, wild-type *hepaCAM* and hCAM_mt1 were inserted at the NH_2-terminal of the V5 tag of the pcDNA6/V5-His vector and designated hepaCAM-V5 and hCAM_mt1-V5, respectively. The constructs, as well as the empty vectors, were transfected into MCF7 cells, and the expressed proteins were analyzed by Western blotting using anti-GFP and anti-V5 antibodies accordingly (Fig. 1, *B* and *C*). Subsequently, MCF7 cells stably expressing pEGFP-N2 vector (MCF7/pEGFPN2), hepaCAM-GFP (MCF7/

[1] The abbreviations used are: BS3, bis(sulfosuccinimidyl) suberate; DTSSP, 3,3′-dithiobis (sulphosuccinimidyl propionate); GFP, green fluorescent protein; TRITC, tetramethylrhodamine isothiocyanate.

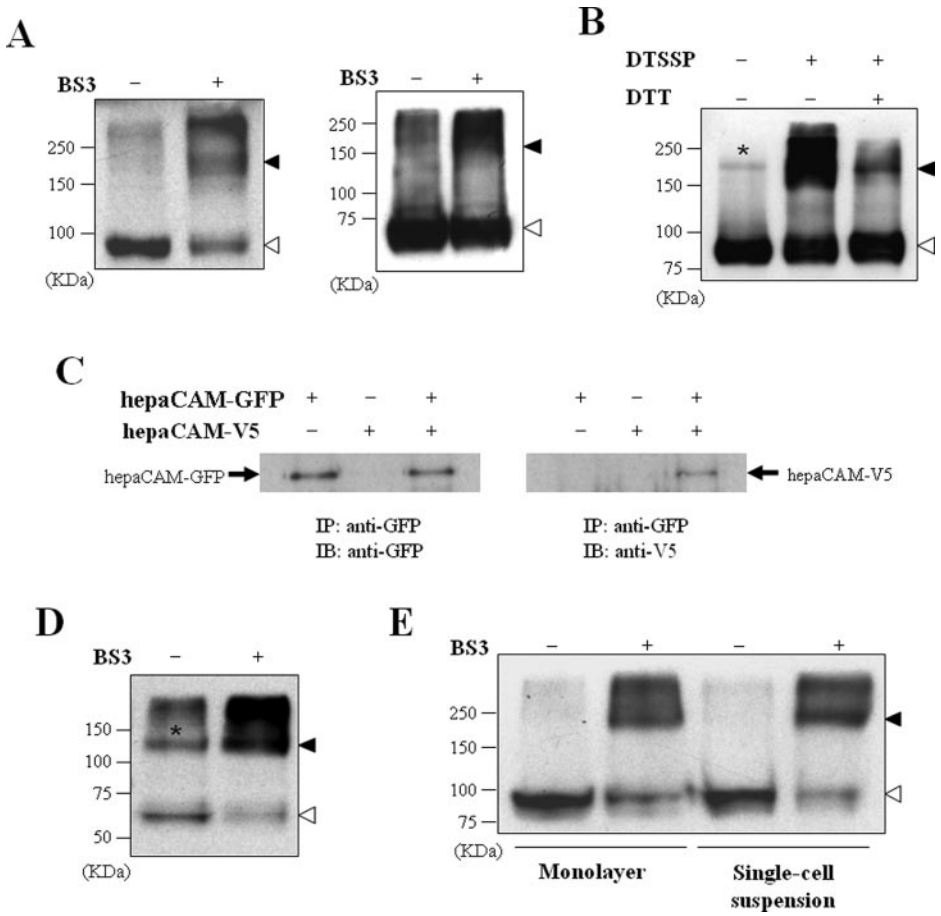

FIG. 4. **Homophilic *cis*-dimerization of hepaCAM and mutant.** *A*, cross-linking of hepaCAM-GFP (*left panel*) and hepaCAM-V5 (*right panel*) on the cell surface. A monolayer of MCF7/hepaCAM-GFP or MCF7/hepaCAM-V5 cells was untreated (−) and treated (+) with 3 mM BS3 prior to protein sample preparation in lysis buffer containing 10 mM iodoacetamide. Protein samples were subjected to Western blotting with anti-GFP antibody or anti-V5 antibody, respectively. *B*, a monolayer of MCF7/hepaCAM-GFP was untreated (−) and treated (+) with 3 mM DTSSP prior to protein sample preparation in lysis buffer containing 10 mM iodoacetamide. Protein samples were resuspended in Laemmli sample buffer in the presence (+) or absence (−) of dithiothreitol. *C*, co-immunoprecipitation of hepaCAM-GFP and hepaCAM-V5. MCF7 cells were transfected with hepaCAM-GFP, hepaCAM-V5, or both. Protein samples were prepared, immunoprecipitated with anti-GFP antibody, and subjected to Western blotting using anti-GFP antibody (*left panel*) or anti-V5 antibody (*right panel*). The signals corresponding to hepaCAM-GFP and hepaCAM-V5 molecules are marked with *arrows*. *D*, a monolayer of MCF7/hCAM_mt1-GFP cells was untreated (−) and treated (+) with 3 mM BS3 prior to protein sample preparation in lysis buffer containing 10 mM iodoacetamide. Protein samples were subjected to Western blotting with anti-GFP antibody. *E*, a monolayer and a single cell suspension of MCF7/hepaCAM-GFP were incubated in the absence (−) or presence (+) of 3 mM BS3. Protein samples were subjected to Western blotting with anti-GFP antibody. *Solid* and *open arrowheads* indicate signals for dimeric and monomeric proteins, respectively. *, dimer in un-cross-linked sample. The positions of the molecular size markers are shown on the *left* of each panel.

hepaCAM-GFP), hCAM_mt1-GFP (MCF7/hCAM_mt1-GFP), hCAM_mt2-GFP (MCF7/hCAM_mt2-GFP), pcDNA6 vector (MCF7/pcDNA6), hepaCAM-V5 (MCF7/hepaCAM-V5) and hCAM_mt1-V5 (MCF7/hCAM_mt1-V5) were generated and cloned.

Phosphorylation of the hepaCAM Cytoplasmic Domain—We generated a polyclonal antiserum that recognizes the hepaCAM cytoplasmic domain but in its dephosphorylated form. The recombinant His bacterial fusion protein used for immunization contained residues 260–416 of hepaCAM. Western analysis showed that the resulting antiserum could specifically detect the bacterial fusion protein, otherwise undetectable by the pre-immune serum. However, when the antiserum was tested on the cell lysate of MCF7/hepaCAM-V5, no specific band was observed (data not shown). We suspected that the antiserum was unable to recognize the cytoplasmic domain of hepaCAM because of the presence of post-translational modifications, *e.g.* phosphorylation. Evaluation of the region selected for antibody generation by the NetPhos version 2.0 server predicted 28 potential serine-, threonine-, or tyrosine-phosphorylated residues scattered along the cytoplasmic domain of hepaCAM protein, with 20 of them giving a potential phosphorylation >0.5 (Fig. 2*A*). To verify that the hepaCAM cytoplasmic domain is phosphorylated, we dephosphorylated cell lysates of C3A cells expressing endogenous hepaCAM and MCF7/hepaCAM-V5 cells expressing exogenous hepaCAM with calf intestinal alkaline phosphatase. The untreated cell lysates were included as controls. Indeed, calf intestinal alkaline phosphatase-treated endogenous and exogenous hepaCAM were detected by the rabbit antiserum (Fig. 2*B*), confirming that the cytoplasmic domain of hepaCAM is phosphorylated.

N-Linked Glycosylation of hepaCAM—Sequence analysis of hepaCAM predicted six *N*-linked glycosylation sites on its extracellular domain (Fig. 3*A*). To investigate whether hepaCAM was glycosylated, the MCF7/hepaCAM-GFP cell lysate was enzymatically digested with peptide *N*-glycosidase F to release putative *N*-linked oligosaccharides. An untreated sample was included as the control. The molecular mass of hepaCAM-GFP, shown by Western analysis to be ~100 kDa, was shifted to ~75 kDa after deglycosylation. Consistently, when MCF7 cells transfected with hepaCAM-GFP were treated with tunicamycin (an antibiotic that inhibits *N*-linked glycosylation) at dif-

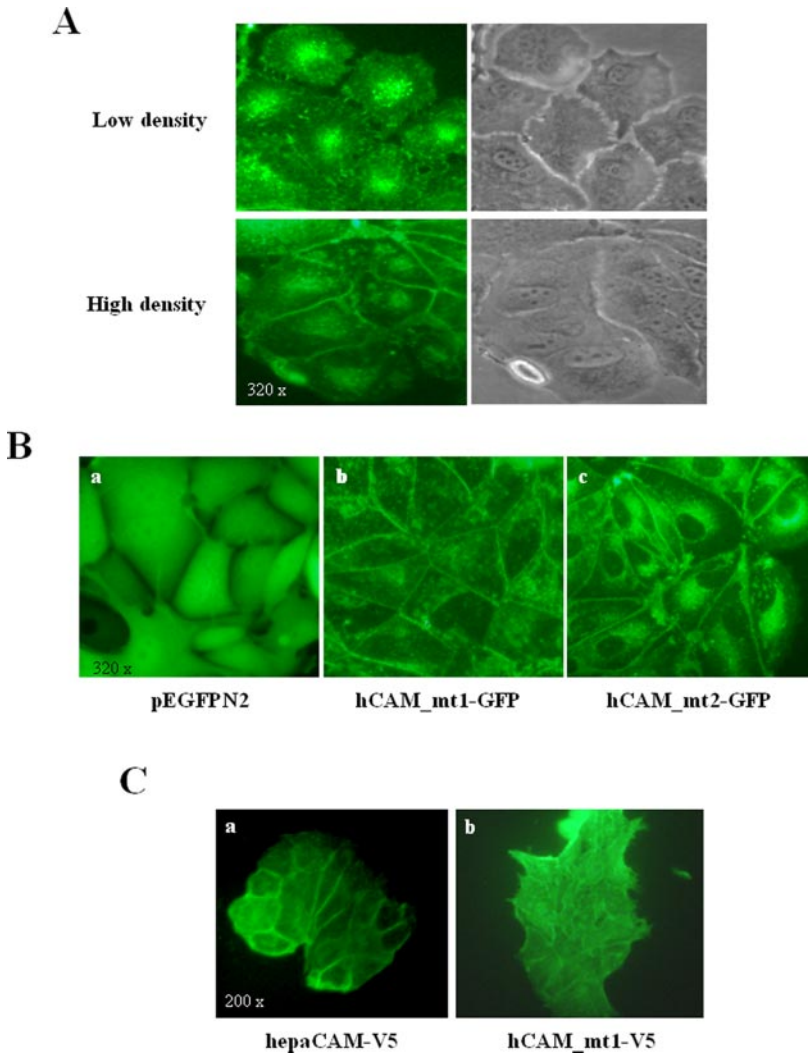

FIG. 5. **Subcellular localization of hepaCAM and mutants in MCF7 cells.** *A*, the localization of hepaCAM-GFP in MCF7 cells is cell density-dependent. MCF7/hepaCAM-GFP cells were seeded at low density and cultured for a few days. Cells at areas of low density (*top panels*) and high density (*bottom panels*) were observed under a fluorescence (*left panels*) or inverted microscope (*right panels*). Magnification is ×320. *B*, the expression of pEGFP-N2 (*a*), hCAM_mt1-GFP (*b*), and hCAM_mt2-GFP (*c*) in MCF7 cells was detected by fluorescence microscopy. Magnification is ×320. *C*, MCF7/hepaCAM-V5 (*a*) and MCF7/hCAM_mt1-V5 (*b*) cells were immunostained with anti-V5 antibody to detect localization of hepaCAM and mutant under a fluorescence microscope. Magnification is ×200.

ferent doses for 24 h, a band at ~75 kDa was also observed (Fig. 3*B*). The results verified that hepaCAM is a glycoprotein. By subtracting the molecular mass of GFP, *i.e.* 27 kDa, the deglycosylated form of hepaCAM is ~48 kDa.

Dimerization of hepaCAM and Mutant on Plasma Membrane—We evaluated the pre-existing forms of hepaCAM on cell membrane by incubating a monolayer of MCF7/hepaCAM-GFP cells with BS3, a noncleavable membrane-impermeable cross-linker. The cell lysate was prepared in the presence of iodoacetamide to inhibit the formation of nonspecific disulfide bonds (10). An untreated sample was included as the control. The samples were analyzed by Western blotting with anti-GFP. In the presence of BS3, a band of ~200 kDa appeared, which seemed to represent the dimerized form of hepaCAM-GFP, accompanied with the disappearance of the hepaCAM monomers. Similarly, treatment of MCF7/hepaCAM-V5 cells with BS3 resulted in a decrease of the ~75-kDa monomeric form of hepaCAM and an accumulation of the higher molecular weight species at ~150 kDa, although no distinct band was noted (Fig. 4*A*). It is possible that the anti-V5 antibody did not recognize the higher molecular weight species as efficiently as monomers. To examine whether hepaCAM forms a homodimer on the cell surface, MCF7/hepaCAM-GFP cells were treated with DTSSP, a reducible membrane-impermeable cross-linker. In the absence of the reducing agent dithiothreitol, a significant increase in the 200-kDa species was observed. However, when dithiothreitol was added into the sample buffer, the higher molecular mass was reduced to the monomeric form to a level closely comparable with that of the untreated cells (Fig. 4*B*). Additionally, we co-expressed hepaCAM-GFP and hepaCAM-V5 in MCF7 cells, immunoprecipitated the cell lysate with anti-GFP antibody, and immunoblotted with anti-V5 or anti-GFP. The result revealed co-immunoprecipitation of hepaCAM-GFP with hepaCAM-V5 (Fig. 4*C*), demonstrating that hepaCAM molecules dimerized through homophilic interaction. To examine whether tailless hepaCAM proteins form dimers, MCF7/hCAM_mt1-GFP cells were treated with BS3 and analyzed by Western blotting (Fig. 4*D*). The monomeric form of hCAM_mt1-GFP was diminished and replaced with its dimeric form at ~125 kDa in the BS3-treated sample. Interestingly, in the untreated sample of hepaCAM-GFP and hCAM_mt1-GFP, protein species that seemed to represent the dimeric form of the proteins were observed. This phenomenon could be due to covalent bonding between the dimers of hepaCAM-GFP or hCAM_mt1-GFP. To determine whether hepaCAM-GFP forms *cis*- or *trans*-dimers on the cell surface, both adherent monolayer and single cell suspension of MCF7/hepaCAM-GFP cells were treated with BS3 (Fig. 4*E*). The extent of dimerization was comparable in both adherent and suspension cells, indicating that hepaCAM homodimerization occurs predominantly through *cis*-interactions rather than *trans*-interactions within the plane of the membrane of individual cells.

Subcellular Localization of hepaCAM and Mutants in MCF7 Cells—We explored the subcellular distribution of wild-type hepaCAM in MCF7/hepaCAM-GFP cells at low and at high cell densities by fluorescence and inverted microscopy (Fig. 5*A*). When

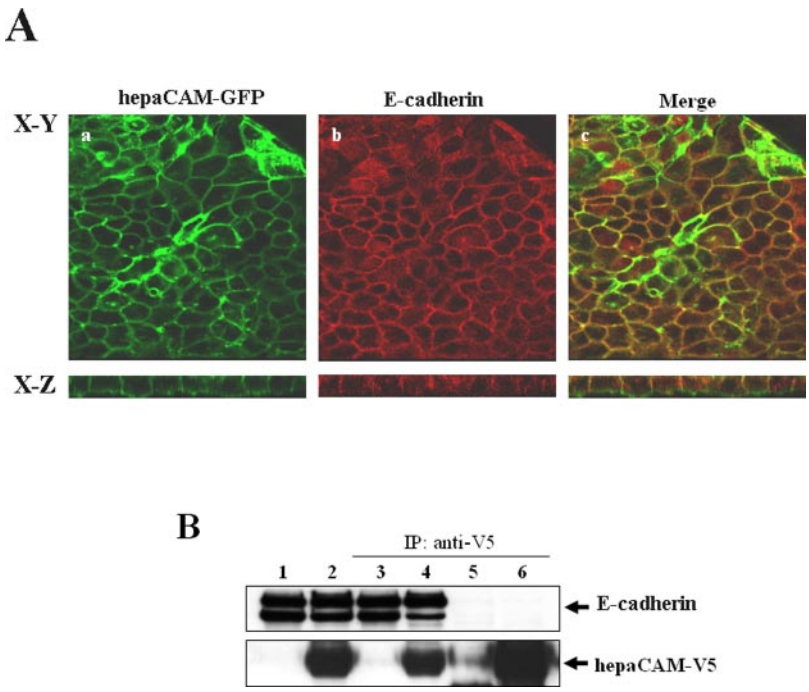

FIG. 6. **Co-localization of hepaCAM with E-cadherin.** *A*, MCF7/hepaCAM-GFP cells grown to confluence on the Transwell filter unit were fixed, permeabilized, and immunostained with anti-E-cadherin. Laser scanning confocal microscopy was performed with a filter set suitable for fluorescein and rhodamine detection. The representative sets of X-Y and X-Z sections are indicated. *a*, hepaCAM-GFP stained *green*; *b*, E-cadherin stained *red*; *c*, confocal images of the hepaCAM-GFP and E-cadherin were merged to show regions of co-localization. *B*, co-immunoprecipitation of hepaCAM-GFP and E-cadherin. Equal amounts of cell lysate prepared from MCF7/pcDNA6 or MCF7/hepaCAM-V5 cells was immunoprecipitated (*IP*) with anti-V5 antibody and subjected to Western blotting using anti-E-cadherin (*top panel*) or anti-V5 antibody (*bottom panel*). The signals corresponding to E-cadherin and hepaCAM-V5 molecules are marked with *arrowheads*. *Lane 1*, cell lysate of MCF7/pcDNA6 before IP; *lane 2*, cell lysate of MCF7/hepaCAM-V5 before IP; *lane 3*, cell lysate of MCF7/pcDNA6 after IP; *lane 4*, cell lysate of MCF7/hepaCAM-V5 after IP; *lane 5*, precipitate of MCF7/pcDNA6; *lane 6*, precipitate of MCF7/hepaCAM-V5.

cells were well spread, hepaCAM protein was localized to punctuate structures in the perinuclear membrane, cytoplasm, and at the tip of the cell surface protrusions, which were about to make contact with adjacent cell surfaces, forming zipper-like structures. Once the cells became confluent, the protein was localized at a lesser extent in the perinuclear membrane and cytoplasm and predominantly on the plasma membrane, particularly in the areas of cell-cell contacts. The results suggest that the subcellular localization of hepaCAM is cell density-dependent. We also examined the effect of hepaCAM cytoplasmic domain in its plasma membrane localization. hCAM_mt1-GFP and hCAM_mt2-GFP were both recruited to the plasma membrane of MCF7 cells (Fig. 5*B*). Similarly, MCF7/hepaCAM-V5 and MCF7/hCAM_mt1-V5 cells immunostained with anti-V5 showed that hepaCAM and its mutant were predominantly expressed on cell membranes (Fig. 5*C*). The results indicate that the cytoplasmic domain is dispensable for membrane localization.

Co-localization of hepaCAM with E-cadherin—The distribution of hepaCAM was further examined in confluent polarized MCF7/hepaCAM-GFP cells by confocal laser scanning microscopy (Fig. 6*A*). The cells were also stained for E-cadherin, which localizes in the lateral cell surface, to compare its localization with that of hepaCAM. In the X-Y sections, hepaCAM-GFP was distributed to honeycomb-like structures at cell-cell boundaries, which significantly co-localized with E-cadherin. In the X-Z vertical cross-section, the distribution of E-cadherin along the entire lateral cell surface coincided with hepaCAM-GFP. Moreover, hepaCAM was detected at the basal membrane that was in contact with the Transwell membrane. Because hepaCAM and E-cadherin appeared to co-localize, we investigated whether there were any physical interactions between them by co-immunoprecipitation (Fig. 6*B*). Cell lysate prepared from MCF7/hepaCAM-V5 was precipitated with the anti-V5 antibody and subjected to Western blotting using the anti-E-cadherin or anti-V5 antibodies. MCF7/pcDNA6 cell lysate was included in the experiment as the control. No co-immunoprecipitation was observed, suggesting that E-cadherin and hepaCAM do not physically interact.

Cell-Matrix Interaction by hepaCAM and Mutant—We evaluated the adhesive properties of V5-tagged *hepaCAM* and mutant constructs on the MCF7 cells through cell aggregation, cell adhesion, and detachment assays. No clear change in cell aggregation was observed among MCF7/pcDNA6, MCF7/hCAM_mt1-V5, and MCF7/hepaCAM-V5 cells (data not shown), but hepaCAM was capable of modulating cell-matrix adhesion significantly. Fig. 7 shows that ~60 and 79% of the MCF7/hepaCAM-V5 cells exhibited spread morphology on fibronectin at 30 min and 2 h of incubation, respectively, in contrast to 40.8 and 58.2% of the MCF7/hCAM_mt1-V5 cells and 7.3 and 18% of MCF7/pcDNA6 cells ($p < 0.001$). Similarly on matrigel, MCF7/hepaCAM-V5 cells showed the fastest spreading, followed by MCF7/hCAM_mt1-V5 cells, and then MCF7/pcDNA6 cells ($p < 0.001$). In the cell detachment assay (Fig. 8), MCF7/hepaCAM-V5 cells detached 18.9 and 21.6 times slower than MCF7/pcDNA6 cells at 5 and 15 min, respectively. MCF7/hCAM_mt1-V5 cells, on the other hand, detached ~4 and 2.2 times slower than MCF7/pcDNA6 cells at time points 5 min and 15 min ($p < 0.001$). The results showed that, in addition to its extracellular and transmembrane domains, hepaCAM needs its cytoplasmic domain to mediate strong cell-matrix adhesion.

Cell Motility by hepaCAM and Mutant—Cell motility of hepaCAM and mutant was assessed by matrigel invasion and wound-healing assays. Barely any MCF7 cells expressing pcDNA6, hCAM_mt1, and hepaCAM migrated through the 8-μm Transwell membrane (data not shown). This observation could be explained by the poorly invasive nature of MCF7 cells.

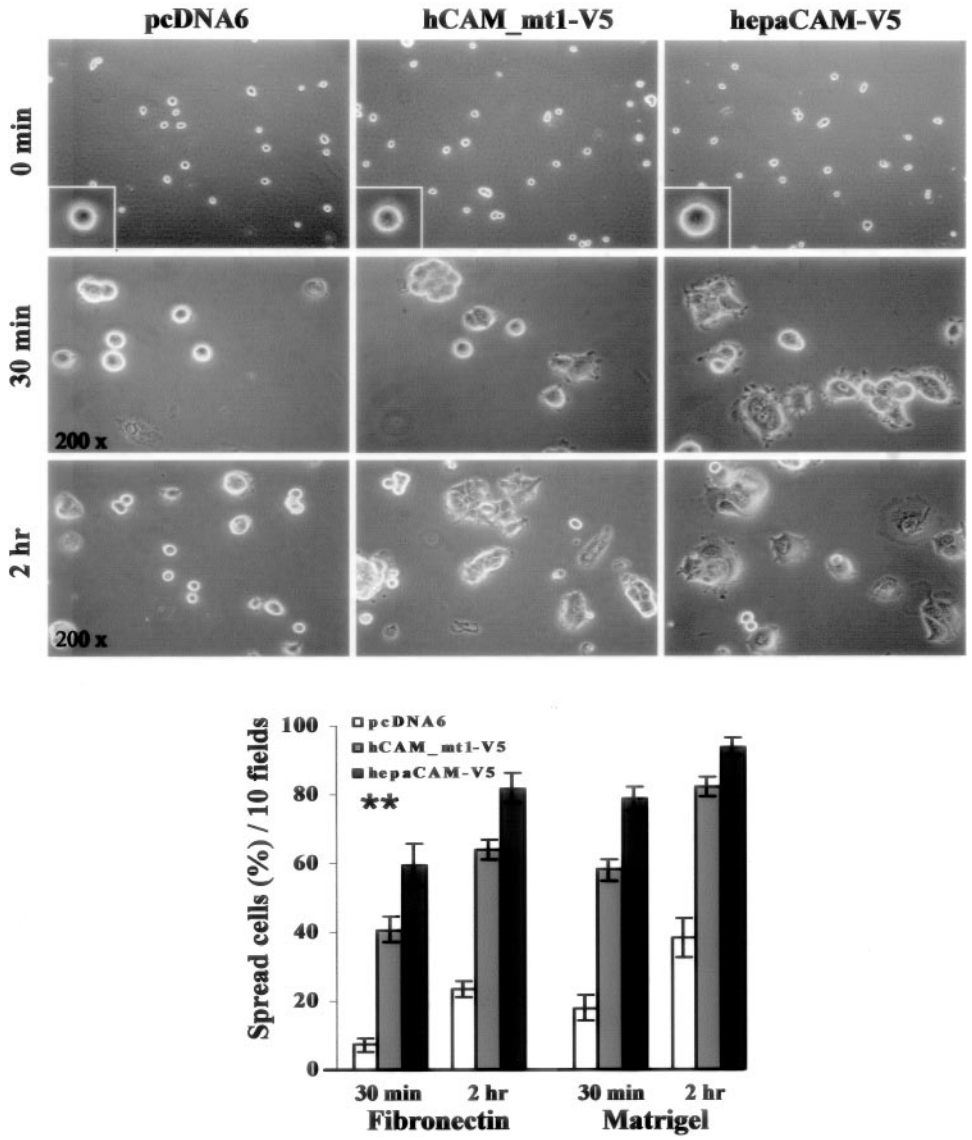

FIG. 7. **Cell spreading assay.** MCF7/pcDNA6 (*left panels*), MCF7/hCAM_mt1-V5 (*middle panels*) and MCF7/hepaCAM-V5 (*right panels*) cells were allowed to spread on matrigel-coated coverslips for 30 min or 2 h. *Insets*, cell morphology before spreading. The microscopic photos were taken under ×200 magnification. Shown is the percentage of spread cells on fibronectin and matrigel. At 30 min or 2 h after plating, the total number of cells showing spread morphology were counted in ten randomly selected fields, and the percentage of cell spreading was then computed. The data represent means ± S.D. ($n = 6$); **, $p < 0.001$ as assessed by analysis of variance.

Moreover, MCF7/hepaCAM cells were enlarged, therefore retarding migration. However, in the wound-healing assay (Fig. 9), we demonstrated that, after 24 h of incubation, MCF7/hepaCAM-V5 cells filled 59.3% of the scratched area ($p < 0.01$), compared with 36.3% by MCF7/hCAM_mt1-V5 cells ($p > 0.05$) and 33.1% by MCF7/pcDNA6 cells. After 48 h, MCF7/hepaCAM-V5 cells closed 83.7% of the wound ($p < 0.01$), compared with 55.2% by MCF7/hCAM_mt1-V5 cells ($p > 0.05$) and 49.5% by MCF7/pcDNA6 cells. Hence, the cytoplasmic domain is important for cell motility modulated by hepaCAM.

DISCUSSION

In our previous work, we identified a novel Ig-like molecule, hepaCAM, which exhibits typical structural characteristics of adhesion molecules of the immunoglobulin superfamily (7). In this study, we demonstrated physiological and biological characteristics of hepaCAM and the relationship between its structure and function, particularly with respect to the cytoplasmic domain.

Sequence analysis revealed that the cytoplasmic domain of hepaCAM contains a proline-rich region that provides putative binding sites for SH3 domains and potential phosphorylation sites of serine/threonine and tyrosine kinases. Experimentally, we showed that the cytoplasmic domain is phosphorylated, suggesting an important role of the hepaCAM cytoplasmic domain in signaling cascades controlling cellular adhesion, motility, morphology, and all processes depending on the cytoskeleton. To evaluate the significance of the cytoplasmic domain, we transfected wild-type and cytoplasmic domain-truncated constructs of *hepaCAM* into MCF7 cells and analyzed their effects on hepaCAM functions.

Biochemical analysis revealed that hepaCAM is a glycosylated protein and forms a *cis*-homodimer on the cell surface. Deletion of the cytoplasmic domain did not interfere with dimer formation, suggesting that dimerization may be stabilized by the extracellular and/or transmembrane domains but not the cytoplasmic domain. Notably, chemical cross-linking of hepaCAM or its mutated protein both showed the presence of high molecular weight proteins, indicating that hepaCAM may form large complexes with other endogenously expressed cellular proteins through its extracellular and/or transmembrane do-

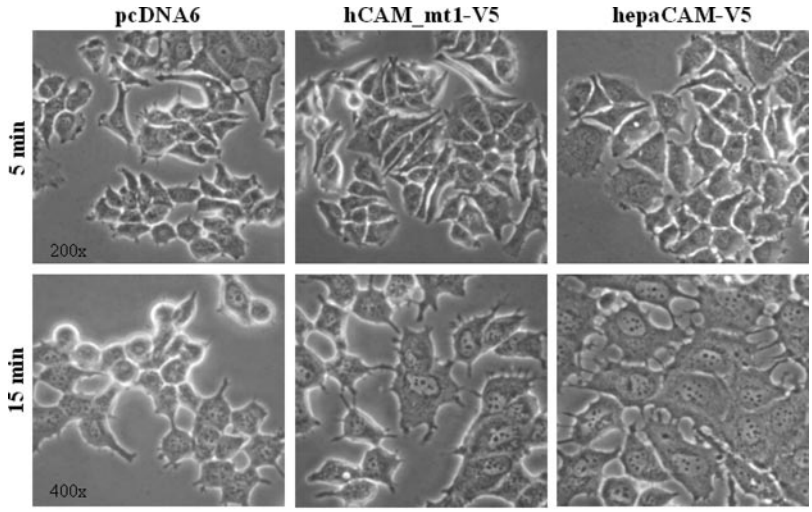

FIG. 8. **Cell detachment assay.** MCF7/pcDNA6 (*left panels*), MCF7/hCAM_mt1-V5 (*middle panels*), and MCF7/hepaCAM-V5 (*right panels*) cells were detached in 1 mM EDTA for 5 min or 15 min. The microscopic photos were taken under ×200 and ×400 magnifications. At 5 min or 15 min after incubation, the total number of detached cells was counted in ten randomly selected fields, and the percentage of cell detachment was then computed. The data represent means ± S.D. ($n = 6$), **, $p < 0.001$ as assessed by analysis of variance.

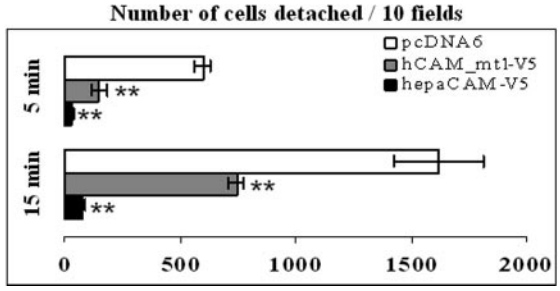

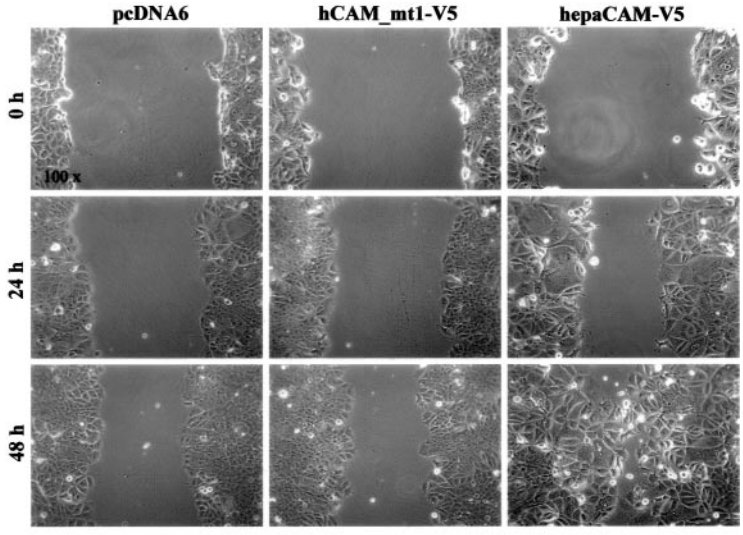

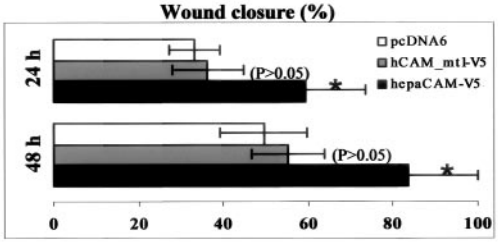

FIG. 9. **Wound-healing assay.** Wounds were made by pipette tip on confluent MCF7/pcDNA6 (*left panels*), MCF7/hCAM_mt1-V5 (*middle panels*), and MCF7/hepaCAM-V5 (*right panels*) cells and allowed to heal for 24 and 48 h. The microscopic photos were taken under ×100 magnification. The diameters of wounds were measured on the microscopic photos at 0, 24, and 48 h after wounding. Changes in wound diameter were computed into percentage (means ± S.D.%, $n = 6$) to represent wound closure. *, $p < 0.01$ as assessed by analysis of variance.

mains. Alternatively, it may represent higher order homo-oligomers of hepaCAM or its mutant. It is interesting to observe the seemingly dimeric form of hepaCAM and its mutant in their respective un-cross-linked samples. Although the mechanism resulting in such interaction is unknown to us, Hunter *et al.* (5) and others (12) have observed a similar phenomenon in C-CAM and raise the possibility that C-CAM dimers become covalently linked, perhaps through the action of transglutaminase, an enzyme which catalyzes the formation of γ-glutamyl-ε-lysine bonds in a restricted number of cellular proteins.

Subcellular localization of hepaCAM in nonpolarized MCF7 cells showed that hepaCAM molecules were recruited to the cytoplasmic membranes at sites of cell-cell attachment. In polarized cells, hepaCAM was preferentially expressed in the lateral and basal membranes. Co-localization analysis demonstrated that hepaCAM co-localized laterally with E-cadherin, but no physical interaction between the two molecules was detected. We also showed that partial truncation and complete deletion of the cytoplasmic domain did not alter the plasma membrane localization. It has been reported that the CEACAM1 cytoplasmic domain regulates its lateral localization. Differing in their cytoplasmic domains, isoform CEACAM1-S distribution is exclusively apical, whereas isoform CEACAM1-L occurs both in apical and lateral cell surfaces (13). However, whether the loss of cytoplasmic domain affects the lateral and basal localization of hepaCAM remains to be determined.

Functionally, hepaCAM is capable of modulating cell-matrix interaction. Cell adhesion to the substratum plays a crucial role in cell migration, which is a key aspect of many normal and abnormal biological processes, including embryonic development, immunity, wound healing, and metastasis of tumor cells (14, 15). The distribution of hepaCAM on the basal membrane of cells, in addition to the spread morphology of MCF7/hepaCAM-V5 cells, hinted at possible *trans*-interaction between hepaCAM and the substrate. Evidently, cell spreading, cell detachment, and wound-healing assays revealed increased cell-substrate affinity and cell motility mediated by hepaCAM. Deletion of the cytoplasmic domain reduced, but did not completely abrogate, cell-matrix adhesion mediated by the wild-type hepaCAM, implicating that, to a considerable extent, the extracellular and transmembrane domains are able to initiate adhesion. However, the rate of wound healing of cells expressing mutant hepaCAM was close to the level of the control cells, indicating that the cytoplasmic domain is essential for mediating wound recovery. The data implies that cell-matrix adhesion and cell motility are controlled separately, and phosphorylation of the cytoplasmic domain may play a pivotal role in the regulation. Indeed, phosphorylation of CD44 was shown to regulate melanoma cell and fibroblast migration on, but not attachment to, a hyaluronan substratum (16). Additionally, it has been proposed for the cadherins (8, 17, 18) and for CEA (19) that *cis*-dimerization will lead to strengthened cell adhesion, and *cis*-homodimer formation of ICAM-1 enhances its binding to a leukocyte β2-integrin (20). However, the functional significance of hepaCAM post-translational modification and dimerization in regulating cell-matrix interaction is still under investigation.

In conclusion, we have shown that hepaCAM is a phosphorylated glycoprotein, forms *cis*-homodimers on the cell surface, and modulates cell-matrix interaction. The cytoplasmic domain, although unessential for cell surface localization and dimerization, is required to maintain a complete functional form of hepaCAM as a modulator of cell-matrix interaction.

Acknowledgment—We thank Asha Reka Das for her assistance whenever and wherever needed.

REFERENCES

1. Edelman, G. M. (1986) *Annu. Rev. Cell Biol.* **2,** 81–116
2. Edelman, G. M. (1984) *Proc. Natl. Acad. Sci. U. S. A.* **81,** 1460–1464
3. Edelman, G. M., and Crossin, K. L. (1991) *Annu. Rev. Biochem.* **60,** 155–190
4. Takeichi, M. (1991) *Science* **251,** 1451–1455
5. Hunter, I., Sawa, H., Edlund, M., and Obrink, B. (1996) *Biochem. J.* **320,** 847–853
6. Rosales, C., O'Brien, V., Kornberg, L., and Juliano, R. (1995) *Biochim. Biophys. Acta* **1242,** 77–98
7. Moh, M. C., Lee, L. H., and Shen, S. (2005) *J. Hepatol.* **42,** 833–841
8. Takeda, H., Shimoyama, Y., Nagafuchi, A., and Hirohashi, S. (1999) *Nat. Struct. Biol.* **6,** 310–312
9. Cheung, P. H., Luo, W., Qiu, Y., Zhang, X., Earley, K., Millirons, P., and Lin, S. H. (1993) *J. Biol. Chem.* **268,** 24303–24310
10. Masuda, M., Yageta, M., Fukuhara, H., Kuramochi, M., Maruyama, T., Nomoto, A., and Murakami, Y. (2002) *J. Biol. Chem.* **277,** 31014–31019
11. Richardson, A., Malik, R. K., Hildebrand, J. D., and Parsons, J. T. (1997) *Mol. Cell. Biol.* **17,** 6906–6914
12. Greenberg, C. S., Birckbichler, P. J., and Rice, R. H. (1991) *FASEB J.* **5,** 3071–3077
13. Sundberg, U., Beauchemin, N., and Obrink, B. (2004) *J. Cell Sci.* **117,** 1091–1104
14. Dedhar, S., and Hannigan, G. E. (1996) *Curr. Opin. Cell Biol.* **8,** 657–669
15. Xie, H., Pallero, M. A., Gupta, K., Chang, P., Ware, M. F., Witke, W., Kwiatkowski, D. J., Lauffenburger, D. A., Murphy-Ullrich, J. E., and Wells, A. (1998) *J. Cell Sci.* **111,** 615–624
16. Peck, D., and Isacke, C. M. (1996) *Curr. Biol.* **6,** 884–890
17. Shapiro, L., Fannon, A. M., Kwong, P. D., Thompson, A., Lehmann, M. S., Grubel, G., Legrand, J. F., Als-Nielsen, J., Colman, D. R., and Hendrickson, W. A. (1995) *Nature* **374,** 327–337
18. Nagar, B., Overduin, M., Ikura, M., and Rini, J. M. (1996) *Nature* **380,** 360–364
19. Bates, P. A., Luo, J., and Sternberg, M. J. (1992) *FEBS Lett.* **301,** 207–214
20. Reilly, P. L., Woska, J. R., Jr., Jeanfavre, D. D., McNally, E., Rothlein, R., and Bormann, B. J. (1995) *J. Immunol.* **155,** 529–532

93rd American Association for Cancer Research. April 6-10, 2002.

A novel intronless putative tumor suppressor gene, hepn1, frequently inactivated in hepatocellular carcinoma and multiple tumor types

Mei Chung Moh, Shali Shen, *Department of Physiology, National University of Singapore, Singapore.*

A novel gene, identified in human liver and designated as hepn1, is frequently silenced in hepatocellular carcinoma (HCC) and multiple tumor types. Reverse transcription-PCR demonstrated a suppression of hepn1 in 78% (68/87) of HCC patients and 84% (16/19) of human tumor cell lines. The full-length hepn1 cDNA, isolated from normal liver, is 1448 base pairs long which contains an open reading frame (OFR) of 267 nucleotides encoding a protein of 88 amino acids. For functional exploration, the ORF of hepn1 was transfected and expressed in HepG2 cells, a hepn1-deficient HCC cell line with wild-type p53. Forty-eight hours after the transfection, the cell viability decreased 27.8% that coincided with the optimized transfection efficiency; however, the expression of p53 in the transfected cells remained unchanged. Through the green fluorescence protein, we localized hepn1 protein in the cytoplasm and observed a hepn1-induced cell death in HepG2. Sequence analysis against the available databases revealed that, at the amino acid level, hepn1 did not have any homology to known proteins/peptides; at the EST level, hepn1 had significant alignments with a number of fragmented sequences obtained from the brain and the breast; and at the genomic level, hepn1 was indicated to be an intronless gene located at human chromosome 11q24. These data suggest that the intronless gene, hepn1, may encode a novel tumor suppressor and its function may be p53-independent.

95th American Association for Cancer Research. March 27-31, 2004.

Identification and characterization of CAMSIT as a novel immunoglobulin-like cell adhesion molecule that exhibits growth inhibitory effect on human cancer cells

Mei Chung Moh, Lay Hoon Lee, Chunli Zhang, Shali Shen. *National University of Singapore, none, Singapore and National University of Singapore, Singapore*.

Alterations of cell adhesion molecules have increasingly been implicated in disruption of cell organization, signaling and growth control, leading to tumor development and progression. In this study, using the technique of suppression subtractive hybridization, we examined differential gene expression in human hepatocellular carcinoma (HCC) and identified a new member of the immunoglobulin superfamily, designated as CAMSIT (cell adhesion molecule suppressed in tumors). Real-time RT-PCR showed that CAMSIT lacked tissue specificity and was widely expressed in normal human tissues, such as liver, brain, skeletal muscle, colon and blood. Its expression was significantly decreased in 20/23 of HCC specimens and undetectable in 17/19 cell lines derived from various human tumors. Sequence analyses revealed that gene CAMSIT, mapped to chromosome 11q24, had no significant similarities to any known genes. The predicted protein of 416 amino acids displayed a typical structure of Ig-like adhesion molecules, including two extracellular Ig-like domains, a transmembrane segment and a cytoplasmic tail. Through transfection studies on HepG2 and MCF7 cells, we explored the biochemical characteristics and biological functions of CAMSIT. The subcellular localization of CAMSIT appeared to be cell density-dependent. In well-spread cells, CAMSIT was distributed in punctuate structures in the cytoplasm and at the cell surface protrusions. In confluent cells, CAMSIT was predominantly localized on the cytoplasmic membrane, particularly in the areas of cell-cell contacts, but absent at free cell borders. Crosslinking assay suggested that, independent of the cytoplasmic tail, CAMSIT formed *cis*-dimers on cell surface. Western analysis following deglycosylation and dephosphorylation indicated that CAMSIT protein, approximately 75 kDa, was glycosylated and phosphorylated. Re-expression of CAMSIT reduced cell colony formation by 10 folds ($P = 0.0022$), inhibited cell proliferation by 14 folds ($P < 0.001$), and induced senescence-like phenotype. In addition, cellular interaction assays demonstrated that CAMSIT was capable of enhancing cell-matrix adhesion and cell migration, but not cell aggregation. More intriguingly, the cytoplasmic domain of CAMSIT, a 27 kDa phophorylated fragment, was consistently detectable by western analysis, and it was translocated into cell nuclei and triggered cell death through apoptosis when exogenously expressed in cells. In conclusion, gene CAMSIT is frequently downregulated in a variety of human tumors. The gene encodes a new Ig-like cell adhesion molecule which modulates cell-matrix adhesion and cell motility. The activated CAMSIT, possibly through phosphorylation, may undergo proteolytic cleavage and consequently be involved in cell signaling and growth control.

5th Human Genetics Organization (HUGO) Pacific Meeting & 6th Asia-Pacific Conference on Human Genetics. November 17-20, 2004.

Identification and characterization of a putative noncoding RNA gene in human hepatocellular carcinoma

Mei Chung Moh, Lay Hoon Lee, Shali Shen. *Department of Physiology, Faculty of Medicine, National Univ. of Singapore, 2 Medical Drive, Singapore 117597*.

Hepatocellular carcinoma (HCC) is one of the most common malignancies worldwide, especially in Africa, China and Southeast Asia. Genetic changes have been defined as the hallmark of cancers as they are responsible for the differences between normal and malignant phenotypes. A widely accepted approach to study genetic instability is to identify cancer-related genes, in particular, the two major groups of growth regulatory genes – oncogenes and tumor suppressor genes. The long-term goal of this research is to identify the common genetic changes that lead to HCC of different etiologies, and to understand the correlation between these changes and tumor progression. Using the technique of suppression subtractive hybridization (SSH), we identified a large number of genes whose expression was either down- or up- regulated in HCC. Quantitative real-time RT-PCR demonstrated that a novel gene transcript, HEPT3, was overexpressed in 95% (22/23) of HCC patients and in all the 5 HCC cell lines tested. Sequence analysis and bioinformatics performed on the full-length cDNA revealed that HEPT3 is an intronless gene mapped to chromosome 6q13-14 and the gene transcript lacks extensive open reading frame, indicating a noncoding RNA. Antisense studies on an HCC cell line C3A showed that cell growth was significantly inhibited, possibly through G2/M arrest, when HEPT3 expression level was reduced. Furthermore, endogenous HEPT3 expression could be regulated when cells were treated with anti-cancer agents, such as 5-FU and etoposide. Our data suggest that HEPT3 may be a functional noncoding gene and its RNA may play a role in the malignant transformation of hepatocytes.

18th Asia Pacific Cancer Conference. September 7-9, 2005.

Structural and functional analyses of a novel immunoglobulin-like cell adhesion molecule hepaCAM that is suppressed in a variety of human cancers

Mei Chung Moh, Lay Hoon Lee, Shali Shen. *Department of Physiology, Faculty of Medince, National University of Singapore, 2 Medical Drive, Singapore 117597.*

Purpose: Previously, we identified a new member of the immunoglobulin superfamily, hepaCAM, in normal human liver. In this study, we examined the expression and characteristics of hepaCAM as well as the relationship between its structure and function. **Methods:** Real-time RT-PCR was used to determine gene expression. Bioinformatics was performed for sequence analyses. Transfections, coupled with immunochemistry, cellular interaction analyses, cell motility assays, and colony formation, were employed to elucidate the characteristics and functions of hepaCAM. **Results:** Gene hepaCAM was widely expressed in normal human tissues, such as liver, brain, skeletal muscle, colon and blood, but was significantly suppressed in 20/23 of HCC specimens and in 17/19 cell lines derived from various human tumors. Mapped to chromosome 11q24, hepaCAM had no significant similarities to any known genes. The predicted protein of 416 amino acids displayed a typical structure of Ig-like adhesion molecules, including two extracellular Ig-like domains, a transmembrane segment and a cytoplasmic tail. The subcellular localization of hepaCAM appeared to be cell density-dependent. In well-spread cells, hepaCAM was distributed in punctuate structures in the cytoplasm and at the cell surface protrusions. In confluent cells, hepaCAM was predominantly localized on the cytoplasmic membrane, particularly in the areas of cell-cell contacts, but absent at free cell borders. The 75 kDa protein was glycosylated and phosphorylated, and formed *cis*-dimers on cell surface. Functionally, hepaCAM reduced cell colony formation ($P = 0.0022$), inhibited cell proliferation ($P < 0.001$), and induced senescence-like phenotype. In addition, hepaCAM increased cell spreading on matrices fibronectin and matrigel, and enhanced cell migration. When the cytoplasmic domain was deleted, the mutant could less significantly increase cell-matrix adhesion, cell motility and growth inhibition compared to the wildtype. **Conclusion:** Gene hepaCAM is frequently downregulated in a variety of human tumors. The gene encodes a new membrane-associated glycoprotein, an Ig-like cell adhesion molecule, modulating cell-matrix adhesion, cell motility and cell growth. The cytoplasmic domain of hepaCAM is essential to its function.

Keywords: Ig-like cell adhesion molecule, glycoprotein, growth inhibition, cellular interactions,

ASBMB Annual Meeting and Centennial Celebration. April 1-5, 2006.

hepaCAM, a novel immunoglobulin-like cell adhesion molecule, is associated with the actin cytoskeleton and the lipid rafts and is involved in cell-matrix interaction

Mei Chung Moh, Shali Shen. *Department of Physiology, National University of Singapore, Yong Loo Lin School of Medicine, Singapore 117597, 2 Medical Drive, Singapore.*

We have recently identified a novel gene hepaCAM which encodes a cell adhesion molecule of the immunoglobulin superfamily. Biochemical analyses reveal that hepaCAM is an N-linked glycoprotein phosphorylated in the cytoplasmic domain, and forms homodimers through cis-interaction on cell surface. Immunocytochemistry shows that the wild-type hepaCAM colocalizes with filamentous actin (F-actin) on the plasma membrane while depolymerization of F-actin leads to an increased solubilization and a disruption of the subcellular distribution of hepaCAM. Sucrose density gradients demonstrate that hepaCAM partitions into the lipid rafts while dispersion of cholesterol in the lipid rafts alters the buoyancy of hepaCAM. In addition, hepaCAM colocalizes with the lipid raft markers, caveolin-1 and fyn. Functionally, hepaCAM increases cell spreading on matrices fibronectin and matrigel, delays cell detachment, and enhances wound healing. Furthermore, when the cytoplasmic domain is deleted, hepaCAM mutants do not affect cell surface localization and dimer formation; however, these mutants are less significantly involved in cell-matrix adhesion and cell motility. Overall, these data indicate that hepaCAM interacts with the actin cytoskeleton and resides in the lipid rafts, and that the cytoplasmic domain of hepaCAM is essential to its function on cell-matrix interaction and cell motility.